UNIVERSITAT DE BARCELONA

Arming oncolytic adenoviruses with bi-specific T-cell engagers to improve antitumor efficacy

Carlos Alberto Fajardo Calderón

UNIVERSITAT DE BARCELONA

FACULTAT DE FARMÀCIA I CIÈNCIES DE L'ALIMENTACIÓ

DEPARTAMENT DE BIOQUÍMICA I BIOLOGIA MOLECULAR

PROGRAMA DE DOCTORAT EN BIOMEDICINA

ARMING ONCOLYTIC ADENOVIRUSES WITH BI-SPECIFIC T-CELL ENGAGERS TO IMPROVE ANTITUMOR EFFICACY

CARLOS ALBERTO FAJARDO CALDERÓN

2017

UNIVERSITAT DE BARCELONA

FACULTAT DE FARMÀCIA I CIÈNCIES DE L'ALIMENTACIÓ

DEPARTAMENT DE BIOQUÍMICA I BIOLOGIA MOLECULAR

PROGRAMA DE DOCTORAT EN BIOMEDICINA

ARMING ONCOLYTIC ADENOVIRUSES WITH BI-SPECIFIC T-CELL ENGAGERS TO IMPROVE ANTITUMOR EFFICACY

CARLOS ALBERTO FAJARDO CALDERÓN

2017

Memòria presentada per Carlos Alberto Fajardo Calderón per optar al grau de Doctor per la Universitat de Barcelona

Dr. Ramon Alemany Bonastre	Dr. Francesc Viñals Canals	Carlos Alberto Fajardo Calderón
Director	Tutor	Autor

Agradecimientos

Empezando a escribir estas páginas se me vienen tantas personas a la cabeza a las que me gustaría agradecer, que necesitaría casi un documento igual de largo a la tesis para lograrlo. A pesar de esto, voy a hacer mi mejor esfuerzo para sintetizar, corriendo el riesgo de que se me olvide alguien o de quedarme corto en palabras para algunos.

En primer lugar quiero agradecer a Ramón Alemany. Gracias, **Ramón**, por haber confiado en mí para llevar a cabo este proyecto tan original y motivante. Cada vez es más difícil innovar en el campo de la viroterapia, pero tú lo sigues consiguiendo y este proyecto es una muestra de ello. Gracias por darme la libertad de desarrollar mis propias ideas, pero también por guiarme cuando no encontraba el rumbo. Gracias por tu paciencia cuando iba a explotarte la cabeza con mis ideas locas y por transmitirme calma cuando las cosas se ponían difíciles. Gracias por siempre tener la puerta de tu oficina abierta para hablar de ciencia, pero también para dar consejos personales en momentos de incertidumbre. De ti he aprendido mucho estos años. He aprendido que se puede ser un gran científico sin necesidad de abandonar la humildad y la sencillez. Estoy convencido de que el mundo científico sería mucho mejor si hubiera más jefes como tú. En fin, muchas gracias por todo!

Claramente, muchos de los agradecimientos tienen que ir para los RATGitos. En especial al consejo de sabios de Maquinitas' Day. A **Rafa**, la maquina más máquina del grupo. Ramón es la brújula, pero tú eres el motor del barco y el grupo tiene suerte de tenerte. Muchas gracias por el apoyo profesional y personal durante estos años. Gracias por siempre arrancarme una sonrisa con tus apuntes con acento andaluz. Gracias por las caminatas de Navidad (cómo las voy a extrañar!), que hicieron que pudiera olvidarme de la tesis por unos instantes! Y gracias por haber hecho que mi adaptación al grupo fuera muy fácil desde el comienzo. Gracias por todo, illo! A **Luisin**, con quien sufrimos estos últimos meses de escritura de tesis. Gracias por hacer que los debates científicos tuvieran "salsa". Pero sobre todo gracias por los buenos momentos: San Sebastián, Logroño, reggaetones en versión burlería, dudo, Bonfiest, entre muchos otros. Gracias por tu humor y por sacarme siempre una sonrisa (aunque con retraso por aquello de no entender las bromas). Te deseo lo mejor en esta nueva etapa que vas a empezar, aunque estoy seguro de que triunfarás allá donde vayas! Y como no agradecer a **Marcelino**, el crack más sabio del consejo y la persona con la que más he conectado en estos años de tesis. Vuelvo y te lo repito: cuando sea grande quiero ser como tú. Contigo se me vienen a la cabeza muchas palabras en desorden: noches de Dudo con ron-colas, Mario Kart 64, debates musicales, Upsala, fiestas de Sants/Gracia,

Logroño…en fin, tú ya sabes a lo que me refiero. Muchas gracias por los innumerables debates acerca de la vida y por siempre estar ahí para escucharme y darme consejos cuando los necesité. Estoy seguro de que nos seguiremos viendo por el camino! Y como grupo, gracias al consejo de sabios por las tardes de videojuegos y los buenos momentos durante estos años. Sé que siempre podré contar con ustedes, así como ustedes pueden hacerlo conmigo.

También quiero agradecer a los RATGitos actuales. A **Ahmed**, por ser una persona generosa, paciente y alegre. Y perdón porque te ha tocado aguantar mi impaciencia en estos últimos meses de tesis. Espero que encuentres el camino que quieres después de la tesis! A **Jana**, por tu carácter alegre, descomplicado y sereno. Espero haberte podido transmitir un poco de motivación, a pesar del estrés estos últimos meses. Y espero que sigas a tope como lo has estado hasta el momento. El proyecto de los BiTEs queda en muy buenas manos! A **Martí**, el canterano del grupo, por siempre transmitir alegría. Sé que la ciencia puede ser frustrante, pero no te desanimes! Poco a poco las cosas irán cogiendo su rumbo. Dale duro! A **Silvia**, mi vecina del Eixample. A pesar de picarme con el Barça (cough, cough…), has tenido siempre palabras de apoyo y te has preocupado mucho por mí. Gracias! Y no creas que no me acuerdo del crepe de manzana que se ha aplazado por la tesis! A **Loli**, por tu carácter amable y alegre y por transmitir calma en tanto caos RATG. Gracias también a las chicas de VCN **Sara, Ana y Patri**.

Y por supuesto tengo que agradecer a los RATGitos que ya no están, pero con los que compartí muy buenos momentos. A **Sonia**, una persona muy especial. Fuimos muy afortunados de tener en el grupo a una persona con tu experiencia en inmunoterapia. Gracias por darle un salto de calidad al proyecto del cBiTE y por creer en la combinación del virus con las CAR T cells. Gracias por corregir esta tesis. Gracias por las innumerables e interminables discusiones de ciencia. Pero sobre todo, gracias por haber estado ahí para apoyarme durante los momentos más difíciles de mi tesis. Siempre lograste arrancarme una sonrisa y he aprendido mucho de ti! Gracias por todo! A **Albita**, porque fuiste de las personas que más me acogió desde el principio y con una de las que más conecté en estos años. Fueron muchas noches de salsa, de música y de risas. Gracias por todo! A **Marta** por acogerme desde el principio y hacer que mi adaptación al grupo fuera más fácil. Por último, quiero agradecer a **Raúl, Cris y Edu** con quienes compartí los primeros años en el laboratorio.

Gracias también a las niñas del LRT1. A **Mariona**, por escucharme y por siempre tener una sonrisa que ofrecer. Siempre recuerdo aquellos días cantando Alosque a todo pulmón o tus cumpleaños desenfrenados que se han vuelto costumbre año tras año. A **Roser**, por tu motivación y por las horas de desahogo mutuo que espero que te hayan servido como a mí. A **Elisenda**, por ser de las personas que me abrió las puertas desde mi primer día en el ICO y con la que aún sigo contando. A **Natalia G** por tu alegría y positividad. A **Nerea**, por tu sencillez y por tus consejos. A **Iratxe**, por los incontables debates acerca de la vida. Gracias también al resto de personas del LRT1 que de alguna u otra forma hicieron que mi adaptación y el trabajo estos años en el laboratorio fueran más fáciles. **A Nick, Carmen, Gorka, Samu, Agnés, Gaby, Julia, María, Mar, Paqui, Susana, Nadia, Mónica, Sara, Alba Natalia Casado, Laura Bernaus y a todos los jefes**. De todos ellos tengo buenos recuerdos que me motivan a ponerlos en esta larga lista para decirles gracias! También quiero agradecer a la gente del LRT2 por su ayuda en varios momentos de esta tesis.

Pero también fuera del LRT1 hay mucha gente a la que tengo que agradecer. A **Jack**, el italiano más crack que conozco. Gracias por tu carácter alegre inagotable y por los buenos momentos durante estos años. Siempre admiraré tu forma de ver la vida y de tratar a la gente! A **Eric**, el crack madridisti. Tengo muy buenos recuerdos de aquellos fines de semana trabajando en el lab cuando el ICO asustaba por su soledad. Y qué decir de los buenos momentos futbolísticos: cuevas/templos, la décima, la undécima e infinidad de debates futbolísticos. Gracias por todo, crack! A **Curro**, el sevillano más bromista que conozco. Gracias por acogerme desde el principio y hacer que mi adaptación al ICO fueras más fácil. Por el padel, los debates futbolísticos, por los momentos de desorden y por mostrarme los mejores restaurantes de Barcelona! A **Francis**, por tu tranquilidad y alegría que han hecho que seas uno más del grupo! A **Ali**, la persona más alegre de este mundo! Gracias por siempre sacarme un sonrisa! A **Karinna**, por hacer que sintiera nuestras tierras muy cerca del ICO. Por último, quiero agradecer a **Elena Senís** por su apoyo durante los primeros años de esta tesis.

No puedo olvidarme de mis amigos de Colombia, a quienes he "abandonado" sin mala intención durante la escritura de esta tesis. Muchas gracias por estar ahí incondicionalmente siempre que lo he necesitado. Espero que podamos adelantar cuaderno al concluir esta etapa!

Quiero agradecer de todo corazón a mi familia. A todos mis tíos, primos y a mi abuela, quienes han seguido mi carrera y siempre se han alegrado con mis logros. A todos ellos que

me han enviado artículos de actualidad científica porque se acordaron de mí, o simplemente porque querían saber mi opinión sobre temas científicos. A todos ellos un millón de gracias! A mi prima **Paula**, mi mejor amiga. Gracias por estar siempre ahí, en las buenas y en las malas. Sé que puedo contar contigo siempre y sabes que es reciproco. TQM! A mi hermana **Vero** y a **Al** porque, a pesar de mi frecuente ingratitud por culpa de la tesis, han sido un apoyo muy importante para mí durante estos años en Barcelona. Gracias por todo!

Dicen que lo mejor se deja para el final y no puedo cerrar estas páginas sin agradecer a las tres personas más importantes de mi vida: mis papás y mi hermano Santiago. Son ellos los que me han apoyado desde el primer momento y son ellos los que me motivan a seguir haciendo lo que hago. Gracias por estar ahí en cada paso que doy. Por haber estado en los momentos más alegres de mi carrera: la defensa de mi tesis de pregrado, cuando me aceptaron para el master en Heidelberg, cuando Ramón me aceptó para hacer el doctorado en su grupo y ahora cuando termino esta tesis. Pero sobre todo gracias por estar ahí para darme apoyo en los momentos más difíciles. Porque hemos reído, pero también llorado juntos. A mi **papá**, por ser mi héroe y mi modelo a seguir. Gracias por mostrarme lo que es ser un buen profesional, pero, sobre todo, por enseñarme lo que es ser una excelente persona. A mi **mamá**, la persona más amorosa que conozco. Nadie se preocupa tanto por mí ni hace las cosas con tanto cariño como tú. No tengo palabras para expresar lo mucho que te quiero. Eres única! A mi **hermano**, gracias por el apoyo incondicional y por creer en mí. A pesar de que no hablamos mucho, siempre lo siento muy cerca y sé que siempre tendré alguien en quien apoyarme. A los tres quiero darles las gracias por la paciencia durante estos últimos meses en los que el estrés y el mal humor se apoderaron de mí. Los quiero mucho y quiero que sepan que nada de esto hubiera sido posible sin su apoyo. Gracias… TOTALES!

Table of contents

ABBREVIATIONS 9
RESUMEN 15
SUMMARY 19
1. INTRODUCTION 23
1.1 Virotherapy of cancer 25
1.2 Adenoviruses: general biology 28
1.2.1 General features and classification 28
1.2.2 Virion structure 29
1.2.3 Genome organization 31
1.2.4 Adenovirus infection cycle 32
1.2.4.1 Adenovirus cell entry 32
1.2.4.2 Genome transcription and replication 33
1.3 Oncolytic Adenoviruses 36
1.3.1 Development of tumor-selective OAds 36
1.3.1.2 Transductional targeting 36
1.3.1.3 Post-entry targeting 37
1.3.2 ICOVIR-15K 39
1.3.3. Arming oncolytic adenoviruses with therapeutic transgenes 40
1.3.4. Clinical experience with oncolytic adenoviruses 41
1.3.5 Challenges for oncolytic adenoviruses 43
1.3.5.1 Oncolytic adenovirus tumor delivery and targeting 43
1.3.5.2 Tumor stromal barriers 45
1.3.5.3 Immune responses in the tumor microenvironment 46
1.4 Antitumor immune responses 46
1.4.1 Tumor immune escape 48
1.4.2 Oncolytic adenovirus-mediated antitumor immune responses 49
1.5 Strategies to improve antitumor immune responses with oncolytic adenoviruses 50
1.5.1 Oncolytic adenoviruses expressing cytokines and chemokines 50
1.5.2 Oncolytic adenoviruses expressing co-stimulatory molecules 51
1.5.3 Combination of oncolytic viruses with other immunotherapies 52
1.5.3.1 Checkpoint inhibitors 52

1.5.3.2 Adoptive transfer of tumor-infiltrating lymphocytes 53
1.5.3.3 Chimeric antigen receptor T-cell therapy 55
1.5.3.3.1 Challenges for CAR T-cell therapy 57
1.5.3.3.2 Combination of CAR T-cell therapy and oncolytic adenoviruses 57
1.6 Antiviral immune responses in the tumor microenvironment 58
1.7 Bi-specific T-cell engagers (BiTEs) 59
1.7.1 Structure of BiTEs 59
1.7.2 Mode of action of BiTEs 60
1.7.3 Clinical application of BiTEs 62
2. OBJECTIVES 65
3. MATERIALS AND METHODS 69
3.1 Handling of bacteria 71
3.1.1 Preparation of electrocompetent bacteria 71
3.1.2 Transformation of bacteria by electroporation 71
3.1.3 Small and large scale isolation of Plasmid DNA 72
3.1.4 Homologous recombination in bacteria 72
3.2 Cell culture techniques 75
3.2.1 Cell lines 75
3.2.2 Maintenance of cell cultures 76
3.2.3 Cell counting 76
3.2.4 Cryopreservation and thawing of cell lines 76
3.2.5 Mycoplasma test 77
3.2.6 Isolation, cryopreservation and thawing of human PBMCs and T cells 77
3.2.7 Isolation of mouse splenocytes 78
3.2.8 Fluorescent labeling of cancer cells with CFSE 78
3.2.9 Fluorescent labeling of human PBMCs and mouse splenocytes with CFSE 78
3.3 Recombinant adenoviruses 79
3.3.1 BiTE design 79
3.3.2 Construction of BiTE-expressing oncolytic adenoviruses 80
3.3.3 Generation of oncolytic adenoviruses by calcium phosphate transfection 80
3.3.4 Virus clone isolation by plaque purification assay 81
3.3.5 Amplification and large-scale production of oncolytic adenoviruses 81
3.3.6 Purification of oncolytic adenoviruses 82

3.3.7 Determination of the total number of virus particles by spectrophotometry 83
3.3.8 Determination of functional viral particles by anti-hexon staining 83
3.3.9 Isolation of viral DNA from infected cells 84
3.3.10 Isolation of viral DNA from viral particles 84
3.3.11 Characterization of viral genomes by restriction analysis 84
3.3.12 Characterization of viral genomes by sequencing 85
3.4 Adenovirus-based *in vitro* assays 86
3.4.1 Adenoviral transduction assay 86
3.4.2 Adenovirus-mediated cytotoxicity assay 86
3.4.3 Adenovirus production assay 86
3.4.4 Production of supernatants 87
3.5 Production and titration of lentiviral vectors 87
3.6 Immunology techniques 88
3.6.1 Antibodies and flow cytometry 88
3.6.2 Preactivation and expansion of human T cells 90
3.6.3 Generation of genetically-modified T cells 91
3.6.4 Binding assays 91
3.7. Coculture-based *in vitro* assays 91
3.7.1 Rosette formation assay 91
3.7.2 T-cell activation assays 92
3.7.3 Cytokine production assay 92
3.7.4 CFSE-based T-cell proliferation assay 93
3.7.5 Luciferase-based T-cell proliferation assay 93
3.7.6 Counting beads-based T-cell proliferation assay 94
3.7.7 Inhibitory markers expression assay 94
3.7.8 Cell-mediated cytotoxicity assays 94
3.7.8.1 CFSE/7-AAD cytotoxicity assay 94
3.7.8.2 Bystander killing assay 95
3.7.8.3 Oncolysis and cell-mediated cytotoxicity assay 95
3.8 *In vivo* studies 96
3.8.1 Mouse models and procedures 96
3.8.2 Immunohistofluorescence of OCT-embedded tumor sections 96
3.8.3 Immunohistochemistry of paraffin-embedded tumor sections 97

3.8.4 Detection of transgene and viral transcripts in tumors by Real-Time PCR 97
3.9 Statistical analysis 99
4. RESULTS 101
4.1 Bispecific T-cell engager-armed oncolytic adenoviruses 103
4.1.1 A BiTE-armed oncolytic adenovirus targeting human EGFR and human CD3 103
4.1.1.1 Generation and characterization of ICO15K-cBiTE 103
4.1.1.2 Cells infected with ICO15K-cBiTE secrete cBiTE antibodies which specifically bind to target and effector cells 106
4.1.1.3 Supernatants from ICO15K-cBiTE-infected cells enhance T-cell function 110
4.1.1.4 ICO15K-cBiTE-mediated oncolysis enhances T-cell function and induces T-cell-mediated bystander effect 113
4.1.1.5 ICO15K-cBiTE increases the persistence and accumulation of tumor infiltrating T cells 118
4.1.1.6 cBiTE and viral transcripts are detected in tumors treated with ICO15K-cBiTE 120
4.1.1.7 ICO15K-cBiTE enhances antitumor efficacy *in vivo* 121
4.1.1.8 ICO15K-cBiTE-mediated oncolysis increases the expression of immune checkpoints on T cells 125
4.1.2 An oncolytic adenovirus encoding a murine surrogate of cBiTE targeting murine EGFR and murine CD3 127
4.1.2.1 Generation and characterization of ICO15K-mBiTE 127
4.1.2.2 Cells infected with ICO15K-mBiTE fail to secrete functional mBiTE antibodies 129
4.1.3 An oncolytic adenovirus encoding a chimeric BiTE targeting human EGFR and murine CD3 130
4.1.3.1 Generation and characterization of ICO15K-mcBiTE 130
4.1.3.2 Cells infected with ICO15K-mcBiTE secrete mcBiTE antibodies which specifically bind to target and effector cells 132
4.1.3.3 Generation and characterization of B16CAR cells expressing the human EGFR 133
4.1.3.4 Supernatants from ICO15K-mcBiTE-infected cells enhance splenocyte function 135
4.1.3.5 Supernatants from ICO15K-mcBiTE-infected cells induce T-cell-mediated cell killing 136
4.1.3.6 B16CAR-EGFR cells produce lower levels of mcBiTE compared to the parental cell line 136
4.1.3.7 B16CAR-EGFR cells fail to generate tumors in C57BL/6 mice 138
4.2. Combination of CAR T-cell therapy and ICO15K-cBiTE 138
4.2.1 Generation of CAR T cells targeting mesothelin 139
4.2.2 ICO15K-cBiTE supernatants activate CAR T-cells in the absence of mesothelin 141

4.2.3 CAR T-cell preparations show increased cytokine productionin combination with ICO15K-cBiTE supernatants 142

4.2.4 CAR T-cell preparations show increased proliferation in combination with ICO15K-cBiTE supernatants 144

4.2.5 ICO15K-cBiTE improves the cytotoxic potential of CAR T-cell preparations *in vitro* 145

5. DISCUSSION 147

5.1 BiTE-ARMED ONCOLYTIC ADENOVIRUSES 149

5.1.1 Molecular considerations for the design of BiTE-armed oncolytic adenoviruses 149

5.1.2 The promise and challenges of BiTE-armed oncolytic adenoviruses 152

5.2 THE CHALLENGE OF ESTABLISHING MURINE MODELS FOR THE *IN VIVO* EVALUATION OF BiTE-ARMED ONCOLYTIC ADENOVIRUSES 158

5.2.1 Humanized mouse models of cancer 158

5.2.2 Immunocompetent mouse models of cancer 162

5.3. COMBINATION OF ICO15K-cBiTE WITH CAR T-CELL THERAPY 165

5.4 Outlook and future perspectives 169

6. CONCLUSIONS 171

7. REFERENCES 175

8. ANNEXES 201

List of figures

Figure 1. The principle of virotherapy of cancer 25
Figure 2. Mode of action of oncolytic viruses. 26
Figure 3. Oncolytic viruses currently used in clinical trials. 27
Figure 4. Structure of adenovirus virions 31
Figure 5. Adenovirus genome organization 32
Figure 6. Infection cycle of human adenoviruses 35
Figure 7. Δ24-based oncolytic adenoviruses 38
Figure 8. Characteristics of ICOVIR-15K 40
Figure 9. Challenges for oncolytic adenoviruses. 44
Figure 10. The cancer-immunity cycle 47
Figure 11. Mechanisms of immune evasion by tumors 49
Figure 12. Activating and inhibitory interactions regulating T-cell activation 54
Figure 13. Chimeric antigen receptors 55
Figure 14. Overview of CAR T-cell therapy 56
Figure 15. BiTE design. 60
Figure 16. Mode of action of BiTEs 61
Figure 17. Comparison of TCR-MHC-I- and BiTE-mediated T-cell responses 62
Figure 18. Schematic representation the ICO15K-cBiTE genome. 104
Figure 19. *In vitro* characterization of ICO15K-cBiTE 106
Figure 20. EGFR and CD3 profiles of the cell lines used in the study. 107
Figure 21. cBiTE antibodies are expressed from ICO15K-cBiTE-infected cells and specifically bind to target cells 108
Figure 22. cBiTE antibodies expressed from ICO15K-cBiTE-infected cells bind to effector T cells 109
Figure 23. Supernatants from ICO15K-cBiTE-infected cells engage T cells towards cancer cells 110
Figure 24. cBiTE antibodies expressed from ICO15K-cBiTE-infected cells induce T-cell activation. 111
Figure 25. cBiTEs expressed from ICO15K-cBiTE-infected cells induce T-cell proliferation. 112
Figure 26. cBiTEs expressed from ICO15K-cBiTE-infected cells enhance T-cell-mediated cytotoxicity 113
Figure 27. ICO15K-cBiTE-mediated oncolysis leads to T-cell activation and proliferation 114
Figure 28. Characterization of adenovirus infection in A431 cells. 115
Figure 29. ICO15K-cBiTE-mediated oncolysis induces T-cell-mediated cytotoxic bystander effect 116
Figure 30. Preactivated T cells produce proinflammatory cytokines and show higher killing capacities than unstimulated T cells when engaged by the cBiTE 117
Figure 31. Preactivated T cells improve the cytotoxic potential of ICO15K-cBiTE 118
Figure 32. Luciferase- and GFP-expressing T cells retain their proliferative capacities *in vitro* 119
Figure 33. ICO15K-cBiTE induces accumulation and increased persistence of tumor-infiltrating T cells *in vivo* 120
Figure 34. cBiTE mRNA transcripts are detected in tumors treated with ICO15K-cBiTE 121
Figure 35. ICO15K-cBiTE shows improved antitumor efficacy *in vivo* 122
Figure 36. ICO15K-cBiTE shows improved antitumor efficacy in an aggressive model of cancer 124
Figure 37. ICO15K-cBiTE-mediated oncolysis induces the expression of inhibitory receptors on T cells 126
Figure 38. Schematic representation of the design of ICO15K-mBiTE 128

Figure 39. Cells infected with ICO15K-mBiTE fail to secrete functional mBiTE antibodies 129
Figure 40. Schematic representation of the design of ICO15K-mcBiTE 131
Figure 41. *In vitro* oncolytic properties of ICO15K-mcBiTE 132
Figure 42. mcBiTE antibodies are expressed from ICO15K-cBiTE-infected cells and specifically bind to target and effector cells 133
Figure 43. Characterization of B16CAR-EGFR cells 134
Figure 44. mcBiTE antibodies expressed from ICO15K-mcBiTE-infected cells induce mouse T-cell activation and proliferation 135
Figure 45. mcBiTEs expressed from ICO15K-cBiTE-infected cells enhance splenocyte-mediated cytotoxicity 136
Figure 46. B16CAR-EGFR cells produce lower levels of mcBiTEs compared to the parental cell line . 137
Figure 47. Schematic representation of the SS1 chimeric antigen receptor construct 139
Figure 48. Generation and characterization of anti-mesothelin CAR T-cell preparations 140
Figure 49. ICO15K-cBiTE supernatants activate CAR T cells in the absence of mesothelin 142
Figure 50. CAR T-cell preparations show increased cytokine production in combination with ICO15K-cBiTE supernatants 143
Figure 51. CAR T-cell preparations show increased proliferation in combination with ICO15K-cBiTE supernatants 144
Figure 52. ICO15K-cBiTE-mediated oncolysis improves the cytotoxic potential of CAR T cells 145
Figure 53. Proposed mode of action of ICO15K-cBiTE 156
Figure 54. Proposed model of the combined action of ICO15K-cBiTE and CAR T cells 169

ABBREVIATIONS

%	Percentage
Δ24	*delta*24 mutation, deletion of 24 bp in E1A protein
°C	Centigrade degrees
µg	microgram
µl	microliter
µm	micrometer
AAALAC	Association for Assessment and Accreditation of Laboratory Animal Care
ACK	Ammonium-chloride-potassium
ACT	Adoptive T cell therapy
Ad	Adenovirus
ADP	Adenovirus Death Protein
AFP	Alpha-Fetoprotein Promoter
ALL	Acute Lymphocytic Leukemia
AML	Acute myeloid leukemia
APC	Antigen-Presenting Cell
ATCC	American Type Cell Culture
ATP	Adenosine triphosphate
BAC	Bacterial Artificial Chromosome
BCA	Bicinchoninic Acid Assay
BCMA	B-cell maturation antigen
BiTE	Bi-specific T-cell engager
bp	base pairs
BRAF	v-Raf murine sarcoma viral oncogene homolog B
BSA	Bovine Serum Albumin
$CaCl_2$	Calcium chloride
CAF	Cancer-Associated Fibroblast
CAR	Coxsackievirus and Adenovirus Receptor or Chimeric Antigen Receptor
CCE	Clarified Cell Extract
CD3ζ	CD3 zeta chain
CD4 and 8	Cluster of differentiation 4 and 8
cDNA	complementary DNA
CE	Cell Extract
CEA	Carcinoembryonic antigen
Cm	Chloramphenicol
cm	centimeter
CMV	Citomegalovirus
CO_2	Carbon dioxide
CPE	Cytopathic effect
CRC	Colorectal cancer
CsCl	Cesium chloride
CTL	Cytotoxic T Lymphocyte

CTLA-4	Cytotoxic T-Lymphocyte-Associated Protein 4
DAMP	Damage-Associated Molecular Pattern
DC	Dendritic cell
ddH_2O	bi-distilled water
DMEM	Dulbecco's Modified Eagle's Medium
DMSO	Dimethyl sulfoxide
DNA	Deoxyribonucleic Acid
dNTP	Nucleoside triphosphate
EC_{50}	Half maximal effective concentration
ECM	Extracellular Matrix
EDTA	Ethylenediaminetetraacetic acid
EGFR	Epidermal growth factor receptor
Epcam	Epithelial cell adhesion molecule
EphA2	EphA2 Ephrin receptor tyrosine kinase A2
ER	Endoplasmic Reticulum
FACS	Fluorescence Activated Cell Sorting
FAP	Fibroblast activation protein
FasL	Fas Ligand
FBS	Fetal Bovine Serum
FDA	Food and Drug Administration
FX	Coagulation factor X
g	acceleration of gravity
g	gram
GM-CSF	Granulocyte Macrophage-Colony Stimulating Factor
h	hour
H_2O_2	Hydrogen peroxide
HCl	Chloridric acid
HEPES	4-(2-hydroxyethyl)-1-piperazineethanesulfonic acid
Her2	Human EGF receptor 2
HMGB1	High Mobility Group Box 1 Protein
HSP	Heat Shock Protein
HSPG	Heparan-Sulphate-Glycosaminoglicans
HSV	Herpes Simplex Virus
hTERT	Human telomerase reverse transcriptase
HVR	Hypervariable region
Hyal	Hyaluronidase
IC_{50}	Inhibitory Concentration 50
ICD	Immunogenic Cell Death
ICOS	Inducible T cell Co-stimulator
IDD	Immunodominant Determinants
IDO	Indoleamine 2,3-dioxigenase
IFN	Interferon
Ig	Immunoglobulin
IL	Interleukin
IP	Intraperitoneal

IRES	Internal Ribosome Entry Site
IT	Intratumoral
ITR	Inverted Terminal Repeats
IV	Intravenous
Kan	Kanamycin
Kbp	kilobase pair
KC	Kupffer Cell
Kd	Dissociation constant
KRAS	V-Ki-ras2 Kirsten rat sarcoma viral oncogene homolog
L	Litre
LAG-3	Lymphocyte activation gene 3
mA	milliampere
mAb	Monocloncal antibody
MDSC	Myeloid-derived supressor cell
MDSC	Myeloid-derived Suppressor Cell
μF	microfarad
mg	milligram
MHC-I	Class I Major Histocompatibility Complex
min	minute
miRNA	MicroRNA
mL	milliliter
MLP	Major Late Promoter
MLU	Major Late transcription Unit
mm	millimeter
mM	millimolar
mm^3	cubic millimeter
MMP	Matrix Metalloprotease
MOI	Multiplicity of Infection
mRNA	Messenger Ribonucleic Acid
MSC	Mesenchymal Stem Cell
MV	Measles virus
NAbs	Neutralizing antibodies
NaCl	Sodium chloride
NaH_2PO_4	Monosodium phosphate
NaOH	Sodium hydroxide
NDV	Newcastle disease virus
ng	nanogram
NK	Natural killer
nm	nanometer
NOD-Scid	Non-obese diabetic
NPC	Nuclear Pore Complex
NSCLC	Non-Small Cell Lung Carcinoma
NSG	Nod Scid Gamma
OAd	Oncolytic adenovirus
OCT	Optimum Cutting Temperature compound

OD	Optical Density
OV	Oncolytic virus
PAMP	Pathogen-Associated Molecular Pattern
PBMCs	Peripheral blood mononuclear cells
PBS	Phosphate Buffered Saline
PCR	Polymerase Chain Reaction
PD-1	Death Protein-1
PD-L1	Death Protein Ligand-1
PE	R-phycoerythrin
pg	picogram
PIK3CA	Phosphatidylinositol-4,5-bisphosphate 3-kinase
pmol	picomol
PRR	Pattern Recognition Receptor
PS	Penicillin-Streptomycin
PSA	Prostate-Specific Antigen
PTEN	Phosphatase and tensin homolog
Rb	Retinoblastoma
RGD	Arginine-glycine-aspartic acid
RNA	Ribonucleic Acid
rpm	revolutions per minute
RPMI	Roswell Park Memorial Institute
RT	Radiation Therapy or Room Temperature
RT-PCR	Real-Time PCR
scFV	Single chain fragment variable
Scid	Severe combined immunodeficiency
SD	Standard Deviation
SDS	Sodium dodecyl sulfate
SEM	Standard Error of the Mean
SPARC	Secreted Protein Acidic and Rich in Cysteine
ssDBP	single-stranded DNA binding protein
Strep	Streptomycin
TAA	Tumor-Associated Antigen
TAM	Tumor-associated macrophages
TAP	Transporter Associated to Antigen Processing
TCR	T Cell Receptor
TE	Tris-EDTA
TGF-β	Transforming Growth Factor-β
TIL	Tumor-Infiltrating Lymphocyte
TIM-3	T-cell immunoglobulin and mucin-domain containing-3
TLR	Toll-Like Receptor
TME	Tumor microenvironment
TNF-α	Tumor Necrosis Factor alpha
TP	Terminal Protein
TPL	Tripartite Leader
TRAIL	TNF-related apoptosis-inducing ligand

T_{reg}	Regulatory T cell
Tris	Tris(hydroxymethyl)aminomethane
TU	Transducing Unit
UTD	Untransduced
V	Volt
V	Volume
VA	Virus-Associated
VEGF	Vascular Endothelial Growth Factor
vp	viral particle
VSV	Vesicular stomatitis virus
VV	Vaccinia Virus
WHO	World Health Organization
WT	Wild-type

Amino acids

F Phe, phenylalanine	**S** Ser, serine	**Y** Tyr, tyrosine	**K** Lys, lysine	**W** Trp tryptophan
L Leu, leucine	**P** Pro, proline	**H** his, histidine	**D** Asp, aspartic acid	**R** Arg, arginine
I Ile, isoleucine	**T** Thr, threonine	**Q** Gln, glutamine	**E** Glu, glutamic acid	**G** Gly, glycine
M Met, methionine	**A** Ala, alanine	**N** Asn, asparragina	**C** Cys, cysteine	**V** Val, valine

Nucleotides

A adenine T thymine **G** guanine **C** cytosine **U** uracil

RESUMEN

Los virus oncolitos, capaces de infectar selectivamente células cancerosas sin afectar aquellas sanas, han despertado interés en los últimos años como nueva terapia contra el cáncer. Sin embargo, los ensayos clínicos con estos virus han demostrado que el sistema inmune supone un obstáculo para el éxito de los mismos en pacientes con cáncer. A pesar de la inmunosupresión que se observa en el ambiente tumoral, las células cancerosas infectadas por el adenovirus pueden ser eliminadas eficientemente por los linfocitos T anti-adenovirales sin comprometer la carga tumoral. La hipótesis de esta tesis es que adenovirus oncoliticos expresando *bi-specific T-cell engagers* (*BiTEs* por sus siglas en inglés) capaces de redirgirir los linfocitos T para atacar las células cancerosas, puede favorecer la respuesta inmune antitumoral sobre la antiviral. El genoma del adenovirus oncolitico ICOVIR-15K fue modificado genéticamente para expresar *BiTEs* contra el receptor del factor de crecimiento epidérmico (*EGFR* por sus siglas en inglés) bajo el control del promotor mayor tardío. El virus ICOVIR-15K expresando un *BiTE* que reconoce el *EGFR* y el CD3 humanos (ICOVIR-15K-cBiTE) fue generado y retuvo propiedades oncoliticas similares a la del virus parental *in vitro*. La expresión y secreción del cBiTE fue detectada en los sobrenadantes de células infectadas ICOVIR-15K-cBiTE, y sus propiedades de unión a células $CD3^+$ o $EGFR^+$ fueron confirmadas *in vitro*. En experimentos de cocultivos, la oncolisis generada por ICOVIR-15K-cBiTE indujo la activación y proliferación de los linfocitos T, e indujo un incremento en la citotoxicidad de células cancerosas. La inyección de este adenovirus aumentó la persistencia y la acumulación de linfocitos infiltrantes de tumor *in vivo.* Adicionalmente, experimentos en modelos murinos de cáncer basados en la administración combinada de ICOVIR-15K-cBiTE y linfocitos humanos demostraron un aumento en la eficacia antitumoral comparado con el virus parental. Tambien demostramos que otro adenovirus oncoliticos expresando un BiTE quimera que reconoce el EGFR humano y el CD3 murino (ICOVIR-15K-mcBiTE) induce la activación y proliferación de linfocitos T murinos *in vitro*. Este virus podrá ser utilizado en un futuro como sustituto de ICOVIR-15K-cBiTE para estudios farmacológicos y toxicológicos de adenovirus armados con BiTEs. Por último, hemos demostrado que la combinación de ICOVIR-15K-cBiTE y linfocitos T con receptores de antígeno quiméricos (CAR por sus siglas en inglés) pueden superar muchas de las carencias que tienen ambas terapias. Los resultados de esta tesis demuestran que los adenovirus oncoliticos expresando BiTEs tienen propiedades que puede superar muchas de las limitaciones de la viroterapia del cáncer, y alienta a continuar su evaluación y desarrollo a nivel clínico.

SUMMARY

Oncolytic adenoviruses that selectively replicate in cancer cells while sparing normal tissue have gained considerable attention as novel anticancer drugs. However, clinical trials with these viruses have identified the immune system as a major hurdle for their success in cancer patients. Despite the existence of a highly immunosuppressive tumor environment, adenovirus-infected cells can nonetheless be efficiently cleared by virus-specific infiltrating cytotoxic T lymphocytes without compromising tumor burden. We hypothesize that arming oncolytic adenoviruses with bi-specific T-cell engagers (BiTEs), a new class of antibodies that re-direct T-cells to cancer cells, might favor antitumor rather than anti-viral immune responses. We have engineered the oncolytic adenovirus ICOVIR-15K to express EGFR-targeting BiTEs under the control of the major late promoter. ICOVIR-15K armed with a BiTE targeting human CD3 and EGFR (ICOVIR-15K-cBiTE) was successfully rescued and it showed similar oncolytic properties as the parental virus. cBiTE expression and secretion was detected in supernatants from ICOVIR-15K-cBiTE-infected cells, and the secreted BiTEs bound specifically to both $CD3^+$ and $EGFR^+$ cells. In cell co-culture assays, ICOVIR-15K-cBiTE-mediated oncolysis resulted in robust T-cell activation, proliferation, and bystander cell-mediated cytotoxicity. Notably, intratumoral injection of this cBiTE-expressing adenovirus increased the persistence and accumulation of tumor-infiltrating T cells *in vivo.* Moreover, in two distinct tumor xenograft models, combined delivery of ICOVIR-15K-cBiTE with peripheral blood mononuclear cells or T cells enhanced the antitumor efficacy achieved by the parental counterpart. We also demonstrate that another oncolytic adenovirus expressing a chimeric BiTE targeting human EGFR and mouse CD3 (ICOVIR-15K-mcBiTE) induce robust mouse T-cell activation, proliferation, and cell-mediated cytotoxicity of cancer cells *in vitro*. Thus, ICOVIR-15K-mcBiTE is a promising surrogate of ICOVIR-15K-cBiTE that will aid in future pharmacological and toxicological preclinical studies of BiTE-armed oncolytic adenoviruses. Finally, we show that the combination of ICOVIR-15K-cBiTE with chimeric antigen receptor T-cell therapy can overcome some of the limitations encountered by both agents as monotherapies. The results described in this thesis demonstrate that BiTE-armed oncolytic adenoviruses hold properties with the potential of solving key limitations in oncolytic virotherapy, and encourage its further evaluation and development.

1. INTRODUCTION

1.1 Virotherapy of cancer

Virotherapy stands as a promising candidate for cancer therapy [1]. This approach is based on the use of oncolytic viruses (OVs) that selectively replicate in tumor cells without harming normal cells (Figure 1). Virotherapy takes advantage of the vast knowledge on viruses, which makes it easy to modify their genomes in order to obtain highly specific anti-cancer drugs. Furthermore, OVs can replicate and produce more cancer-specific progeny virions, conferring them an uncommon feature in the field of pharmacology: a selective drug that amplifies itself within the body of the patient.

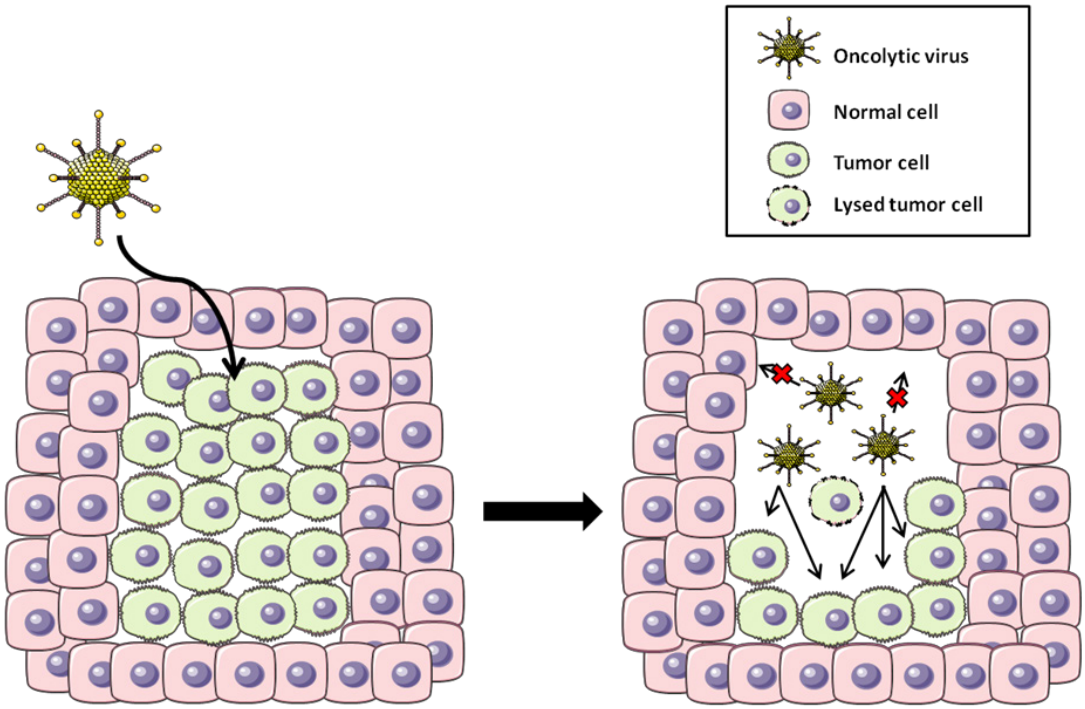

Figure 1. The principle of virotherapy of cancer. This strategy is based on replication-competent viruses which selectively kill tumor cells without harming normal cells. Oncolytic viruses replicate in tumor cells, which leads to cell death and progeny release. Newly produced viruses can spread and infect other tumor cells (black arrows) while sparing normal cells (red crosses).

Most of the attractiveness of OVs relies on their multimodal mechanisms to kill cancer cells. In addition to the direct killing of cancer cells, OV-mediated oncolysis results in the release of tumor-associated antigens (TAAs), pathogen-associated molecular pattern (PAMPs), damage-associated molecular patterns (DAMPs) and proinflammatory cytokines, all of which can trigger antitumor immune responses (Figure 2, [2]). Finally, OVs can be armed with therapeutic genes which can aid in the killing of bystander uninfected cancer cells.

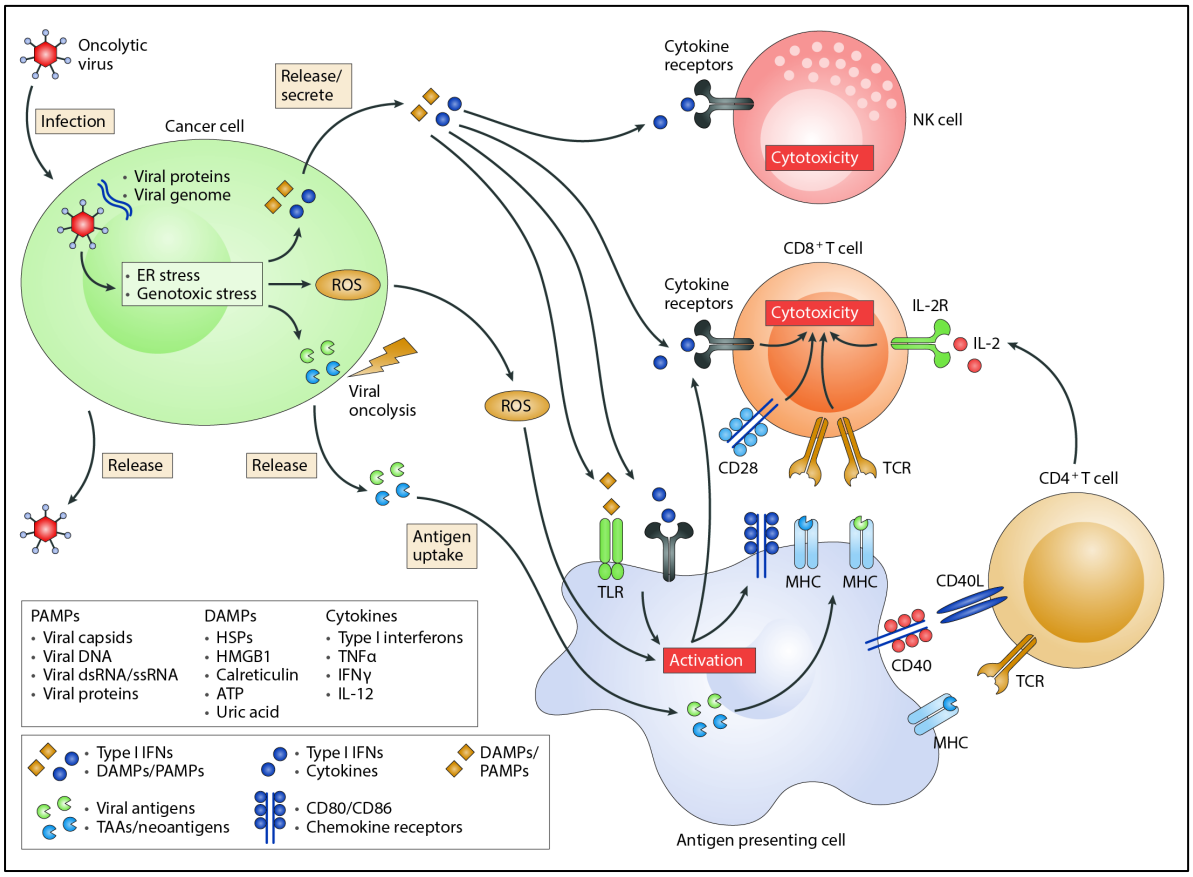

Figure 2. Mode of action of oncolytic viruses. The infection and replication of oncolytic viruses in cancer cells leads to direct cell lysis and release of virus progeny. Oncolysis induces the release PAMPs, DAMPs, cytokines and TAAs that can activate antigen-presenting cells. These events lead to the generation of antitumor and antiviral immune responses that determine the therapeutic efficacy of oncolytic viruses. Image adapted from [2].

To date viruses from 9 families with different characteristics are under investigation as OVs in clinical trials (Figure 3, [3]). OVs can be generally classified in two groups: naturally occurring or genetically engineered OVs. Naturally occurring OVs, such as parvoviruses or reoviruses, are those that exert selective tumor replication without the need of any further genetic modification. The second group is based on the genetic manipulation of viral genes to increase tumor selectivity and reduce their pathogenicity. Example of such viruses include herpes simplex viruses (HSV), vaccinia viruses (VV), adenoviruses, vesicular stomatitis viruses (VSV), measles viruses (MV), and Newcastle disease viruses (NDV) [4].

The development of OVs has risen significantly in the past 20 years, with many of these entering advanced stages in clinical trials and even receiving approval for some clinical indications. To date, two genetically engineered OVs have been approved for marketing as cancer therapeutics. Oncorine (also known as ONYX-015), an oncolytic adenovirus (OAd),

was approved in China in 2005 for the treatment of head and neck cancer [5]. More recently, the Granulocyte-macrophage colony-stimulating factor (GM-CSF)-expressing HSV T-Vec (also termed IMLYGIC or talimogene laherparepvec) was approved in the USA, Europe and Australia for the treatment advanced melanoma [6].

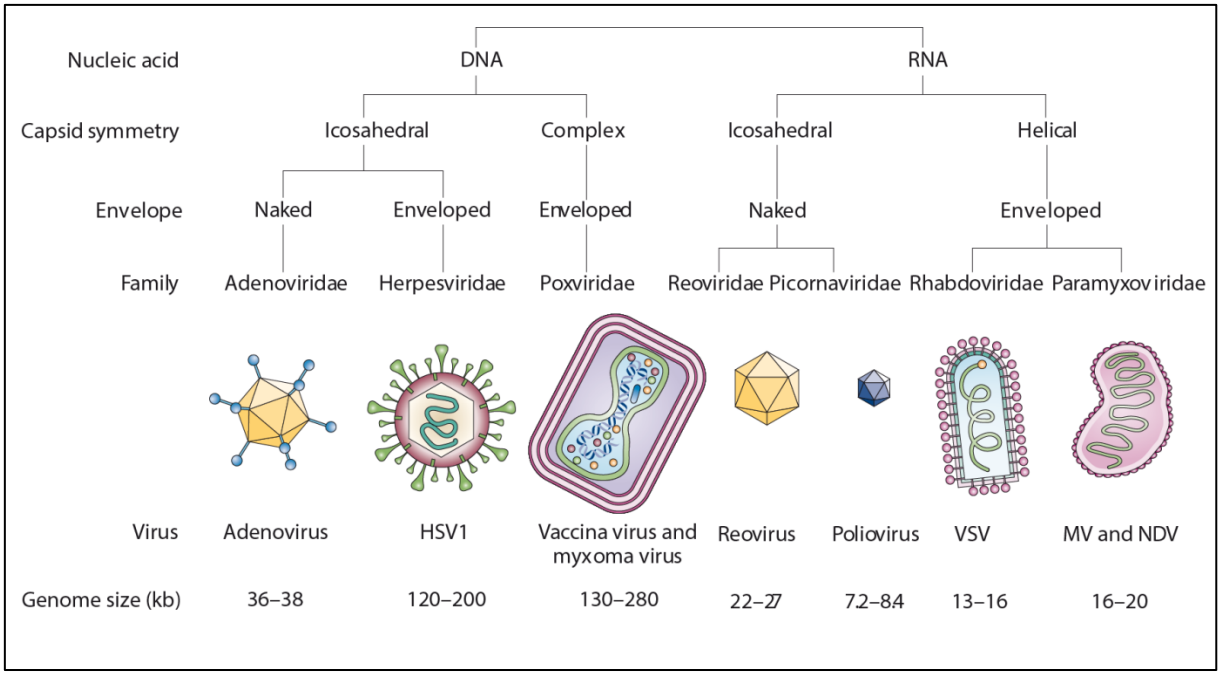

Figure 3. Oncolytic viruses currently used in clinical trials. The most representative oncolytic viruses among different virus families that are under investigation in different clinical trials. Image adapted from [3]

From the OVs studied to date, adenoviruses (Ads) hold features that make them good virotherapy candidates. These include low pathogenicity, a lytic replication cycle, the ability to infect proliferating and quiescent cells, and potent and efficient genome transfer machinery. Furthermore, Ads have been key models in molecular biology by contributing to the progress of understanding processes such as DNA replication, RNA splicing, cell cycle control and oncogenic transformation, among others [7, 8]. This wide knowledge about the molecular biology of Ad infection makes it fairly easy to modify its genome. Additionally, OAds have favorable toxicity profiles after systemic or intratumoral administration in cancer patients [9], and their potential is exemplified by the virus DNX-2401 which has received fast-track status and orphan drug designation by the FDA for the treatment of malignant glioma [10].

1.2 Adenoviruses: general biology

1.2.1 General features and classification

Adenoviruses (Ads) are non-enveloped, icosahedral, double-stranded (ds)DNA viruses of animals [11]. They belong to the family *Adenoviridae*, which comprises four genera based on the host range: *Mastadenovirus* (mammals), *Aviadenovirus* (birds), *Atadenovirus* (reptiles, birds, mammals) and *Siadenovirus* (reptiles and birds) [11, 12]. Human adenoviruses (HAds) are classified in serotypes within subgroups (also termed species) (Table 1). Serotypes are defined by the sensitivity to neutralizing antibodies, while species are determined by their hemmaglutination profiles. So far, 57 human adenoviruses serotypes have been described which are grouped into seven species (A to G) [13].

Ads are common human pathogens that cause respiratory and enteric infections, among others. Ad infections are mild and self-limiting in immunocompetent hosts, whereas in immunocompromised individuals and neonates these infections can lead to death [14].

Table 1. Classification of human Ads (Adapted from [13])

Species	Serotypes	Common associated disease	Primary attachment molecule	Oncogenic potential in rodents
A	12, 18, 31	Gastroenteritis	CAR	High
B	3, 7, 16, 21, 50, 55 (B1) 11, 14, 34, 35 (B2)	Respiratory (B:1) or urinary tract disease (B:2)	CD46/CD80/CD86 and Desmoglein-2	Moderate
C	1, 2, 5, 6, 57	Respiratory disease	CAR	Low/none
D	8, 9, 10, 13, 15, 17, 19, 20, 22–30, 32, 33, 36–39, 42–49, 51, 53, 54, 56	Keratoconjunctivitis	CAR (sialic acid for 8, 19, 37 and CD46 for 37)	Low/none
E	4	Respiratory disease/conjunctivitis	CAR	Low/none
F	40, 41	Gastroenteritis	CAR (for long fiber; short fiber unknown)	Unknown
G	52	Gastroenteritis	Unknown	Unknown

1.2.2 Virion structure

Ads virions are composed of 13 structural proteins, 7 of which form the icosahedral capsid and 6 of which are packaged with the linear double-stranded DNA in the core of the particle (Figure 4) [15, 16]. Most of the components of the virion have been designated II to X according to their apparent decreasing mass in polyacrylamide gels. Three major proteins constitute the capsid: hexon, penton base, and fiber. The faces and edges of the capsid are formed by 240 copies of the hexon homotrimer. The penton base is a pentameric protein found at each of the 12 vertices of the capsid, from which trimeric fiber proteins protrude. The fiber is a homotrimer composed of three domains: an N-terminal tail, a central shaft and a C-terminal knob. The tail is responsible for the attachment to the penton base protein at the vertices of the capsid. The fiber shaft extends to the outside of the capsid and is formed by amino acid repeats. The knob monomer is as an antiparallel β-sandwich, composed of β-strands with interspersing loop regions of variable lengths [16]. Besides being responsible for the binding to the primary receptor, the knob domain plays a key role in the formation of fiber trimers [17]. Minor capsid proteins (polypeptides IIIa, VI, VIII and IX) are located beneath the primary protein coat and hold important features for Ad structure and replication (Table 2). Finally, other accessory proteins (protease, IIIa, VI, VII, VIII, X and TP) are found in the core of the particle along with the viral genome, and play important roles in virus replication, genome packaging and assembly [13].

Table 2. Adenovirus virion proteins and their function. Adapted from [13]

Polypeptide/name	Location	Function
II (hexon)	Facets of icosahedron	Major structural component, forms facets of the capsid
III (penton base)	Capsid vertices	Contains an RGD motif which facilitates interaction with cellular integrins*
IIIa	Underside of penton base	Stabilizes the vertices
IV (fiber)	Projecting from the penton base	Mediates the initial attachment to host cells
V	Core	Links core to capsid, possibly aids nuclear localization
VI	Inner hexon cavity	Protease cofactor, assembly, endosome disruption and nuclear import of hexon
VII	Core	Targets viral genome to the nucleus and condenses DNA
VIII	Between hexons	Stabilization of peripentonal hexon–hexon interactions
IX	External faces of the capsid	Stabilization of virion. Transcriptional activator
TP	5'-End of the genome	Primes DNA replication
Mu	Core	DNA condensation
IVa2	Core	DNA packaging
Ad protease	Core	Cleaves precursor proteins

* except for Ads of species F.

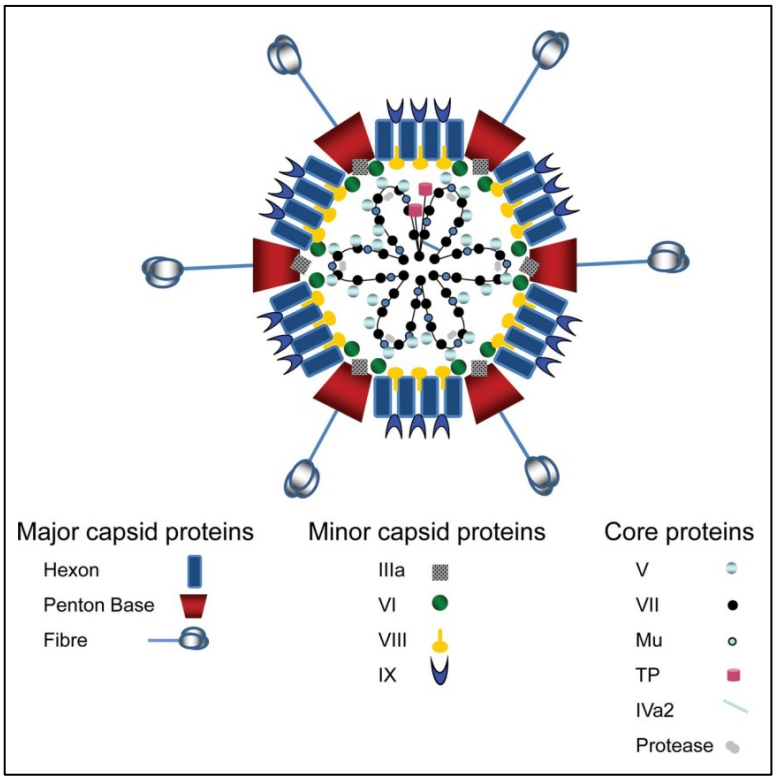

Figure 4. Structure of adenovirus virions. Ads have icosahedral capsids. The capsid outer coat is composed of three major proteins: the hexon, the penton base and the fiber. The hexon surrounds the faces and edges of the capsid. The penton base is located at each of the 12 vertices of the capsid from which the antenna-like fiber proteins protrude. Minor proteins locate underneath the primary coat, while core proteins are located in the inside of the virus particle along with the double stranded DNA. Taken from [13].

1.2.3 Genome organization

HAds bear a linear dsDNA of 30-36 kb flanked by two inverted terminal repeats (ITRs) at both ends of the molecule, which play a key role in the replication of the genome. HAd genomes are organized in well-defined transcription units which are divided into three classes depending on the timing of use during infection: six early (E) transcription units (*E1A, E1B, E2A, E2B, E3* and *E4*), three delayed-early transcription units (IX, Iva2 and E2 late), and one late (L) transcription unit that is processed to generate five families of late mRNAs (*L1-L5*) (Figure 5) [12, 18]. Each of these transcription units is defined by particular sets of promoters and polyadenylation signals giving rise to mRNA transcripts which can be further processed by alternative RNA splicing. In total, HAds genome code for approximately 50 proteins [18]. Additionally, Ad genomes code for one or two virus-associated (VA) RNAs which are involved in translational control during infection.

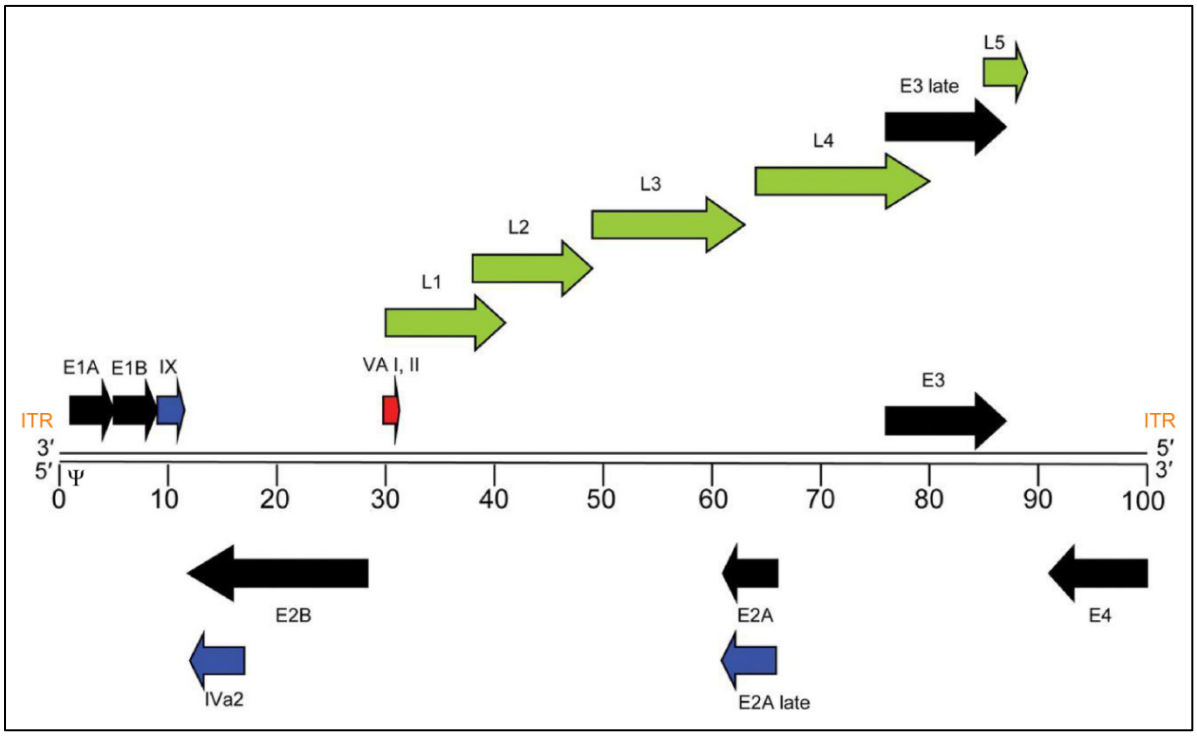

Figure 5. Adenovirus genome organization. Schematic representation of the HAd5 genome. Early (black), intermediate (blue) and late (green) mRNAs are shown as arrows. Rightwards reading transcripts are shown on top, leftwards reading transcripts at the bottom. The inverted terminal repeats (orange), the packaging signal (Ψ) and the VA-RNAs (red) are also depicted. The genome is divided into 100 map units (approximately 350nt per map unit) Adapted from [13].

1.2.4 Adenovirus infection cycle

1.2.4.1 Adenovirus cell entry

HAd5 cell entry involves two steps: a first attachment process to its primary receptor, followed by secondary interactions that lead to internalization via clathrin-coated vesicles (Figure 6, steps 1 and 2). The first step is accomplished by the high affinity interaction of the knob domain with the the coxakie- and adenovirus receptor (CAR) [19]. Once attachment has occurred, secondary interactions between the exposed arginine-glycine-aspartic acid (RGD) motif on the penton base and integrins take place [20]. This, in turn, leads to clathrin-mediated endocytosis resulting in virus internalization within endosomes (Figure 6, step 3). Subsequent acidification of the endosome leads to the release of protein VI, which holds membrane disruption activity, promoting thus endosome lysis and virion release into the cytosol [21]. Ad capsids can further interact via the hexon with dyneins, leading to their transport across microtubules to the nuclear pore complex (NPC) (Figure 6, step 4) [22].

Once at the NPC, the viral genome is disengaged from the capsid and is further transported into the nucleus for transcription and replication (Figure 6, step 5).

1.2.4.2 Genome transcription and replication

Once the viral genome enters the nucleus, the *E1A* transcription unit is the first to be expressed. This is possible as its promoter only requires cellular proteins for its expression. The *E1A* transcription unit produces multiple mRNAs and several proteins due to alternative RNA splicing. From these mRNAs, two are predominantly produced in the early infection phase: the 12s and 13s (s stands for Svedberg units in sucrose gradients). The 12s mRNA codes for the 243R protein and the 13s mRNA codes for the 289R protein (R stands for amino acid residues) [15]. The main function of these proteins is to act as trans-activators of the other early transcription units (*E1B, E2A, E2B, E3, and E4*) and to induce the cells to enter the S phase. This latter function, which is a prerequisite for Ad replication, is achieved by the sequestration of members of the retinoblastoma (RB) family of tumor suppressor proteins and by the subsequent release of the transcription factor E2F [7, 23]. These E2F transcription factors are crucial in cell-cycle regulation as they promote the expression of S phase-related genes. As a result of this E1A-mediated S-phase induction and of its trans-activator activities, the other early transcription units are expressed and produce proteins which cover key functions in the replication cycle of Ads. The main function of the *E1B* gene products (19K and 55K) is the inhibition of apoptosis. The 55K protein inactivates the pro-apoptotic tumor suppressor p53, whose accumulation is triggered by the E1A-mediated cell cycle deregulation, while the 19K protein inactivates down-stream mediators of p53-independent apoptotic pathways. E2 gene products, whose expression is triggered by E2F, are important in viral DNA replication and include the Ad DNA polymerase (Ad pol), the preterminal protein (pTP) and the single-stranded DNA binding protein (ssDBP). *E3* gene products are involved in the evasion of the host antiviral immune response by triggering mechanisms such as the blocking of viral antigen presentation by the major histocompatibility complex (MHC) class I pathway or by reducing chemokine receptors on the cell surface [24-26]. Finally, *E4* gene products are involved in the modulation of DNA replication and apoptosis, and in mediating transcriptional and translational regulation.

Once the gene products of the early phase have accumulated, viral genome replication begins (Figure 6, steps 14-15). As mentioned above, DNA replication is carried out by Ad pol, pTP and ssDBP proteins, in addition to host cell factors. After the onset of viral DNA replication, the major late transcription unit (MLTU) is expressed from a single promoter, known as the major late promoter (MLP) (Figure 6, steps 16-19). The primary transcript or pre-mRNA is further processed by alternative splicing or by polyadenylation. Late phase genes code for structural and scaffold proteins, a protease and other proteins required for virion assembly. Once late phase genes are expressed, structural proteins are transported to the nucleus, where DNA encapsidation and virion assembly takes place (Figure 6, steps 20-21). At this point, the Ad protease proceeds to cleave a subset of the structural proteins into their mature form in order to generate infectious Ad particles. Finally, cell lysis and progeny release occurs, mediated by the adenovirus death protein (ADP) which is expressed from the *E3* transcription unit (Figure 6, step 22). This is the only early gene that is expressed during the late phase.

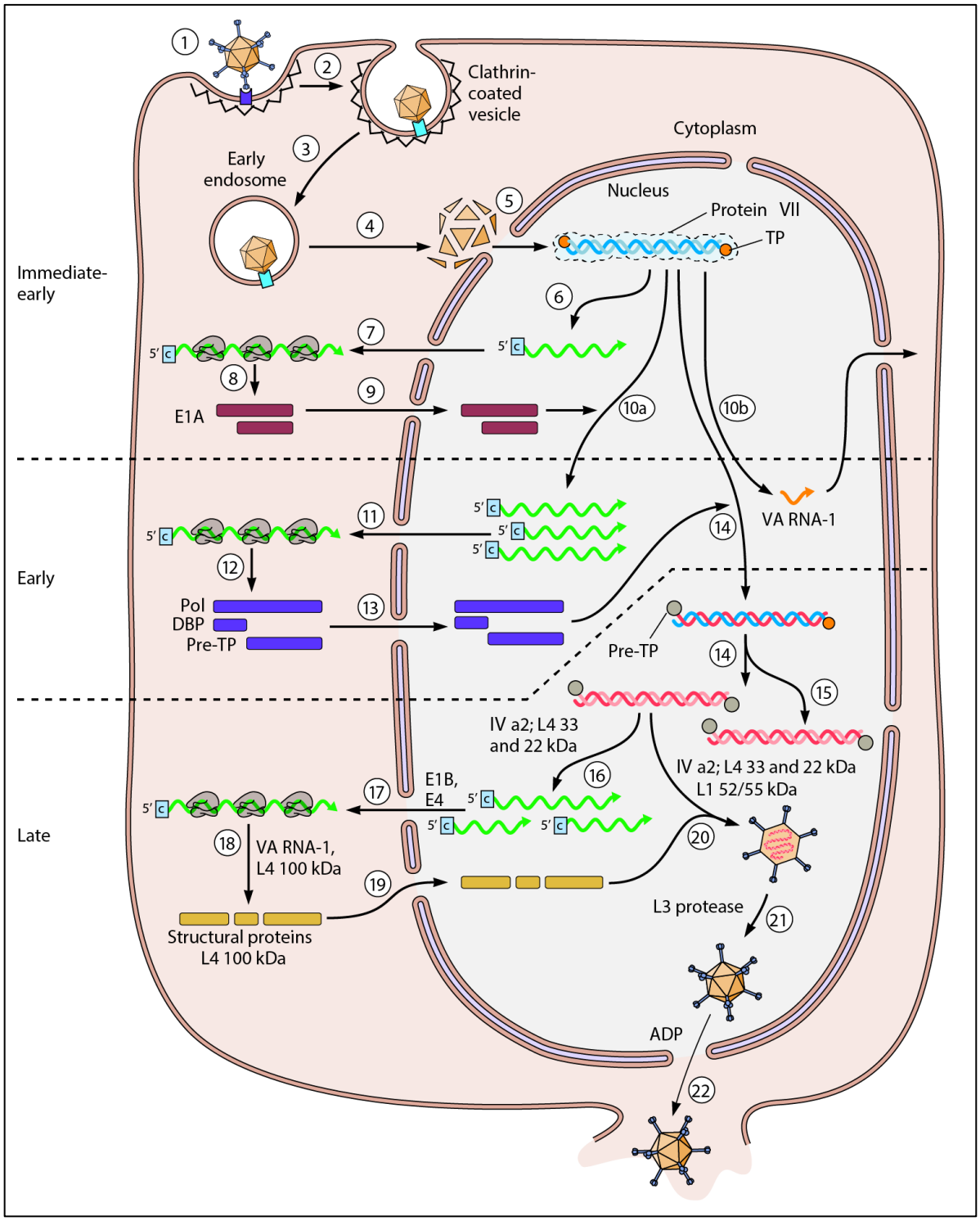

Figure 6. Infection cycle of human adenoviruses. The infection cycle of adenoviruses can be divided into time-specific events: adenovirus cell entry (steps 1-3), capsid disassembly and genome import into the nucleus (steps 4-5), immediate-early E1A gene expression (steps 6-9), E1A-mediated transcription of viral early genes (step 10a), translation of viral early proteins (steps 11-13), viral DNA replication (steps 14-15), transcription and translation of viral late genes (steps 16-19), capsid assembly and virion maturation (steps 20-21) and progeny virus release (step 22). Image taken from [27]

1.3 Oncolytic Adenoviruses

1.3.1 Development of tumor-selective OAds

A fundamental requirement in the development of OAds is to restrict their replication to tumor cells by means of genetic engineering. There are two main strategies to achieve this. The first is the transductional targeting of Ads, which aims at restricting Ad entry to tumor cells at the level of virus receptor binding. The second strategy is based on the restriction of Ad replication to tumor cells by manipulating the different Ad transcription units and is termed post-entry targeting.

1.3.1.2 Transductional targeting

Ads have broad tissue tropism which impairs a specific and efficient infection of target cells *in vivo* [19]. Moreover, although the HAd5 primary cellular receptor CAR is ubiquitously expressed in normal epithelial cells, its expression negatively correlates with tumor progression and it is often downregulated in cancer cells [28-30]. These drawbacks have limited the efficacy of Ads in cancer therapy.

To overcome these challenges, OAds can be transductionally targeted by strategies that involve one or two modifications of the viral capsid: a first (optional) detargeting step to ablate the native tropism of the virus, and a second retargeting step to direct it towards cancer-specific receptors. Three strategies have been developed to detarget Ads which involve: (i) genetic ablation of the native interactions with cellular receptors and factors (CAR, integrins and heparan sulfate proteoglycans (HSPGs), (ii) chemical modifications (*i.e.* shielding) of the capsid, and (iii) 'genetic pseudotyping' between different Ads serotypes [31, 32]. Regarding retargeting, systems to modify Ad tropism are based either on the addition of an adapter molecule to crosslink the virus to a target cellular receptor, or the genetic modifications of the viral capsid [31]. Generally, transductional targeting strategies based on genetic modifications are preferred in virotherapy because they will be carried by the progeny of the virus, whereas chemical or other non-genetic modifications will be lost after the first round of replication in cancer cells.

Ads can be genetically modified for retargeting purposes at different positions in the capsid such as the fiber, the penton base, some hypervariable regions (HVRs) of the hexon, and the minor capsid protein IX [31-33]. Although all capsid locations used so far show

potential for further applications, the most common Ad retargeting strategy involves the incorporation of peptide ligands into different sites of the fiber knob domain. This approach takes advantage of the exposed loops connecting the β-sheets or the C-terminus to incorporate short peptides, generally identified by phage display, in order to modify Ad tropism. Indeed, some tissue-specific-targeting peptides have been successfully incorporated into the knob domain of several Ad species, rendering them tumor-specific tropism [32]. From these, the most successful to date is the incorporation of the RGD-4C peptide that binds with high affinity to $\alpha_v\beta_3$ and $\alpha_v\beta_5$ integrins, which are commonly overexpressed in different types of cancer [34]. This peptide has been the best model of transductional re-targeting of Ads, as it has been genetically incorporated into different locales of the fiber of Ad species B, C and F [35-39]. Furthermore, the efficacy of the insertion of the RGD-4C peptide into the HI loop of the fiber from an oncolytic adenovirus is currently being tested in clinical trials for glioma and ovarian cancer [40].

1.3.1.3 Post-entry targeting

Although transductional targeting of Ads is an important step in the development of OAds, retargeted Ads can also infect normal cells that express the receptor that is being targeted by the virus. Thus, restriction of virus replication to cancer cells is the most important step in developing OAds.

Two main strategies have been developed to achieve this. The first is based on mutations or deletions in key Ad replication genes, which can be compensated only in cancer cells [41]. One of the best examples is the AdΔ24 which carries a 24-base pair deletion in the *E1A* region responsible for the interaction with the pRB [42]. As mentioned before, E1A-mediated sequestration of pRB releases the E2F transcription factor, leading to S-phase induction and viral replication in normal cells. Importantly, the pRB pathway is deregulated in almost 90% of cancers, resulting in constitutively E2F-mediated transcription of cell cycle control genes. Thus, in normal cells in which no pRB deregulation is observed, the Δ24-E1a protein will fail to interact with the pRB protein, resulting in halted viral gene transcription and replication (Figure 7). Conversely, the constitutive E2F-mediated transcription of S phase genes in cancer cells allows viral gene transcription and replication.

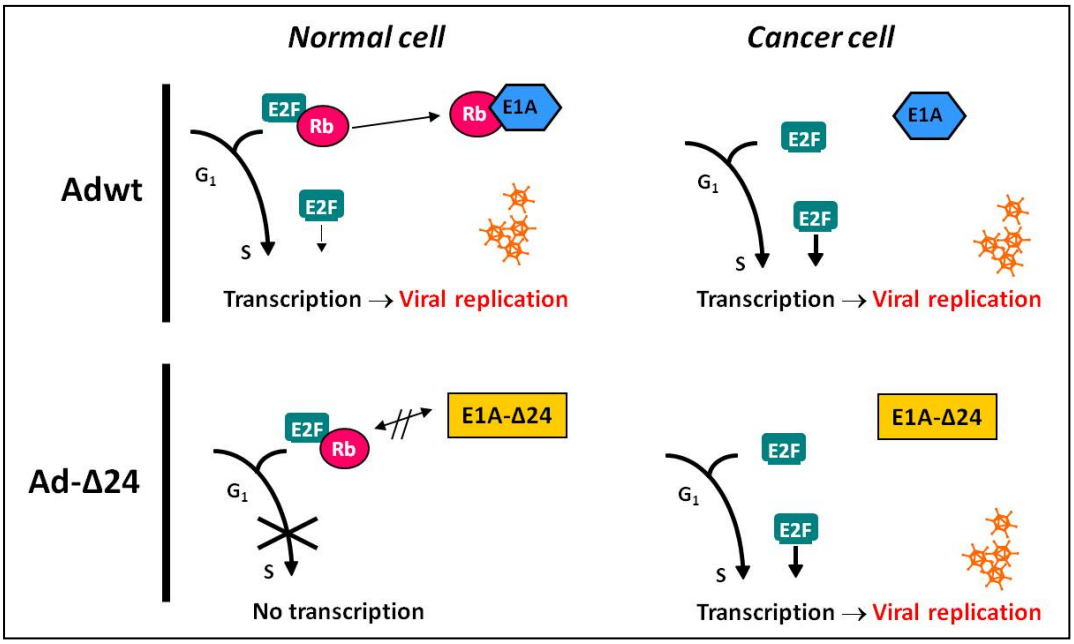

Figure 7. Δ24-based oncolytic adenoviruses. In normal cells, the transcription factor E2F is sequestered by the retinoblastoma protein (Rb). The E1a protein from wild-type Ad (Adwt) sequesters Rb, releasing E2F and thus promoting viral replication. On the contrary, Δ24-mutated proteins fail to mediate Rb sequestration and thus virus replication is halted in normal cells. However, Rb pathway deregulation and constitutive E2F activity in cancer cells allows the replication of the Δ24 oncolytic adenovirus. Image taken from [43].

The second strategy to restrict virus replication to cancer cells is termed transcriptional targeting. This approach is based on the incorporation of tumor-specific promoters or other regulatory sequences in the Ad genome to drive viral gene expression only in cancer cells. The promoters commonly used in this strategy should be specifically active in cancer cells and should support gene activation outside the chromatin context [44]. Examples that have been successfully engineered in OAds include the promoters of the genes encoding proteins such as the prostate-specific antigen (PSA), human telomerase reverse transcriptase (hTERT), MUC1, AFP and tyrosinase, among others [41]. More recently, the restriction of virus replication to cancer cells by incorporating microRNA (miRNA)-regulated sequences has been proposed. In this strategy, binding sites for miRNAs that are ubiquitously expressed in normal cells but downregulated in cancerous ones are inserted in the 3' untranslated region of the *E1A* gene to promote the degradation of its mRNA [45, 46].

1.3.2 ICOVIR-15K

Our group has combined several of the targeting strategies described above to generate highly cancer-specific OAds such as ICOVIR-15K (ICO15K). This virus combines transductional and post-entry targeting modifications which have shown tumor selectivity (Figure 8). Regarding transductional targeting, ICO15K incorporates an RGDK motif replacing the KKTK heparan sulfate glycosaminoglycan-binding domain in the fiber shaft. This modification, which targets integrins, increases tumor transduction and improves tumor-to-liver transduction ratios, resulting in reduced Ad-mediated hepatotoxicity and improved antitumor efficacy *in vivo* [39, 47]. As for post-entry targeting, ICO15K combines the deletion of viral functions complemented by cancer cells, and transcriptional targeting. The former is achieved by incorporating the *E1a* Δ24 mutation described above. Transcriptional targeting of ICO15K is achieved by incorporating eight E2F-responsive sites organized in four palindromes and one extra binding site for the SP-1 transcription factor in the *E1a* endogenous promoter [48]. In this way, transcription of *E1a* is directed to pRB deregulation in cancer cells and is further potentiated by the cooperation of E2F and SP-1 transcription factors which are known to potentiate transcription [49]. This modified promoter confers the virus with high selectivity for actively dividing cells and also allows the incorporation of bigger transgenes due to its small size compared to other tumor-specific promoters. ICO15K has shown potent antitumor efficacy and favorable toxicity profiles *in vivo*, and a modified version of it expressing hyaluronidase is currently under clinical investigation for the treatment of pancreatic cancer [50, 51].

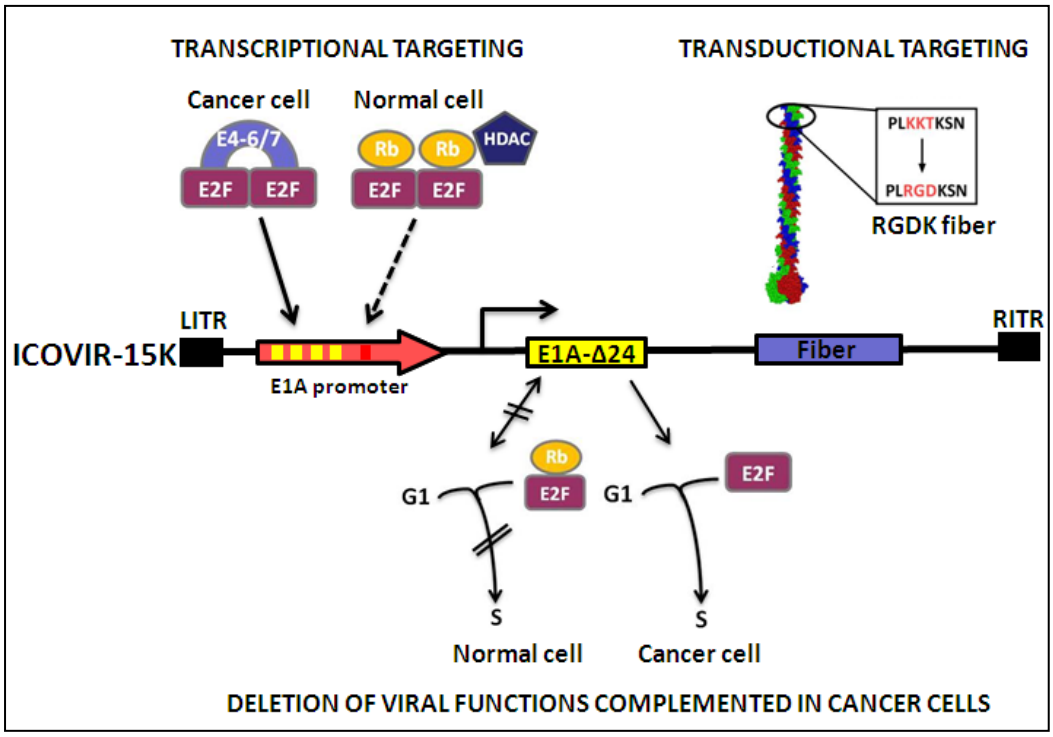

Figure 8. Characteristics of ICOVIR-15K. Schematic representation of the different modifications in the genome of ICOVIR-15K. At the transductional targeting level, the fiber shaft of this virus exchanges the KKT motif for an integrin-binding RGD motif. Replication restriction to cancer cells is mediated by the Δ24 mutation in the *E1A* gene. Transcriptional targeting is achieved incorporating eight E2F-responsive sites organized in four palindromes and one extra binding site for the SP-1 transcription factor in the *E1a* endogenous promoter. Image taken from [43].

1.3.3. Arming oncolytic adenoviruses with therapeutic transgenes

Clinical trials with OAds (see section 1.3.4) have demonstrated that developing viruses with improved efficacy will be required in order to have therapeutic benefit in patients. Scientists have achieved this by exploiting the vast knowledge about adenovirus biology in order incorporate therapeutic transgenes in the virus genome. In fact, Ads have long been identified as one of the most efficient gene transfer vectors, and this is corroborated by being the most frequently used viral vector for gene therapy applications [52]. OAds have been engineered to express therapeutic transgenes with varying modes of action including induction of apoptosis, chemotherapy-mediated prodrug activation, immunostimulation or antioangionesis. Transgenes can be either inserted as a cassette with its own promoter and polyadenylation (polyA) signal, or as an extra adenoviral transcription unit controlled by the viral gene expression machinery [44]. For the former, transgene expression can be controlled by constitutive promoters (*e.g.* CMV) or by tissue-specific promoters to add another level of specificity. For the second strategy, transgenes can be linked to viral proteins such as E1a via

sequences that will not affect protein function (*e.g.* internal ribosome entry site, IRES) or by adding a splice acceptor and a polyA signal that will promote transgene expression from the MLP [53]. Controlling transgene expression from viral promoters is particularly appealing for the generation of armed OAds, since restricting its expression to virus replication adds another level of selectivity. Additionally, MLP-driven transgene expression will be restricted to the late phase of the replication cycle, which is important in cases where the therapeutic protein can target the infected cells, thereby impairing the completion of the infection cycle. Transgenes cassettes have been successfully inserted in different regions of the adenovirus genomes including *E1*, *E3* or *E4*. Also, some of these regions (*e.g. E3*) can be fully replaced by the transgene without altering virus replication [44]. Transgenes coupled to splice acceptors and polyA signals can be inserted in various regions downstream of the MLP [54]. One drawback of OAds compared to other bigger viruses is the restriction in transgene size that can be incorporated in its genome. The maximum packaging size for the Ad genome is 38kb, which is approximately 2kb over the wild-type (wt) size [55, 56]. Since some OAds are modified with tumor-specific promoters, this further restricts the space available for transgene insertion. In the case of ICO15K, which has a genome size of 36.1kb, the maximum tolerated transgene size to be inserted is approximately 1.9kb. As mentioned above, a strategy to increase available space in the Ad genome involves the replacement of some regions such as *E3*.

1.3.4. Clinical experience with oncolytic adenoviruses

The first clinical trial evaluating replication-competent Ads was conducted more than 60 years ago [57]. In that study, 30 women with cervical carcinoma received intratumoral or systemic administrations of WT Ads from different serotypes. Ad injections were well tolerated and only some mild flu-like symptoms were observed. Necrotic areas in tumor biopsies were observed in more than 50% of the patients. Importantly, the extent of tumor necrosis was negatively affected by high titers of NAbs. However, and despite the signs of necrosis in tumors, no complete responses were observed and disease progressed in all patients. Interestingly, all patients showed an increase in NAbs after virus administration, and no virus could be recovered from cervical swaps two weeks after treatment. This suggested that antiviral immune responses could have been responsible for the clearance of the virus from the tumor site. Overall, this study demonstrated the favorable toxicity profile of Ads, but also highlighted the need of developing more potent OAds. It also suggested that

antiviral immune responses could represent a limitation for the success of oncolytic virotherapy with OAds.

After that trial, and with the advent of DNA technologies, a wide range of genetically modified Ads were developed. The first modified OAd to be evaluated in clinical trials was ONYX-015. This virus had a deletion of the *E1B55K* gene, which is responsible for binding and inactivation of the master cell cycle regulator p53 [58]. Thus, replication of the mutant virus was, in theory, restricted to cells with inactivated or mutant forms of p53 such as cancer cells [59]. The intratumoral administration of ONYX-105, in combination with chemotherapy, was evaluated in phase I and II clinical trials for the treatment of head and neck cancer. These studies, conducted in the United States, confirmed the favorable safety profile of OAds and reported unprecedented clinical responses in the field with 14% and 50% of the patients showing complete responses and stable disease, respectively [60, 61]. Further clinical studies with ONYX-105 were canceled due to corporate reasons, but independent groups in China patented the OAd H101, which also incorporated the *E1B55K* deletion. A Phase III trial evaluating the intratumoral administration of H101 in combination with cisplatin-based chemotherapy showed an overall response rate of 79% [62]. These results led to the China's approval of the combination of H101 and chemotherapy for the treatment of nasopharyngeal cancer. Despite these results, further studies revealed that the *E1B55K* deletion negatively affected the oncolytic properties of these OAds, and that the E1B55K-based cancer selectivity was more complex than simply targeting p53 [63]. These facts prompted the development of more potent and selective OAds.

The virus DNX-2401, formerly called Delta-24-RGD, is a Δ24-based OAd which incorporates the RGD4C peptide in the HI loop of the fiber knob (see sections 1.3.1.2 and 1.3.1.3). This virus is currently under clinical investigation, and early clinical trials have contributed important data with relevance for the field. A phase I clinical trial evaluating the intraperitoneal administration of DNX-2401 in ovarian cancer patients revealed similar toxicity profiles to those observed in the clinical trials described above [64]. Interestingly, signs of virus replication were observed in ascites from these patients, as virus DNA copy numbers raised in 30% of the patients 3 days after inoculation. A more recent trial has evaluated the potential of DNX-2401 for the treatment of recurrent malignant glioma. Complete regressions and partial responses were observed in patients receiving intratumoral virus administrations, and data suggest that antitumor immune responses complement the oncolytic action of the virus [65]. As mentioned above, DNX-2401 received

fast-track status and orphan drug designation by the FDA for the treatment of malignant glioma in 2016 [10].

The studies described above have encouraged the development of new OAds with improved properties. As described in section 1.3.3, OAds can be armed with a wide range of transgenes to potentiate their action. Furthermore, OAds can be combined with other cancer therapies to maximize their antiutmor effect. To date, more than 25 clinical trials for the treatment have been registered to evaluate different unarmed or armed OAds alone or in combination with different cancer therapies [2].

1.3.5 Challenges for oncolytic adenoviruses

Despite the potential of OAds as anticancer agents, limited clinical responses have been observed when they are administered as monotherapy to cancer patients. These results are most likely explained by the many hurdles OVs encounter after systemic administration into patients. These challenges include: virus delivery, tumor targeting, stromal barriers and different immune responses in the tumor microenvironment (Figure 9).

1.3.5.1 Oncolytic adenovirus tumor delivery and targeting

Given their pathogenic nature, OAds interact with several host factors, limiting their delivery into tumors after systemic administration into patients. Humans exposed to Ad5 (up to 90% seroprevalence depending on the geographical region) show high levels of circulating neutralizing antibodies (NAbs) against capsid proteins [66, 67]. These Nabs mainly target the HVRs of the hexon protein [68, 69], leading to interference with the infection cycle of the virus [70]. Additionally, the phagocytosis of Ad5 by liver macrophages (*i.e.* Kupffer cells) promotes the saturation of the reticuloendothelial system, thereby increasing the uptake of Ads by hepatocytes [71, 72]. This hepatic tropism reduces the distribution of the infused Ads into tumors. Finally, Ad particles directly interact with several other blood components such as platelets, complement proteins, CAR-expressing erythrocytes and coagulation factors, all of which can negatively impact the delivery of adenoviral vectors to specific tissues [52].

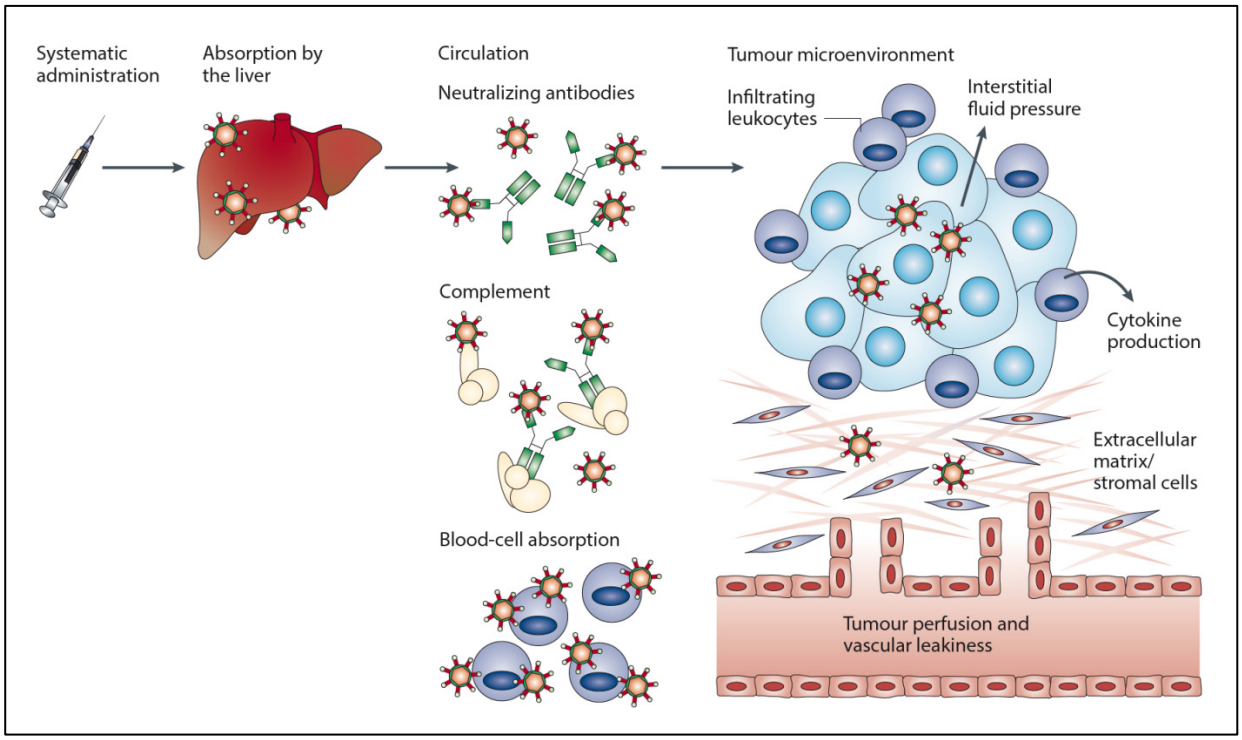

Figure 9. Challenges for oncolytic adenoviruses. Virus Delivery: systemically administered oncolytic adenoviruses can be sequestered by Kupfer cells in the liver or can be neutralized by antibodies recognizing viral proteins. Tumor stroma: once in the tumor, oncolytic adenovirus spread can be hindered by the exctracellular matrix and fibroblast that are resistant to oncolysis. Immune responses: given their pathogenic nature, oncolytic adenoviruses can be cleared from the tumor microenvironment by virus-specific CTLs. Image adapted from [73].

Several strategies have been developed to avoid these negative interactions. Regarding neutralization of the virus, chemical shielding of the adenovirus capsid with synthetic polymers or the replacement of the HVR from one Ad serotype to another have shown promise as strategies to evade NAbs [74-76]. Furthermore, our group has recently shown that inserting an albumin-binding domain in the hexon protein shields the virus from Nabs and improves its blood persistence as a result of albumin coating of the virus after systemic administration into mice [77]. Another strategy to overcome NAbs is based on the use of patient-derived autologous cells, such as mensenchymal stem cells (MSCs) or monocytes, as carriers for OAd [78, 79]. These cells can be seen as 'trojan horses' which hide viruses from the antiviral immune response and deliver them efficiently to the tumor site due to their intrinsic homing properties. Evidence of the feasibility of this approach comes from an exploratory study in which MSCs loaded with ICOVIR-5, a pRB-regulated OAd which selectively replicates in cancer cells, were infused to four children with refractory metastatic neuroblastoma [80]. Notably, infusions were well tolerated and one of the patients showed complete clinical response with remission of metastases up to 6 years after treatment.

The main strategies to solve liver tropism rely on the combination of modifications in the Ad capsid that will allow simultaneous liver detargeting and tumor retargeting. For instance, Ads shielded with polyethylene glycol incorporating a vasculature homing peptide have shown increased tumor transduction and increased liver detargeting compared to the unmodified Ad [81]. As described above, another strategy that has been used in our group is the replacement of the HSG-binding KKT fiber shaft domain with the RGD peptide, which results in reduced liver tropism, increased bioavailability of the virus and increased tumor transduction *in vivo* [39, 47].

1.3.5.2 Tumor stromal barriers

After reaching the tumors, OAds face several physical barriers that limit their spread across the tumor microenvironment. The major component contributing to this is the tumor stroma, which is composed of cancer-associated fibroblasts (CAFs), immune cells, MSCs, a extracellular matrix (ECM) built by structural and adhesive proteins (*e.g.* fibronectin, laminin, collagen and elastin), proteoglycans, and glycoproteins [82, 83]. In contrast to cancer cells, CAFs are partly resistant to OAd infection and thus represent a physical barrier for virus spread *in vivo* [84, 85]. Additionally, the complex and tight structure of ECM increases the interstitial fluid pressure which limits the access of drugs or viral vectors to the tumor [86-88].

The major strategies to improve OAd spread within the tumor rely on the targeting of ECM components or CAFs. OAds expressing ECM-degrading enzymes such as hyaluronidase or acti-resitant DNaseI have shown improved intratumoral spread and enhanced antitumor efficacy *in vivo* [50, 89]. Of note, the hyaluronidase-expressing virus VCN-01 developed in our group has shown favorable toxicity profiles and potent antitumor efficacy in different mouse and Syrian hamster models of cancer [51, 90], and is currently under clinical investigation for the treatment of advanced pancreatic cancer (NCT02045602). Other strategies to target tumor stroma involve the generation of OAds expressing ECM-modifiers which can inhibit collagen and induce expression of matrix metalloproteases (MMP). Specifically, OAds expressing relaxing or decorin enhance virus penetration and spread in tumors, leading to improved antitumor efficacy [91, 92]. Regarding the targeting of CAFs, two different approaches have been evaluated. Lopez *et al.* have generated OAds whose *E1a* expression is controlled by the cancer- and stroma-specific SPARC (secreted protein, acidic, rich in cysteine) promoter [85, 93]. These viruses induce oncolysis in fibroblasts and have

shown potent *in vitro* cytotoxicity in stroma-rich tumor explants from ovarian cancer. A different approach developed in our lab aimed at selecting Ads from a mutagenized stock by serial passages in human CAFs. Ad clones selected by this process contained a C-terminally truncated form of the i-leader protein which resulted in enhanced cytotoxicity of CAFs and improved antitumor efficacy in mouse models of desmoplastic tumors [94].

1.3.5.3 Immune responses in the tumor microenvironment

Besides delivery and stromal barriers, the immune system has long been identified as a major challenge for the success of OAds in cancer patients. Paradoxically, the two most important immunological hurdles for virotherapy with OAds are rather opposing. On the one hand, cancer cells have evolved numerous mechanisms to create an immunosuppressive tumor microenvironment (TME) in order to bypass antitumor immune responses. On the other hand and despite this immunosuppressive TME, OAds are rapidly cleared from tumors by adaptive immune responses, thereby reducing their antitumor efficacy. These opposing views opened the debate whether the immune system is a friend or a foe for OAds. This debate has been long present in the field of virotherapy and has been extensively reviewed by our group and others [95, 96]. However, the fact that OVs can promote antitumor immune responses has made it clear that the immune system represents both an ally and an enemy of OAds and that balancing the immunological responses described above will be crucial for the success of virotherapy.

The work described in this thesis mainly focuses on overcoming some of the immunological limitations encountered to date by OAds in the TME. In the coming sections, the different immunological hurdles for OAds and strategies developed to overcome these will be discussed in detail.

1.4 Antitumor immune responses

The onset of cancer has long been associated with accumulation of several genetic alterations in key regulatory genes of the cell. These alterations lead to the expression of mutated proteins with altered amino acid sequences and functions, compared to their wild-type counterparts. Importantly, $CD8^+$ T cells can recognize epitopes of these proteins (also termed neoantigens) presented by MHC-I on the surface of cancer cells. This evidence has set the foundations to better understand how antitumor immune responses are triggered, a process also known as immunosurveillance [97]. Mounting immune responses against cancer

cells is a stepwise process (Figure 10, [98]). Immunogenic cell death (ICD) of cancer cells leads to the release of neoantigens that can be captured and processed by dendritic cells (DCs) for their presentation on MHC-I and MHC-II molecules. Consequently, mature DCs migrate to the draining lymph nodes where antigen presentation and priming of T cells occurs. Activated CTLs then traffic through blood vessels in order to infiltrate tumors, where they recognize neoantigen-expressing cancer cells via TCR-MHC interactions. This recognition leads to CTL-mediated killing of cancer cells and release of more neoantigens that amplify the overall antitumor immune response.

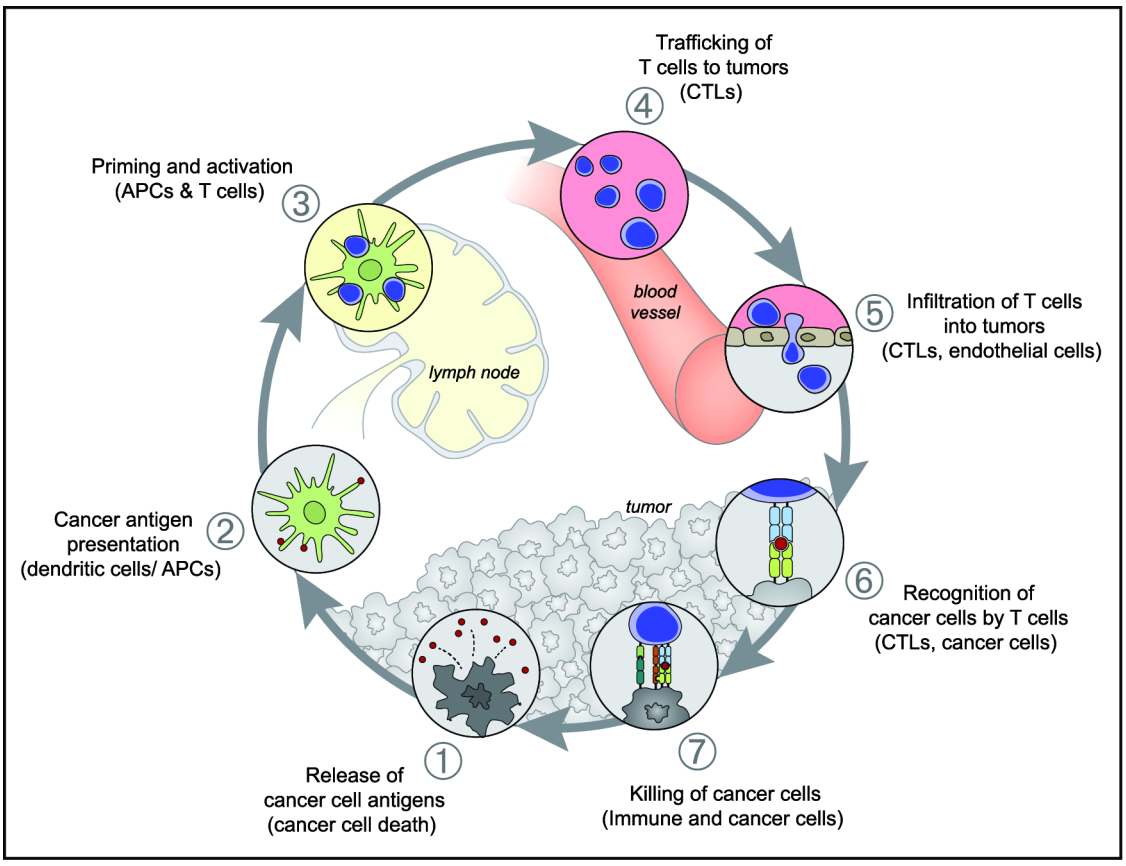

Figure 10. The cancer-immunity cycle. Dying cancer cells release antigens (step 1) that can ben engulfed and processed by APCs/DCs (step 2). Activated DCs can migrate to the lymph nodes where antigen presentation to T cells occur (step 3). Antigen-specific CTLs travel to the tumor through the circulation (step 4) and infiltrate tumors after extravasation from the blood vessels (step 5). CTLs then recognize TAAs presented by cancer cells on MHC-I (step 6). Finally, activated T cells kill cancer cells (step 7). Image taken from [98].

1.4.1 Tumor immune escape

Although the anitutmor immunity seems straightforward, cancer cells have developed numerous strategies to evade every step of such responses (Figure 11, [97]). For instance, tumor cells secrete factors such as the vascular endothelial growth factor (VEGF) or transforming growth factor-β (TGF-β) which impair DC activation and maturation. Additionally, tumor cells impair DC migration to the lymph nodes by secreting ligands that inhibit the expression of the CC chemokine receptor 7 on DCs via the liver X receptor-α [99]. Even if DCs bypass these evasions mechanisms and successfully migrate and activate T cells in the lymph nodes, tumors exploit several strategies to evade or impair CTL function. Cancer cells often bear mutations in genes involved in the processing and presentation of antigens via MHC-I, thus evading their recognition by CTLs via the TCR [100, 101]. Furthermore, a wide spectrum of tumor-secreted immunomodulatory factors promote the infiltration of regulatory T cells (T_{regs}), M2 tumor-associated macrophages (TAMs) and myeloid-derived suppressor cells (MDSCs), which impair T-cell functions. Tumor cells also induce apoptosis of CTLs by expressing FAS and TRAIL ligands on their membrane. Another important evasion mechanism that has gained considerable attention as target for cancer immunotherapies is the deregulation of immune checkpoint signaling in CTLs as a result of the expression of inhibitory ligands on the membrane of cancer cells, which suppresses antitumor T-cell effector mechanisms (See section 1.5.2.1). Finally, cancer cells accumulate mutations in genes involved ICD, thereby reducing the immunogenicity of cell death processes [102].

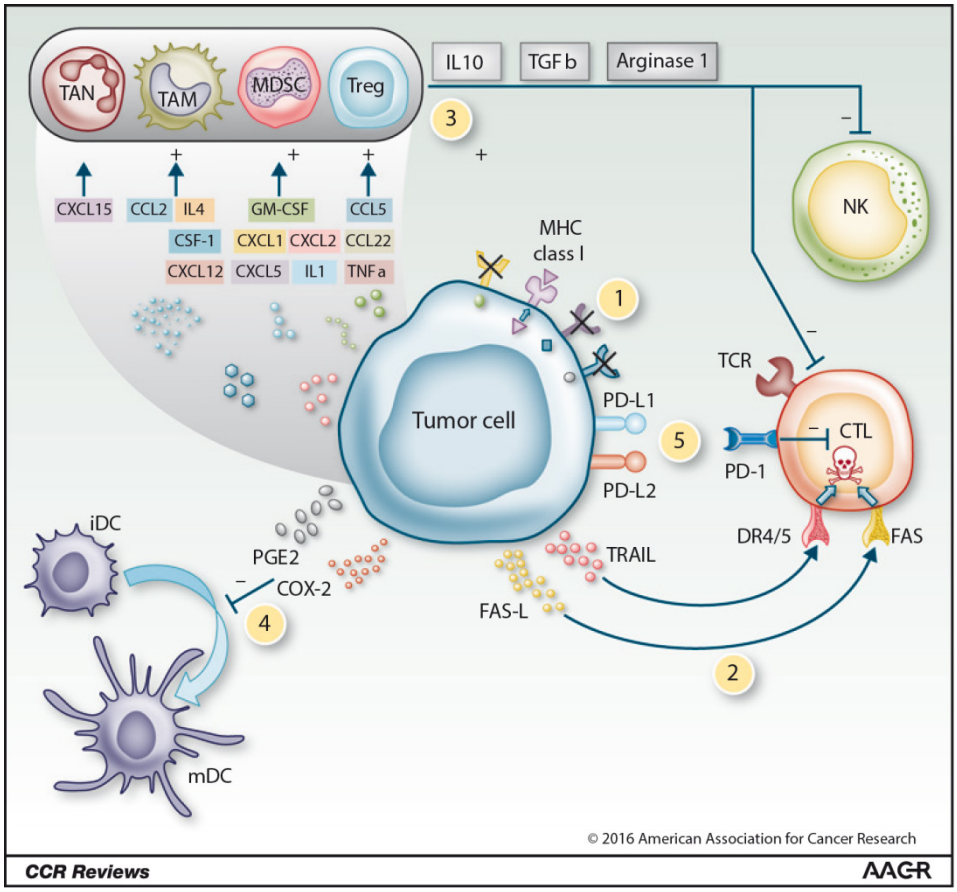

Figure 11. Mechanisms of immune evasion by tumors. Tumor cells can evade antitumor immune responses by: (1) downregulating antigen presentation via MHC-I, (2) inducing apoptosis of CTLs, (3) secreting a wide range of cytokines and chemokines that recruit immunosupressor cells into the tumor, (4) inhibiting DC maturation and migration, and (5) expressing T-cell inhibitory ligands on their cell membrane. Image taken from [103].

1.4.2 Oncolytic adenovirus-mediated antitumor immune responses

Oncolysis meadited by OAds has been shown to induce antitumor immune responses directed to neoepitopes in preclinical and clinical studies [104, 105]. Although the exact mechanism by which OAds trigger these responses is not fully elucidated, compiling evidence suggest that OAds induce cell death mechanisms that, in contrast to the silent physiological apoptosis process, are highly immunogenic. For instance, OAd replication can lead to the secretion of uric acid, a key molecule involved in DC maturation [106]. Moreover, OAds induce the secretion of the high-mobility group box-1 (HMGB1) protein, as well as the exposure of calreticulin on the surface of tumor cells *in vitro* and *in vivo* [107]. All these molecules are known immunogenic DAMPs that are associated with ICD. In addition to this, OAds have been shown to induce autophagy in cancer cells to promote oncolysis [108, 109]. The combination of OAds with Temozolomide and Cyclophosphamide increases the levels of autophagic cell death *in vitro*, as evidenced by ultrastructural changes and by the release of

DAMPs such as HMGB1 and adenosine triphosphate (ATP) [110]. More importantly, cancer patients receiving the same combination therapy showe high levels of circulating HMGB1 which correlated with antitumor T-cell responses in 88% of the patients. Thus, all the data described above suggest that OAd-mediated oncolysis leads to the accumulation of TAAs, PAMPs and DAMPs, all of which can contribute to the induction of antitumor immune responses.

Despite this evidence, further studies have also suggested that oncolysis alone will likely not be sufficient to induce long lasting antitumor immune responses. *In vitro* studies have demonstrated that oncolysates from OAd-infected melanoma cells fail to induce DC maturation unless cytokines and co-stimulatory signals are added to the cultures [111]. Furthermore, OAds alone have been reported to fail at promoting tumor-specific antitumor immune responses in immunocmpetent mice, and only their combination with tumor peptide-loaded DCs could trigger such responses [112]. This data, in combination with the strong evidence of the importance of antitumor immune responses for virotherapy, has promoted the development of OAds with improved immunomodulatory properties.

1.5 Strategies to improve antitumor immune responses with oncolytic adenoviruses

1.5.1 Oncolytic adenoviruses expressing cytokines and chemokines

As mentioned above, tumors have encountered several strategies to exploit cytokine and chemokine profiles within the TME in their favour. OAds represent an ideal tool to modulate this profile by arming them with cytokine or chemokine genes. One of the best examples is the case of OAds engineered to express granulocyte–macrophage colony-stimulating factor (GM-CSF), a potent inducer of antitumor immunity. OAds expressing GM-CSF have shown promise as potent inducers of antitumor immunity in preclinical and clinical studies [113-115]. As an example, a Phase I clinical trial with the GM-CSF-armed OAd CG0070 showed complete response rate of 48.6% in bladder cancer patients [116]. IL-12 is another cytokine that has been widely studied in this context. This pro-inflammatory cytokine links innate and adaptive immune responses by activating NK cells, polarizing naïve $CD4^+$ T cells and promoting differentiation and survival of memory T cells [117]. OAds co-armed with this cytokine and other molecules have shown enhanced immunological and antitumor properties *in vivo* [118-121]. Importantly, it has been shown that restricting IL-12 expression

to virus replication in tumors can reduce IL-12-mediated off-target effects, supporting the use of OAds as tools for tumor delivery of this kind of transgenes [122]. Examples of other cytokines that have been encoded in OAd genomes are IL-2, IL-15, IL-18, IL-23, IL-24 and IFN-α [123-125].

Chemokines are implicated in the circulation, homing and activation of immune cells, and their role in dictating the course of antitumor immune responses has been extensively studied [126]. The chemotactic and immunostimulatory properties of chemokines have encouraged the generation of OAds expressing such genes in order to promote infiltration of effector T cells into tumors as well as activation of immune cells.

1.5.2 Oncolytic adenoviruses expressing co-stimulatory molecules

Co-stimulation is essential for the generation of antitumor immune responses, including those induced by OAds. From the perspective of DCs, co-stimulatory molecules expressed on the surface of T cells induce DC activation and maturation. However, and as mentioned above, there is evidence demonstrating that oncolysates from OAd-infected melanoma cells fail to induce DC maturation unless cytokines and co-stimulatory signals are added to the cultures [111]. To overcome this, OAds have been engineered to express co-stimulatory molecules. One of the best examples is Ad5/3-hTERT-E1A-hCD40L, a chimeric OAd coding for the CD40 ligand (CD40L) in the E3 region and whose replication is controlled by the tumor-restricted human telomerase reverse transcriptase (hTERT) promoter. CD40L is a T-cell derived molecule which triggers DC activation by interacting with the CD40 receptor (CD40R) expressed on DCs [127]. Ad5/3-hTERT-E1A-hCD40L showed enhanced efficacy and immunomodulatory properties compared to the parental virus *in vitro* and *in vivo* [107]. Furthermore, Ad5/3-hTERT-E1A-hCD40L has been evaluated in patients with advanced solid tumors, showing disease control in 5 of 6 patients [128]. Importantly, high levels of virus, CD40L, RANTES and tumor-specific $CD8^+$ T-cells were detected in tumor biopsies from these patients.

From the perspective of T cells, MHC-dependent T-cell activation requires the co-stimulatory interaction of CD28 with B7-1 and B7-2 ligands expressed on APCs [129]. However, these ligands are not expressed in most tumor cells, and are often absent on APCs if these are not activated. To overcome this hurdle, OAds have been engineered to express B7-1 ligands on the surface of infected tumor cells. OAds co-expressing B7-1 ligand with GM-

CSF or IL-12 have shown enhanced T-cell infiltration and antitumor efficacy in immunocompetent mice bearing B16-F10 tumors [130, 131].

1.5.3 Combination of oncolytic viruses with other immunotherapies

1.5.3.1 Checkpoint inhibitors

Compiling evidence from the past 20 years have demonstrated that, besides triggering T-cell activation, engagement of T cells through TCR-MHC-I interactions further induces the upregulation of pathways that can stop immunologic responses. These mechanisms are known as immune checkpoints or co-inhibitory pathways. The central inhibitory pathway is mediated by the cytotoxic T lymphocyte antigen 4 (CTLA-4). Normal T-cell activation requires the co-stimulation of CD28 through its binding to B7-1 or B7-2 ligands expressed on APCs. However, once activated, T cells induce the expression of CTLA-4 which has a higher affinity for ligands on APCs than the CD28, thereby preventing co-stimulation by competition and negative signaling [132]. Another important T-cell-intrinsic regulatory pathway is that mediated by PD-1 (programmed death 1) and its ligands PD-L1 and PD-L2 [133]. Contrary to CTLA-4, PD-1 expression on T cells does not compete with other ligands expressed on APCs. Instead, PD-1 interaction with its ligands transduces signals that directly compete with and inhibit T-cell receptor signals. After the discovery of CTLA-4 and PD-1, other inhibitory receptors expressed on T cells such as lymphocyte activation gene 3 (LAG-3), T cell immunoglobulin mucin 3 (TIM-3) and CD200 have been described (Figure 12, [134]).

Immune checkpoints have drawn much attention in the field of cancer therapy due to their role in cancer pathogenesis. For instance, PD-L1 is expressed on many cancer types and, thus, it has been proposed as one of the major mechanism by which tumors bypass immune responses [97, 103, 135]. Some of the most promising novel cancer therapies aim at interfering with the interaction of inhibitory receptors and their ligands. Anti-CTLA-4, anti-PD-1 and anti-PD-L1 monoclonal antibodies have shown outstanding clinical results for the treatment of different types of cancer [136, 137]. Consequently, the FDA has granted approval for many of these antibodies which are currently being further developed in combinatorial clinical trials [138].

Given their potential of restoring T-cell function within the TME, checkpoint inhibitors are currently being evaluated in combination with other therapies such as virotherapy. One strategy that has been evaluated in preclinical studies is the generation of OAds expressing full-length anti-CTLA-4 antibodies. An example of this is the chimeric virus Ad5/3-D24aCTLA4

has been engineered to secrete anti-CTLA-4 mAbs from infected cells. Supernatants from Ad5/3-D24aCTLA4-infected cells have been shown to increase activation of PBMCs from cancer patients when compared to the parental virus. Another strategy that is currently under investigation is the direct combination of OAds with FDA-approved checkpoint inhibitors [139]. Up to four clinical trials have been recently registered to evaluate the combination of different OAds with anti-PD1 and anti-PD-L1 blocking antibodies for the treatment of different malignancies (NCT02636036, NCT02798406, NCT03003676, NCT02798406).

1.5.3.2 Adoptive transfer of tumor-infiltrating lymphocytes

Another promising immunotherapy is adoptive cell transfer (ACT) of TILs. This therapy is based on the *ex vivo* isolation and expansion TILs which are then infused back to the patients. This immunotherapy approach has shown promising results over the years for different malignancies. Specifically, ACT of TILs has shown up to 50% complete responses in patients with metastatic melanoma [140]. Moreover, enriching TIL preparations to contain high percentages of T cells recognizing tumor-specific mutations has shown impressive clinical responses in a patient with metastatic cholangiocarcinoma [141]. Currently, several strategies are being developed to improve the clinical responses with ACT of TILs [142].

The intrinsic immunomodulatory properties of OAds have encouraged their combination with ACT of TILs as a strategy to improve antitumor efficacy. Tähtinen and colleagues used the B16.OVA tumor model to demonstrate that intratumoral administrations of a chimeric Δ24-based OAd improved the efficacy of adoptively transferred OVA-specific $CD8^+$ T cells [143]. More recently, the combination of OAd with TILs from pancreatic and melanoma tumors from Syrian hamsters has shown improved antitumor efficacy compared to the virus or TIL transfer alone [144]. This study is particularly interesting, since OAds show permissive replication in the Syrian hamster cancer model and thus represent a scenario that more closely resembles the oncolytic process in humans. These studies suggest that OAds might be promising tools for improving ACT of TILs.

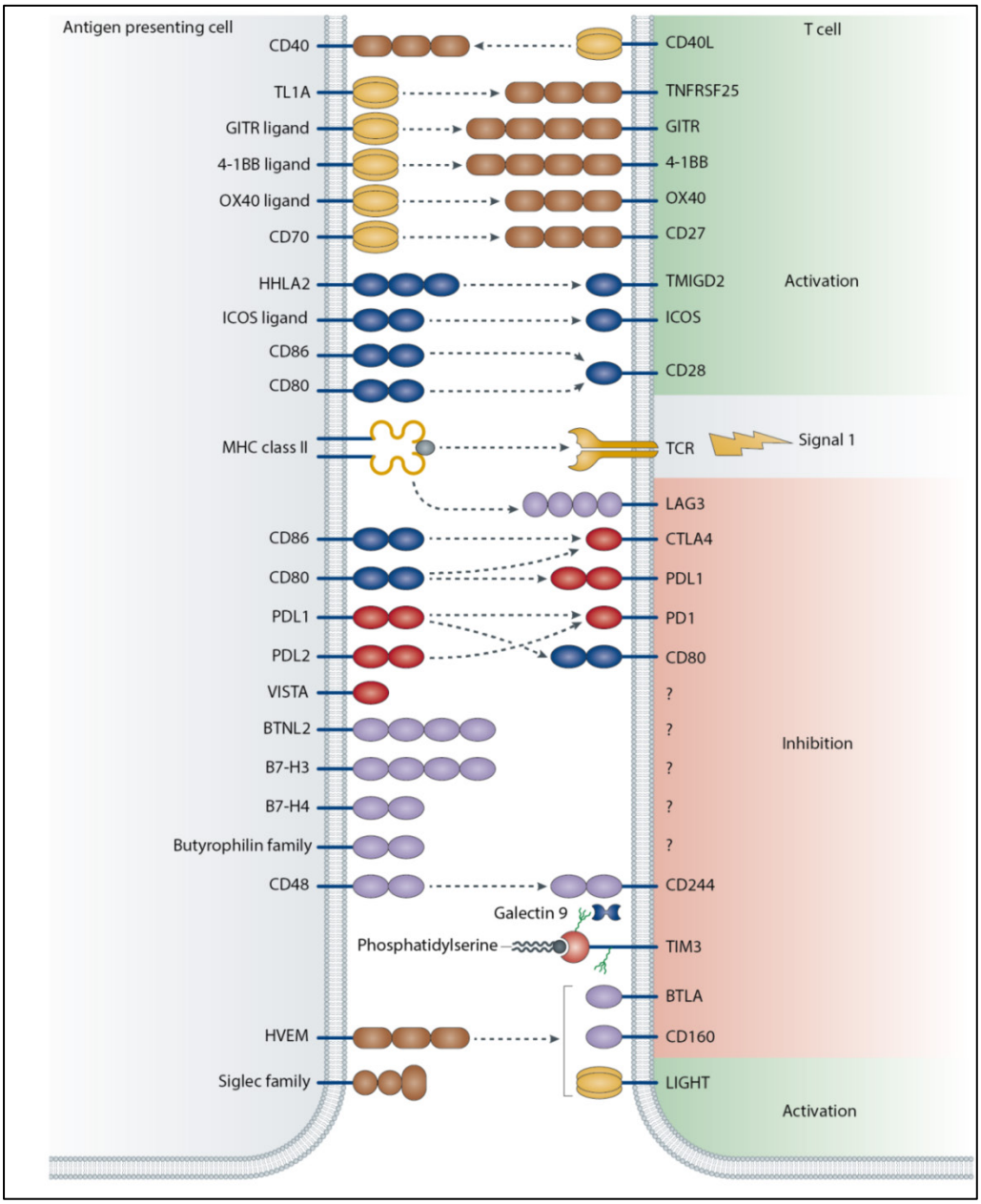

Figure 12. Activating and inhibitory interactions regulating T-cell activation. T cell activation is triggered after TCR-MHC-I interactions (signal 1) followed by co-stimulation via CD28 (signal 2). Additional interactions between ligands and activating (green shading) or inhibitory (red shading) receptors further regulate T-cell activation. These second signals include co-stimulatory ligands and receptors (blue), immune checkpoint ligands and receptors (red), tumor necrosis factor (TNF) receptor superfamily (brown) members and their trimeric TNF superfamily ligands (light brown), and additional members of the immunoglobulin superfamily (purple). BTLA, B and T lymphocyte attenuator; BTNL2, butyrophilin-like protein 2; CTLA4, cytotoxic T lymphocyte antigen 4; GITR, glucocorticoid-induced TNFR-related protein; HHLA2, HERV-H LTR-associating protein 2; HVEM, herpes virus entry mediator; ICOS, inducible T cell co-stimulator; LAG3, lymphocyte activation gene 3 protein; PD1, programmed cell death protein 1; PDL, programmed cell death 1 ligand; siglec; sialic acid-binding immunoglobulin. Image and part of the figure legend adapted from [138].

1.5.3.3 Chimeric antigen receptor T-cell therapy

Chimeric antigen receptor (CAR) T cell-therapy has emerged as one of the most promising immunotherapies in the past years. CAR T cells are genetically programmed to specifically redirect immune responses towards TAAs. CARs are chimeric molecules composed of an extracellular antigen-recognition domain and an intracellular module (Figure 13). The extracellular domain consists of a scFV derived from monoclonal Abs recognizing TAAs, and it is anchored to the cell membrane by a transmembrane domain [145]. The intracellular module is composed of domains responsible for transducing T-cell activating signals upon receptor engagement. All CAR constructs developed to date use the CD3 zeta chain (CD3ζ) as their core signaling domain. Depending on the arrangement and components of the intracellular module, CAR can be classified in three groups. First generation CARs only bear the CD3ζ signaling domain, whereas second generation CARs include a co-stimulatory domain such as CD28, 4-1BB or ICOS, linked to the CD3ζ domain. Third generation CARs incorporate three or more signaling domains.

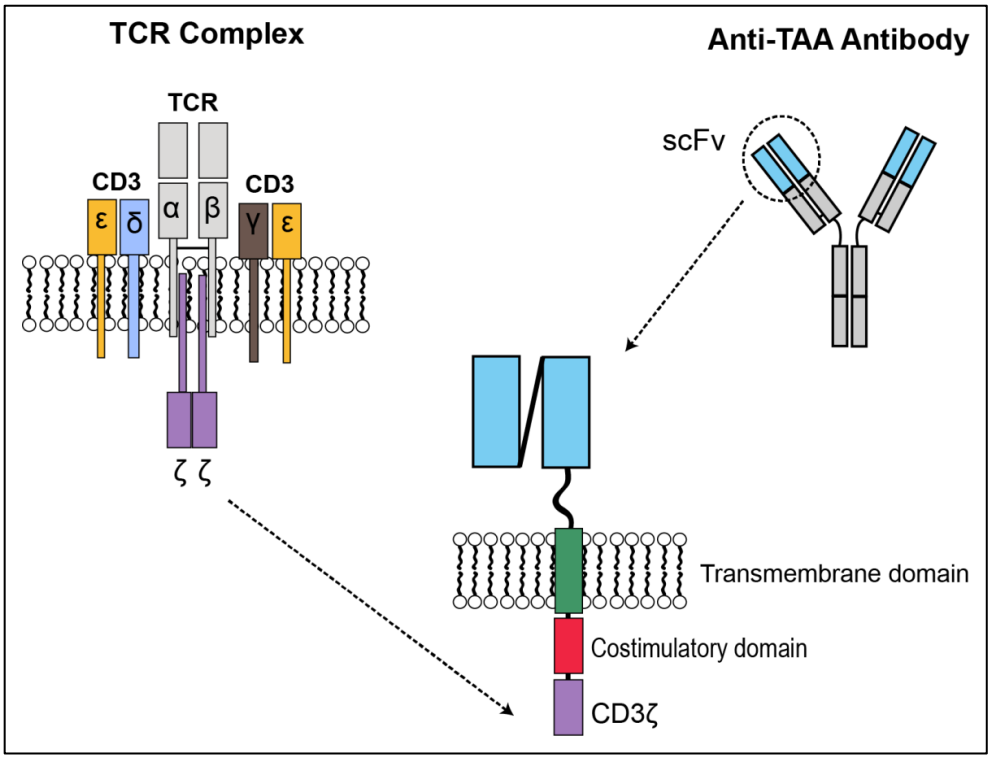

Figure 13. Chimeric antigen receptors. Schematic representation of CARs, which are composed an extracellular antigen-recognition domain and an intracellular module. The extracellular domain consists of a scFV derived from monoclonal Abs recognizing TAAs, and it is anchored to the cell membrane by a transmembrane domain. The intracellular module is responsible for transducing T-cell activating signals, and it is composed of the ζ chain of the TCR complex and different costimulatory domains. Image kindly provided by Sonia Guedan.

Clinical-grade CAR T cells are generated *ex vivo* before being infused to cancer patients (Figure 14, [146]). To this end, T cells from patients are isolated by leukapheresis, followed by activation with anti-CD3/anti-CD28-coated beads. Activated T cells are then transduced with a viral vector encoding the CAR construct. After bead removal, T cells are further expanded, processed and subjected to quality control prior to infusion into patients. CAR T-cell preparations generated this way result in mixed populations of transduced (*i.e.* CAR^+) and untransduced (*i.e.* CAR^-) T-cell populations, with the CAR-expressing population representing between 5% and 45% of total T cells [147].

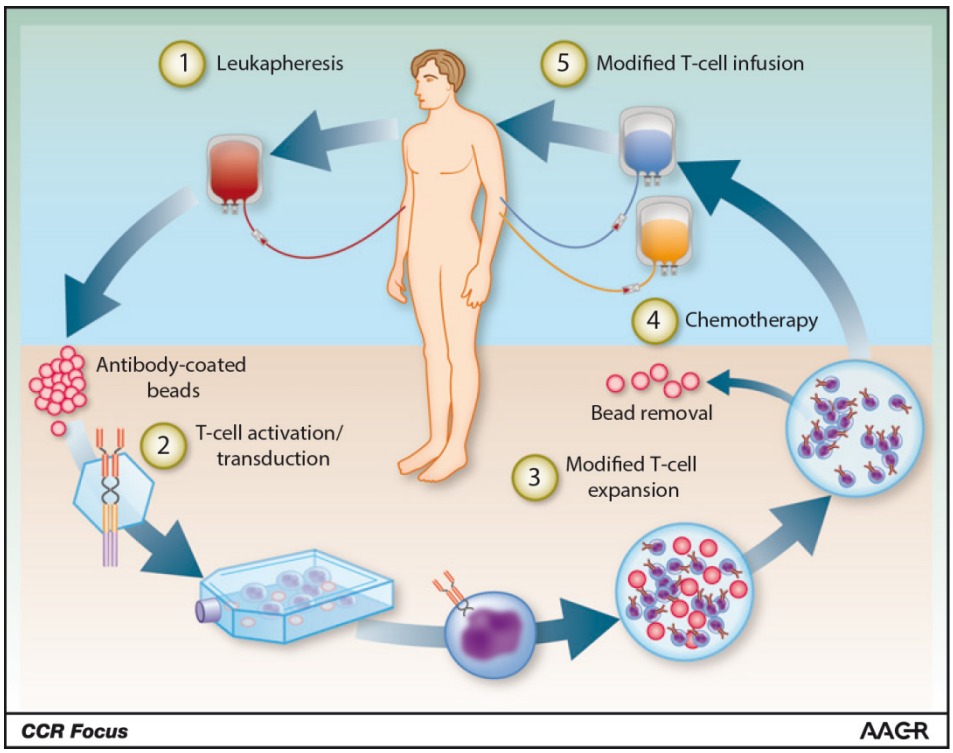

Figure 14. Overview of CAR T-cell therapy. T cells are isolated from cancer patients by leukapheresis (1). T cells are then stimulated with antibody-coated beads simulating antigen-presenting cells, and transduced with a lentiviral vector encoding the CAR (2). After activation and transduction, beads are removed and T cells are further expanded and processed to generate infusion preparations (3). After lymphodepleting chemotherapy (4), CAR T-cells are infused into the patients (5). Image taken from [148].

Clinical trials with CAR T-cell therapy for hematological malignancies have reported outstanding clinical responses. Response rates of 50 to 100% have been observed in patients with relapsed and refractory B-cell acute lymphablastic leukemia (B-ALL), diffuse large B cell lymphoma, follicular lymphoma, or chronic lymphocytic lymphoma who were treated with the CAR T cells targeting CD19 [148]. These exciting results have encouraged the

development of CAR T cells targeting different antigens. To date, CAR T cells directed to one of more than 24 different TAAs are under investigation in clinical trials for the treatment of hematological malignancies and solid tumors [145].

1.5.3.3.1 Challenges for CAR T-cell therapy

Despite the exciting results obtained in clinical trials of hematological malignancies, CAR T cells have shown limited success in solid tumors. Preclinical and clinical trials have identified key hurdles accounting for this low efficacy [149]. As with any other antitumor CTL, CAR T cells have to circumvent factors limiting their trafficking and infiltration into the tumors. Furthermore, the immunosuppressive TME has been shown to induce hypofunctionality in tumor-infiltrating CAR T cells, leading to a reduction in antitumor efficacy in mouse models of cancer [150]. Another major hurdle that is also encountered by CAR T cells and any therapy targeting surface antigens is the tumor immune evasion due to antigen loss. Patients responding to anti-CD19 CAR T-cell therapy can develop $CD19^-$ relapses due to mutations in the *CD19* locus which leads to the expression of truncated forms of the protein [151]. Moreover, preclinical mouse studies with mesothelin-targeting CAR T cells have shown that, after an initial response to the therapy, tumors relapse mainly due to the loss of mesothelin expression within the tumor microenvironment (Sonia Guedan, personal communication and unpublished data). Finally, another concern of the use of CAR T cells for solid tumors is the induction of side effects. Many of the antigens targeted by CAR T cells are expressed on normal tissue, which leads to off-target side effects. Thus, identifying suitable targets and scFV with reduced affinity has been suggested to be an important point to consider.

1.5.3.3.2 Combination of CAR T-cell therapy and oncolytic adenoviruses

OAds have been proposed as attractive tools to circumvent many of the limitations encountered by CAR T cells in the TME of solid tumors. Nishio and colleagues have used a Δ24-based OAd encoding RANTES and IL-15 as a strategy to increase the persistence and infiltration of CAR T cells in the tumors [152]. In line with this, the combination of an OAd encoding TNF-α and IL-2 with CAR T cells targeting mesothelin showed enhanced T-cell proliferation, persistence, function and infiltration in solid tumors, leading to improved antitumor efficacy [153]. These studies highlight the potential of using OAds to improve CAR T-cell therapy.

1.6 Antiviral immune responses in the tumor microenvironment

As mentioned above, OAds can induce antitumor immune responses as one of their main mode of actions. However and given the pathogenic nature of OAds, oncolysis also triggers potent antiviral immune responses. The immunogenicity of viral epitopes often results in biased immune responses against them over other epitopes, a process that is known as immunodominance [154]. Importantly, the immunodominance of adenoviral epitopes has been shown to mask immune responses to delivered transgenes, capsid-displayed TAA and other tumor-restricted epitopes [112, 155, 156]. Additionally, tumor-bearing immunocompetent mice treated with armed OAds show increased antiviral immune responses with concomitant loss of transgene expression in the tumors [157]. Thus, OAd-infected cells are often cleared from the tumor microenvironment by infiltrating virus-specific CTLs without before clinical responses are observed [57]. These facts strongly support the idea that a fine tuning between antiviral and antitumor immune response will be necessary for the success of virotherapy with OAds.

To date, few strategies have been developed to modulate the antiadenoviral immune responses in the TME. Capasso *et al.* have shown that coating of the adenoviral capsid with MHC-I-restricted tumor-specific peptides overcomes the immunodominance of an OAdv by favoring antitumor immune responses *in vivo* [158]. We have also demonstrated that OAds encoding tumor-associated epitopes fused to the viral protein E3-19K promote MHC-I epitope presentation independently from transporter-associated with antigen processing (TAP) protein, leading to antitumor immune responses which compensate adenoviral epitope immundominance [159]. Another interesting approach to favor antitumor rather than antiviral immune responses is the so-called oncolysis-assisted DC vaccination in which DCs loaded with tumor-specific eptiopes are administered during the treatment with oncolytic viruses. Woller and colleagues have shown that the intratumor or intravenous delivery of OAds into immunocompetent mice fails to promote tumor-specific antitumor immune responses as a result of increased antiviral immune responses [112]. However, when combined with DCs loaded with tumor-specific epitopes, OAds promote a shift from virus- to tumor-specific antitumor immune responses.

Although these studies support the need of balancing antiviral and antitumor immune responses, the approaches used by us and others do not fully solve the hurdle of antiviral immune responses. Even if immune responses towards cancer epitopes are favored in these settings, viral epitopes can still be presented and induce antiviral immune responses. Thus,

the approaches described above do not address virus-specific CTL-mediated clearance of the virus from the TME. Moreover, the strategies described above rely on the expression of MHC-I, which is downregulated on cancer cells. Thus, there is a need for developing strategies that can simultaneously promote antitumor immune responses while evading cell-mediated antiviral immunity. In this thesis, we propose the use of bi-specific T-cell engager (BiTE) antibodies as a strategy to achieve this.

1.7 Bi-specific T-cell engagers (BiTEs)

1.7.1 Structure of BiTEs

BiTE antibodies are recombinant proteins composed of two scFV connected through a flexible linker (Figure 15). scFVs are constructed by connecting the variable heavy (V_H) and light (V_L) domains of monoclonal antibodies with a flexible peptide linker. One of the scFV recognizes tumor-associated antigens on target cells, whereas the second scFV bind to the epsilon chain of the CD3 subunit in the T-cell receptor (TCR). BiTEs are commonly produced as monomeric non-glycosylated polypeptide chains of approximately 55 kDa which show high stability. To date, all BiTEs under preclinical and clinical validation are arranged with the TAA-biding scFV located at the N-terminus, while the anti-CD3 scFV is placed C-terminally in the protein.

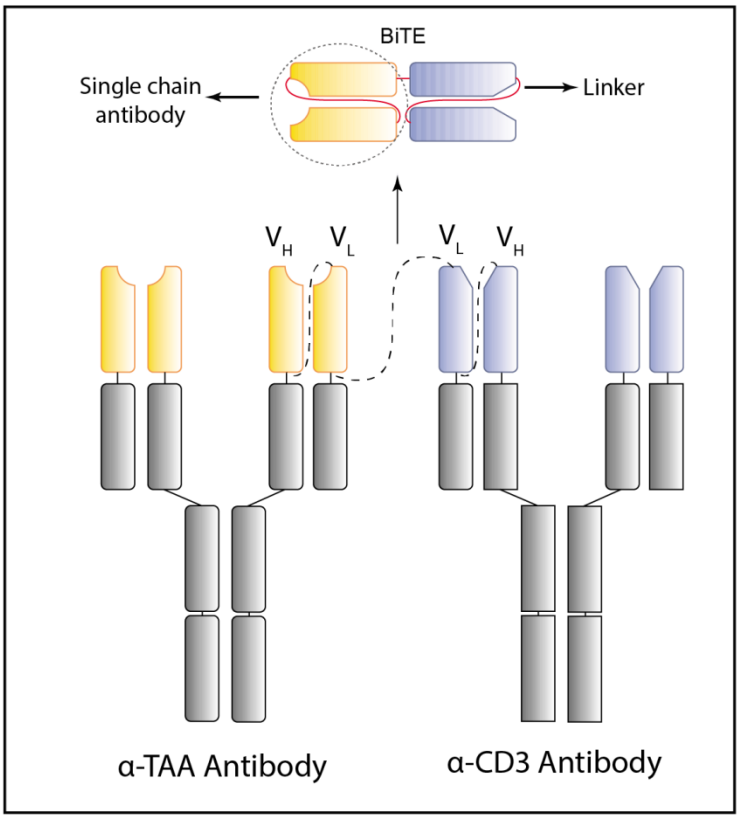

Figure 15. BiTE design. The variable domains of monoclonal antibodies are fused together by linkers, generating single chain antibodies (scFV). One of the scFV recognizes a TAA (yellow) and the other recognizes the epsilon chain of the CD3 coreceptor in the TCR complex (purple). Both scFVs are further linked together by a short flexible peptide. Image adapted from [160].

1.7.2 Mode of action of BiTEs

BiTE antibodies mediate the redirected lysis of cancer cell by T cells after a series of stepwise events. The dual specificity of BiTEs allows their simultaneous binding to T cells and target cells (Figure 16A). This binding brings the membranes of both cells in close proximity, forming an immunological synapse which closely resembles that formed by the TCR-MHC-I interaction between T cells and target cells (Figure 16B). The formation of these synapses induces T-cell activation as evidenced by the expression of activation markers (*e.g.* CD25 and CD69) and cell adhesion molecules, and by the secretion pro-inflammatory cytokines. Once activated, T cells release perforin and granzyme B to the cytolytic synapse thereby eliciting a pro-apoptotic cascade in target cells (Figure 16C). Finally, T cells disengage from dying cells, proliferate and produce new cytotoxic granules before being engaged by BiTEs to neighboring cancer cells (Figure 16D).

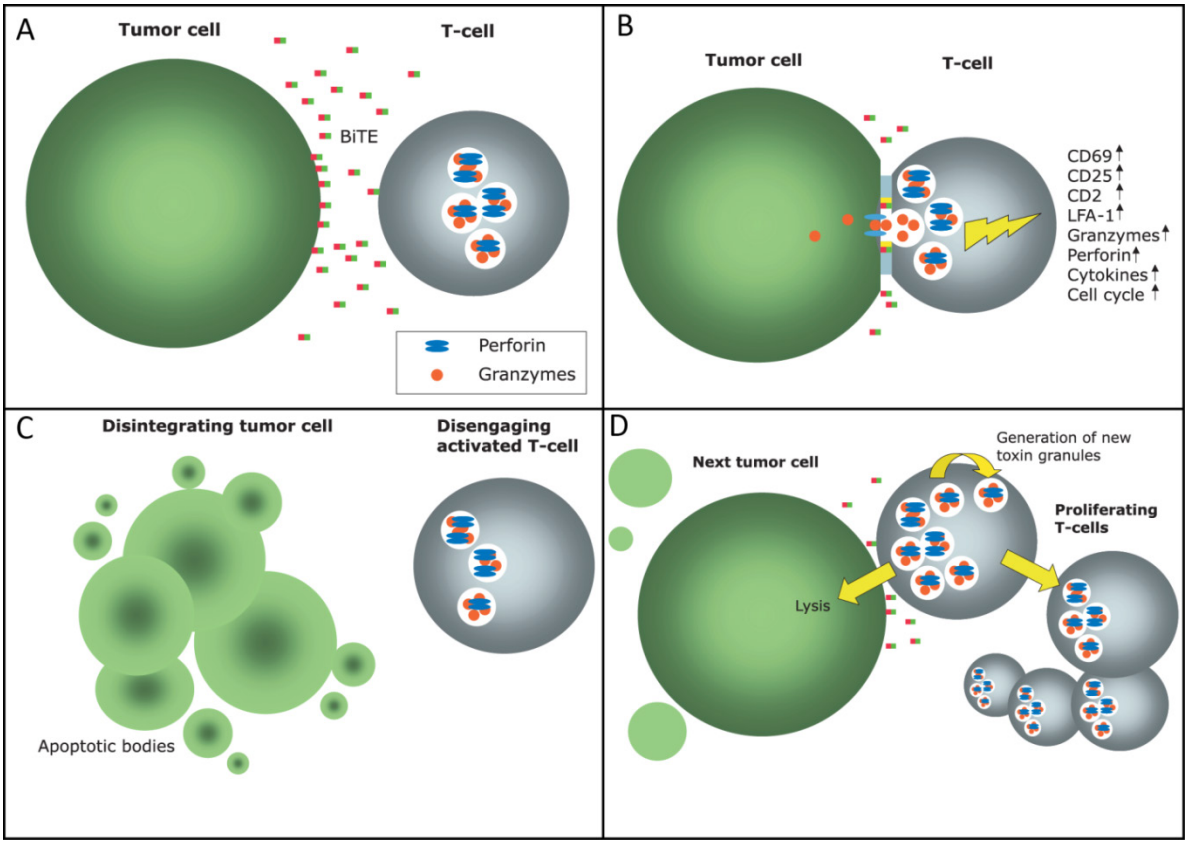

Figure 16. Mode of action of BiTEs. **(A)** BiTEs bind to cancer cells and recruit T cells via the anti-CD3 scFV. **(B)** Simultaneous binding promotes the formation of an immunological synapse and triggers T-cell activation and discharge of cytotoxic granule content (perforin and granzyme). **(C)** These series of events lead to cancer cell death and disengaging of activated T cells. **(D)** Disengaged activated T cells proliferate and can engage in new rounds of killing of neighboring cancer cells. Image adapted from [161].

The mode of action of BiTEs is attractive from the point of view of cancer therapeutics for various reasons. BiTE activity is strictly dependent on the expression of the TAA, and monovalent binding by BiTEs to the CD3 alone does no trigger T-cell activation [162]. BiTEs exert potent cytotoxic activities, with half maximal cell lysis (EC_{50}) typically falling in the femto- and picomolar range (*i.e.* 10-1 × 10^4 pg/ml) [160]. Additionally, the bridging of T cells and cancer cells via BiTE has several advantages over normal TCR-MHC-I-mediated immune responses (Figure 17). BiTEs cannot prime naïve T cells in the absence of co-stimulation by CD28. Instead, the major contribution of the cytotoxic potency of BiTEs comes from effector memory T cells (T_{EM}), which only require CD3 engagement for their activation. Hence, BiTEs can theoretically activate $CD3^+$ T_{EM} in a polyclonal manner, maximizing the overall therapeutic potential. Furthermore, BiTE-mediated T-cell activation is independent of MHC-I antigen presentation. Thus, BiTE antibodies bypass many of the mechanisms employed by cancer cells to evade antitumor immune responses.

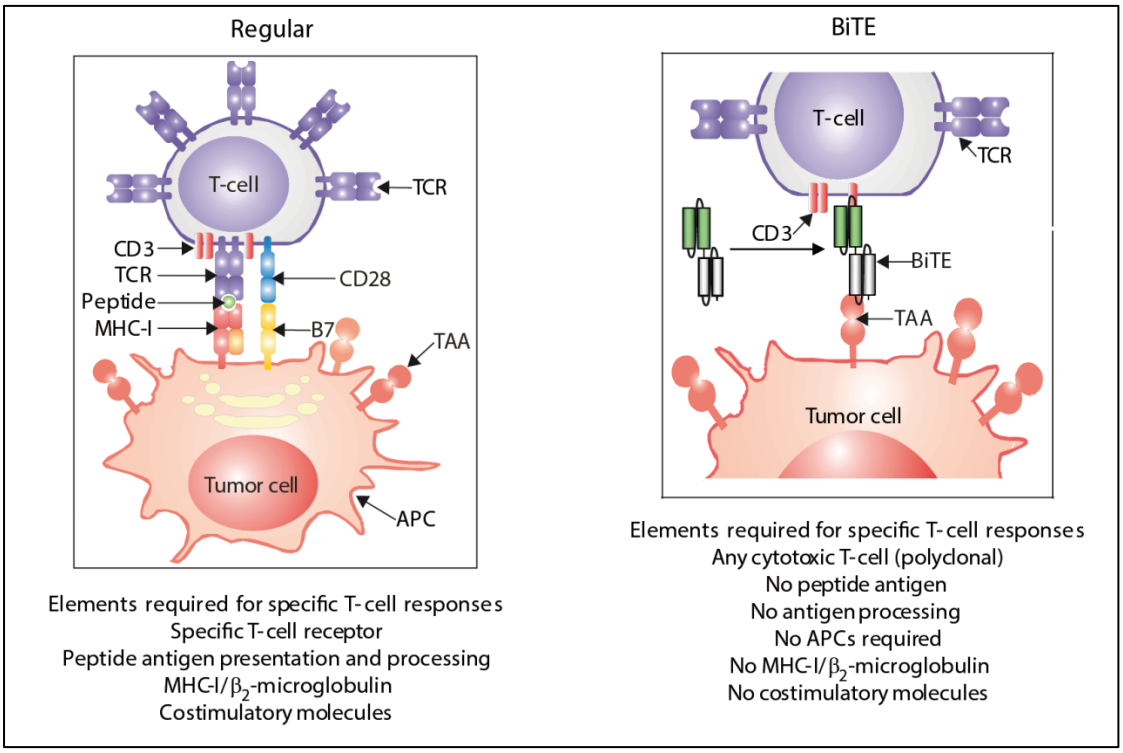

Figure 17. Comparison of TCR-MHC-I- and BiTE-mediated T-cell responses. Regular T-cell mediated antitumor responses (left panel) require the recognition of antigens presented on MHC-I by the TCR, followed by co-stimulatory signals. In contrast, the mode of action of BiTEs (right panel) does not require any of these antigen presentation steps, which are commonly downregulated or absent in cancer cells. Image adapted from [163].

1.7.3 Clinical application of BiTEs

To date, BiTEs targeting one of more than ten different TAAs have been evaluated in preclinical studies (Table 3). From these, those targeting CD33, Ephrin receptor tyrosine kinase A2 (EphA2), carcinoembryonic antigen (CEA), B-cell maturation antigen (BCMA), epithelial cell adhesion molecule (EpCAM) and Prostate-specific membrane antigen (PSMA) are under investigation in Phase I clinical trials for the treatment of different malignancies. Most certainly, the best example of the potential of BiTEs for cancer treatment is Blinatumomab (also named Blincyto), which targets CD19. This BiTE has shown an overall response rate of 40% in patients with Philadelphia chromosome-negative relapsed or refractory B-cell precursor acute lymphoblastic leukemia (R/R ALL), and has been therefore granted approval by the FDA for the treatment of this condition. Blinatumomab has been further evaluated for other hematological malignancies. A recent study of a Phase I clinical trial of Blinatumomab for the treatment of patients with Relapsed/Refractory Non-Hodgkin Lymphoma (R/R NHL) has reported overall response rates of 69% and a Phase II clinical trial is currently ongoing with expanded cohorts [164].

From the pharmacological and toxicological point of view, clinical trials have demonstrated a half-life of 2.11 hours for Blinatumomab in serum, which is accounted for its lack of the fragment crystallizable (Fc) region of mAbs [165]. Despite this short half-life, early clinical trials with Blinatumomab demonstrated that short and spaced intravenous administrations of the BiTE resulted in sever neurological adverse events and cytokine release syndrome (CRS) in patients with high blast burden. Subsequent clinical trials aimed at improving the dosing and schedule of BiTE treatment to mitigate these adverse events. Blinatumomab is currently administered to patients by continuous intravenous infusion in an increasing step dose regime consisting of a first cycle at 9 μg/m^2/day in week 1 and 28 μg/m^2/day thereafter for 3 more weeks [166]. Additionally, patients with more than 50% blasts or a peripheral blast count over 15 × 10^9/L are subjected to a pre-conditioning with dexamethasone to reduce CRS.

Table 3. BiTEs in preclinical and clinical development (Adapted from [163])

BiTE Molecule	TAA Target	Development status	Indications
Blinatumomab (Blincyto)	CD19	FDA-approved Phase II	ALL NHL
MEDI-565 /AMG 211 / MT211	CEA	Phase I	Gastrointestinal cancer
AMG 330	CD33	Phase I	AML
AMG 420	BCMA	Phase I	Multiple Myeloma
AMG 212 / BAY-2010112	PSMA	Phase I	Prostate cancer
AMG 110 / MT 110	EpCAM	Phase I	Solid tumors (Lung, gastric, colorectal)
BscEphA2xCD3	EphA2	Discovery	Ovarian, prostate, cervical, lung and esophageal cancer
C-BiTE	EGFR	Discovery	Lung, colorectal, head and neck and bladder cancer
Her2-BiTE	Her2	Discovery	Breast cancer
MCSP-BiTE	MCSP	Discovery	Melanoma

AML acute myeloid leukemia, B-ALL acute B-cell lymphoblastic leukemia, CEA carcinoembryonic antigen, EGFR epidermal growth factor receptor, EpCAM epithelial cell adhesion molecule, EphA2 Ephrin receptor tyrosine kinase A2, Her2 human EGF receptor 2, MCSP melanoma-associated chondroitin sulfate proteoglycan, NHL non-Hodgkin's lymphoma.

Regarding BiTEs for the treatment of solid tumors, only the results of the Phase I dose-escalation clinical trial with the anti-CEA BiTE MEDI-565/AMG 211 for the treatment of gastrointestinal adenocarcinomas have been reported [167]. The BiTE was given weekly by intravenous infusion over 3 hours on days 1 through 5 for 4 weeks. Different doses were evaluated with or without dexamethasone pre-treatment. MEDI-565 showed similar half-life in serum as Blinatumomab (*i.e.* 2.2 hours) and CRS was observed in patients in the highest dose cohort, although these were mitigated by dexamethasone pre-treatment. No objective responses were observed and 28% showed stable disease as the best response. The results of this study highlight some of limitations of BiTEs for the treatment of solid tumors. As opposed to hematological malignancies, BiTEs will have to penetrate the tumor through the vasculature and reach a concentration high enough to exert their potency. It is likely that the treatment and concentration scheme used in that trial was not sufficient to observe clinical responses, and a regime similar to that used for patients treated with Blinatumomab will potentially improve the performance of this BiTE in the future.

2. OBJECTIVES

Antiviral immune responses are a major hurdle for the success of oncolytic adenoviruses as cancer treatments. Despite the existence of a highly immunosuppressive tumor environment, adenovirus-infected cells can be efficiently cleared by infiltrating virus-specific CTLs. We propose bi-specific T-cell engager (BiTE) antibodies as a strategy to overcome this limitation. Independently of MHC-I antigen presentation, BiTEs can engage T cells towards cancer cells by bridging the CD3 on T cells with a tumor-associated antigen on cancer cells. This means that, theoretically, if BiTEs are present in the tumor microenvironment they could potentially re-direct any $CD3^+$ T cell, including antiviral CTLs, towards cancer cells. Thus, we hypothesize that an oncolytic adenovirus expressing a BiTE might favor anti-tumor rather than anti-viral immune responses.

The general objective of this thesis was to generate and characterize oncolytic adenoviruses armed with BiTEs to redirect immune responses towards cancer cells as a strategy to improve antitumor efficacy.

To achieve this goal, different specific objective were established:

- To generate ICOVIR-15K-based oncolytic adenoviruses expressing BiTEs targeting the EGFR.
- To characterize the oncolytic properties and stability of the BiTE-expressing adenoviruses *in vitro*.
- To characterize the functionality of BiTEs expressed from infected cells.
- To evaluate the antitumor efficacy of BiTE-expressing oncolytic adenoviruses in mouse models of cancer.
- To evaluate the potential of the combination of the BiTE-expressing adenoviruses with novel immunotherapies such as Chimeric Antigen Receptor (CAR) T cells.

3. MATERIALS AND METHODS

3.1 Handling of bacteria

3.1.1 Preparation of electrocompetent bacteria

The *E. coli* DH5α glycerol stock was scrapped with a sterile pipette tip into 10 ml of LB (1% Tryptone, 0.5% Yeast Extract, 0.5% NaCl) and incubated overnight at 37°C and 250rpm. The next day, the 10 ml preculture was added to 1 L of LB and the cultures was incubated at 37°C and 250rpm until the optical density at 600nm (OD_{600}) reached 0.6. The culture was distributed in 250 mL Sorvall bottles and placed on ice for 40 minutes. From this point on, the manipulation of bacteria was performed on ice. Bacteria were centrifuged 15 minutes at 3500 *g* and 4°C in a Sorvall centrifuge. The supernatant was discarded, pellets were gently resuspended with 10ml ice-cold bi-distilled water (ddH_2O) and bottles were filled with more ice-cold ddH_2O. This washing procedure was repeated twice with increasing centrifugation speeds in order to avoid leakiness of the pellets. In the final washing step, the pellet was resuspended in 45 mL of ddH_2O supplemented with 10% (v/v) glycerol. Bottles were centrifuged once more and pellets were resuspended in 3 mL of ddH_2O containing 10% glycerol. The OD_{600} of a 1:100 dilution of the suspension was determined. The OD values were adjusted as close as possible to 1 (which is equivalent to 2.5×10^8 cells/ml). Finally, the suspension was distributed in 50 µl aliquots that were immediately frozen on dry ice. Aliquots were stored at -80°C.

3.1.2 Transformation of bacteria by electroporation

Frozen aliquots (50 µl) of electrocompetent *E. coli* DH5α were thawed on ice and mixed with a maximum of 10 µl pre-cooled DNA (10-1000pg for retransformations or >200ng for recombinations (see section 3.1.4)). The bacteria and the DNA were gently mixed by pipetting and transferred into an ice-cold 0.2 cm electroporation cuvette and electroporated at 50 µF, 1500 V and 125 Ω with an ECM 630 Electroporation System (BTX). After electroporation, bacteria were recovered in 1ml LB medium and incubated at 37°C and shaking conditions for 30-60 minutes. Recovery cultures were plated in LB/Amp plates and incubated at 37°C overnight. For retransformations, cells were streaked on LB agar plates supplemented with the appropriate antibiotic and incubated 37°C overnight. The next day, one clone was inoculated in 6ml (for mini-preps) or 50-200ml (midi-preps) LB supplemented with the corresponding antibiotic. These cultures were used to isolate plasmid DNA as described below.

3.1.3 Small and large scale isolation of Plasmid DNA

For small scale isolation, plasmid DNA (mini-preps) was extracted with alkaline lysis protocol described by Birnboim and Doyle [168]. 6ml of bacterial cultures were incubated overnight at 32°C (for *E. coli* strain SW102) or 37°C (for *E. coli* DH5α). 2ml of the overnight cultures were centrifuged and pellets were resuspended in 200 µl of pre-cooled solution 1 (25 mM Tris-HCl pH 8, 10 mM EDTA, 50 mM glucose, 0.1 mg/mL RNAse). 200 µl of freshly prepared solution 2 (SDS 1%, NaOH 0.2 M) were added, and tubes were mixed by inversion. Finally, 200 µl of pre-cooled solution 3 (3 M potassium acetate, 11.5% acetic acid) were added, and tubes were mixed by inversion. The mixture was incubated for 5 minutes on ice and centrifuged for 15 minutes at 13000 *g*. After centrifugation, the clear supernatant was collected and mixed with 2 volumes of 100% ethanol. The mixture was incubated 15 minutes at room temperature (RT) and plasmid DNA was precipitated by centrifugation for 10 minutes at 13000 *g*. After centrifugation, supernatants were discarded and pellets were washed once with room-temperature 70% ETOH by centrifugation at 13000 *g* for 5 minutes. The supernatants were discarded and the pellet was carefully air-dried, avoiding overdrying. Pellets were resuspended in 40µl ddH_2O.

Large scale isolation of plasmid DNA (midi-preps) was performed with the PureLink HiPure Plasmid Midiprep Kit (Invitrogen) from overnight cultures of 50ml (high copy plasmids) or 200ml (low copy plasmids).

3.1.4 Homologous recombination in bacteria

Genetic modification of the adenovirus genome was carried out with the bacterial artificial chromosome (BAC) recombination-mediated genetic engineering (recombineering) method described by Warming *et al* [169]. Homologous recombination of the BACs is achieved by using the *E. coli* strain SW102, which bears the integrated temperature-sensitive defective λ-prophage. The λ-prophage recombination machinery is controlled by a temperature inducible promoter, whose activation can be triggered by a temperature of 42°C. Electroporation of the heat-shocked bacteria with a DNA fragment flanked by homology arms (>30bp) to the targeted site in the BAC will result in the insertion of the DNA by homologous recombination. This method has been adapted by Stanton *et al* [170] in order for the BAC to carry the whole adenovirus genome, a system known as AdZ (Ad with zero cloning steps). We further adapted the protocol from Stanton *et al*. to replace the *SacB* and

ampicillin resistance genes for the *rpsL-neo* cassette, as it is a faster and more cost-effective method [171]. In the first step of the procedure, termed positive selection, the *rpsL-neo* cassette is inserted in the region of interest of the adenovirus genome. The *neo* gene in the *rpsL-neo* cassette confers resistance to kanamycin. Thus, positive selection can be achieved by plating of the bacteria after electroporation in LB agar plates supplemented with kanamycin (kana) and chloramphenicol (Cm) (the pAdZ BAC backbone confers resistance to this antibiotic). In the second step, termed negative selection, the heat-shocked bacteria containing the pAdZ-rpsL-neo are electroporated with the DNA of interest flanked by homology arms targeting the region where the *rpsL-neo* cassette is inserted. The *E. coli* strain SW102 is intrinsically resistant to streptomycin (Strep) due to mutations in the *rpsL* gene, but introducing the wildt-ype *rpsL* gene into the bacteria exerts dominant phenotypic effects over mutated *rpsL* [172]. Thus, only the bacteria that have replaced the rpsL-neo cassette by the DNA of interest will be able to grown on LB agar plates supplemented with chloramphenicol and streptomycin.

The plasmid pAdZ5-CV5-E3^{+} provided by Richard Stanton was modified by our group in order to obtain the plasmid pAdZ-ICOVIR-15K which has been used for all the recombinations in this thesis. The detailed methodology for recombineering is as follows. For positive selection, the glycerol stock of the bacteria containing the pAdZ-ICOVIR-15K plasmid was scrapped with a sterile pipette tip into 5ml of LB media supplemented with Cm and Strep antibiotics (12.5 µg/ml, and 1 mg/ml, respectively) and incubated overnight at 32°C and constant agitation. The next day, 0.5 ml of the overnight culture were inoculated in 25 ml of LB supplemented with Cm + Strep, and the culture was incubated at 32°C with agitation until the OD_{600} reached 0.5-0.6. The culture was then divided in two Falcon tubes with equal volumes. One of the tubes was kept on ice until further processing. The other tube was induced by heat-shock at 42°C for 15 minutes in a water bath, followed by chilling on ice for 15 minutes. From this point on, manipulation of the bacteria was performed on ice in order to ensure transformation efficiency. Both cultures (induced and uninduced) were centrifuged for 5 minutes at 3200 *g* and 4°C, and supernatants were discarded. Bacteria pellets were resuspended in 12 ml of ice-cold ddH_2O and the centrifugation step was repeated. This washing step was repeated thrice and, after the final step, the pellet was resuspended in approximately 300 µL ddH_20. 50 µL-aliquots of the induced and uninduced cultures were transformed (see section 3.1.2) with >200 ng of the rpsL-neo DNA flanked by the desired homology arms. Bacteria were recovered in 1 mL of LB and incubated for 1 hour at 32°C with constant agitation. From this recovery, 100 µl were plated on LB plates

supplemented with Cm and Kana (12.5 µg/ml, and 15 µg/ml, respectively) and incubated overnight at 32°C. The next day, the number of colonies on the plates of induced and uninduced cultures was counted to determine the recombination efficiency. Colonies were inoculated in 6ml LB supplemented with Cm and Kana and incubated overnight at 32°C and 250rpm. Mini-preps of the overnight cultures were prepared as described in section 3.1.3. For screening of recombinant clones, 17µl of the mini-preps were digested with the corresponding restriction enzymes (New England Biolabs and Takara/Clonetech) at 37°C for 1 hour and separated by electrophoresis on 0.7% agarose gels. Positive clones were stored at -80°C in LB with 15% (v/v) glycerol. The pAdZ-ICOVIR-15K-rpsLNeo plasmid, containing the *rpsL-neo* cassette after the fiber region of the adenovirus genome was previously generated in our group using this positive selection method.

To insert the BiTE transgenes in the ICOVIR-15K genome, the negative selection step was performed. We used the BiTE genes excised from the pUC57 plasmids (see section 3.3.1) which were flanked by 40bp sequences homologue to the sequences flanking the *rpsL-neo* cassette. The plasmid pAdZ-ICOVIR-15K-rpsLNeo was used as backbone for these recombinations. The methodology for the negative selection the same as for the positive selection with the exception of the antibiotics used. After electroporation and the recovery incubation, 100 µL from a 1:10 or 1:25 dilution were plated on LB agar supplemented with Cm and Strep and plates were incubated overnight at 32°C. The next day, colonies were inoculated in 6ml LB supplemented with Cm and Strep and incubated overnight at 32°C and 250rpm. Recombinant clones were screened and stored as above, and the correct insertion of the genes was confirmed by sequencing (see section 3.3.11). Midi-preps from the sequenced positive clones were prepared (see section 3.1.3) and used for transfection (see section 3.3.3).

3.2 Cell culture techniques

3.2.1 Cell lines

The cancer cell lines used in this thesis are outlined in table 4.

Table 4. Cell lines used in this thesis

Cell line	Origin	Tissue of origin	Medium	FBS
A549	Human	Human lung carcinoma	DMEM	10%
A431	Human	Vulval epidermoid carcinoma	DMEM	10%
HEK-293	Human	Embyonic kidney	DMEM	5%
293FT	Human	Embyonic kidney	DMEM + MEM non-essential amino acids	10%
HCT116	Human	Colorectal carcinoma	DMEM-F12	10%
FaDu	Human	Hypopharyngeal carcinoma (squamos cell carcinoma)	DMEM	10%
MDA-MB-453	Human	Breast metastatic carcinoma	DMEM F12	10%
L55	Human	Non-small cell lung carcinoma	DMEM	10%
Jurkat	Human	Acute T-cell leukemia	RPMI	10%
B16CAR	Mouse	Melanoma	DMEM + 0.5 mg/mL hygromycin	10%
EL4	Mouse	Lymphoma (C57/BL)	DMEM	10%

The cancer cell lines A431, MDA-MB-453, A549, HCT116, FaDu, Jurkat and HEK-293 were obtained from the American Type Culture Collection (ATCC, Manassas, VA, USA). L55 cells were kindly provided by Sonia Guedan (University of Pennsylvania). EL4 cells were kindly provided by Silvio Hemmi (University of Zurich). B16CAR cells were obtained from Philippe Erbs (Transgene, France). Cells were maintained in either DMEM, DMEM-F12 or RPMI (Gibco, Thermo Fisher Scientific) supplemented with 5-10% FBS (Gibco, Thermo Fisher Scientific) as indicated in table 4. The A431-GFPLuc cell line was generated by sorting of A431 cells that had previously been transduced with a lentiviral vector encoding GFP and luciferase.

B16CAR-EGFR cells were generated by transfecting the pcDNA3-EGFR plasmid (kindly provided by Frank-D. Böhmer, Jena University Hospital, Germany) into B16CAR cells with Lipofectamine LTX (Thermo Fisher Scientific), according to the manufacturer's instructions.

Transfected cells were selected by 2-week incubation in the presence of 0.5 mg/mL hygromycin and 1 µg/ml G418. EGFR-positive B16CAR cells were selected by Fluorescence-activated cell sorting (FACS) after staining with anti-EGFR antibodies followed by fluorescently labeled secondary antibodies (see section 3.6.1).

3.2.2 Maintenance of cell cultures

Cells were incubated at 37°C in a humidified atmosphere with 5% CO2 in the presence of the corresponding medium. When cultures reached 80-90% confluence, cells were washed once with PBS and detached with trypsin-EDTA. To stop the reaction, cells were resuspended to a final volume of 10ml in the corresponding medium supplemented with 5-10% (v/v) FBS. These cell suspensions were used to split the cells 1:10 to 1:20 depending on the cell line.

3.2.3 Cell counting

To determine the concentration of cells in suspension (trypsinized cells, T cells, etc), manual or automated methods were performed. In both cases, trypan blue staining was used to exclude dead cells. For manual counting, 10 µl from a dilution were pipetted into a Neubauer chamber so that 10-100 cells could be counted in each quadrant. Viable cells in each quadrant were counted and the mean was calculated. Cell concentration was calculated according to the following formula:

$$Concentration\ (cells/ml) = Mean\ viable\ cells\ per\ quadrant \times Dilution\ factor \times 10^4$$

Automated cell counting was performed with a cell counter TC20^{TM} (Bio-Rad) according to the manufacturer's instructions.

3.2.4 Cryopreservation and thawing of cell lines

For long term storage, cells were collected by trypsinization and pelleted by centrifugation. Cell pellets were resuspended in FBS with 10 % (v/v) DMSO and were transferred into Cryovials. Aliquots were put in a container allowing freezing at constant rate of approximately -1 °C per minute and kept at -80 °C overnight before storing them in liquid nitrogen. To thaw frozen cell line stocks, samples were quickly thawed in a water bath at

37°C and washed once with 10 ml of the relevant growth medium by centrifugation before seeding cells at an appropriate density.

3.2.5 Mycoplasma test

Cell lines were routinely tested for mycoplasma contamination by PCR using the following primers:

Table 5. Primers for the detection of mycoplasma

Primer	Sequence (5' → 3')
MICO-1	GGCGAATGGGTGAGTAACACG
MICO-2	CGGATAACGCTTGCGACTATG

As a template for the PCR, medium aliquots from cell cultures that had been in overconfluence and absence of antibiotics for at least 5 days were used. If the result was positive, cells were treated with Plasmocin (Invivogen) at 25 µg/ml for 2 weeks, and tested again for contamination.

3.2.6 Isolation, cryopreservation and thawing of human PBMCs and T cells

All experiments were approved by the ethics committees of the University Hospital of Bellvitge and the Blood and Tissue Bank (BST) from Catalonia. Blood samples were obtained from the BST from Catalonia and the Human Immunology Core of the University of Pennsylvania. Peripheral blood mononuclear cells (PBMCs) of healthy donors were isolated from the blood by ficoll (Rafer) density gradient centrifugation in Leucosep tubes (Greiner Bio-one) following manufacturer's recommendations. Erythrocytes were removed by incubation with ACK lysing buffer (Lonza) and thrombocytes were removed by centrifugation of the PBMCs at 100 *g* for 10 minutes and aspiration of the supernatant. T cells were isolated from blood samples with the RosetteSep Human T-Cell Enrichment Cocktail (STEMCELL Technologies) according to the manufacturer's instructions. PBMCs and T cells were cryopreserved in FBS supplemented with 10% DMSO in aliquots of 1-5 × 10^7 cells/vial. For thawing, PBMCs or T cells cryovials were quickly thawed in a water bath at 37 °C and washed once with 10 ml RPMI supplemented with 10% FBS and 10 mM HEPES (Gibco) by centrifugation. Cells were resuspended at a concentration of 2-3 × 10^6 cells/ml and incubated overnight for the recovery of the cells prior to the experiments.

3.2.7 Isolation of mouse splenocytes

Spleens from CO_2 euthanized C57BL/6 or BALB/c mice were surgically resected under sterile conditions and placed in falcons containing PBS until further processing. Cells strainers (70 μm) were placed in a petri dish containing 5ml RPMI 10% FBS and spleens were mechanically disrupted with the plunger of a syringe by carefully pressing the spleen over the strainer. The medium in the petri dish was periodically passed through the strainer to ensure complete disaggregation of the spleen. Medium was collected and centrifuged for 10 minutes at 400*g* and room temperature. The supernatant was discarded and red blood cells were removed by incubating cells with 1ml of ACK lysis buffer for 5 minutes. Cells were washed three times with PBS and cells were resuspended in RPMI 10% supplemented with 50 μM 2-mercaptoethanol (Gibco, Thermo Fisher Scientific) and adjusted to the desired concentration.

3.2.8 Fluorescent labeling of cancer cells with CFSE

Trypsinized cancer cells (3×10^6) were centrifuged at 300g for 5 minutes and pellets were resuspended in 5ml 1μM Carboxyfluorescein succinimidyl ester (CFSE) (Sigma) diluted in PBS. Cells were incubated at 37°C for 20 minutes protected from light and the reaction was blocked with equal volumes of FBS. Cells were centrifuged at 300g for 5 minutes and pellets were resuspended either in the corresponding medium supplemented with 10% FBS. For experiments involving the use of mouse splenocytes, mouse cancer cells were resuspended in the corresponding medium supplemented with 10% FBS and 2-mercaptoethanol. After resuspension, cells were counted and cell concentration was adjusted as needed.

3.2.9 Fluorescent labeling of human PBMCs and mouse splenocytes with CFSE

PBMCs or splenocytes ($1\text{-}3 \times 10^7$) were resuspended in 1ml PBS and mixed with 1ml of 2 μM CFSE (Sigma) to achieve a final concentration of 1 μM. Cells were incubated for 5 minutes at room temperature protected from light and the reaction was then blocked by adding ten volumes of PBS 5% FBS. Cells were centrifuged at 300*g* for 5 minutes, the supernatant was discarded and pellets were resuspended in 5 ml PBS 5% FBS. This washing step was repeated twice. After the last washing step, pellets were resuspended in RPMI 10% FBS (PBMCs) or RPMI 10% supplemented with 2-mercaptoethanol (splenocytes). Cells were counted and concentration was adjusted as needed.

3.3 Recombinant adenoviruses

All adenoviruses used in this thesis are derived from the human adenovirus serotype 5 (Ad5). The virus ICOVIR-15K (see section 1.3.2) has been previously described [47]. AdTLRGDK is GFP- and luciferase-expressing *E1*-deleted adenovector having the same capsid as ICOVIR-15K, and has been previously described [39]

3.3.1 BiTE design

cBiTE

The anti-EGFR scFV (C225) was derived from the Cetuximab monoclonal antibody and its sequence was obtained from publically available sources. The anti-CD3 scFV corresponds to that of the Blinatumomab BiTE and its sequence was obtained from the World Intellectual Property Organization application WO2004106381. The C225 and anti-CD3 variable regions were connected by a $(G_4S_1)_3$ and a $(G_2S_1)_4GG$ linker, respectively, and both scFV were connected to each other by a GGGS flexible linker. The cBiTE was arranged VL_{C225}-VH_{C225}-VH_{CD3}-VL_{CD3} and it included the peptide signal from the mouse Ig heavy chain and a FLAG tag at the N- and C-terminus of the protein, respectively. The cBiTE construct included a left (upstream of the BiTE starting codon) and a right (downstream of the last BiTE codon) homology arms. The left homology region included the kozac, the IIIa splicing acceptor and extra DNA base pairs from the adenovirus genome. The right homology arm included the stop codon, the polyA signal and extra base pairs from the adenovirus genome. Both arms were homologous to the sequences flanking the *rpsL-neo* cassette in the pAdZ-ICOVIR-15K-rpsL-neo plasmid. The cBiTE-coding region was optimized for human codon usage avoiding Ssp1 and AfeI restriction sites, and the whole construct, including the regulatory and homology sequences, was synthesized by Genscript (Annex 1).

mBiTE

The anti-mouse CD3 scFV was derived from the hamster monoclonal antibody 145.2C11 [173]. The anti-mouse EGFR scFV was derived from the mouse monoclonal antibody 7A7, which recognizes both murine and human EGFR [174]. The 2C11 and 7A7 variable regions were connected by a $(G_4S_1)_3$ and a $(G_2S_1)_4GG$ linker, respectively, and both scFV were connected to each other by a GGGS flexible linker. The mBiTE construct was arranged VH_{2C11}-VL_{2C11}-VH_{7A7}-VL_{7A7} and it included the peptide signal from the mouse Ig heavy chain and a FLAG tag at the N- and C-terminus of the protein, respectively. The mBiTE construct included the same homology arm described for the cBiTE. The mBiTE-coding region was optimized for human

codon usage avoiding Ssp1 and AfeI restriction sites, and the whole construct, including the regulatory and homology sequences, was synthesized by Genscript (Annex 2).

mcBiTE

The chimeric mcBiTE was composed of the scFV C225 from the cBiTE and the 2C11 scFV from the mBiTE. The 2C11 and C225 variable regions were connected by a $(G_4S_1)_3$ and a $(G_2S_1)_4GG$ linker, respectively, and both scFV were connected to each other by a GGGS flexible linker. The mcBiTE construct was arranged VH_{2C11}-VL_{2C11}-VL_{C225}-VH_{C225} and it included the peptide signal from the mouse Ig heavy chain and a FLAG tag at the N- and C-terminus of the protein, respectively. The mcBiTE construct included the same homology arm described for the cBiTE. The mcBiTE-coding region was optimized for human codon usage avoiding Ssp1 and AfeI restriction sites, and the whole construct, including the regulatory and homology sequences, was synthesized by Genscript (Annex 3).

3.3.2 Construction of BiTE-expressing oncolytic adenoviruses

The BiTE constructs were excised from pUC57 plasmids by exploiting the SspI and AfeI restriction sites included in their sequence. These sites were designed so that the overhangs generated after restriction retained the homology to the target sequences in the pAdZ-ICOVIR-15K-rpsL-neo plasmid. The pUC57 plasmids containing the BiTE constructs were digested with SspI and AfeI enzymes (New England Biolabs) according to the manufacturer's instructions. Digestions were separated by gel electrophoresis and the band corresponding to the BiTE constructs were sliced from the gel. DNA gel extraction was performed with the QIAquick gel extraction kit (QIAGEN) according the manufacturer's instructions. This DNA was used for homologous recombination in bacteria in order to generate the plasmids pAdZ-ICO15K-cBiTE, pAdZ-ICO15K-mBiTE and pAdZ-ICO15K-mcBiTE (see section 3.1.4).

3.3.3 Generation of oncolytic adenoviruses by calcium phosphate transfection

Once the incorporation of the BiTEs into the adenovirus genome was confirmed by sequencing (see section 3.3.12), plasmids were transfected into HEK-293 cells to generate the virus. For transfection, monolayers of HEK-293 cells seeded in 6-well plates in a final volume of 2ml until they reached a confluence of 60-80%. For each plasmid to be transfected the following mixture was prepared in a 1.5 mL tube:

- 19.5 µL of $CaCl_2$ 2 M
- 3 µg of DNA
- ddH_2O up to a final volume of 162 µL

This solution was added drop-wise into a tube containing 162 µL of HBS 2X (NaCl 274 mM, HEPES 50 mM, and NaH_2PO_4 1.5 mM in H_2O, pH adjusted to 6.95 – 7.05 with NaOH) and solutions were mixed by finger vortexing. The mixture was incubated for 20 minutes at RT and added drop-wise to the cells. 16 hours post-transfection the medium was removed and exchanged by fresh medium. When cytopathic effect (CPE) foci were visible (approximately 5-7 days post-transfection), cells were collected together with the supernatant and underwent through 3 rounds of freeze/thaw cycles to completely release the viral particles from the cells. This cell extract (CE) was used for further amplification steps.

3.3.4 Virus clone isolation by plaque purification assay

Serial dilutions from the transfection CE, ranging from 10^{-1} to 10^{-7}, were prepared in DMEM 5% FBS. 100 µl of each dilution was used to infect one 6-well of 80% confluent A549 cells for 4 hours at 37°C. After removing the media and washing of the cells with PBS, 3 ml of a 1:1 solution of DMEM 5% FBS and 1% agarose pre-warmed was added to the cells. Once solidified, 2 ml of fresh medium were added over the agarose matrix. The plates were incubated at 37°C until the appearance of plaques was evident (5-8 days post infection). To select clones, the medium was removed and the plaques were picked through the agarose matrix using a pipette tip. The aspirated agarose/medium was resuspended in 500 µl of DMEM 5% FBS and used for further amplifications steps.

3.3.5 Amplification and large-scale production of oncolytic adenoviruses

After clone selection, 250 µl from the clone suspension were used to infect a 6-well of confluent A549 cells. When cytopathic effect (CPE) was observed cells were harvested and subjected to 3× freeze/thaw cycles. From this point on, viruses were sequentially amplified by scaling up as follows: 6-well → 1 × 100mm dish → 1 × 15cm dishes → 14 × 15cm dishes. In general, 1:20 dilutions of the viral suspension from each step were used as inoculum for the next expansion step, while the rest was stored at -80°C as backup stocks. The general process for virus propagation consisted of an infection and harvesting steps. Infections were performed in DMEM 5% FBS and dishes were incubated for 3 days until cells were detached or showed evident signs of CPE. For harvesting, infected cells were collected by pipetting and

subjected to 3× freeze/thaw cycles. In the final harvesting step, cell pelleted by centrifugation and cells were resuspended in a maximum volume of 10 ml before performing freeze/thaw cycles for purification. 50 ml of supernatants were also collected for the first round of ultracentrifugation.

3.3.6 Purification of oncolytic adenoviruses

Oncolytic adenoviruses were purified by cesium chloride (CsCl) density gradient centrifugation. Prior to the preparation of the CsCl gradients, cell pellets were subjected to three freeze/thaw cycles to release the viruses from the cells. Debris was cleared by centrifugation at 1000 *g* for 10 minutes, and the supernatant was collected. Cell pellets were resuspended in 10ml of the supernatant stored in the last step of the amplification process, and tubes were centrifuged again to wash the pellet. This process was repeated until a final volume of 42ml of virus supernatant was reached. Discontinous CsCl gradients were prepared in ultracentrifugation tubes (Beckman Coulter) using 2 solutions at different concentrations. For the first layer of the gradient, 2.5 ml of a solution with a concentration of 1.35 g/ml were added to the bottom of the tubes. The second layer consisted of 2.5 ml of a CsCl solution at 1.25 g/ml, and it was carefully added on top of the first layer. Gradients were completed by carefully adding 7.5 ml of the virus on top of the second layer of the gradient. Tubes were ultracentrifuged for 2 hours at 150000 *g* (35000 rpm, SW40 Ti rotor, Beckman) and 10°C. With these conditions, viral particles are separated from cell debris according to size and appear as 2 bands at the interface between 1.25 and 1.35 g/ml layers. The upper band corresponds to empty viral capsids and was removed by suction. The lower band of interest was collected and placed on ice in a 50 ml Falcon tube. For further purification and concentration, a second centrifugation step using a continuous CsCl gradient was performed. The solution containing the virus was brought up to 24 ml with the CsCl solution at 1.35 g/ml and distributed into 2 ultracentrifuge tubes. The second centrifugation was carried out overnight at the same conditions of the first one. After centrifugation, the upper band was discarded by suction and the band corresponding to the full viral particles was collected in a maximum volume of 2 ml. Buffer exchange was performed with PD-10 desalting columns (GE healthcare Life Sciences) according to the manufacturer's instructions. Viruses were eluted from columns with 2ml Tris-NaCl, supplemented with glycerol to a final concentration of 5% (v/v) and stored in 25 µl- and 50 µl-aliquots at -80°C for long term storage.

3.3.7 Determination of the total number of virus particles by spectrophotometry

Virus stocks were diluted 1:5, 1:10 and 1:20 in lysis buffer (Tris 10 mM, EDTA 1 mM, 0.1% SDS, pH 8.0) and incubated at 56°C for 5 minutes in order to dissociate viral particles. After incubation, the absorbance of each sample was determined at 260nm wavelength using a NanoDrop ND-1000 UV/VIS spectrophotometer. The number of viral particles was calculated according to the following formula:

$$Titer\ (vp/ml) = OD_{260} \times DF \times 1.1 \times 10^{12}$$

Where OD_{260} corresponds to the absorbance of each sample at 260nm and *DF* to the dilution factor of each sample. The final titer is given in viral particles/ml.

3.3.8 Determination of functional viral particles by anti-hexon staining

In order to measure the number of infectious particles, serial 1:10 dilutions of the viral stock were prepared in DMEM 5% FBS in triplicates in a final volume of 100 µl in 96-well plates. HEK-293 cells (1×10^5 cells) were added to the wells in a volume of 50 µl and plates were incubated for 36 hours at 37°C. The medium was then removed and cells were air-dried for 5 minutes at RT. Cold methanol (100 µl) was added to each well and incubated for 10 minutes at -20°C in order to fix the cells. Methanol was removed and wells were washed twice with PBS^{++} containing 1% BSA. Cells were then incubated for 1 hour at 37°C with 1:5 diluted anti-hexon antibody obtained from the hybridoma 2Hx-2 (ATCC, Manasas, VA, USA). Cells were then washed three times more and incubated for 1 hour with 1:500 diluted anti-mouse secondary antibody conjugated with Alexa-488 (Thermo Fisher Scientific). Finally, cells were washed thrice and the viral titer was determined by counting stained cells using an inverted fluorescence microscope. To calculate the concentration of transducing units (TU) in the stock, the following formula was used:

$$Functional\ titer\ (TU/ml) = \frac{Mean\ positive\ cells}{100\ \mu l} \times Dilution\ factor \times 1000\ \mu l$$

3.3.9 Isolation of viral DNA from infected cells

In order to validate the identity of the adenovirus clones isolated from the plaque assay, Hirt DNA extraction was performed. For this, A549 cells seeded in a 100mm plate were infected with the corresponding adenovirus until complete CPE was observed. Cells were harvested, pelleted by centrifugation for 5 minutes at 1000 *g* and washed once with PBS. Cells were then pelleted again by centrifugation, resuspended in 350 µl of ddH_20 and mixed with 350 µl 2x Hirt lysis buffer (10 mM Tris pH 8.0, 20 mM EDTA, 1.2% SDS, and 200 µg/ml proteinase K). Samples were incubated for 1 hour at 56°C. Then, 200 µl of 5M NaCl were added drop-wise to the mixture while vortexing and samples were incubated for 8-16 hours at 4°C until a white precipitate corresponding to the cellular DNA was observed. Samples were then centrifuged for 30 minutes at 13000 *g* and 4°C, and the clear supernatant containing the viral DNA was collected. Supernatants were incubated for 1 hour at 37°C with RNAse at a final concentration 100 µg/µl to remove RNA. Samples were mixed with one volume phenol-chloroform and centrifuged for 5 minutes at 13000 *g*. The upper phase containing the DNA was collected, mixed with two volumes of ethanol supplemented with 2% sodium oxaloacetate and incubated for 1 hour at -20°C. Samples were centrifuged for 20 minutes at 13000 *g*, the supernatant was discarded and pellets were washed once with 70% ethanol. Finally, the supernatant was discarded and air-dried DNA pellets were resuspended in 25 µl TE pH 8.0.

3.3.10 Isolation of viral DNA from viral particles

50-µl aliquots of the purified virus were used. Usually, an input of $2x10^{10}$ vp results in yields of 1 µg viral DNA. Virus aliquots were mixed with 350 µl of a TE-based lysis buffer (final concentrations in the solution: 20 mM EDTA pH 8.0, 0.5% SDS, 200 µg/ml proteinase K). Samples were incubated for 2 hours at 56°C in order to dissociate viral particles. DNA was isolated by phenol-chloroform extraction and ethanol precipitation as described above. DNA pellets were resuspended in 25 µl TE pH 8.0.

3.3.11 Characterization of viral genomes by restriction analysis

Genomes of recombinant adenoviruses were characterized by restriction analysis to confirm genome stability during amplification. For this, 1 µg of adenovirus DNA was digested with 1 unit of the corresponding restriction enzyme according to the manufacturer's

instructions. DNA from the parental adenovirus (*i.e.* ICO15K) was included as a control for comparison. Digestion patterns were evaluated by gel electrophoresis on 1% agarose gels.

3.3.12 Characterization of viral genomes by sequencing

Adenovirus genomes were sequenced to discard potential recombinations with the wild-type *E1a* present in HEK-293 cells during the transfection–mediated adenovirus rescue, and to discard mutations in the BiTE transgenes after the amplification process in A549 cells. The primers for the sequencing of the different regions of the adenovirus genomes are described in table 6.

Table 6. Primers used for the sequencing of adenovirus genomes

Primer name	Sequence 5' → 3'	Description
Fiber up	CAAACGCTGTTGGATTTATG	For the sequencing of the BiTE transgenes
Fiber down2	TTCATTCAGTAGTATAGCC	For the sequencing of the BiTE transgenes
Oligo7	GGAACACATGTAAGCGACGGATGTGG	For the sequencing of the modified *E1a* promoter
Ad670F	ATCTTCCACCTCCTAGCCAT	For the sequencing of the Δ24 mutation

Sequencing was performed with the BigDye™ Terminator v3.1 Cycle Sequencing Kit (Applied Biosystems, Thermo Fisher Scientific). For the sequencing setup, 10 µl-reaction mixes were prepared containing 100-200 ng DNA, 3.2 pmol of the primer, 2 µl 5X Sequencing Buffer, 2 µl Reaction Mix and ddH_2O to complete the final volume. The PCR conditions are listed in table 7.

Table 7. PCR conditions for the sequencing of the adenovirus genomes

Stage	Description	Temperature	Time	Cycles
1	Initial denaturation	96°C	1 minute	1
	Denaturation	96°C	30 seconds	
2	Annealing	50°C	15 seconds	24
	Extension	60°C	2 minutes	
3	Pause	4°C	∞	1

Reactions were sequenced by the core facility from the translational research laboratory at the Catalan Institute of Oncology.

3.4 Adenovirus-based *in vitro* assays

3.4.1 Adenoviral transduction assay

HCT116, A431 or A549 cells (1×10^5) were seeded in 24-well plates in a volume of 400 µl. Cells were infected with 100 µl of the *E1*-deleted and GFP-expressing AdTLRGDK vector to have multiplicities of infection (MOI) ranging from 25 to 400 TU/cell. 24 h post-infection, cells were trypsinized, resuspended in FACS buffer and GFP expression levels were assessed by flow cytometry. A total of 10000 events were acquired. Data was expressed as the mean fluorescence intensity for each cell line.

3.4.2 Adenovirus-mediated cytotoxicity assay

A549 or HCT116 (2×10^4) cells per well were seeded in 96-well plates in DMEM supplemented with 5% FBS. Cells were infected with serial dilutions of ICO15K or ICO15K-cBiTE starting from 200 TU/cell. At day 6 post-infection plates were washed with PBS and stained for total protein content with the bicinchoninic acid (BCA) kit (Pierce Biotechnology). Absorbance was determined and the percentage of cell survival was calculated by normalization to the absorbance values of uninfected wells. The inhibitory concentration 50 (IC_{50}) was calculated with GraphPad Prism v6.02 (GraphPad Software Inc.) by using a dose-response non-linear regression with variable slope.

3.4.3 Adenovirus production assay

A549, A431, MDA-MB-453 or FaDu cells (1×10^5) were seeded in 24-wells plates and incubated overnight. The next day, one of the wells was trypsinized and the total number of cells was determined. Cells were infected with ICO15K or ICO15K-cBiTE at an MOI of 20 in a final volume of 500 µl for 72 hours. After incubation, the cells were collected together with the supernatant and cell extracts were prepared by 3x freeze/thaw cycles. The functional titer was determined with the anti-hexon staining method (see section 3.3.8). Results are expressed as the number of TU produced by a single cell, taking into account the functional titer and the number of cells at the day of the infection.

3.4.4 Production of supernatants

A549 cells (1×10^7) were seeded in 100mm culture plates. The next day, medium was removed and cells were infected with ICO15K or ICO15K-cBiTE (MOI = 20) in a final volume of 10ml of DMEM supplemented with 5% FBS. 72 h post-infection supernatants were harvested, centrifuged at 500 *g* for 5 min to discard dead cells, and stored at -20°C until further use. For effector binding and rosette formation assays, supernatants were concentrated (approximately 20x) with Amicon Ultra-15 centrifugal filter units with a molecular weight cut-off of 30 kDa (Merck Millipore) according to manufacturer's instructions. Supernatants from uninfected cells were used as a negative mock control.

3.5 Production and titration of lentiviral vectors

The lentiviruses used in this thesis were produced with the 3rd-generation plasmids described in table 8. The plasmids pTRPE-CBG-T2A-GFP and pTRPE-SS1-ICOSz were kindly provided by Sonia Guedan (University of Pennsylvania).

Table 8. Plasmids for the generation of lentiviral vectors

Plasmid name	Plasmid type	Description
pRSV-Rev	Packaging	Encodes the Rev protein
pMDLg/pRRE	Packaging	Encodes the Gag and Pol proteins
pMD2.g	Envelope	Encodes the VSV-G envelope
pTRPE-CBG-T2A-GFP	Transfer	Encodes the click beetle green luciferase and GFP
pTRPE-SS1-ICOSz	Transfer	Encodes the SS1 chimeric antigen receptor

For lentivirus production, 293FT cells (8×10^6) were seeded in 15cm plates in a total volume of 30ml. The next day, the plasmids pRSV-Rev (18 µg), pMDLg/pRRE (18 µg), pMD2.g (7 µg) and the CAR- or luciferase-expressing plasmids (15µg) were diluted in Opti-MEM (Gibco, Thermo Fisher Scientific) to a final volume of 1.4ml and mixed with 60 µl plus reagent. The DNA mixture was added drop-wise into a tube containing 1.4 ml Opti-MEM and 60 µl Lipofectamine LTX (Thermo Fisher Scientific), and the tubes was mixed by finger vortexing. Transfection mixtures were incubated at RT for 20 minutes. After incubation, the medium from the 293FT cultures was removed and transfection mixtures were added drop-wise to the cells in order to cover the whole monolayaer. After one-minute incubation, 30ml fresh medium was added to the plate. 24 hours post-transfection, the medium was

harvested and stored at 4°C and fresh medium was added to the plates. The next day, the medium was harvested and both 24h and 48h supernatants were filtered through 0.45 μm filter units. Lentivirus preparations were concentrated by ultracentrifugation for 2 hours at 20000 rpm (82705 *g*) and 4°C with a SW28 Ti rotor (Beckman Coulter), supernatants were discarded and each virus pellet was resuspended in 200-400 µl RPMI 10% FBS. Aliquots (20-50 µl) were stored at -80°C.

Lentiviral stocks were titrated on Jurkat cells. For this, 1:3 dilutions of the lentivirus in a final volume of 100 µl were prepared in 96-well plates. Jurkat cells (2×10^4) were seeded into each well and plates were incubated at 37°C for 72 hours. CBG-expressing Jurkat cells were evaluated by flow cytometry and the percentage of GFP^+ cells was determined for each dilution. For CAR-expressing Jurkat cells, cells were incubated with Biotin-SP Goat Anti-Mouse IgG antibody followed by incubation with APC-conjugated streptavidin (see section 3.6.1). The percentage of CAR^+ cells was determined by flow cytomtery. To calculate the titer for each lentiviral preparation, the following formula was used:

$$Titer\ (TU/ml) = \left(\frac{\%\ positive\ cells}{100}\right) \times (2 \times 10^4\ cells) \times 20 \times Dilution$$

The dilution at which less than 20% of cells expressed the transgene was chosen to calculate the final titer, as it represents the most accurate limiting-dilution titer for the vector sample.

3.6 Immunology techniques

3.6.1 Antibodies and flow cytometry

Flow cytometry analysis was performed with a Gallios cytometer (Beckman Coulter). The antibodies used in this thesis are listed and described in table 9. Surface staining and washes were performed in PBS supplemented with 10% FBS and 0.01% NaN_3. Cells were stained cell viability with LIVE/DEAD fixable stain (Thermo Fisher Scientific) according to the manufacturer's instructions. For indirect surface staining, primary antibodies or isotype controls were incubated for 30 minutes on ice, followed by washing steps and incubation with fluorochrome-coupled secondary antibodies for 30 minutes on ice. Direct surface staining was performed for 30 min on ice. All flow cytometry data were analyzed with the FlowJo software v7.6.5 and v10 (Tree Star).

Table 9. List of antibodies used in this thesis

Antibody	Source	Clonality	Company	Concentration	Application
Anti-human EGFR	Mouse	Monoclonal (528)	Merck Millipore	5µg/ml	EGFR cell profiling
Normal mouse IgG2a	Mouse	-	Santa Cruz Biotechnology	5µg/ml	EGFR cell profiling
Anti-FLAG	Mouse	Monoclonal (M2)	Sigma-Aldrich	5µg/ml	Binding assays with cBiTE and mBiTE
Normal mouse IgG1a	Mouse	-	Santa Cruz Biotechnology	5µg/ml	Binding assays with cBiTE and mBiTE
Anti-FLAG	Rabbit	Polyclonal	Sigma-Aldrich	5µg/ml	Binding assays with mcBiTE
Normal rabbit IgG	Rabbit	-	Santa Cruz Biotechnology	5µg/ml	Binding assays with mcBiTE
Alexa Fluor 488 anti-mouse IgG	Goat	Polyclonal	Thermo Fisher Scientific	5µg/ml	Binding assays with cBiTE and mBiTE. EGFR and CD3 cell profiling
Alexa Fluor 647 anti-mouse IgG	Goat	Polyclonal	Thermo Fisher Scientific	5µg/ml	Binding assays of cBiTE to T cells
Alexa Fluor 488 anti-Rabbit IgG	Goat	Polyclonal	Thermo Fisher Scientific	5µg/ml	Binding assays with mcBiTE
Anti-human CD3	Mouse	Monoclonal (OKT3)	Biolegend	5µg/ml	CD3 profiling of Jurkat cells and PBMCs
APC anti-human CD8	Mouse	Monoclonal (SK1)	Biolegend	Titration-dependent	T-cell activation and proliferation assays
FITC anti-human CD8	Mouse	Monoclonal (SK1)	Biolegend	Titration-dependent	T-cell activation assays
PE anti-human CD4	Mouse	Monoclonal (OKT4)	Biolegend	Titration-dependent	T-cell activation and proliferation assays
FITC anti-human CD25	Mouse	Monoclonal (BC96)	Biolegend	Titration-dependent	T-cell activation assays
APC anti-human CD25	Mouse	Monoclonal (BC96)	Biolegend	Titration-dependent	T-cell and CART-cell activation assays
FITC anti-human CD69	Mouse	Monoclonal (FN50)	Biolegend	Titration-dependent	T-cell activation assays
APC anti-human CD69	Mouse	Monoclonal (FN50)	Biolegend	Titration-dependent	T-cell activation assays
APC Anti-human CD3	Mouse	Monoclonal (HIT3a)	Biolegend	Titration-dependent	T-cell prolfieration assays
Alexa Fluor 488 LAG-3	Mouse	Monoclonal (17B4)	Enzo	Titration-dependent	Inhibitory marker expression assay
PerCP/eFluor710 TIM-3	Mouse	Monoclonal (F38-2E2)	eBioscience	Titration-dependent	Inhibitory marker expression assay
PE/Cy7 anti-human CD200	Mouse	Monoclonal (OX104)	eBioscience	Titration-dependent	Inhibitory marker expression assay
H7/APC anti-human CD8	Mouse	Monoclonal (SK1)	BD Pharmigen	Titration-dependent	Inhibitory marker expression assay
BV510 anti-human CD4	Mouse	Monoclonal (OKT4)	Biolegend	Titration-dependent	Inhibitory marker expression assay
BV605 anti-human CD3	Mouse	Monoclonal (OKT3)	Biolegend	Titration-dependent	Inhibitory marker expression assay

BV711 anti-human PD1	Mouse	Monoclonal (EH12.2H7)	Biolegend	Titration-dependent	Inhibitory marker expression assay
FITC anti-mouse CD4	Rat	Monocloanl (RM4-5)	Biolegend	Titration-dependent	Splenocyte activation assays
PE anti-mouse CD8a	Rat	Monoclonal (53-6.7)	Biolegend	Titration-dependent	Splenocyte activation assays
APC anti-mouse CD25	Rat	Monoclonal (PC61)	Biolegend	Titration-dependent	Splenocyte activation assays
APC anti-mouse CD69	Rat	Monoclonal (H1.2F3)	Biolegend	Titration-dependent	Splenocyte activation assays
APC anti-mouse CD3	Rat	Monoclonal (17A2)	Biolegend	Titration-dependent	Splenocyte proliferation assays
Biotin-SP Goat Anti-Mouse IgG, F(ab')$_2$ Fragment Specific	Goat	Polyclonal	Jackson Immunoresearch	1:20	Detection of Chimeric antigen receptors
APC streptavidin	-	-	Biolegend	2µg/ml	Detection of Chimeric antigen receptors
PE strepatvidin	-	-	Biolegend	2µg/ml	Detection of Chimeric antigen receptors
PercP/Cy5.5 anti-human CD8	Mouse	Monoclonal (SK1)	Biolegend	Titration-dependent	CART-cell activation and proliferation assays
PE anti-human CD45	Mouse	Monoclonal (HI30)	Biolegend	Titration-dependent	CART-cell activation and proliferation assays
FITC anti-human CD4	Mouse	Monoclonal (OKT4)	Biolegend	Titration-dependent	CART-cell activation and proliferation assays

3.6.2 Preactivation and expansion of human T cells

Human T cells (1 × 10^6 cells/ml) were cultured with CD3/CD28 activating Dynabeads (Thermo Fisher Scientific) at a bead-to-cell ratio of 3. On day 3 after bead stimulation, T-cell cultures were fed with ¾ culture volumes of fresh medium. On day 5 after bead stimulation, beads were removed by placing the cultures on DynaMag-15 magnet (Thermo Fisher Scientific) and recovering the supernatants. Cells were counted with the TC20 automated counter by setting the gates from 8 µm to 14 µm (resting T cells have a mean diameter of 6 µm, whereas proliferating T cells have a mean diameter of 10 µm), and cultures were set to 1 × 10^6 cells/ml. From this day on, cells were fed daily to a concentration of 8 x 10^5 cells/ml. Cells were maintained in culture while they were still in the expansion phase and just before they returned to a resting state. This was confirmed by diameter characterization with the TC20 counter and cultures were maintained for 10-11 days after bead stimulation. Aliquots (1-5 × 10^7 cells) were cryopreserved in FBS supplemented with 10% DMSO.

3.6.3 Generation of genetically-modified T cells

For the generation of luciferase- or CAR-expressing T cells, transduction with the corresponding lentiviral vectors was carried out 24 h after bead-mediated T-cell activation (see section 3.6.2). For the generation of luciferase-expressing T cells, cultures were infected with the CBG-T2A-GFP vector at an MOI of 5. For the generation of CAR T cells, cultures were infected with the SS1-ICOSz vector at an MOI of 2 or 20. Transduced T-cell cultures were expanded and handled as described in section 3.6.2. T-cell preparations were characterized for the expression of the transgene and phenotyped for CD4 and CD8 T-cell subpopulations by flow cytometry (see section 3.6.1). CAR T cell preparations were adjusted to contain 50% CAR^+ and 50% CAR^- T cells by adding the appropriate amount of untransduced (UTD) preactivated T cells from the same donor.

3.6.4 Binding assays

Cancer cells (2×10^5) or effector cells (1×10^5) were incubated with the different supernatants for 1 h on ice. Cells were washed 3x followed by incubation with the monoclonal M2 anti-FLAG antibody (Sigma Aldrich) or its corresponding IgG1 isotype control (Santa Cruz Biotechnology) for 1 h on ice. Cells were washed 3x and bound antibodies were detected by incubating cells with an Alexa Fluor 488- or 687-coupled (for binding to CD4 and CD8 T cells) goat anti-mouse IgG secondary antibody (Thermo Fisher Scientific) for 30 min on ice. To asses binding to T cell subsets, cells were further incubated with anti-CD4 or anti-CD8 antibodies for 30min on ice. Cells were evaluated by flow cytometry and 10000 events were acquired.

3.7. Coculture-based *in vitro* assays

3.7.1 Rosette formation assay

Jurkat cells (2.5×10^6) and A431-GFPLuc cells (5×10^5) were seeded in 24-well plates in a volume of 400 µl and 100 µl of the corresponding concentrated supernatants were added to the wells. Cocultures were incubated for 4 hours and contrast and fluorescent microscopy images were acquired. Composite images merging contrast and fluorescent pictures were generated with ImageJ.

3.7.2 T-cell activation assays

To evaluate human T-cell activation induced by the supernatants from virus-infected cells, cancer cells (3×10^4) and PBMCs (1.5×10^5) were seeded in 96-well plates in 100 µl medium. Cocultures were mixed with 100 µl of the supernatants and incubated for 48 hours. Cells were then stained for cell viability with LIVE/DEAD fixable stain (Thermo Fisher Scientific) followed by incubation with antibodies specific for CD8 and CD4 and CD69 or CD25. For the oncolysis-mediated T cell activation assays, 3×10^4 target cells/well (A549 or HCT116) and 1.5×10^5 PBMCs/well (E:T = 5) were seeded in 96-well plates in 100µl DMEM 10%. Cocultures were infected with 100µl of ICO15K or ICO15K-cBiTE (MOI = 20) and incubated for 5 days. Cells were processed as described above. Flow cytometry analysis was performed by acquiring 3×10^4 events per sample for both assays.

To evaluate murine T-cell activation, cancer cells (3×10^4) and splenocytes (3×10^5) were seeded in 96-well plates in 100µl medium supplemented with 100 µM 2-mercaptoethanol so that, after addition of the supernatants, the final concentration in the coculture was 50 µM. Cocultures were mixed with 100µl of the supernatants and incubated for 48 hours. Cells were then stained for cell viability with LIVE/DEAD fixable stain (Thermo Fisher Scientific) followed by incubation with antibodies specific for CD8 and CD4 and CD69 or CD25. Flow cytometry analysis was performed by acquiring 3×10^4 events per sample.

To evaluate the activation of CAR T-cell preparations, cancer cells (3×10^4) were seeded in 96-well plates and incubated overnight. The next day, the medium was removed and UTD or CAR T cells (1.5×10^5) were added to the wells in a final volume of 100 µl. Cocultures were mixed with 100 µl of the corresponding supernatants and incubated for 24 hours. Cells were then stained for cell viability with LIVE/DEAD fixable stain followed by incubation with antibodies for the detection of CAR, CD8, CD4 and CD25. Flow cytometry analysis was performed by acquiring 3×10^4 $CD45^+$ events per sample.

3.7.3 Cytokine production assay

Cancer cells (3×10^4) and PBMCs (1.5×10^5) were seeded in 96-well plates in 100µl medium. Cocultures were mixed with 100 µl of the supernatants and incubated for 48 hours. Coculture supernatants were harvested, centrifuged at 500 *g* for 5 min to discard cells, and stored at -80°C. Supernatants were assessed for cytokines with the human IFN-γ and TNF-α ELISA development kits (Peprotech) according to the manufacturer's instructions.

To evaluate cytokine production by CAR T-cell preparations, cancer cells (3×10^4) were seeded in 96-well plates and incubated overnight. The next day, the medium was removed and UTD or CAR T cells (1.5×10^5) were added to the wells in a final volume of 100 µl. Cocultures supernatants were harvested and processed as described above.

3.7.4 CFSE-based T-cell proliferation assay

To asses T-cell proliferation induced by the supernatants from virus infected cells, cancer cells (3×10^4) and CFSE-labeled PBMCs (1.5×10^5) were seeded in 96-well plates in 100µl medium. Cocultures were mixed with 100µl of the supernatants and incubated for 6 days. Cells were then stained for cell viability with LIVE/DEAD fixable stain (Thermo Fisher Scientific) followed by incubation with an anti-CD3 antibody. Flow cytometry analysis was performed by acquiring 20000 events per sample. For the oncolysis-mediated T-cell proliferation assays, 3×10^4 target cells/well (A549 or HCT116) and 1.5×10^5 PBMCs/well (E:T = 5) were seeded in 96-well plates in 100µl DMEM 10%. Cocultures were infected with 100 µl of ICO15K or ICO15K-cBiTE (MOI = 20) and incubated for 7 days. Cells were processed for cell viability as describe above, followed by surface staining for CD4 and CD8. Flow cytometry analysis was performed by acquiring 30000 events per sample.

To evaluate murine T-cell proliferation, cancer cells (3×10^4) and CFSE-labeled splenocytes (3×10^5) were seeded in 96-well plates in 100 µl medium supplemented with 100 µM 2-mercaptoethanol so that, after addition of the supernatants, the final concentration in the coculture was 50 µM. Cocultures were mixed with 100µl of the supernatants and incubated for 5 days. Cells were then stained for cell viability with LIVE/DEAD fixable stain (Thermo Fisher Scientific) followed by incubation with antibodies specific for CD8 and CD4. Flow cytometry analysis was performed by acquiring 30000 events per sample for both assays.

3.7.5 Luciferase-based T-cell proliferation assay

Luc-T cells (1×10^5) were cocultured with HCT116 cells (E:T= 5) in 96-well plates. Cocultures were mixed with the supernatants (100 µl) and incubated for 6 days. Cells were transferred to a round-bottom 96-well plate and centrifuged at 500 *g* for 5 minutes. Supernatants were carefully discarded and cells were resuspended in 50 µl Reporter lysis buffer (Promega) containing protease inhibitor cocktail (Roche), followed by a freeze-thaw cycle to ensure cell lysis. Lysates were centrifuged and 8 µl of the supernatants were mixed

with 20 µl of Luciferase Assay Reagent (Promega). Luciferase activity was measured in a Berthold Junior luminometer (Berthold GmbH & Co.). Results are expressed as relative light units.

3.7.6 Counting beads-based T-cell proliferation assay

To evaluate the proliferation of CAR T-cell preparations, cancer cells (3×10^4) were seeded in 96-well plates and incubated overnight. The next day, the medium was removed and UTD or CAR T cells (1.5×10^5) were added to the wells in a final volume of 100 µl. Cocultures were mixed with 100 µl of the corresponding supernatants and incubated for 5 days. Cells were then stained for cell viability with LIVE/DEAD fixable stain followed by incubation with antibodies for CD45, CD8 and CD4. Cells were resuspended in a final volume of 200 µl with a known amount of CountBright Absolute Counting Beads (Thermo Fisher Scientific). Flow cyometry analysis was performed by acquiring a total of 2000 bead events. The absolute number of the corresponding T-cell subpopulation was calculated according to the manufacturer's instructions. The absolute T-cell number at day 5 was normalized to that of samples from day 0 which had been processed as described above.

3.7.7 Inhibitory markers expression assay

This experiment was carried out in collaboration with Sonia Guedan at the University of Pennsylvania. L55 tumor cells (1×10^5) were seeded in 48 well/plates and infected with ICO15K or ICO15K-BiTE at an MOI of 1. T cells (2×10^5) were added 24 hours after virus infection. 6 days after coculture, cells were collected, and stained with live/dead viability stain, followed by surface staining for CD3, CD4, CD8, PD1, TIM-3, LAG-3 and CD200. Cells were analyzed on a BD Fortessa as described by the manufacturer.

3.7.8 Cell-mediated cytotoxicity assays

3.7.8.1 CFSE/7-AAD cytotoxicity assay

CFSE-labeled target cells (3×10^4) were cocultured with PBMCs (3×10^5) in 100 µl medium in 96-well plates. Cocultures were mixed with 100 µl of the supernatants and incubated for 24 h. Cocultures were trypsinized and stained with 10 µg/ml 7-amino-actinomycin D (7-AAD) (Enzo Life Sciences) for 30 min on ice. After washing, cells were analyzed by flow cytometry and the percentage of $CFSE^+/7\text{-}AAD^+$ cells was determined. 10000 $CFSE^+$ events were acquired for each sample.

For cytotoxicity assays with murine splenocytes, CFSE-labeled target cells (3×10^4) were cocultured with splenocytes (3×10^5) in 100µl medium in 96-well plates. Cocultures were mixed with 100µl of the supernatants and incubated for 48 h. Cocultures were processed and evaluated as described above. 10000 $CFSE^+$ events were acquired for each sample.

3.7.8.2 Bystander killing assay

A549 cells in suspension were infected with ICO15K or ICO15K-cBiTE at an MOI of 20 for 4 hours. Excess virus was removed by washing the cells with PBS. 2.5×10^4 virus-infected A549 cells per well and 2.5×10^4 A431-GFPLuc per well were cocultured with 1.5×10^5 PBMCs (E:T = 6 with respect to A431-GFPLuc cells) in 96-well plates in a final volume of 200µl medium. Cocultures without PBMCs were used as a control for virus-mediated cell cytotoxicity. 5 days after infection, cocultures were trypsinized and stained with 7-AAD as described in section 3.7.8.1. After washing, cells were resuspended in 200 µl FACS buffer containing a known amount of CountBright Absolute Counting Beads (Thermo Fisher Scientific), and flow cyometry analysis was conducted. A total of 2000 bead events were acquired. The absolute number of live A431-GFPLuc was calculated with counting beads according to the manufacturer's instructions, and the percentage of live A431-GFPLuc was obtained by normalizing the absolute count of the samples to that of culture of untreated A431-GFPLuc cells.

3.7.8.3 Oncolysis and cell-mediated cytotoxicity assay

These experiments were carried out in collaboration with Sonia Guedan at the University of Pennsylvania. Oncolysis-mediated enhanced cell-mediated cytotoxicity was evaluated with the xCELLigence Real-Time Cell Analyzer System (ACEA Biosciences). A549 or HCT116 cells (1×10^4) were seeded and infected with ICO15K or ICO15K-cBiTE at an MOI of 1 in 150 µl of medium. After overnight tumor cell adherence to the well bottom, 50 µl of effector cells (CAR T cells or preactivated T cells) were added at an effector:target ratio of 5. Cell index (*i.e.* relative cell impedance) values were monitored every 20 minutes for 120 h and normalized to the maximal cell index value immediately prior to effector cell plating.

3.8 *In vivo* studies

3.8.1 Mouse models and procedures

All animal experiments were approved by Ethics Committee for Animal Experimentation from the Biomedical Research Institute of Bellvitge (IDIBELL). Animals were housed in the IDIBELL Animal Core Facility (AAALAC Unit 1155). Subcutaneous A549 and HCT116 were established by 100 µl-injections containing 5×10^6 and 2.5×10^6 cells, respectively, into both flanks of 8-week old female SCID/beige mice (Envigo). When tumors reached ~100mm^3 mice were randomized and treated as described below.

For the T-cell biodistribution study, tumors received a 50 µl-injection of 2×10^9 VP of the indicated viruses or PBS. After 5 days, mice received an intravenous injection of 1×10^7 cell preparations containing 59% preactivated CBG luciferase-expressing T cells, followed by an intraperitoneal dose of 1500 IU IL-2 (Peprotech). Mice were imaged daily until day 9 with the IVIS Lumina XRMS Imaging System (PerkinElmer) after administering intraperitoneal injections of a 15 mg/ml D-luciferin firefly potassium salt solution (Biosynth AG). Tumor radiance was measured by drawing a region of interest around the tumor contour.

For antitumor efficacy, A549 tumors received a 50 µl-injection of 2×10^9 VP of the indicated viruses or PBS. After 4 and 18 days, PBS or 1×10^7 unstimulated human PBMCs were administered to the mice by intravenous injection. Mice bearing HCT116 tumors received a 200-µl intravenous injection of 1×10^{10} VP of the indicated viruses or PBS. After 4, 8 and 11 days, mice received an intravenous injection of 1×10^7 preactivated T cells followed by an intraperitoneal injection of 1500 IU IL-2. In both models, tumors were measured every 2-4 days and the volume was calculated as V (mm^3) = $\pi/6 \times W^2 \times L$, where W and L are the width and the length of the tumor, respectively.

3.8.2 Immunohistofluorescence of OCT-embedded tumor sections

OCT-embedded tumor sections were thawed at room temperature for 20 minutes. Slides were then fixed with 4% paraformaldehyde for 5 minutes at room temperature. Paraformaldehyde excess was removed by washing slides in bi-distilled water and subsequent 3x 5-minute washing steps in PBS 0.1% Triton. Unspecific binding was blocked by incubating sections with PBS 20% goat serum for 1 hour at room temperature in a humidity chamber. Excess liquid was carefully removed and primary rabbit anti-E1a antibody (diluted

1:50 in PBS 5% goat serum) was applied to one of both section in the slide. The other section was incubated with PBS 5% goat serum as a control for unspecific binding. Slides were incubated overnight at 4°C in a humidity chamber. The next day, slides were brought to room temperature for 20 minutes and excess liquid was carefully removed. Slides were washed 3x with PBS 0.1% Triton. Next, an Alexa488-coupled goat anti-rabbit IgG secondary antibody diluted in PBS 5% goat serum was applied to the section and incubated for 1 hour at RT. Slides were washed with PBS, Vectashield (Vectorlabs) mounting medium was applied and coverslips were mounted on top of the sections. Fluorescence microscopy was carried out with a Nixon Microscope.

3.8.3 Immunohistochemistry of paraffin-embedded tumor sections

The detection of FLAG tag by immunohistochemistry was performed by the histopathology core facility of the Institute for Research in Biomedicine (IRB) as follows. 3 µm Paraffin-embedded tumor sections were air dried and further dried at 60°C over-night. For immunohistochemical detection, sections were dewaxed and antigen retrieval process was done with citrate buffer pH6 for 20 min at 97°C using a PT Link (Dako – Agilent). Quenching of endogenous peroxidase was performed by 10 min of incubation with Peroxidase-Blocking Solution (Dako). Blocking of unspecific unions was done using 10% goat normal serum (Life technologies) and 1% of bovine serum albumin (Sigma-Aldrich). Rabbit monoclonal anti-FLAG primary antibody (Cell signalling) was diluted 1:20 and incubated over night at 4°C. The secondary antibody used was BrightVision Poly-HRP-Anti Rabbit IgG Biotin-free (Immunologic). Antigen–antibody complexes were reveled with 3-3'-diaminobenzidine (Dako), with the same time exposure per antibody (10 min). Sections were counterstained with hematoxylin (Dako) and mounted with Toluene-Free Mounting Medium (Dako) using a Dako CoverStainer. Specificity of staining was confirmed by omission of the primary antibody.

3.8.4 Detection of transgene and viral transcripts in tumors by Real-Time PCR

Frozen tumor samples were disrupted using a mortar and pestle under liquid nitrogen. Approximately 25mg of tissue were homogenized with Qiashredder homogenizers, and RNA was isolated with the RNeasy kit (Qiagen) including on-column DNase I digestion to remove genomic DNA. RNA (1 µg) was retrotranscribed with the High-capacity cDNA Reverse Trancription kit (Thermo Fisher Scientific). cDNA samples were diluted 1:5 with ddH_2O.

Real time was performed using a LightCycler ® 480 Instrument II (Roche) in the presence of SYBR Green I Master (Roche). PCR reactions (10 µl) were prepared containing 4µl of the diluted cDNA sample, 5 µl of SYBR Green I Master 2x, 4 pmol of each primer and ddH_2O to complete the volume. The primers used for the detection of cBiTE and hexon cDNA are listed in table 10 and PCR conditions are listed in table 11. Standard curves for cBiTE and hexon were prepared by serial dilutions of known copy numbers of pUC57-cBiTE or purified ICO15K genomes, respectively. Non-retrotranscribed RNA samples, equivalent to the amount cDNA loaded in the PCR, were run to discard genomic DNA contamination. After PCR, melting curve analysis was performed to discard primer dimer formation or unspecific product amplification.

Table 10. Primers for the detection of cBiTE and hexon cDNA

Primer name	Sequence 5' → 3'	Description
qBiTE F	CGGCGAGAAAGTGACAATGAC	For the detection of cBiTE cDNA
qBiTE R	TTGGTGAGGTGCCACTTTTC	For the detection of cBiTE cDNA
Ad18852	CTTCGATGATGCCGCAGTG	For the detection of hexon cDNA
Ad19047R	ATGAACCGCAGCGTCAAACG	For the detection of hexon cDNA

Table 11. PCR conditions for the detection of cBiTE and hexon cDNA

Stage	Description	Temperature	Time	Cycles
1	Activation	95°C	10 minutes	1
2	Amplification Cycles	95°C	15 seconds	40
		60°C	1 minute	
		72°C	7 seconds	

3.9 Statistical analysis

For comparisons of 2 groups, two-tailed unpaired t tests were used. For comparison of more than two groups, One-way ANOVA with Tukey post-hoc tests was used. Statistical significance was established as $P < 0.05$. Data are presented as the mean ± SD or SEM. All statistical analyses were calculated with the GraphPad Prism software v6.02.

4. RESULTS

4.1 Bispecific T-cell engager-armed oncolytic adenoviruses

The antiviral immune response represents one of the major hurdles for the success of oncolytic adenoviruses (OAds) in cancer patients. Despite the highly immunosuppressive environment at the tumor site, Ad-infected cells can be efficiently cleared from the organism by infiltrating Ad-specific CTLs without compromising the tumor burden [57]. We hypothesize that arming OAds with BiTEs might favor antitumor rather than antiviral immune responses by activating and redirecting any T cell that infiltrates the tumor.

4.1.1 A BiTE-armed oncolytic adenovirus targeting human EGFR and human CD3

To test our hypothesis, we envisioned an OAd that, upon infection of cancer cells, leads to the secretion of a BiTE that redirects T cells towards cancer cells. Since the OAd platforms developed in our laboratory are intended for the treatment of solid tumors, the selection of a BiTE targeting a TAA expressed within the tumor microenvironment is mandatory. Several antigens overexpressed in solid tumors have been evaluated in preclinical studies as targets for BiTEs [175-179]. From these, the EGFR is an attractive target due to the vast knowledge of its molecular biology, and due to its well-documented overexpression in several human solid tumors [180, 181]. We therefore chose the EGFR as a target for our BiTE-armed OAd.

4.1.1.1 Generation and characterization of ICO15K-cBiTE

We have previously reported the generation of the OAd ICO15K, an E1a-Δ24-based Ad which incorporates palindromic E2F binding sites in the *E1a* promoter and bears an RGDK motif replacing the KKTK heparan sulfate glycosaminoglycan-binding domain in the fiber shaft [47]. This virus has shown favorable toxicity profiles and increased tumor targeting *in vivo*, and we therefore chose it as a platform to incorporate a BiTE targeting the EGFR (cBiTE) into its genome (Figure 18).

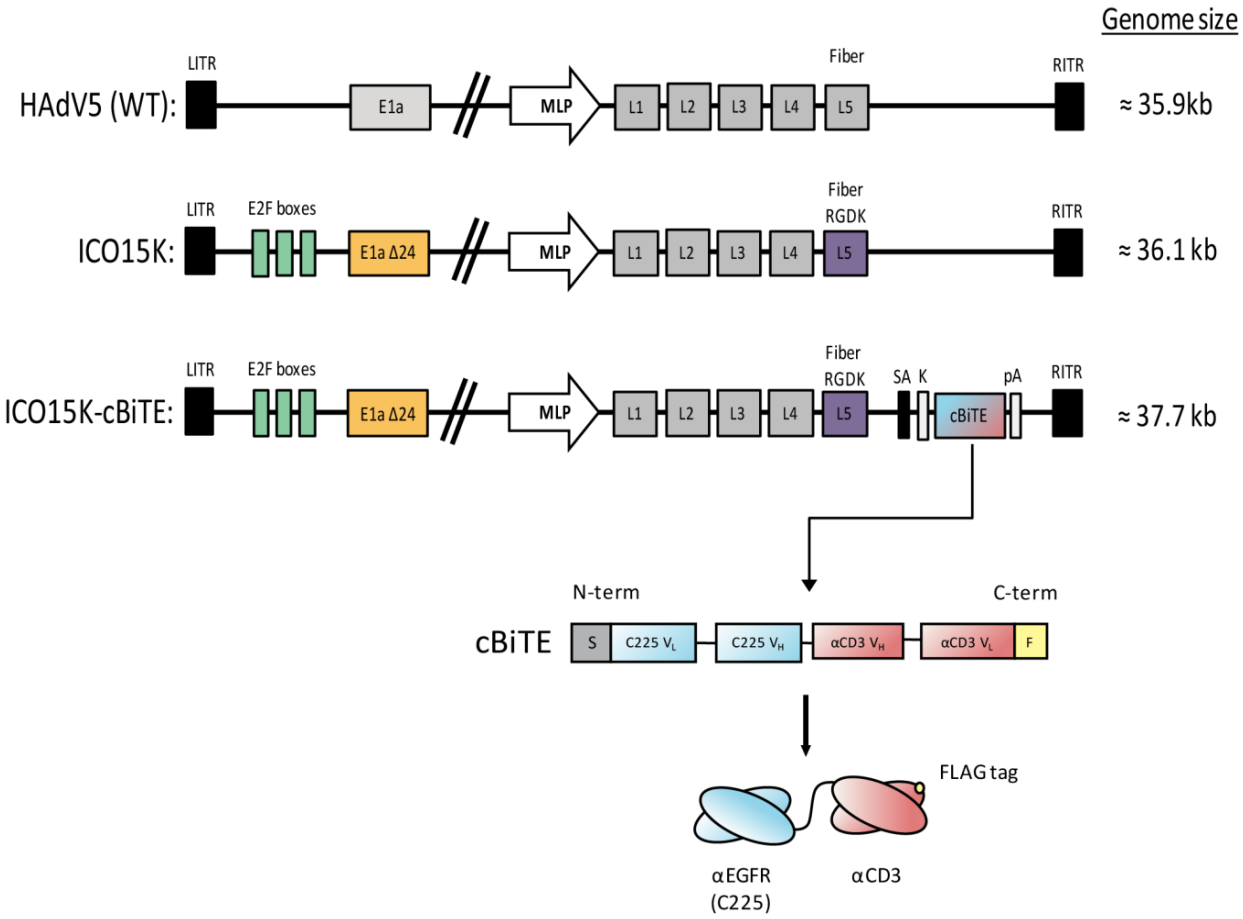

Figure 18. Schematic representation the ICO15K-cBiTE genome. The virus ICO15K carries the Δ24 mutation in the *E1a* gene and its expression is controlled by palindromic E2F binding sites located in the promoter of the gene. This virus also contains an RGDK motif replacing the KKTK heparan sulfate glycosaminoglycan-binding domain in the shaft of the fiber (L5). The cBiTE gene contains a signal peptide sequence (S), an anti-EGFR scFV derived from the Cetuximab antibody (C225), an anti-CD3 scFV derived from the blinatumomab BiTE and a FLAG tag (F) for detection purposes. For proper expression of the BiTE, the gene was flanked by a kozac sequence (K) and a polyadenylation signal (pA). The cBiTE gene was located after the fiber gene, and it was placed under the control of the major late promoter (MLP) by including a splicing acceptor (SA) upstream of the kozac sequence.

We designed the cBiTE by joining a scFV version of the FDA-approved monoclonal antibody Cetuximab and the anti-CD3 scFV from Blinatumomab through a peptide linker. The cBiTE gene also encodes the signal peptide from the mouse Ig heavy chain at the N-terminus of the protein to support its secretion from the cell, and a FLAG tag at the C-terminus for detection purposes. For enhanced and correct translation of the protein, the construct included a kozak sequence upstream of the starting codon, and a polyA site downstream of the stop codon. The adenovirus IIIa splicing acceptor was placed upstream of the kozak sequence in order to control the cBiTE expression from the MLP. This strategy was

chosen to avoid a potential BiTE-mediated interference with virus replication. The genome of ICO15K was genetically engineered by homologous recombination in bacteria to place the cBiTE construct downstream of the fiber gene as an L6 unit. The virus ICO15K-cBiTE was successfully rescued and amplified to similar physical and functional titers as those of ICO15K (Table 12).

Table 12. Virus production quality control

Virus	Physical titer (VP/ml)	Functional titer (TU/ml)	Physical:functional ratio
ICO15K	2.66×10^{12}	1.47×10^{11}	18.1
ICO15K-cBiTE	3.32×10^{12}	1.68×10^{11}	19.8

To characterize the oncolytic properties of the modified virus, dose-response cytotoxicity assays with cancer cells were performed. Although ICO15K-cBiTE showed dose-dependent oncolytic properties *in vitro*, its IC_{50} values increased 2.1- and 1.4-fold compared to its parental counterpart in A549 and HCT116 cancer cells, respectively (Figure 19A). To further evaluate this loss in cytotoxicity, we compared virus production in a panel of cancer cell lines after 72h of infection. The total production of ICO15K-cBiTE was reduced 1.3-fold in A549 cells compared to ICO15K, which may explain the loss in oncolysis observed in the cytotoxicity assays (Figure 19B).

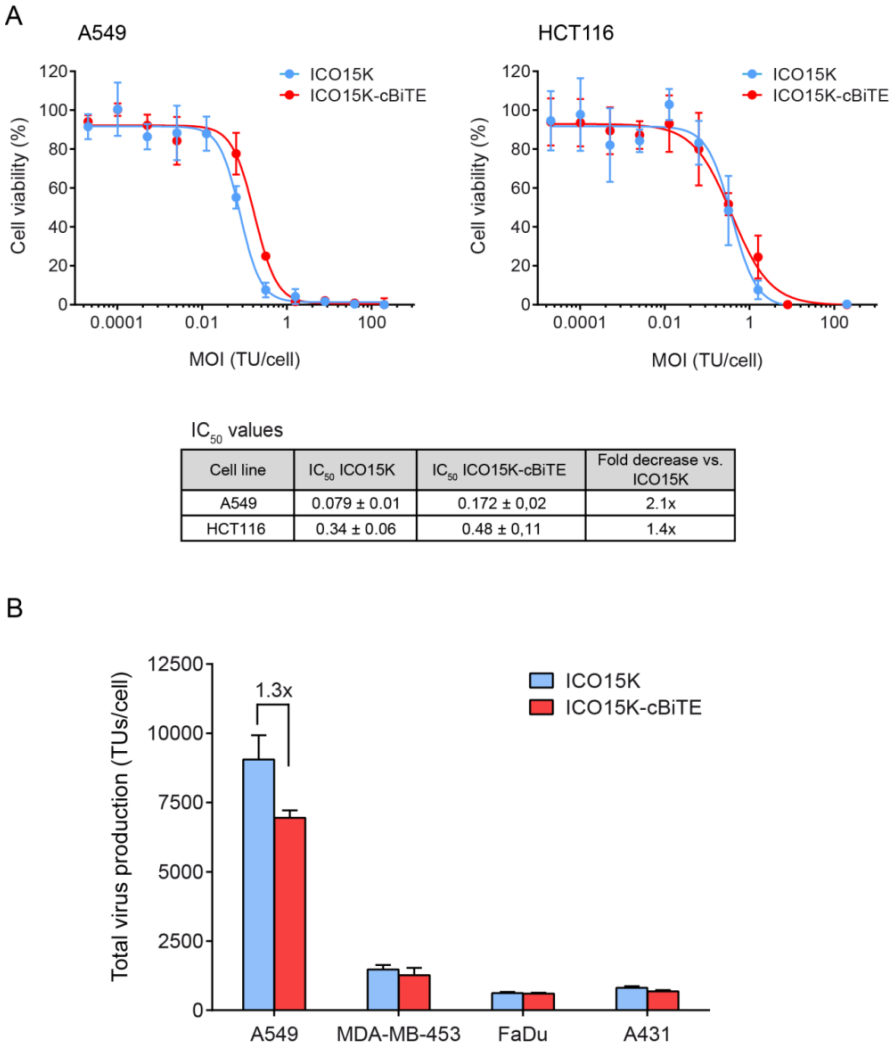

IC_{50} values

Cell line	IC_{50} ICO15K	IC_{50} ICO15K-cBiTE	Fold decrease vs. ICO15K
A549	0.079 ± 0.01	0.172 ± 0,02	2.1x
HCT116	0.34 ± 0.06	0.48 ± 0,11	1.4x

Figure 19. *In vitro* characterization of ICO15K-cBiTE. (A) A549 and HCT116 cell lines were incubated with serial dilutions of ICO15K or ICO15K-cBiTE, with multiplicity of infections (MOIs) ranging from 200 to 0 TU/cell. 6 days post-infection, cell viability was determined and the IC_{50} for each virus was calculated. The mean ± SD of triplicates is shown. **(B)** The indicated cell lines were infected with ICO15K or ICO15K-cBiTE at an MOI of 20 for 4 hours. Excess virus was then washed and cells were incubated for 72 hours. Total virus production in the culture cell extracts was determined with anti-hexon staining method. Results are expressed as transducing units produced per cell. The mean ± SD of triplicates is shown.

4.1.1.2 Cells infected with ICO15K-cBiTE secrete cBiTE antibodies which specifically bind to target and effector cells

To characterize the cBiTE, a panel of cancer cell lines with varying EGFR expression levels and also $CD3^+$ Jurkat and human peripheral blood mononuclear cells (PBMCs) were used (Figures 20A and B).

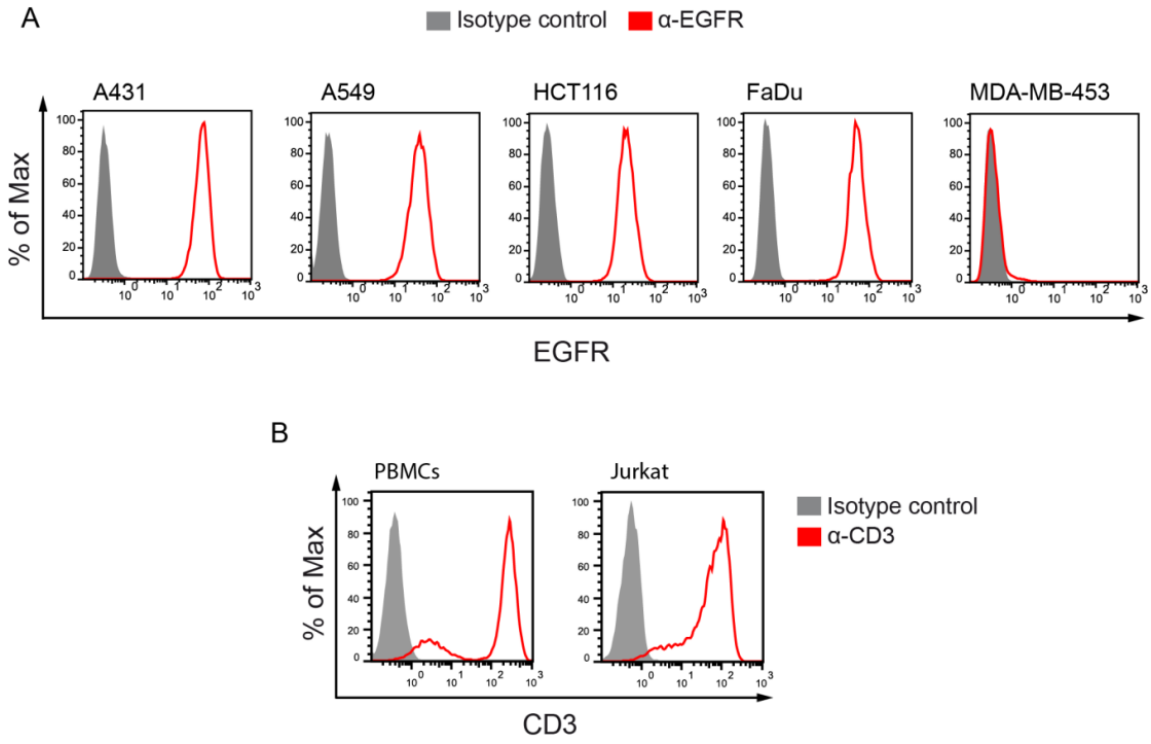

Figure 20. EGFR and CD3 profiles of the cell lines used in the study. (A) A panel of cancer cell lines was evaluated for EGFR expression by flow cytomery. Cells were incubated with an anti-EGFR antibody or its corresponding isotype control, followed by the incubation with an Alexa488-coupled secondary antibody. **(B)** Jurkat cells and human PBMCs from healthy donors were evaluated for CD3 expression by flow cytometry. Cells were incubated with the OKT3 anti-CD3 antibody or its corresponding isotype control, followed by the incubation with an Alexa488-coupled secondary antibody. For PBMCs samples, the CD3 analysis was performed after gating the lymphocyte population on the FSC vs. SSC plot.

To evaluate the secretion of the cBiTE by infected cells, flow cytometry-based binding assays were performed by exploiting the FLAG tag encoded in the transgene. cBiTE antibodies were only detected in the supernatants of ICO15K-cBiTE-infected cells, and they specifically bound to $EGFR^+$ (A431, A549, HCT116 and FaDu) but not $EGFR^-$ (MDA-MB-453) cancer cells (Figure 21A). To demonstrate that the anti-EGFR scFV retained the specificity of the cetuximab antibody as a BiTE molecule, a competition binding assay with Cetuximab was performed. The preincubation of A431 cells with Cetuximab impaired the binding of the cBiTE to the cells in a dose-dependent manner, confirming the specificity of the Cetuximab-derived scFV in the cBiTE (Figure 21B).

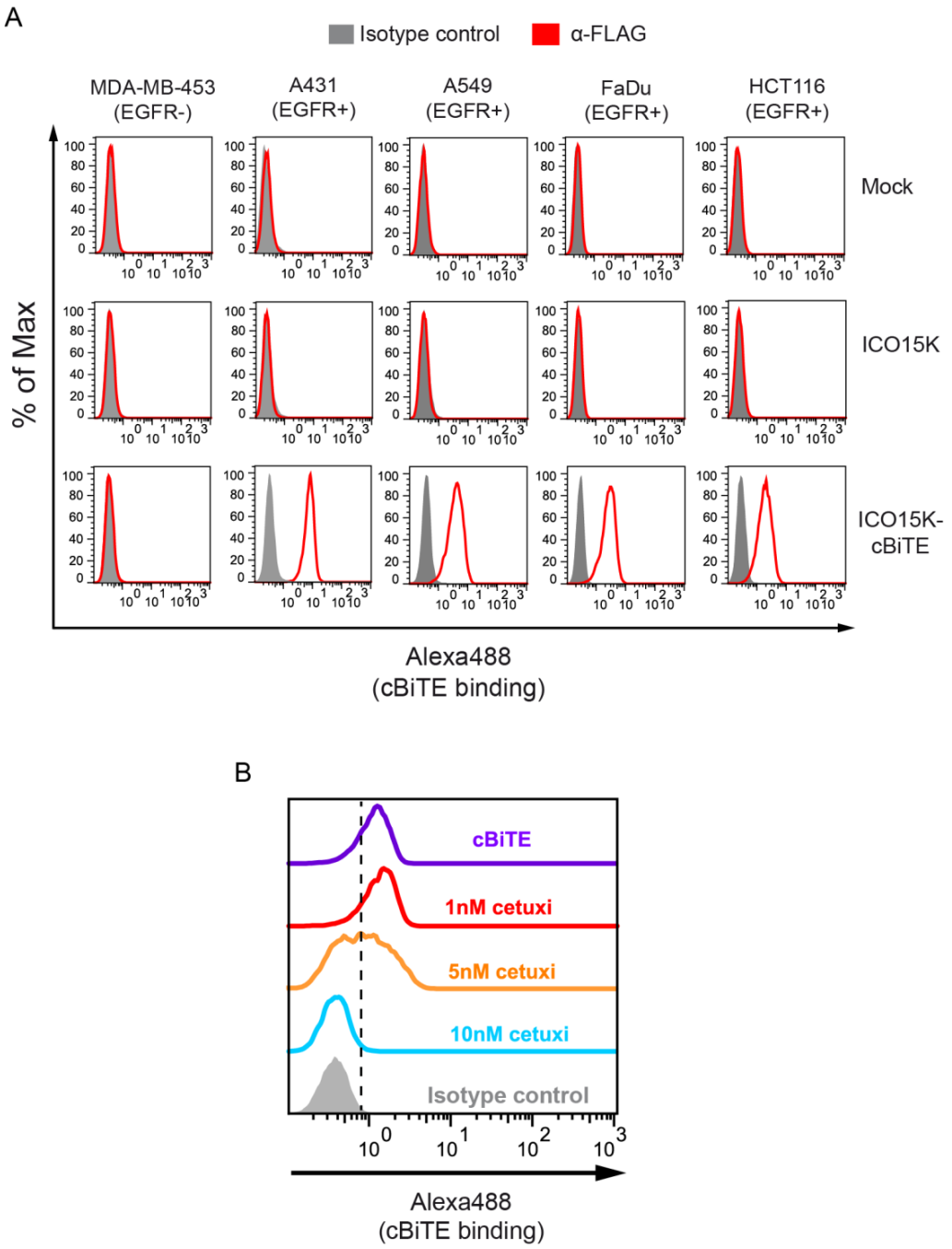

Figure 21. cBiTE antibodies are expressed from ICO15K-cBiTE-infected cells and specifically bind to target cells. **(A)** The indicated cell lines were incubated with the supernatants of ICO15K- or ICO15K-cBiTE-infceted A549 cells. The supernatants from uninfected cells (mock) were used as a negative control. cBiTE binding was detected by incubating cells with an anti-FLAG antibody and an Alexa488-coupled secondary antibody. Cells were analyzed by flow cytometry. The corresponding isotype control for the anti-FLAG antibody was used as a negative control. **(B)** A431 cells were preincubated with the indicated concentrations of Cetuximab. Cells were then incubated with the supernatant of ICO15K-cBiTE-infected A549 cells, and cBiTE binding was detected by flow cytometry as in A.

cBiTE antibodies also bound to $CD3^+$ Jurkat cells and human PBMCs, and this binding was more pronounced when supernatants were concentrated (Figure 22A). Furthermore, the binding of the cBiTE to $CD4^+$ and $CD8^+$ T cells within the PBCMs was further confirmed (Figure 22B).

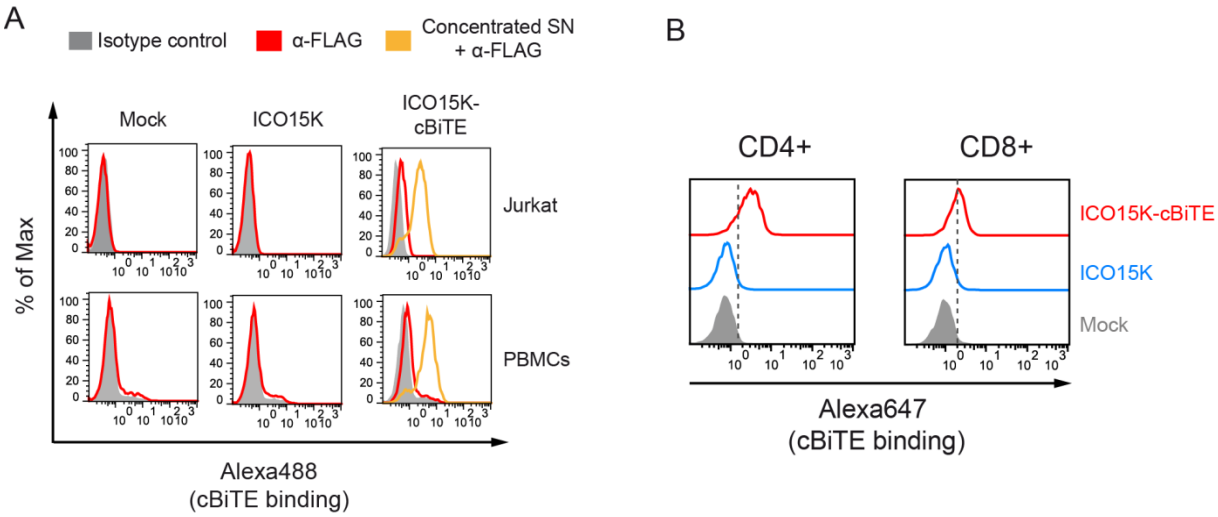

Figure 22. cBiTE antibodies expressed from ICO15K-cBiTE-infected cells bind to effector T cells. (A) Human PBMCs and Jurkat cells were incubated with the indicated supernatants. cBiTE binding was detected by incubating cells with an anti-FLAG antibody and an Alexa488-coupled secondary antibody. For PBMCs samples, binding analysis was performed after gating the lymphocyte population on the FSC vs. SSC plot. **(B)** Human PBMCs were incubated with the indicated concentrated supernatants. cBiTE binding to $CD4^+$ and $CD8^+$ T cells was detected by incubating cells with an anti-FLAG antibody and an Alexa647-labeled secondary antibody, followed by staining of CD4 and CD8. Cells were analyzed by flow cytometry. The corresponding isotype control for the anti-FLAG antibody was used as a negative control.

We then assessed whether cBiTE molecules could engage T cells towards cancer cells by binding to the EGFR and CD3 simultaneously. For this, a rosette-formation assay was conducted by coculturing trypsinized A431-GFPLuc cells with Jurkat cells and the different supernatants for 4 hours. Microscopy analysis revealed the aggregation of Jurkat cells around fluorescent cancer cells only in the cocultures that included the supernatant of ICO15K-cBiTE (Figure 23). Furthermore, rosettes (*i.e.* T cells surrounding a cancer cell) were clearly identified in the same cocultures when images were taken at higher magnifications, confirming the cBiTE-mediated recruitment of T cells towards cancer cells.

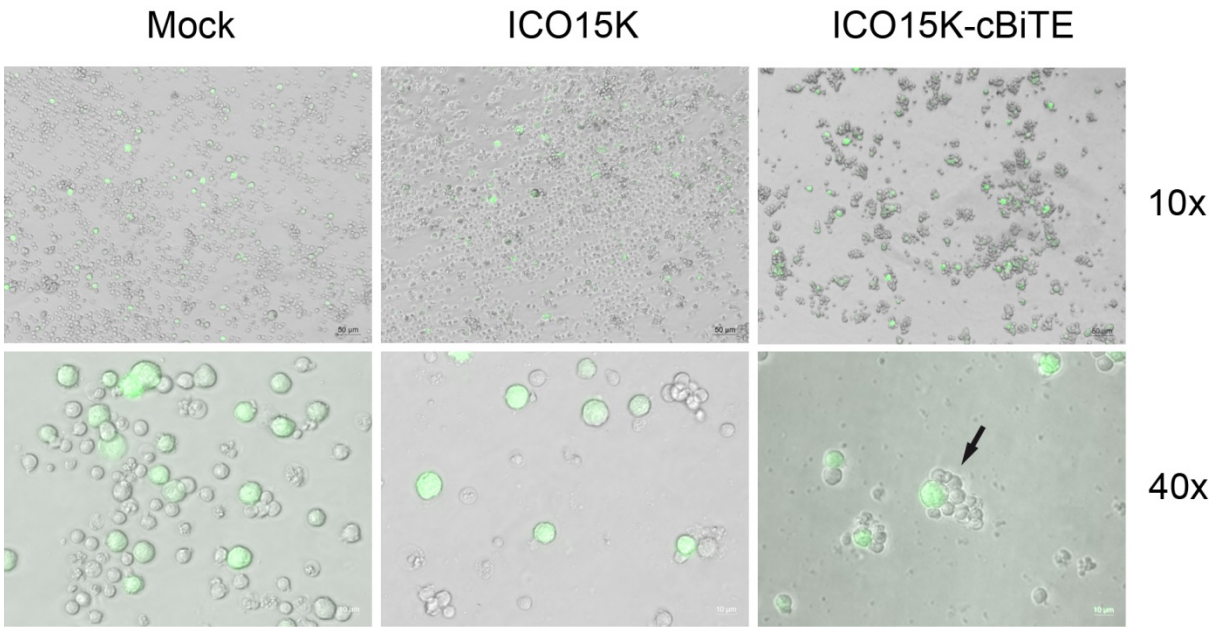

Figure 23. Supernatants from ICO15K-cBiTE-infected cells engage T cells towards cancer cells. Cocultures of A431-GFPLuc cells and Jurkat cells were treated with concentrated supernatants from uninfected (mock), ICO15K or ICO15K-cBiTE-infected A549 cells. 4 hours after coculture fluorescent and light microscopy images were taken from the same field of view and composite images were generated with the ImageJ software. Images were evaluated for Jurkat cell aggregation around fluorescent A431 cells (green), also known as Rosettes (black arrow).

4.1.1.3 Supernatants from ICO15K-cBiTE-infected cells enhance T-cell function

We then evaluated the functionality of the secreted cBiTE in coculture experiments of cancer cells with human PBMCs. ICO15K-cBiTE supernatants specifically induced $CD8^+$ and $CD4^+$ T-cell activation, as indicated by an increase in the expression of the activation markers CD25 and CD69 when PBMCs were cocultured with EGFR+ cell lines (Figure 24A). To confirm this activation, we assessed cytokine production by PBMCs in coculture assays with a panel of cancer cell lines. IFN-γ and TNF-α were detected at high levels only when ICO15K-cBiTE supernatants were cocultured with PBMCs and $EGFR^+$ cell lines. Importantly, the cBiTE-containing supernatants did not induce T-cell activation when cocultured alone or with the $EGFR^-$ cell line MDA-MB-453 (Figure 24B).

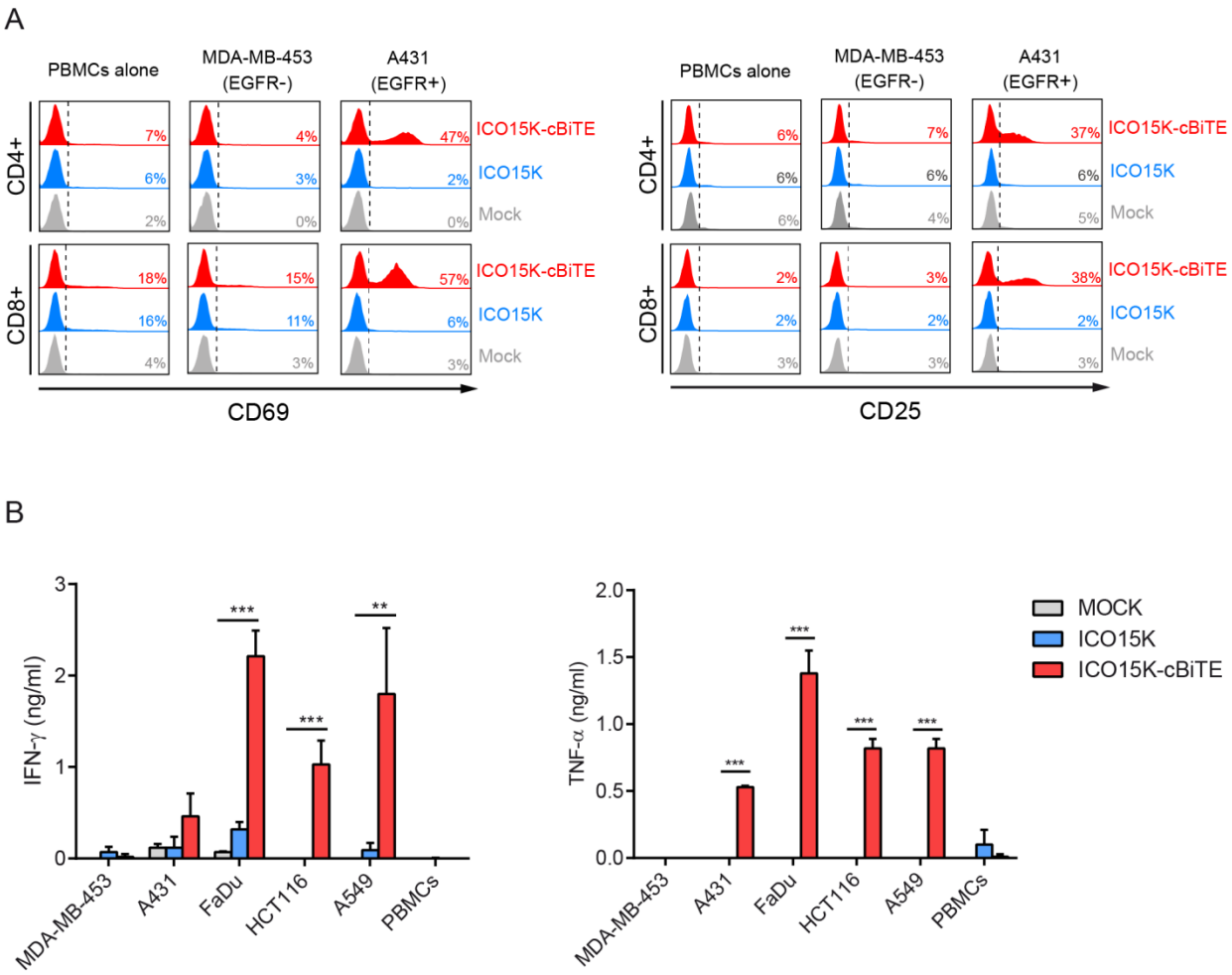

Figure 24. cBiTE antibodies expressed from ICO15K-cBiTE-infected cells induce T-cell activation. (A) Human PBMCs were cocultured with A431 or MDA-MB-453 cells (E:T = 5) in the presence of supernatants from uninfected (mock), ICO15K or ICO15K-cBiTE-infected A549 cells. 48h after coculture, the expression levels of CD25 and CD69 on $CD4^+$ and $CD8^+$ T cells were assessed by flow cytometry. Representative results from one of two healthy donors are shown. **(B)** A panel of cancer cell lines was cocultured with PBMCS (E:T = 5) in the presence of the indicated supernatants. 48 h after cocultures, supernatants were harvested and cytokine production was evaluated by ELISA. Representative results from one of two healthy donors are shown. Bars represent the mean ± SD of triplicates. **, $P < 0.01$; ***, $P < 0.001$ by One-way ANOVA with Tukey post-hoc test.

Another important indicator of T-cell activation is their proliferative capacity. Proliferation was assessed by flow cytometry after coculture of CFSE-labeled PBMCS with cancer cells and the corresponding supernatants. $CD3^+$ T cells underwent multiple rounds of proliferation only when PBMCs were cocultured with $EGFR^+$ A431 cells and ICO15K-cBiTE supernatants, as evidenced by the dilution of CFSE after 6 days of incubation (Figure 25).

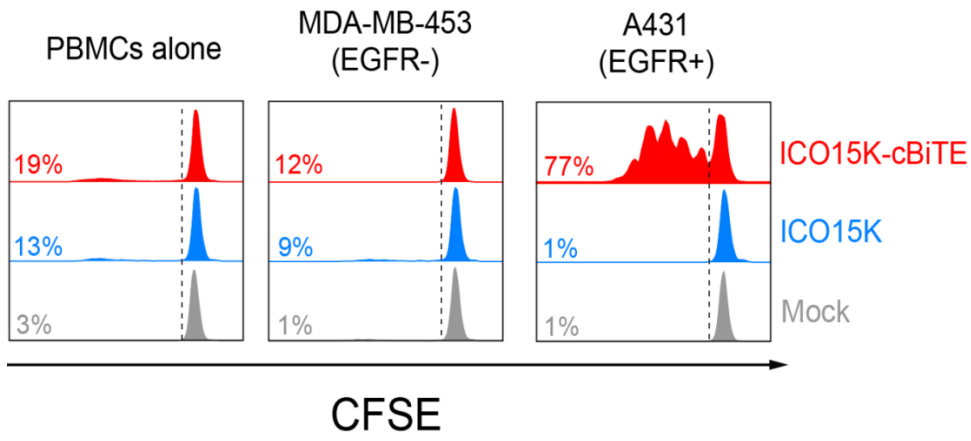

Figure 25. cBiTEs expressed from ICO15K-cBiTE-infected cells induce T-cell proliferation. CFSE-labeled PBMCs were cocultured with A431 or MDA-MB-453 cells (E:T = 5) in the presence of the indicated supernatants. 5 days after coculture, CFSE dilution (*i.e.* cell proliferation) in $CD3^+$ cells was evaluated by flow cytometry. Representative results from one replicate from one of two healthy donors are shown.

The ultimate goal of BiTE antibodies is to retarget T-cell-mediated cytotoxicity towards cancer cells. To confirm this, we performed flow cytometry-based cell-mediated cytotoxicity assays by coculturing CFSE-labeled A431 or MDA-MB-453 cells with PBMCs and the different supernatants for 24 hours. The coculture of A431 but not of MDA-MB-453 cells with the cBiTE-containing supernatants and PBMCs led to a significant increase in cell cytotoxicity compared to ICO15K and the mock control (Figure 26A). Further assays demonstrated that PBMCs preparations from different donors induce a significant increase in the cytotoxicity of A431 cells in the presence of the cBiTE, and the extent of cell death was donor-dependent (Figure 26B).

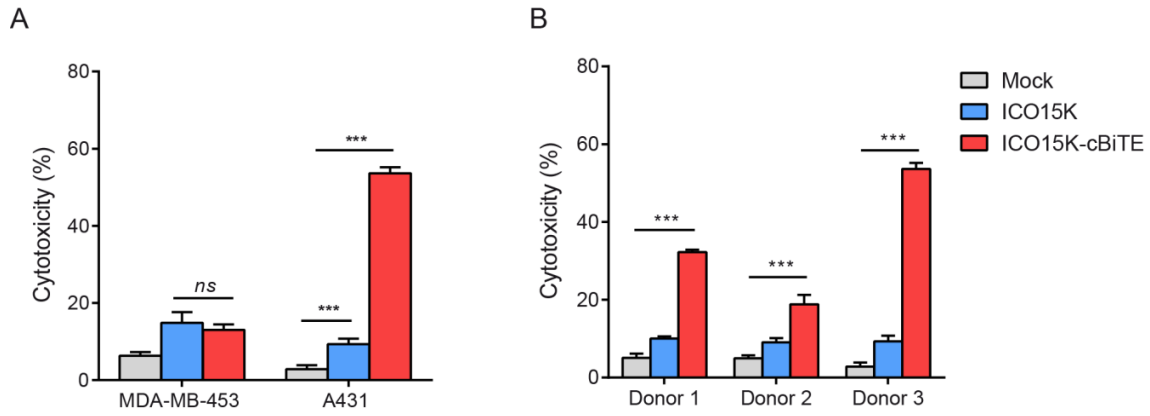

Figure 26. cBiTEs expressed from ICO15K-cBiTE-infected cells enhance T-cell-mediated cytotoxicity. (A) Cocultures of PBMCs with CFSE-labeled MDA-MB-453 or A431 cells (E:T = 10) were treated with the different supernatants. 24 h after coculture, cells were stained with 7-AAD and the percentage of cytotoxicty on target cells ($CFSE^+/7AAD^+$) was assessed by flow cytometry. Representative results from one of three healthy donors are shown. **(B)** Cytotoxicity of A431 cells under the same conditions described in (A) with PBMCs from three different healthy donors. Bars represent the mean ± SD of triplicates ***, $P < 0.001$ by One-way ANOVA with Tukey post-hoc test.

4.1.1.4 ICO15K-cBiTE-mediated oncolysis enhances T-cell function and induces T-cell-mediated bystander effect

The experiments described above were performed with supernatants of infected cells that contained the cBiTE. We next wanted to evaluate the cBiTE-expressing virus in a setting that more closely resembles a therapeutic oncolytic process. For this, cocultures of human PBMCS with either A549 or HCT116 $EGFR^+$ cell lines were infected at an MOI of 20 with respect to cancer cells. Cells were incubated for 5 or 7 days to address activation or proliferation, respectively. These incubation times were chosen in order to allow a full replication cycle of the virus and the proper action of the cBiTE. ICO15K-cBiTE-mediated oncolysis led to an increase in $CD25^+$ and $CD69^+$ T cells and to extensive proliferation of both T-cell subsets only when cancer cells were present (Figures 27A and B).

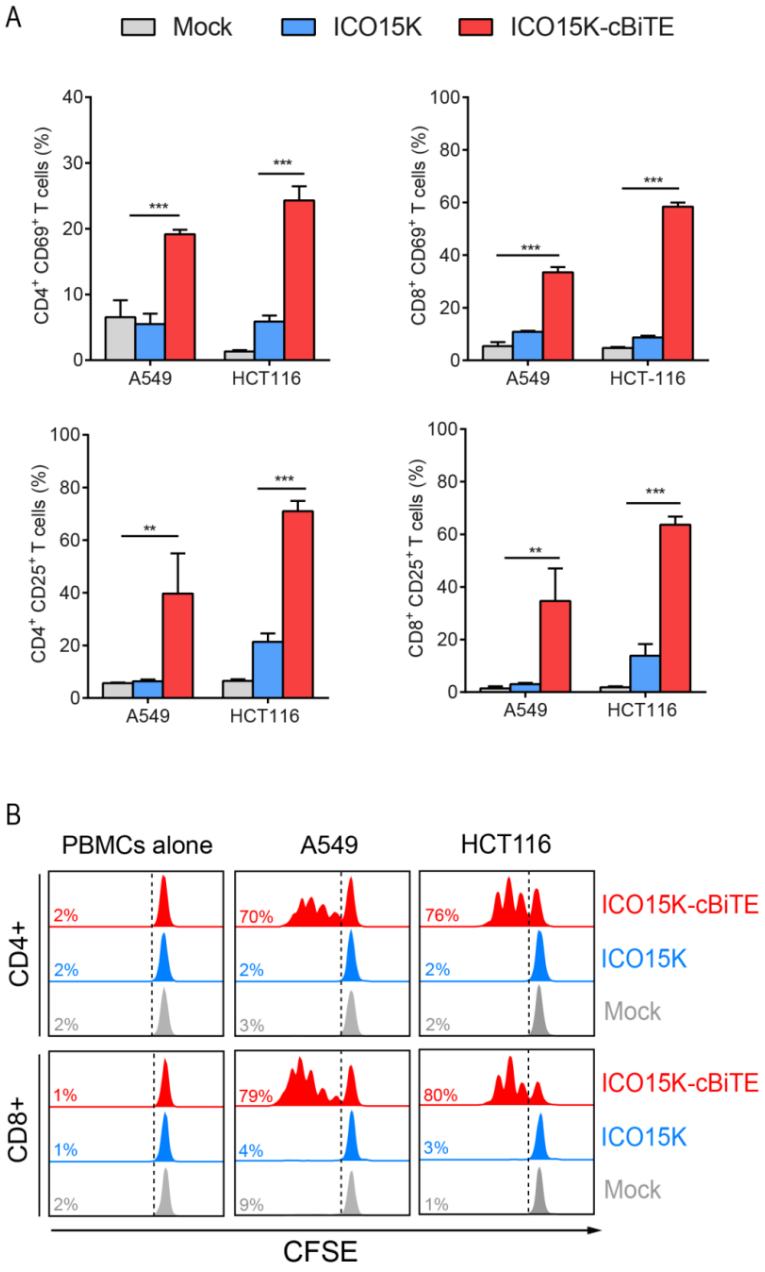

Figure 27. ICO15K-cBiTE-mediated oncolysis leads to T-cell activation and proliferation. **(A)** Cocultures of PBMCS with A549 or HCT116 cells (E:T =5) were infected with ICO15K or ICO15K-cBiTE at an MOI of 20. Uninfected (mock) cocultures were used a negative controls. 5 days after coculture, $CD8^+$ and $CD4^+$ T cells were assessed by flow cytometry for the expression of CD25 and CD69 activation markers. The mean ± SD of triplicates is shown.**, $P < 0.01$; ***, $P < 0.001$ by One-way ANOVA with Tukey post-hoc test. **(B)** Cocultures of CFSE-labeled PBMCS with A549 or HCT116 cells (E:T =5) were infected with ICO15K or ICO15K-cBiTE at an MOI of 20. Uninfected (mock) cocultures were used a negative controls. 7 days after coculture the CFSE content in $CD4^+$ and $CD8^+$ T cells was determined by flow cytometry. A representative result from triplicates is shown.

Another important feature of a secreted BiTE is its ability to generate a bystander effect. To test this without the interfering cytotoxicity of the virus, we sought a cell line which could partly resist ICO15K infection for 72 hours. The $EGFR^+$ cell line A431 has been reported to express low levels of the coxsackie and adenovirus receptor (CAR), and we therefore decided to characterize it as a candidate for a bystander effect assay. A431 cells were poorly transduced by AdTLRGDK, an *E1*-deleted and GFP-expressing adenoviral vector bearing the same capsid as ICO15K, even at high MOI (Figure 28A).

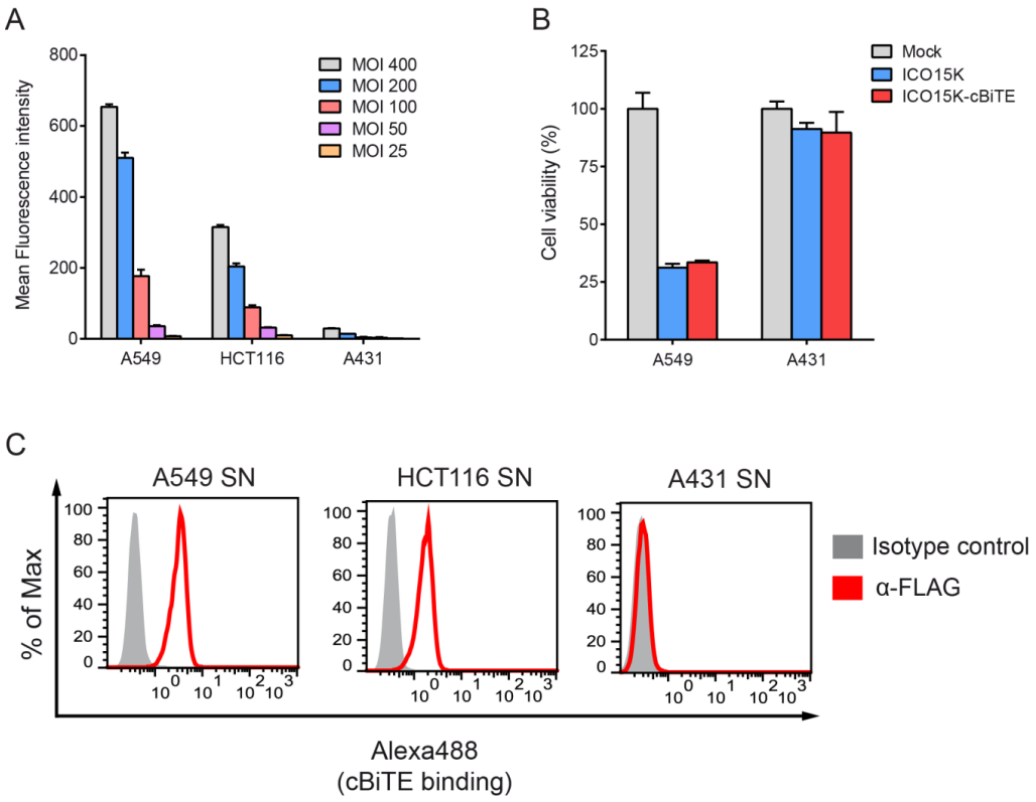

Figure 28. Characterization of adenovirus infection in A431 cells. (A) A549, HCT116 or A431 cells were infected with the GFP-encoding AdTLRGDK vector at MOIs ranging from 25 to 400 TU/cell. 24 h post-infection, GFP expression levels were assessed by flow cytometry. The mean fluorescence intensity ± SD of triplicates is shown. **(B)** A549 and A431 cells were infected with ICO5K or ICO15K-cBiTE at an MOI of 10. 3 days post-infection cell viability was determined with alamar blue. The percentage of viable cells was determined by normalizing to the viability observed in the uninfected (mock) control. The mean ± SD of triplicates is shown. **(C)** A549, HCT116 and A431 cells were infected with ICO15K-cBiTE at an MOI of 10 TU/cell. 3 days post-infection supernatants were harvested and incubated with A431 to evaluate cBiTE production. Bound cBiTE was detected by incubating cells with an anti-FLAG antibody and an Alexa488-labeled secondary antibody. Cells were analyzed by flow cytometry. The corresponding isotype control for the anti-FLAG antibody was used as a negative control.

Furthermore, A431 cells showed low OAd-mediated cytotoxicity at an MOI of 10 compared to A549 cells after 72 hours of incubation (Figure 28B). We then evaluated whether A431 cells could produce cBiTE antibodies in the presence of the virus (MOI = 20) for 72 hours. In contrast to the high levels of cBiTE observed in the supernatants of ICO15K-cBiTE-infected A549 or HCT116 cells, no cBiTE signal was detected in the supernatants of A431 cells (Figure 28C). Altogether, these results validate the A431 cell line as a suitable model for the bystander assay. In order to have a stable fluorescent signal for flow cytometry discrimination of these cells in cocultures, a GFP- and luciferase-expressing version of the A431 cell line (A431-GFPLuc) was generated.

For the bystander effect assay, A431-GFPLuc cells were cocultured with ICO15K- or ICO15K-cBiTE infected A549 cells in the presence or absence of human PBMCs for 5 days. Thus, in this setting, A549 cells act as BiTE producers, while A431-GFPLuc cells represent the targets of the T cells. ICO15K-cBiTE-infected A549 cells induced a significant decrease in the percentage of live A431-GFPLuc cells compared to ICO15K-infected cells when cocultured with PBMCS from two different donors (Figure 29). This increased cytotoxicity was dependent on the presence of PBMCS, as ICO15K and ICO15K-cBiTE induced similar levels of cell death in the absence of PBMCs.

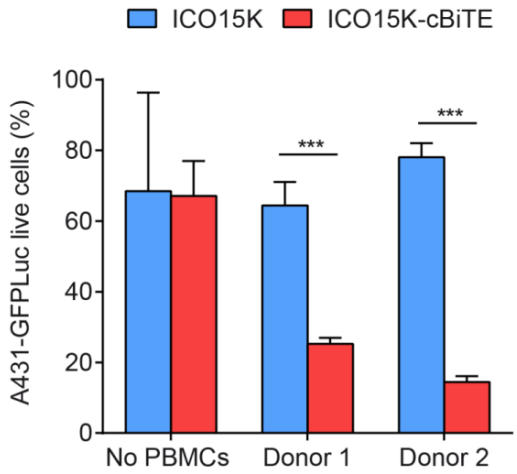

Figure 29. ICO15K-cBiTE-mediated oncolysis induces T-cell-mediated cytotoxic bystander effect. A549 cells were infected with ICO15K or ICO15K at an MOI of 20 for 4 hours. After washing the excess of virus, the infected A549 cells were cocultured with A431-GFPLuc cells (1:1 ratio) and with PBMCs from two different donors (E:T = 6 with respect to A431-GFP-Luc cells). Cocultures with no PBMCs were used as a negative control. 5 days after infection, cocultures were stained with 7-AAD and the absolute count of live A431-GFPLuc cells was determined by flow cytometry with counting beads. The percentage of live A431-GFPLuc was obtained by normalizing the absolute count of the samples to a culture of untreated A431-GFPLuc cells. The mean ± SD of triplicates is shown. ***, $P < 0.001$ by One-way ANOVA with Tukey post-hoc test.

We then tested whether the infection of cancer cells with ICO15K-cBiTE at low MOIs could provide an advantage during oncolysis over the non-modified virus when cocultured with T cells in time-course experiments. For these assays, preactivated T cells were used. These cells have a phenotype that more closely resembles that of Ad-specific CTLs, which is the main T-cell population expected to infiltrate tumors during oncolysis. We found that preactivated T cells produce high amounts of proinflammatory cytokines (Figure 30A). Furthermore, these cells show enhanced cytotoxic potential compared to unstimulated T cells when engaged by cBiTE antibodies (Figure 30B).

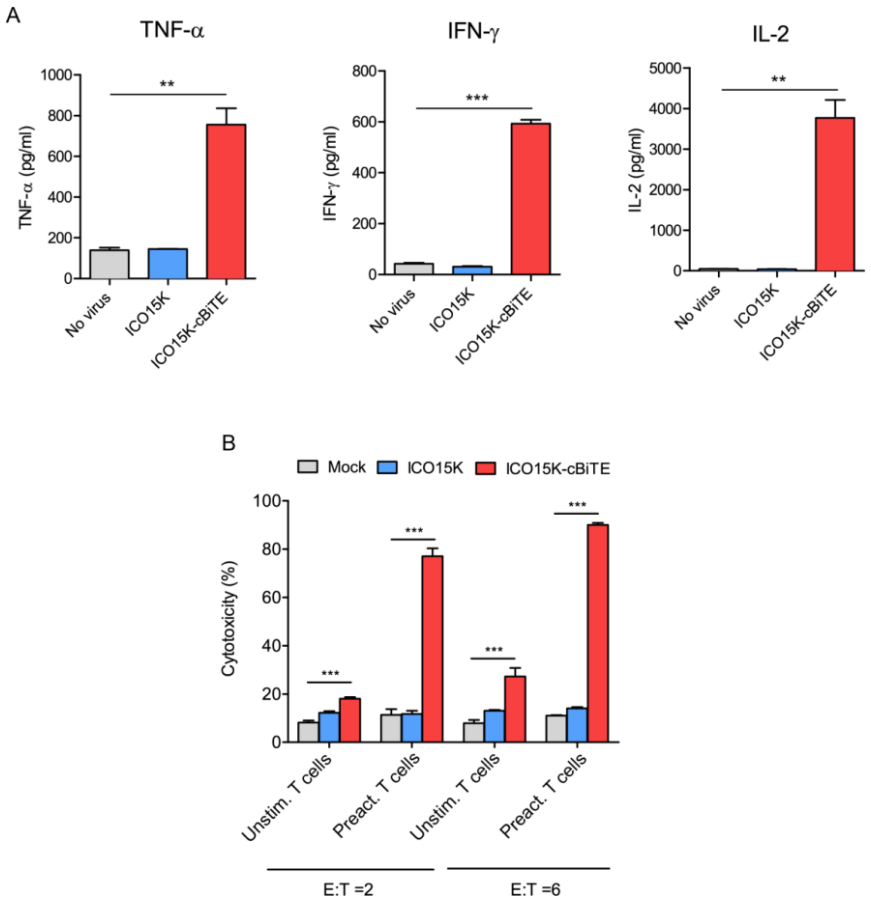

Figure 30. Preactivated T cells produce proinflammatory cytokines and show higher killing capacities than unstimulated T cells when engaged by the cBiTE. **(A)** HCT116 cells were infected with ICO15K/ICO15K-cBiTE at an MOI of 10. 24 hours later, preacivated T cells were added to the cultures (E:T =2). 48 hours after coculture supernatants were harvested and assessed for cytokine production by ELISA. Uninfected (mock) cells were used as negative controls. One representative experiment from three independent T-cell preparations from different healthy donors is shown. The mean ± SD of triplicates is shown. **(B)** CFSE-labeled A431 cells were cocultured with unstimulated or preactivated T-cells from the same donor (E:T = 2 or 6) in the presence of supernatants from uninfected or ICO15K/ICO15K-cBiTE-infected A549 cells. 24h after coculture cells were stained with 7-AAD and the percentage of cytotoxicity ($CFSE^+/7AAD^+$ cells) was determined by flow cytometry. The mean ± SD of triplicates is shown. **, $P < 0.01$; ***, $P < 0.001$ by One-way ANOVA with Tukey post-hoc test.

For the time-course assays, cell death was assessed using the xCELLigence system, which allows real-time monitoring of cell death by measuring the change in the impedance of attached cells. HCT116 or A549 cells were infected at an MOI of 1 and T cells were added to the cultures 24 hours after seeding and infection. The combination of ICO15K-cBiTE and T cells showed a remarkable additive effect by reducing by half the time to complete death of A549 and HCT116 cells when compared to any of the other virus treatments (Figure 31).

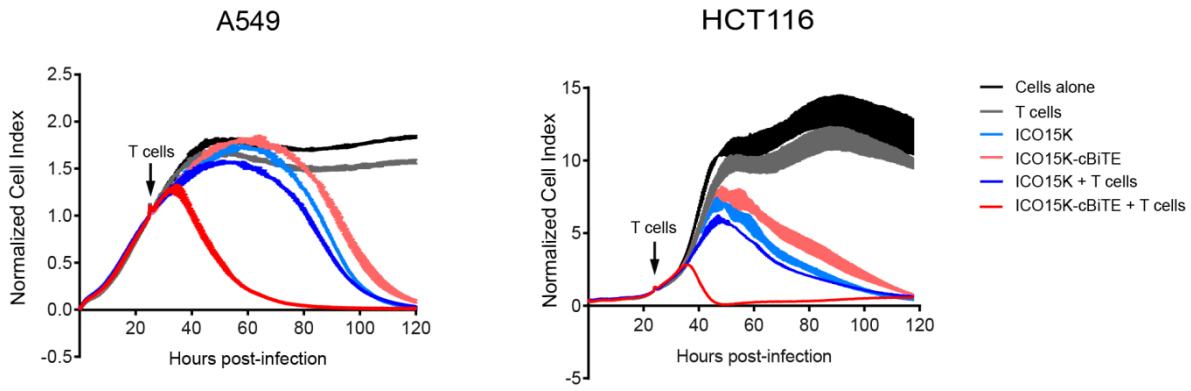

Figure 31. Preactivated T cells improve the cytotoxic potential of ICO15K-cBiTE. The xCELLigence system was used to evaluate the lysis of A549 and HCT116 cells over a 120 h period. Tumor cells were seeded and infected with ICO15K or ICO15K-cBiTE at an MOI of 1 at t_0. Preactivated T cells were added 24 hours later (E:T = 5). Impedance at well bottoms was measured every 20 min for 120h and normalized to baseline impedance values with medium only. The mean ± SD of duplicates is shown. One representative experiment from three independent T cell preparations from different healthy donors is shown.

4.1.1.5 ICO15K-cBiTE increases the persistence and accumulation of tumor infiltrating T cells

To address the potential of ICO15K-cBiTE *in vivo*, we first evaluated the persistence and biodistribution of human T cells in SCID/beige mice. To this end, isolated T cells from a healthy donor were pre-activated and transduced with a lentiviral vector encoding the Click Beetle Green (CBG) luciferase and GFP. CBG was chosen over firefly luciferase due to its superior photon emission which facilitates in vivo bioluminescence imaging [182]. T-cell preparations had 59% transduced (*i.e.* GFP^+) cells and retained the ability to proliferate *in vitro* (Figures 32A and B).

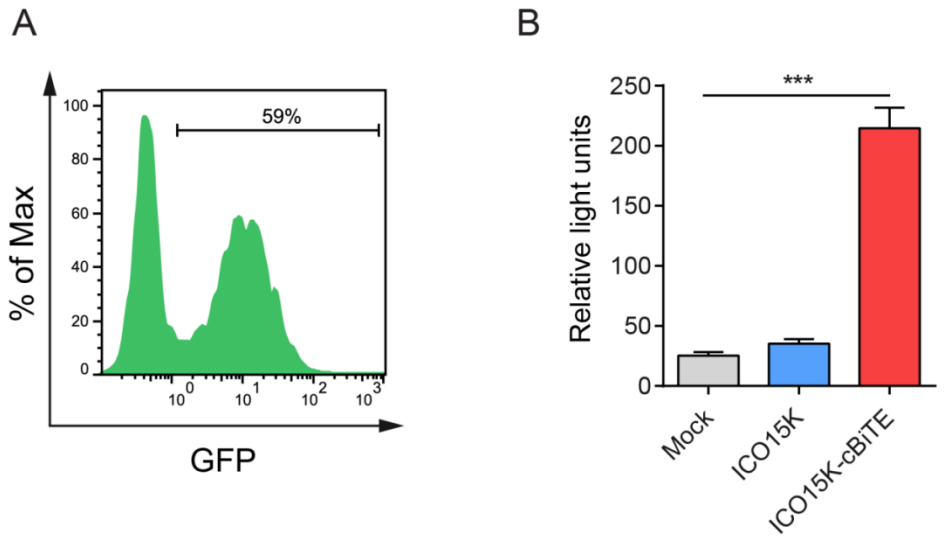

Figure 32. Luciferase- and GFP-expressing T cells retain their proliferative capacities *in vitro*. (A) Flow cytometry analysis of GFP expression by preactivated T cells that had been transduced with a lentiviral vector encoding the click beetle green (CBG) luciferase and GFP. **(B)** Luc-T cells were cocultured with HCT116 cells (E:T = 5) in the presence of the indicated supernatants. 5 days after coculture, cells were lysed and assessed for luciferase expression by a luminometric-based assay. The mean relative light units (RLU) ± SD of triplicates is shown. ***, $P < 0.001$ by One-way ANOVA with Tukey post-hoc test.

To test the biodistribution and persistence of these Luc-T cells *in vivo*, SCID/beige mice bearing subcutaneous EGFR$^+$ HCT116 tumors were injected intratumorally with PBS, ICO15K-cBiTE, or the parental virus. Five days after virus administration, mice received an intravenous injection of the CBG-Luc T-cell preparations (1×10^7 total cells) and tumor and body luminescence was measured daily thereafter by *in vivo* imaging. T cells were mainly distributed in the lymphoid organs one day after infusion and the signal generally decreased within 3 days. Tumor radiance was measured from day 3 on to avoid background signal coming from the initial engraftment in the lymphoid organs. Tumors treated with ICO15K-cBiTE induced T-cell accumulation from day 3 with a peak at day 4, and with the signal lasting for 9 days until reaching the levels of PBS- or ICO15K-treated tumors (Figure 33A). Half of the tumors treated with ICO15K-cBiTE, but none of those treated with PBS or ICO15K, showed a detectable increase in bioluminescent signal after 3 days of adoptive T-cell transfer (Figure 33B).

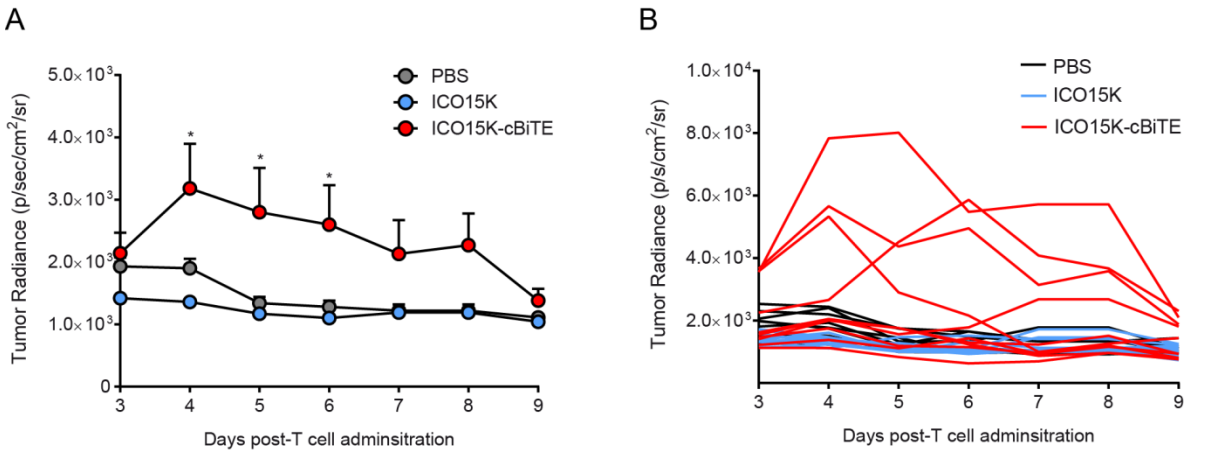

Figure 33. ICO15K-cBiTE induces accumulation and increased persistence of tumor-infiltrating T cells *in vivo*. **(A)** SCID/beige mice bearing subcutaneous HCT116 tumors on both flanks were intratumorally injected with PBS, ICO15K or ICO15K-cBiTE (*n* = 10 per group). 5 days later mice received an intravenous injection of 1 × 10^7 preactivated T cells expressing the click beetle green luciferase (Luc-T cells), followed by an intraperitoneal injection of IL-2. Body luminescence was monitored by *in vivo* imaging for 9 days. The mean tumor radiance ± SEM is shown from day 3, to avoid false positive signal from primary lymphoid organs. *, *P*< 0.05 ICO15K-cBiTE vs. ICO15K by students *t* test. **(B)** Radiance from individual tumors from the experiment described in A.

4.1.1.6 cBiTE and viral transcripts are detected in tumors treated with ICO15K-cBiTE

We also evaluated whether the cBiTE is expressed at the transcriptional level using a similar experimental setting to that of the biodistribution experiment. For this, SCID/beige mice bearing subcutaneous HCT116 tumors were injected intratumorally with PBS, ICO15K-cBiTE, or the parental virus. Seven days after virus administration, mice received an intravenous injection of 1 × 10^7 preactivated T cells. On day 4 after adoptive T-cell transfer, tumors were resected and processed for real-time PCR analysis. cBiTE transcripts were detected at variable levels only in the tumors treated with ICO15K-cBiTE (Figure 34A). Furthermore, hexon mRNA copies were detected at high levels in both ICO15K- and ICO15K-cBiTE-treated mice, confirming the presence of the viruses in the tumors (Figure 34B). Importantly, the mean levels of hexon mRNA copies were similar for both virus-treated groups, indicating that no short-term detrimental effect of the cBiTE-engaged T cells on the persistence of ICO15K-cBiTE in tumors.

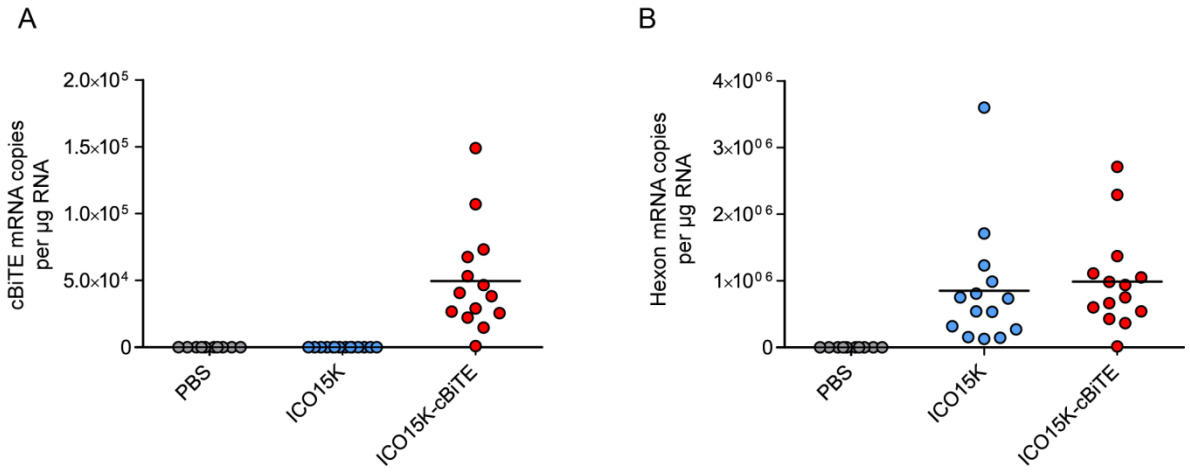

Figure 34. cBiTE mRNA transcripts are detected in tumors treated with ICO15K-cBiTE. SCID/beige mice bearing subcutaneous HCT116 tumors on both flanks were intratumorally injected with PBS (*n* = 10), ICO15K or ICO15K-cBiTE (*n* = 14). 7 days later mice received an intravenous injection of 1 × 10^7 preactivated T cells followed by an intraperitoneal injection of IL-2. Mice were sacrificed 4 days after T-cell administration and the presence of cBiTE **(A)** and hexon **(B)** mRNA transcripts was evaluated by qPCR after cDNA synthesis from RNAs extracted from tumor samples.

4.1.1.7 ICO15K-cBiTE enhances antitumor efficacy *in vivo*

We then assessed the antitumor efficacy of ICO15K-cBiTE in mouse xenograft models of cancer. To this end, SCID/beige mice bearing subcutaneous A549 tumors were injected intratumorally with PBS, ICO15K-cBiTE, or the parental virus. At 4 and 18 days post-virus administration mice received intravenous injections of either 1 × 10^7 unstimulated human PBMCs or PBS. The PBS groups showed the fastest tumor growth and the cBiTE-expressing Ad showed a similar antitumor efficacy as the parental virus in the absence of PBMCs (Figure 35A). Notably, the administration of human PBMCs significantly enhanced the antitumor efficacy of ICO15K-cBiTE but not that of ICO15K. Histological analysis of the tumors revealed the expression of the E1a protein at day 49 in all groups treated with any of the Ads in the study, indicating that PBMC-mediated cytotoxicity had no effect on the persistence of the virus in the tumor (Figure 35B). Additionally to histological analysis, tumors were processed to evaluate the presence of infiltrating T cells by flow cytometry. No $CD3^+$ T cells could be detected in any of the analyzed tumors. These results are likely explained by the low persistence of human T cells in SCID/Beige mice.

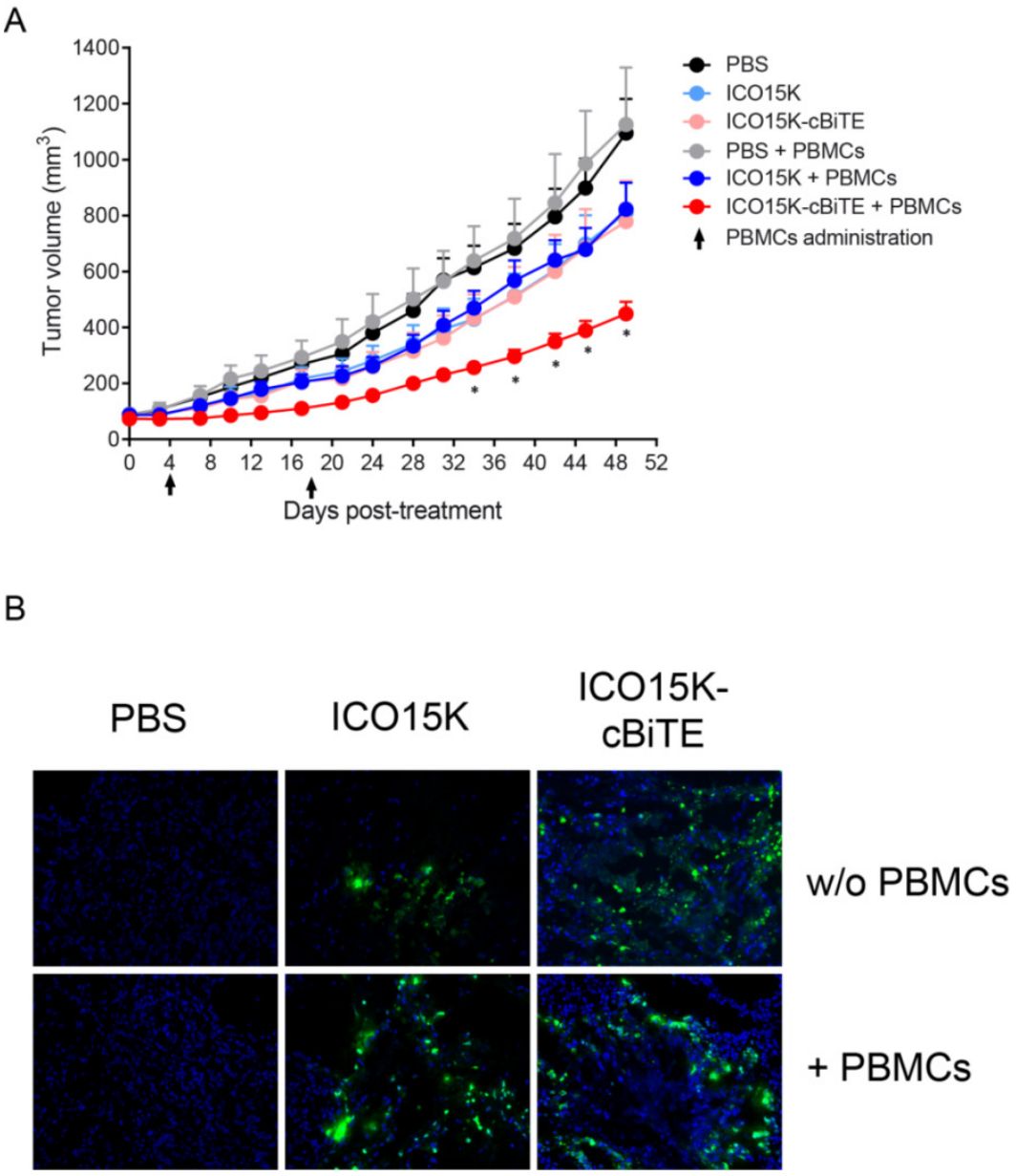

Figure 35. ICO15K-cBiTE shows improved antitumor efficacy *in vivo.* **(A)** SCID/beige mice bearing subcutaneous A549 tumors were intratumorally injected with PBS or 2 × 10^9 VP/tumor of ICO15K or ICO15K-cBiTE. 4 and 18 days post-virus administration, mice received either an intravenous injection of 1 × 10^7 PBMCs (*n* = 9-10 per group) or PBS (*n* = 10 per group). Tumor volume was monitored every 3-4 days until the end of the study. The mean tumor volume ± SEM is shown. *P* < 0.05 ICO15K-cBiTE + PBMCs vs. all groups by student*s*t test. **(B)** OCT-embedded cryosections from the tumors described in (A) were stained for the adenovirus E1a protein (green) and for nuclei with DAPI (blue). Representative composite images from each group are shown.

We also tested the effect of delivering ICO15K-cBiTE intravenously, a setting which is more therapeutically relevant for OAds. SCID/beige mice bearing subcutaneous HCT116 tumors were injected intravenously with PBS or 1×10^{10} VPs of either ICO15K or ICO15K-cBiTE. On days 4, 8, and 11 post-virus administration, mice received an intravenous injection of 1×10^{7} preactivated T cells followed by an intraperitoneal injection of IL-2. This regime was chosen based on the results of the persistence study in which T-cell tumor infiltration peaked at day 4, and it aimed at maximizing the presence of T cells in the tumor during the first weeks after virus treatment. Ad-treated mice had smaller tumor size than those treated with PBS, with ICO15K-cBiTE-treated ones having the smallest tumor volume after T-cell administration (Figure 36A). Although these differences were not statistically significant for tumor volume, ICO15K-cBiTE showed significant reduction in tumor growth compared to PBS and ICO15K from day 7 post-virus administration (Figure 19B). Importantly, the presence of virus and cBiTE in tumors was confirmed at the end of the study by immunohistological analysis (Figure 36C).

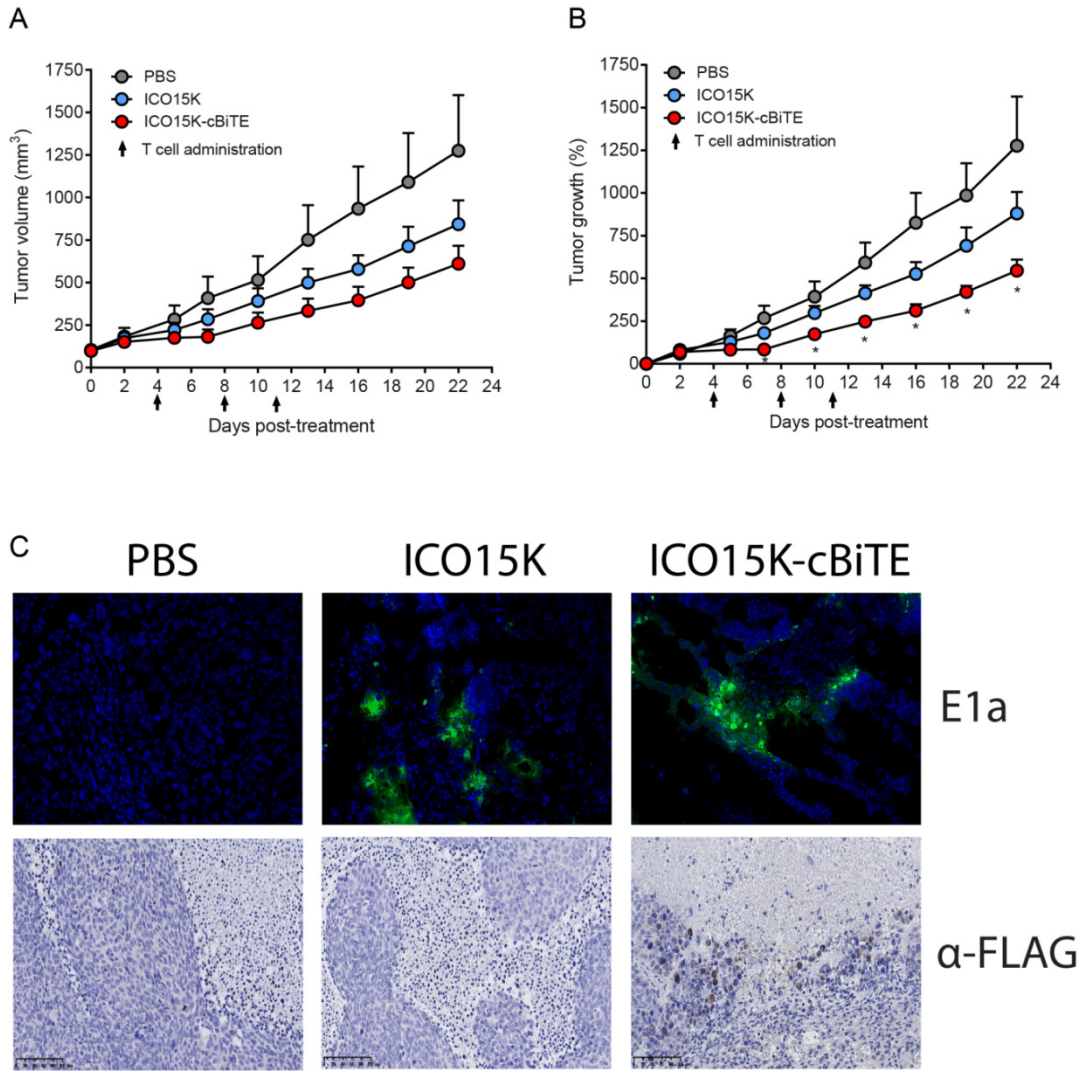

Figure 36. ICO15K-cBiTE shows improved antitumor efficacy in an aggressive model of cancer. (A) SCID/beige mice bearing subcutaneous HCT116 tumors were intravenously injected with PBS or ICO15K or ICO15K-cBiTE. 4, 8 and 11 days post-virus administration, mice received an intravenous injection of preactivated T cells followed by an intraperitoneal injection of IL-2. Tumor volume was monitored every 2-3 days. The mean tumor volume ± SEM is shown. **(B)** Tumor growth of the experiment described in A. The mean tumor growth ± SEM is shown. *, $P < 0.05$ ICO15K-cBiTE vs all groups. **(C)** Immunohistological detection of adenovirus and cBiTE in tumor samples. Upper panel, OCT-embedded cryosections from the tumors described in (A) and (B) were stained for the adenovirus E1a protein (green) and for nuclei with DAPI (blue). Representative composite images from each group are shown. Lower panel, paraffin-embedded sections from the tumors described in A and B were stained for anti-FLAG tag (*i.e.*cBiTE expression). Representative images from each group are shown. Scale bar: 100 µm.

4.1.1.8 ICO15K-cBiTE-mediated oncolysis increases the expression of immune checkpoints on T cells

The expression of inhibitory immune checkpoints as a result of T-cell activation is now recognized as a key factor to take into account when developing immunotherapies of cancer [138]. To evaluate the behavior of T cells during ICO15K-cBiTE oncolysis, cocultures of $EGFR^+$ L55 cells and preactivated T cells were mock-treated or infected with ICO15K or ICO15K-cBiTE for 6 days, and the expression of a panel of inhibitory checkpoints (PD-1, TIM-3, CD200 and LAG-3) on $CD4^+$ and $CD8^+$ T cells was assessed by flow cytrometry. Only a small proportion of $CD4^+$ and $CD8^+$ cells expressed the evaluated inhibitory markers in the mock- or ICO15K-treated cocultures (Figure 37A). In contrast, cocultures infected with ICO15K-cBiTE showed a marked increase in the frequency of $CD4^+$ and $CD8^+$ cells expressing inhibitory markers. Overall, the frequency of T cells expressing any of the markers was higher for the $CD4^+$ subpopulation compared to $CD8^+$ cells. These results demonstrate that ICO15K-cBiTE-mediated oncolysis induces robust T-cell activation, leading to the upregulation of immune checkpoints.

Given that co-expression of inhibitory receptors has been associated with a dysfunctional (*i.e.* exhausted) T-cell phenotype [183, 184], a deeper Boolean analysis of the flow cytometry data from the same experiment was performed to determine the number of inhibitory markers expressed on T cells after ICO15K-cBiTE treatment. Consistent with the results described in figure 37A, ICO15K-cBiTE-mediated oncolysis of L55 cells increased the percentage of T cells co-expressing inhibitory markers compared to untreated or ICO15K-infected cocultures (Figure 37B). Approximately 68% of $CD4^+$ and 49% of $CD8^+$ T cells in ICO15K-cBiTE-treated cocultures co-expressed ≥ 2 inhibitory markers, whereas only 4% and 6% of $CD4^+$ and 2% and 4% of $CD8^+$ T cells did so in mock- or ICO15K-treated cocultures, respectively. These results suggest that cBiTE engagement of T cells towards the EGFR can lead to phenotypes that resemble T-cell exhaustion. However, further molecular and functional analyses are needed to determine if the increased co-expression of markers is the result of T-cell exhaustion or if it is rather an indication of robust and transient T-cell activation.

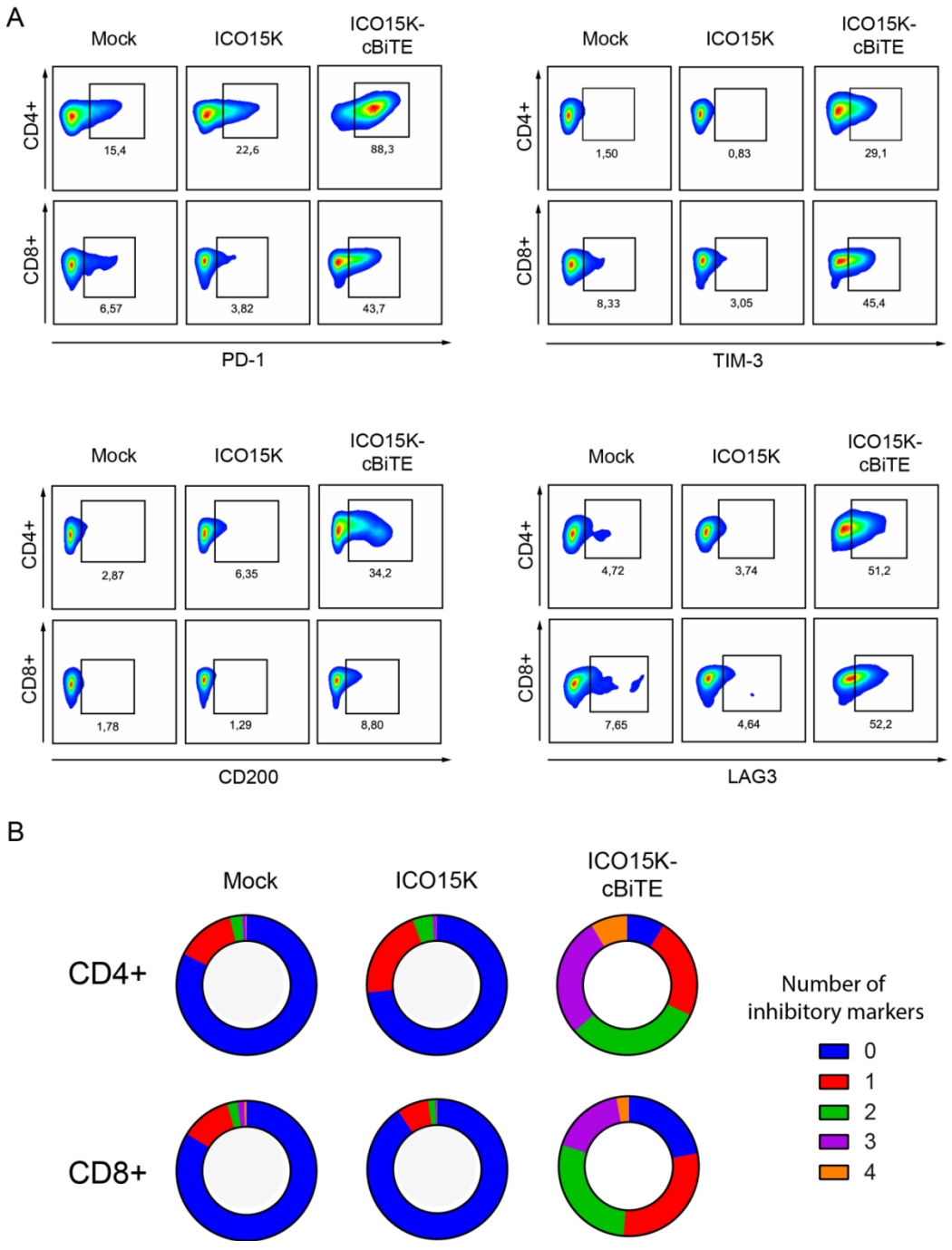

Figure 37. ICO15K-cBiTE-mediated oncolysis induces the expression of inhibitory receptors on T cells. (A) L55 cells were seeded and infected with ICO15K or ICO15K-cBiTE at an MOI of 1. Preactivated T cells were added 24 hours later at an E:T ratio of 1. After 6 days of coculture, the expression of the indicated checkpoint inhibitory markers on $CD4^+$ and $CD8^+$ subpopulations was evaluated by flow cytometry. Plots represent fluorescence for each marker as a function of CD4 or CD8 expression. Uninfected cocultures were used as a mock control. **(B)** The percentage of T cells co-expressing the indicated number of inhibitory markers was determined by Boolean gating analysis with FlowJo.

Altogether, the results from this section demonstrate that BiTE-armed OAds show enhanced immunostimulatory properties which results in enhance antitumor efficacy *in vivo*.

Since the humanized mouse models used in this section do not support deep immunological analysis after ICO15K-cBiTE treatment, we next evaluated the possibility of generating fully murine surrogates of the cBiTE which can be evaluated in immunocompetent mouse models.

4.1.2 An oncolytic adenovirus encoding a murine surrogate of cBiTE targeting murine EGFR and murine CD3

The *in vivo* results described above with ICO15K-cBiTE encourage the further development of this virus to a clinical setting. However, several of the pharmacological and toxicology aspects of this virus and the cBiTE cannot be studied in the SCID/Beige mouse model due to its immunodeficiency. For instance, the short persistence of T cells in this mouse model prevents us to study the behavior of the cBiTE in a scenario where anti-adenovirus CTLs are constantly infiltrating the tumor. Additionally, the possible side effects of the virus are neglected in our model since the scFVs used in the cBiTE only recognize human targets with no cross reactivity with mouse.

A common strategy used to solve these limitations is the use of surrogate BiTEs recognizing murine tumor antigens and murine CD3. This strategy has been well characterized for BiTEs targeting Epcam which has led to important observations regarding the pharmacokinetics and toxicology profiles of BiTEs [178, 185, 186].

4.1.2.1 Generation and characterization of ICO15K-mBiTE

In an attempt to generate a murine version of the cBiTE, we exploited the scFV versions of two antibodies that are well characterized in the literature. The first one, the hamster monoclonal antibody 145.2C11, recognizes the mouse CD3 and it has been previously used as scFV in different BiTE studies. The second, the mouse monoclonal antibody 7A7, recognizes both murine and human EGFR and it has been used as a preclinical model for the evaluation of anti-EGFR monoclonal antibodies [174].

The mBiTE was designed by joining the 145.2C11 and 7A7 scFVs through a peptide linker. In contrast to the cBiTE, the arrangement of the mBiTE comprised the anti-CD3 scFV at the N-terminus and the anti-EGFR scFV at the C-terminus (Figure 38). This arrangement was

chosen based on the literature describing a better performance of the 145.2C11 scFV in this location [173]. The mBiTE held the same structure as the cBiTE, including the signal peptide, the FLAG tag, the kozac sequence, the polyA site and the IIIa splicing acceptor to control its expression from the MLP. The genome of ICO15K-mBiTE was generated by homologous recombination in bacteria and the virus was successfully rescued.

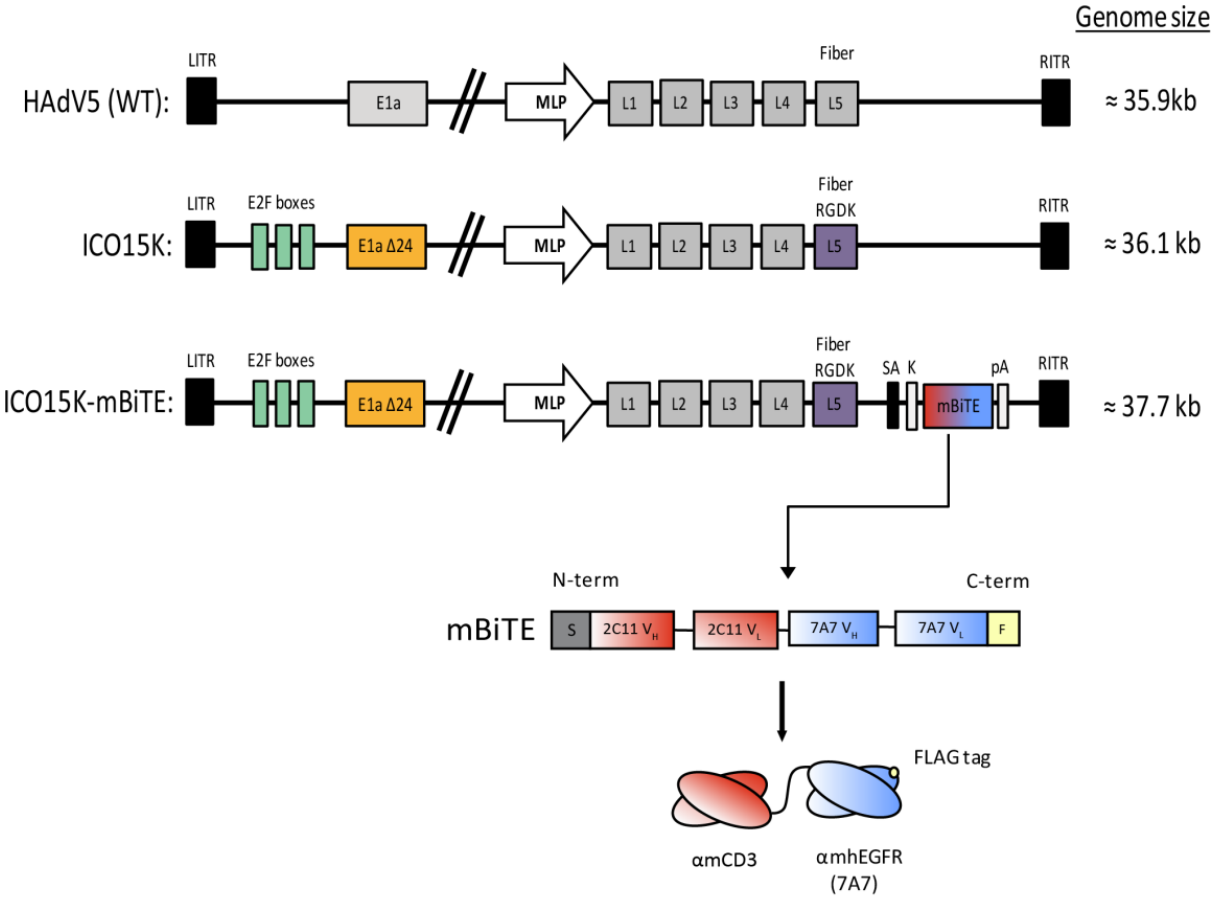

Figure 38. Schematic representation of the design of ICO15K-mBiTE. The mBiTE gene contains a signal peptide sequence (S), the scFV from the anti-mouse CD3 monoclonal 145.2C11 antibody, the scFV of the anti-mouse EGFR 7A7 monoclonal antibody and a FLAG tag (F) for detection purposes. For proper expression of the BiTE, the gene was flanked by a kozac sequence (K) and a polyadenylation signal (pA). The mBiTE gene was incorporated into the genome of ICO15K after the fiber gene, and it was placed under the control of the major late promoter (MLP) by including a splicing acceptor (SA) upstream of the kozac sequence.

4.1.2.2 Cells infected with ICO15K-mBiTE fail to secrete functional mBiTE antibodies

We next evaluated the secretion and functionality of the mBiTE which should be detected in supernatants from infected cells. Since the 7A7 scFV binds both to human and murine EGFR [174], we designed a flow cytometry-based binding assay similar to the one used to evaluate cBiTE expression and secretion. No mBiTE antibodies could be detected in the supernatants from ICO15K-mBiTE-infected A549 cells, as evidence by the lack of shift in fluorescence in A431 cells compared to the positive control (ICO15K-cBiTE supernatant) (Figure 39A).

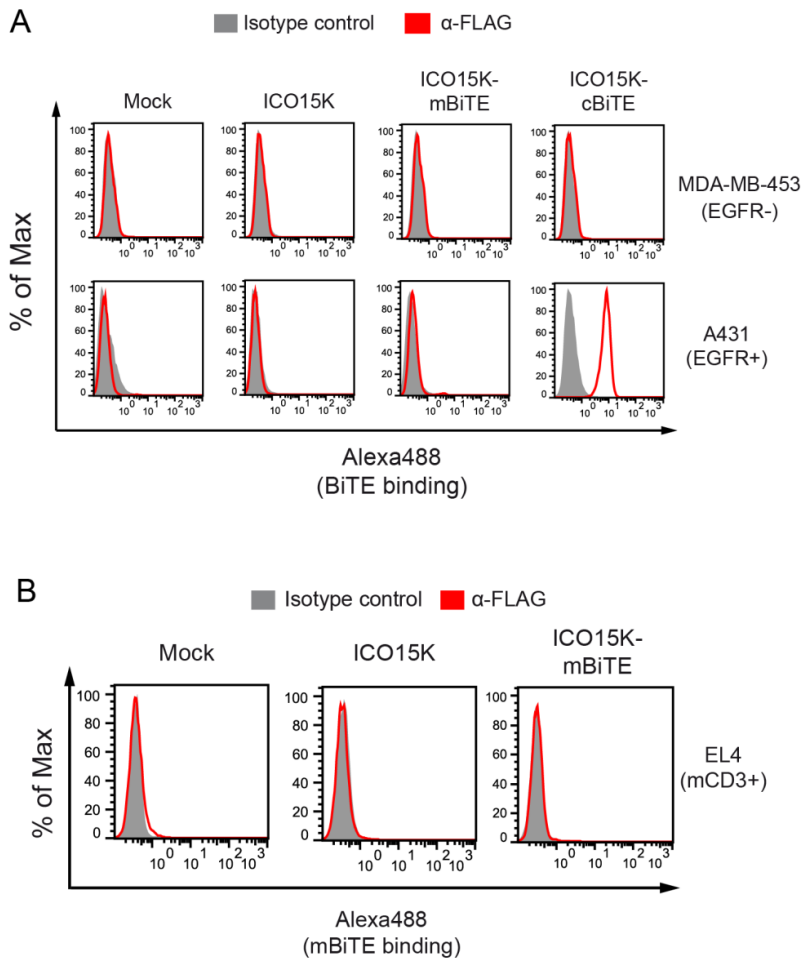

Figure 39. Cells infected with ICO15K-mBiTE fail to secrete functional mBiTE antibodies. MDA-MB-453 or A431 cells **(A)**, and mCD3$^+$ EL4 cells **(B)** were incubated with the supernatants of ICO15K- or ICO15K-mBiTE-infceted A549 cells. The supernatants from uninfected cells (mock) were used as a negative control. mBiTE binding was detected by incubating cells with an anti-FLAG antibody and an Alexa488-coupled secondary antibody. Cells were analyzed by flow cytometry. The corresponding isotype control for the anti-FLAG antibody was used as a negative control.

These results prompted us to determine whether we could detect the mBiTE via binding to the mCD3, which would also imply that the 7A7 scFV might have lost its activity as a BiTE molecule. For this, we performed binding assays with the mouse $CD3^+$ EL4 cell line. No binding to EL4 cells was detected in the supernatants of ICO15K-mBiTE-infected cells (Figure 39B). Furthermore, these results were confirmed even in binding assays with concentrated supernatants (data not shown). Altogether, these results indicate a lack of function of the mBiTE with the arrangement, design and scFVs we selected.

Since there is no certainty of the functionality of the 7A7 scFV in BiTE antibodies and, to our knowledge, there is no other anti-mouse EGFR antibody described in the literature, we decided not to continue with this project and change the strategy to generate chimeric BiTEs which can be evaluated in mouse cell lines expressing the human EGFR.

4.1.3 An oncolytic adenovirus encoding a chimeric BiTE targeting human EGFR and murine CD3

Another strategy used to evaluate BiTEs in immunocompetent mouse models is the construction of chimeric BiTEs which are composed of a scFV targeting a human TAA, and a second one targeting the mouse CD3. For this approach, mouse cancer cell lines are commonly modified to express the human TAA so that they can be targeted by mouse T cells in syngeneic mouse models of cancer. Different BiTEs targeting human antigens such as Epcam have been successfully evaluated using this approach [179].

4.1.3.1 Generation and characterization of ICO15K-mcBiTE

We designed a chimeric BiTE, termed mcBiTE, by joining a scFV derived from the hamster anti-mouse CD3 monoclonal antibody 145.2C11 (see section 1.2.1) and the same anti-hEGFR scFV used for the cBiTE (Figure 40). The mcBiTE followed the same arrangement as the mBiTE, with the anti-CD3 scFV located at the N-terminus and the anti-EGFR scFV placed at the C-terminus to improve the functionality of the 145.2C11 scFV (see section 1.2.1). The mcBiTE construct also included the splicing acceptor, kozak, signal peptide, FLAG tag and polyA sequences described for the cBiTE (see section 1.1.1). The genome of ICO15K was genetically engineered by homologous recombination in bacteria to place the mcBiTE construct downstream of the fiber gene as an L6 unit under the control of the MLP. The virus ICO15K-mcBiTE was successfully rescued and amplified to similar physical and functional titers as those of ICO15K (Table 5).

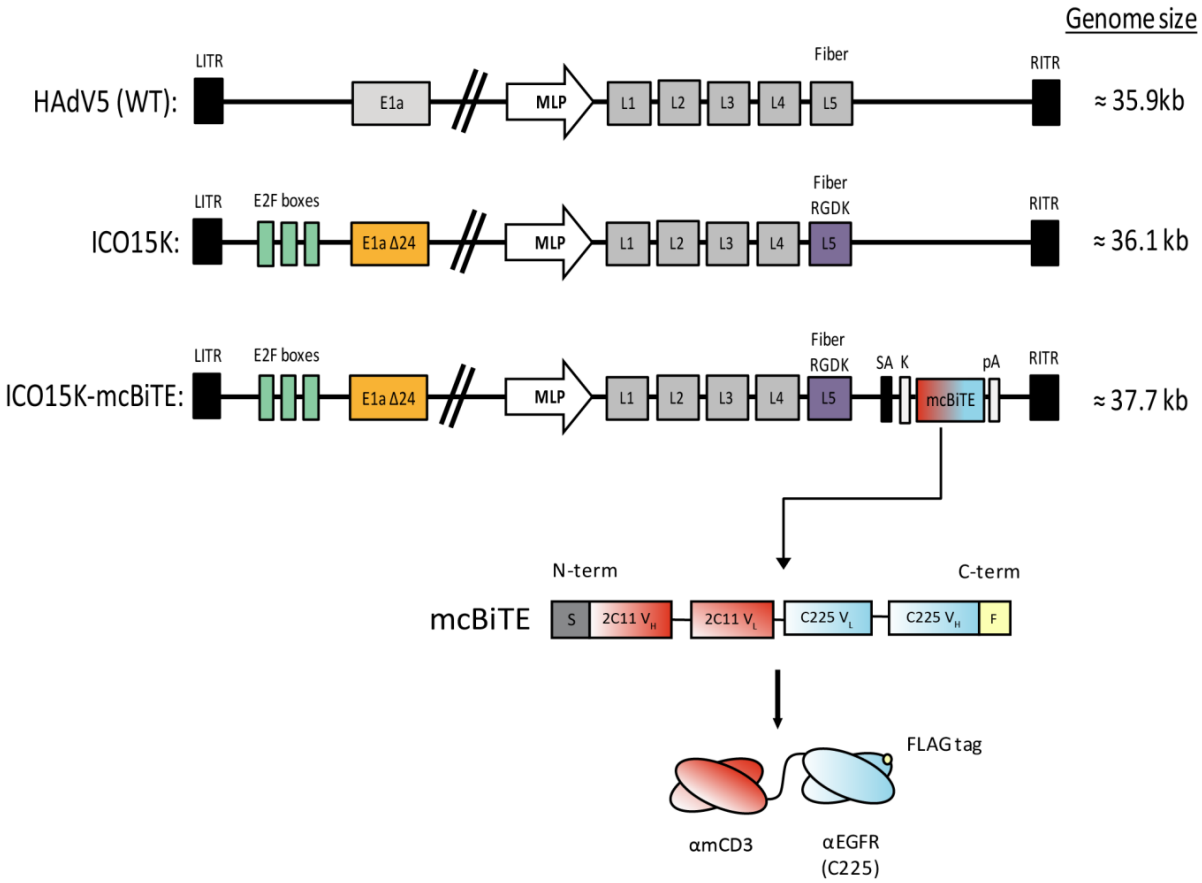

Figure 40. Schematic representation of the design of ICO15K-mcBiTE. The chimeric mcBiTE gene contains a signal peptide sequence (S), the scFV from the anti-mouse CD3 monoclonal 145.2C11 antibody, the anti-EGFR scFV derived from the Cetuximab antibody (C225) and a FLAG tag (F) for detection purposes. For proper expression of the BiTE, the gene was flanked by a kozac sequence (K) and a polyadenylation signal (pA). The mcBiTE gene was incorporated into the genome of ICO15K after the fiber gene, and it was placed under the control of the major late promoter (MLP) by including a splicing acceptor (SA) upstream of the kozac sequence.

Table 13. Virus production quality control

Virus	Physical titer (VP/ml)	Functional titer (TU/ml)	Physical:functional ratio
ICO15K	2.66×10^{12}	1.47×10^{11}	18.1
ICO15K-cBiTE	2.53×10^{12}	1.16×10^{11}	21.8

To characterize the oncolytic properties of ICO15K-mcBiTE, a dose-response cytotoxicity assay with A549 cells was performed. The mcBiTE-expressing virus retained oncolytic properties *in vitro*, although its IC_{50} value was increased 1.9-fold compared to ICO15K (Figure 41).

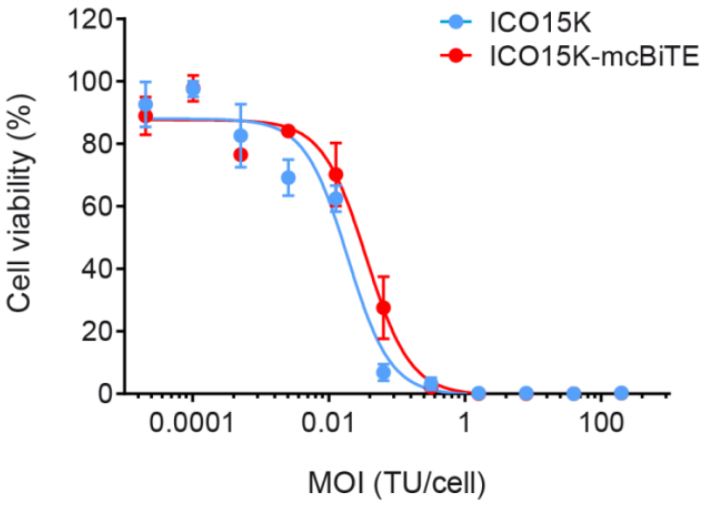

IC_{50} ICO15K	IC_{50} ICO15K-mcBiTE	Fold decrease vs. ICO15K
0.019 ± 0.03	0.036 ± 0.02	1.9x

Figure 41. *In vitro* oncolytic properties of ICO15K-mcBiTE. A549 cells were incubated with serial dilutions of ICO15K or ICO15K-mcBiTE, with multiplicity of infections (MOIs) ranging from 200 to 0 TU/cell. 6 days post-infection, cell viability was determined, and the IC_{50} for each virus was calculated. The mean ± SD of triplicates is shown.

4.1.3.2 Cells infected with ICO15K-mcBiTE secrete mcBiTE antibodies which specifically bind to target and effector cells

As performed with the above-described BiTEs, we next tested whether ICO15K-mcBiTE-infected cells could produce and secrete functional BiTEs. To assess the production and binding of the mcBiTE, the human A431 and MDA-MB-453, and the mouse EL4 cell lines were used for binding assays. mcBiTE molecules were only detected in the supernatants of ICO15K-mcBiTE-infcted cells and they specifically bound to EGFR-expressing cancer cells (Figure 42A) . Furthermore, mcBiTEs bound to the $mCD3^+$ EL4 cell line (Figure 42B).

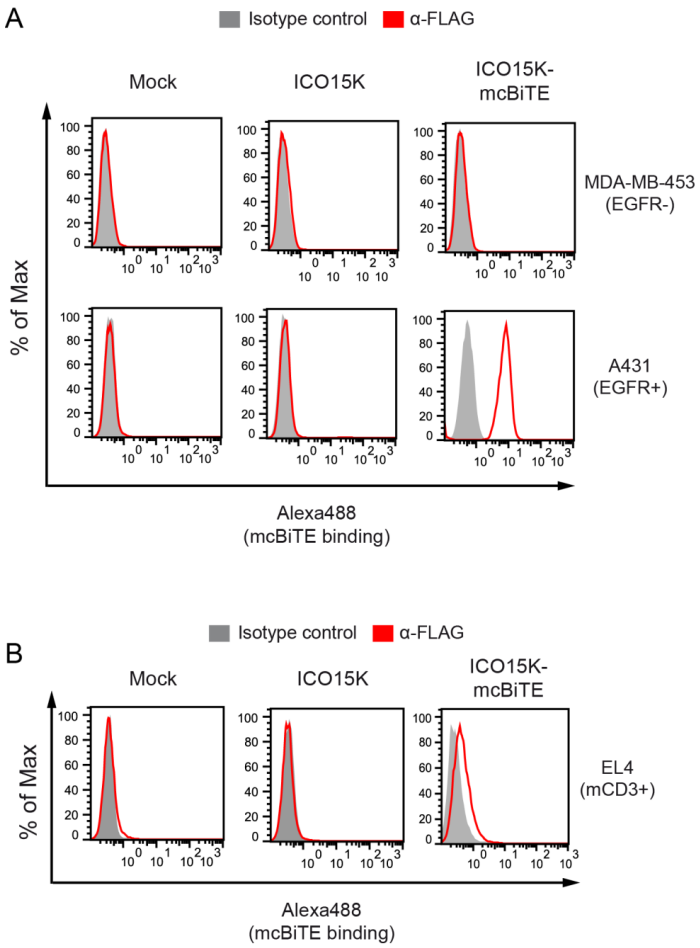

Figure 42. mcBiTE antibodies are expressed from ICO15K-cBiTE-infected cells and specifically bind to target and effector cells. MDA-MB-453 or A431 cells **(A)**, and mCD3$^+$ EL4 cells **(B)** were incubated with the supernatants of ICO15K- or ICO15K-mcBiTE-infceted A549 cells. Supernatants from uninfected cells (mock) were used as a negative control. mBiTE binding was detected by incubating cells with an anti-FLAG antibody and an Alexa488-coupled secondary antibody. Cells were analyzed by flow cytometry. The corresponding isotype control for the anti-FLAG antibody was used as a negative control.

4.1.3.3 Generation and characterization of B16CAR cells expressing the human EGFR

As mentioned above, in order to evaluate chimeric BiTEs in immunocompetent mouse models, murine cancer cell lines have to be modified to express the human antigen. For the evaluation of ICO15K-mcBiTE, we chose the melanoma B16CAR cell line which has been used for the preclinical evaluation of adenoviral vectors [159, 187]. These cells have been modified to express the coxsackie- and adenovirus receptor (CAR), which favors their transduction by Ad5-based vectors. The B16CAR-EGFR cell line was generated by stable transfection with a plasmid expressing the human EGFR and fluorescence-activated cell sorting of the EGFR-expressing cells. B16CAR-EGFR cells expressed high levels of the human EGFR, and retained the CAR expression, although at lower levels when compared to the

parental B16CAR cell line (Figure 43A). Importantly, binding assays demonstrated that, in contrast to B16CAR cells, the B16CAR-EGFR cell line could be targeted by the mcBiTE antibodies present in the supernatants of ICO15K-mcBiTE-infected cells (Figure 43B).

We then evaluated whether the decrease in CAR expression of B16CAR-EGFR cells could translate into a lower transduction of these cells by Ads. B16CAR and B16CAR-EGFR cells were infected with AdTLRGDK at different MOIs, and the transduction efficiency was determined by flow cytometry. Both cell lines were transduced at similar levels by the adenoviral vector, reaching almost 80% of transduced cells at an MOI of 50 (Figure 43C). Thus, B16CAR-EGFR cells retain the feature of being transduced by adenoviruses, despite the decrease in CAR expression.

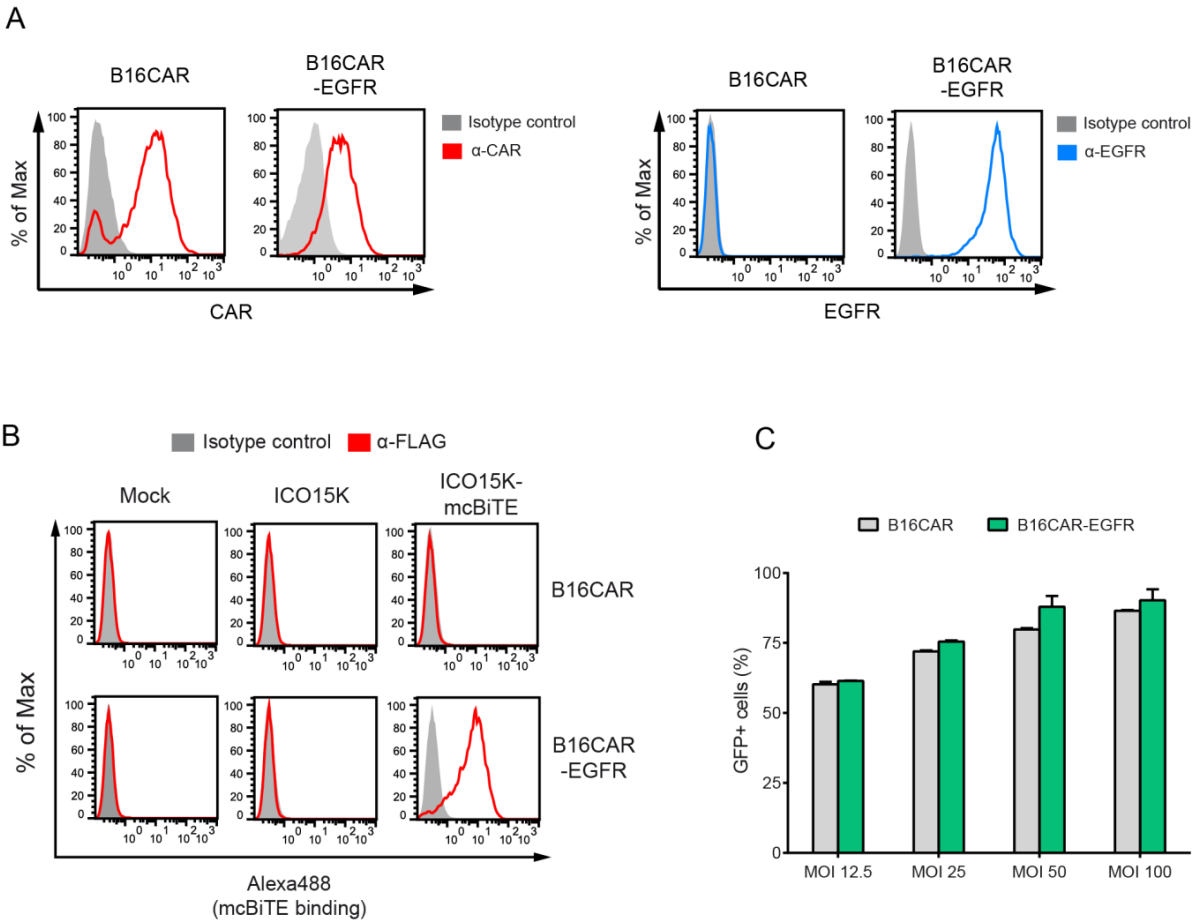

Figure 43. Characterization of B16CAR-EGFR cells. (A) B16CAR or B16CAR-EGFR cells were assessed for coxsackie and adenovirus receptor (CAR; left panel) or EGFR (right panel) expression by flow cytometry. **(B)** B16CAR or B16CAR-EGFR cells were incubated with the indicated supernatants and mcBiTE binding was detected by flow cytometry after incubation with anti-FLAG and an Alexa488-coupled secondary antibodies. **(C)** B16CAR or B16CAR-EGFR cells were infected with the GFP-encoding AdTLRGDK vector at the indicated MOIs (TU/cell). 24 h post-infection, the percentage of GFP^+ cells was assessed by flow cytometry. The mean ± SD of triplicates is shown.

4.1.3.4 Supernatants from ICO15K-mcBiTE-infected cells enhance splenocyte function

In order to test the activity of the mcBiTE secreted fromICO15K-mcBiTE-infected cells, coculture assays were set up with C57BL/6 mice-derived splenocytes and the mouse melanoma cell lines described above. The mcBiTE-containing supernatants induced the expression of the activation markers CD69 and CD25 on $CD4^+$ and $CD8^+$ T cells, only in cocultures that included the EGFR-expressing B16CAR cells (Figure 44A). Furthermore, cocultures of CFSE-labeled splenocytes with B16CAR-EGFR cells and the mcBiTE supernatant induced T-cell proliferation after 5 days of incubation (Figure 44B). This proliferation was clearly skewed towards the $CD8^+$ T-cell subpopulation, with more than 80% of these cells undergoing cell divisions compared to only 10% in the $CD4^+$ subpopulation.

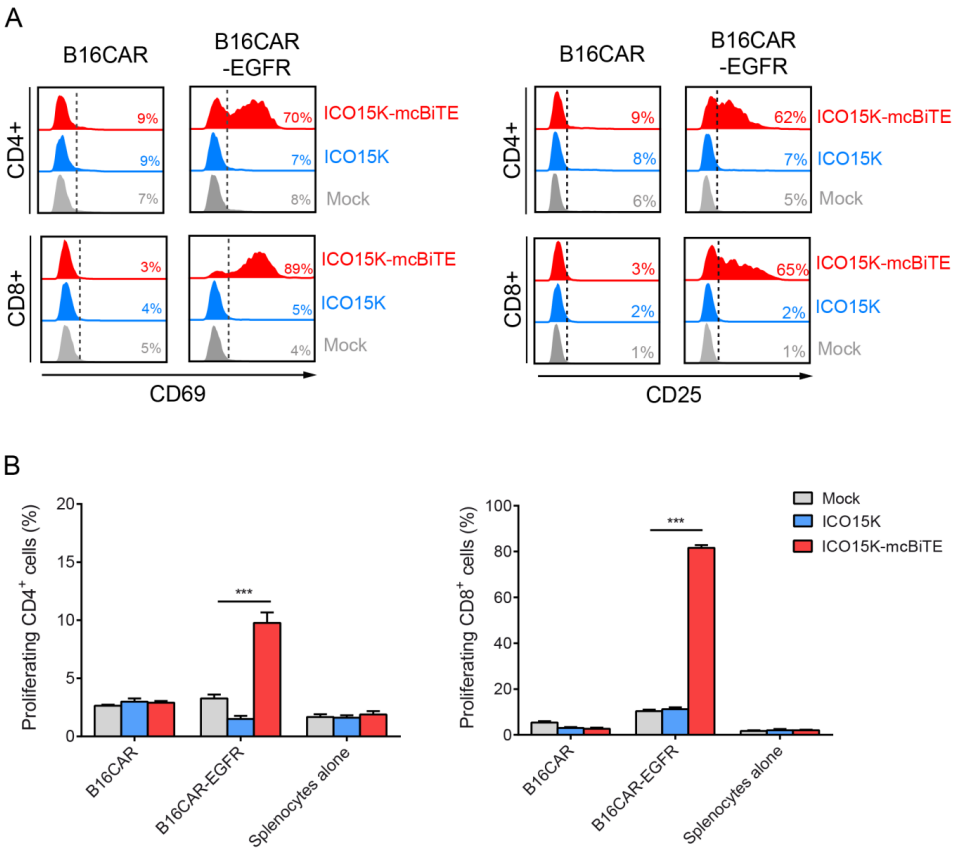

Figure 44. mcBiTE antibodies expressed from ICO15K-mcBiTE-infected cells induce mouse T-cell activation and proliferation. Unlabeled **(A)** or CFSE-labeled **(B)** splenocytes derived from C57BL/6 mice were cocultured with B16CAR or B16CAR-EGFR cells in the presence of the indicated supernatants. **(A)** 48h after coculture, the expression levels of CD25 and CD69 on $CD4^+$ and $CD8^+$ T cells were assessed by flow cytometry. Representative results from triplicates are shown. **(B)** 5 days after coculture, the percentage of proliferating (*i.e.* CFSE-diluted) $CD4^+$ and $CD8^+$ T cells was determined by flow cytometry. The mean ± SD of triplicates is shown.***, $P < 0.001$ by One-way ANOVA with Tukey post-hoc test.

4.1.3.5 Supernatants from ICO15K-mcBiTE-infected cells induce T-cell-mediated cell killing

We next tested whether mcBiTE-engaged mouse splenocytes could induce cell death in B16CAR-EGFR. For this, splenocytes from BALB/c mice were cocultured with B16CAR or B16CAR-EGFR in the presence of the different supernatants for 48 hours, and cell death was assessed by flow cytomerty. This experiment also intended to confirm the MHC-I-independent mode of action of BiTEs, since B16 cells are derived from C57BL/6 mice (haplotype b) while spleonocytes were derived from BALB/c mice (haplotype d). The supernatant containing the mcBiTE induced a significant increase in cell death of B16CAR-EGFR but not of B16CAR cells, confirming mcBiTE-mediated T-cell engagement in an MHC-I-independent manner (Figure 45).

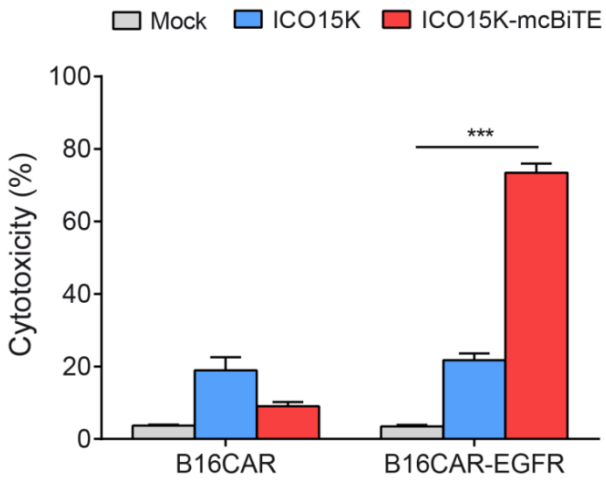

Figure 45. mcBiTEs expressed from ICO15K-cBiTE-infected cells enhance splenocyte-mediated cytotoxicity. Cocultures of BALB/c mice-derived splenocytes with CFSE-labaled B16CAR o B16CAR-EGFR cells were treated with the indicated supernatants. 48 h post-treatment, the percentage of cytotoxicty on target cells ($CFSE^+/7AAD^+$ cells) was assessed by flow cytometry. The mean ± SD of triplicates is shown ***, $P < 0.001$ by One-way ANOVA with Tukey post-hoc test.

4.1.3.6 B16CAR-EGFR cells produce lower levels of mcBiTE compared to the parental cell line

In order for the B16CAR-EGFR cell line to be a good model for the *in vivo* evaluation of ICO15K-mcBiTE, the BiTE transgene has to be successfully produced and secreted from the cells. Although productive Ad replication is species-specific, reports in the literature have

demonstrated the expression of MLP-driven genes in different syngeneic mouse cancer cell lines, including B16CAR [43, 188].

We therefore further characterized the ability of B16CAR-EGFR cells to produce mcBiTEs. To this end, B16CAR and B16CAR-EGFR cells were infected with ICO15K-mcBiTE at an MOI of 20 for 72 hours. The supernatants of infected cells were then assessed for the presence of mcBiTEs by binding assays with $EGFR^+$ A431 cells. Although moderate levels of mcBiTE were detected in the supernatant of B16CAR cells, no mcBiTEs could be detected in the supernatants of B16CAR-EGFR cells (Figure 46A). To rule out the possibility that mcBiTE was not produce in this cell line, further infection experiments were performed at higher MOIs (*i.e.* 50). The supernatants of these infected-cultures were assessed for the presence of mcBiTE by binding assays with either B16CAR or B16CAR-EGFR cells. In contrast to the high levels of mcBiTE detected in the supernatants of B16CAR cells, very low levels of mcBiTE were detected in the supernatants of B16CAR-EGFR cells (Figure 46B). These results might be a consequence of the competition of the CAR, EGFR and viral genes for the transcription and translation machinery of the cells.

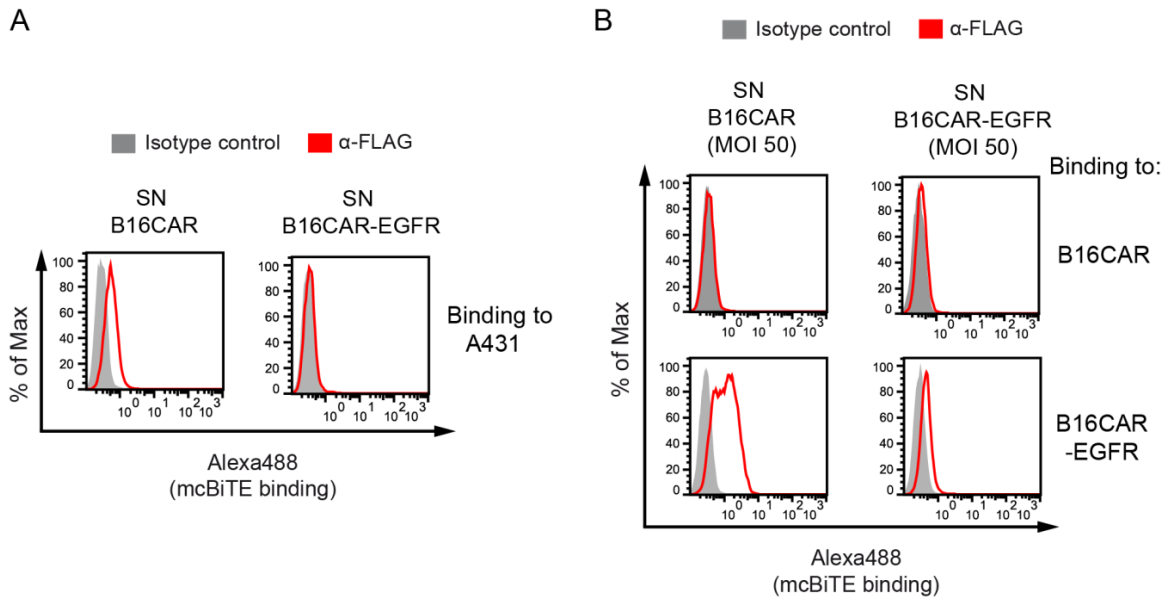

Figure 46. B16CAR-EGFR cells produce lower levels of mcBiTEs compared to the parental cell line. (A) B16CAR or B16CAR-EGFR were infected with ICO15K-mcBiTE at an MOI of 20 for 72 hours. The supernatants from infected cells were incubated with A431 cells and mcBiTE detection was assessed by flow cytometry as described above. **(B)** B16CAR or B16CAR-EGFR cells were infected with ICO15K-mcBiTE at an MOI of 50 for 72 hours. The supernatants from infected cells were incubated with B16CAR or B16CAR-EGFR cells and mcBiTE detection was assessed by flow cytometry as described above.

4.1.3.7 B16CAR-EGFR cells fail to generate tumors in C57BL/6 mice

Although B16CAR-EGFR cells produced less mcBiTE than B16CAR cells, these levels might be enough to exert the full potential of BiTEs. Indeed, BiTEs are known to exert all their functions even in the picomolar range. Thus, we decided to evaluate the B16CAR-EGFR cell line as a potential model for the *in vivo* assessment of ICO15K-mcBiTE. To this end, B16CAR or B16CAR-EGFR cells were implanted subcutaneously in the flanks of C57BL/6 mice and tumor growth was monitored every 2-3 days. As expected, B16CAR cells developed palpable and measurable tumors in all mice after 7-10 days of implantation. However, B16CAR-EGFR cells failed to develop palpable or measurable tumors in all animals even after 2 months of implantation. When these animals were sacrificed, the necropsy revealed a black spot at the inoculation site consistent with B16CAR cells but no evidence of growth was observed, suggesting the rejection of the cells by the immune system of the host reacting against the human EGFR. These results demonstrate that B16CAR-EGFR cells cannot be used as a model for the *in vivo* assessment of ICO15K-mcBiTE. Since we did not have any other chimeric cancer cell line expressing the human EGFR, the potential of ICO15K-mcBiTE could not be evaluated in a fully immunocompetent *in vivo* setting. However, the development of different mouse cell lines expressing the human EGFR is considered as a future direction of this project.

4.2. Combination of CAR T-cell therapy and ICO15K-cBiTE

CAR T-cells have shown exciting results in clinical trials for hematological malignancies, but their efficacy in solid tumors is still limited. Some of the major hurdles faced by CAR T-cells on solid tumors include poor T-cell infiltration and proliferation due to the highly immunosuppressive tumor microenvironment, and poor efficacy due to tumor immune evasion by antigen loss. OAds have already been used as attractive immunostimulatory agents to revert tumor immunosuppression, favoring thus CAR-T infiltration and function [152]. We hypothesize that combining the cBiTE-expressing OAd might further favor CAR T-cell therapy by: (i) redirecting CAR-negative untransduced (UTD) T cells (commonly present in CAR T-cell preparations infused to patients) to cancer cells and (ii) minimizing tumor immune evasion by antigen loss due to targeting of two distinct tumor antigens.

4.2.1 Generation of CAR T cells targeting mesothelin

The favorable characteristics of ICO15K-cBiTE prompted us to evaluate whether this virus could aid in overcoming many of the limitations encountered by CAR T-cell therapies in solid tumors. To this end, we used a CAR construct that contains the SS1 scFV, which recognizes the tumor antigen mesothelin (Meso) [189]. The full CAR construct is composed of the SS1 scFV, the CD8 hinge region, the ICOS transmembrane and intracellular signaling domains and the TCR-ζ signal transduction domain (Figures 47A and B), as previously described [190].

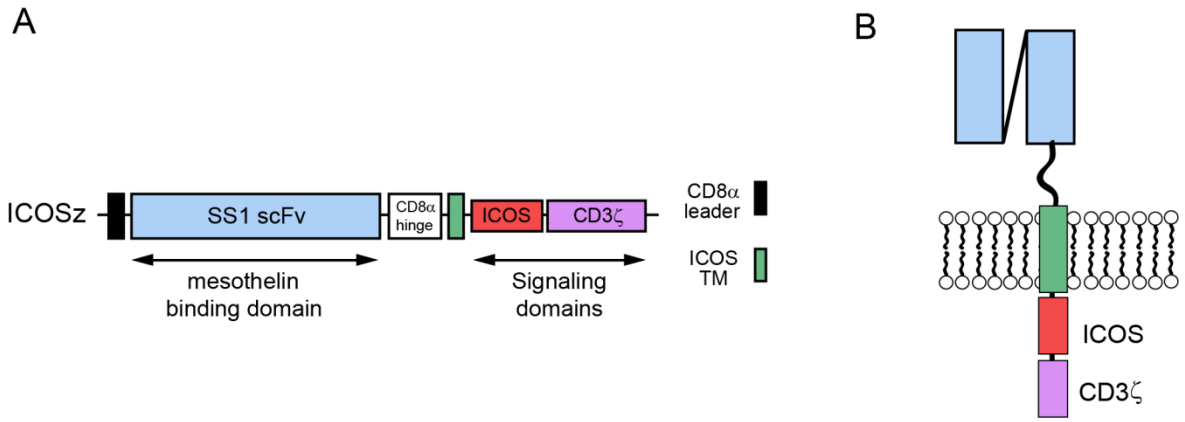

Figure 47. Schematic representation of the SS1 chimeric antigen receptor construct. (A) The SS1 CAR construct is composed of the CD8α leader sequence, followed by the anti-mesothelin SS1 scFV , the CD8 hinge region, the ICOS transmembrane (TM) and intracellular signaling domains and the TCR-ζ signal transduction domain. **(B)** SS1-modified T cells express the scFV as an extracellular domain, which, upon binding to mesothelin, transduces signals through both ICOS and CD3ζ domains.

To generate CAR T cells targeting Meso, isolated human unstimulated T cells are activated with anti-CD3/anti-CD28-coated beads, transduced with lentiviral particles encoding the CAR construct, and further expanded for 9-11 days until storage (Figure 48A). This process leads, depending on the MOI of lentivirus used, to the generation of mixed population of transduced (*i.e.* CAR^+) and untransduced (*i.e.* CAR^-) T cells. We generated CAR T cells from two different donors at two different MOI (2 and 20) to ensure one of these conditions to have at least 50% transduced cells. In parallel, as negative controls, untransduced (UTD) T cells from the same donor were activated, expanded and cryopreserved.

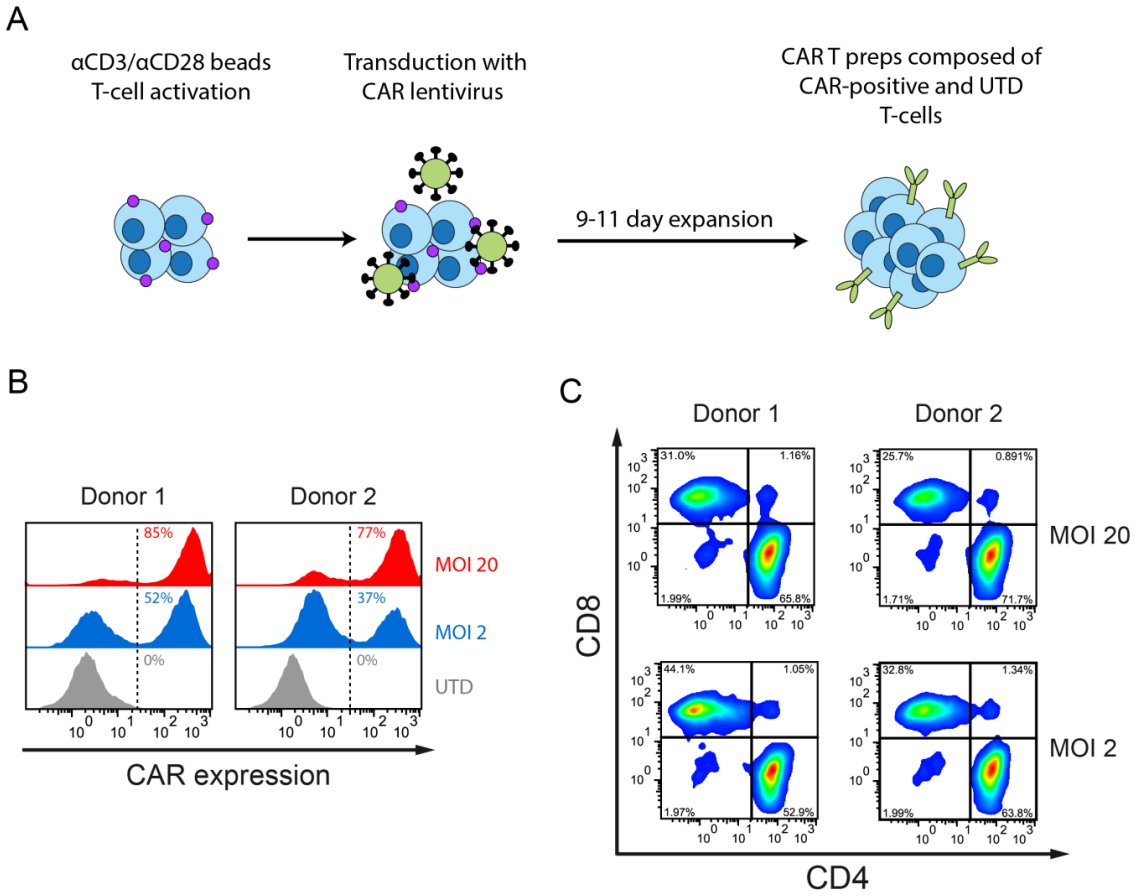

Figure 48. Generation and characterization of anti-mesothelin CAR T-cell preparations. (A) Schematic representation of the protocol for the production CAR T-cell preparations. **(B)** Activated T cells from two different donors were infected with the CAR-encoding lentiviral vector at an MOI of 2 or 20. CAR expression was evaluated by flow cytometry. Untransduced (UTD) T cells from the same donors were used as negative controls. **(C)** CD8 and CD4 subpopulations within the CAR^+ populations was determined by flow cytometry.

We obtained CAR preparations with varying levels of CAR-expressing cells, depending on the MOI used. The level of transduced CAR^+ cells under both lentivirus MOI was donor-dependent (Figure 30B). In both donors, the MOI = 20 led to preparations with >75% of transduced cells and similar frequencies of $CD4^+$ and $CD8^+$ T cells (65-70% and 25-31%, respectively) (Figures 48B and C). At an MOI of 2, CAR expression on T cells varied between both donors, with 52% and 37% for donor 1 and donor 2, respectively. For all functional assays, preparations from MOI = 20 infections were normalized for equivalent CAR expression by adding the required amount of UTD T cells. Thus, CAR T-cell preparations contained approximately 50% CAR^+ and 50% CAR^- (UTD) cells, a similar setting to that of clinical trials with CAR T-cell therapies.

4.2.2 ICO15K-cBiTE supernatants activate CAR T-cells in the absence of mesothelin

To study whether the cBiTE-expressing OAd could activate CAR T cells in a mesothelin-negative context, we chose A431 ($EGFR^+$ and $Meso^-$) and L55 ($EGFR^+$ and $Meso^+$) cells to perform coculture assays in the presence of ICO15K-cBiTE supernatants. Thus, in this setting, L55 cells would represent a condition prior to antigen loss, whereas A431 cells would mimic the scenario of mesothelin loss while EGFR expression still occurs.

We first evaluated T-cell activation in 24 h cocultures by staining of the CD25 activation marker within the $CD8^+$ subpopulation. In L55 cells, two distinct $CD8^+$ populations ($CD25^-$ and $CD25^+$) at similar frequencies (approximately 50% each) were observed in cocultures containing the ICO15K or Mock supernatants (Figure 49A). Interestingly, in the presence of the cBiTE supernatant, the majority (>80%) of $CD8^+$ T cells were positive for CD25. In A431 cells, in which no mesothelin is expressed, $CD25^+$ $CD8^+$ T cells could only be detected in CAR T-cell cocultures that contained ICO15K-cBiTE supernatants. As expected, cocultures containing UTD T cells were activated in both cell lines in the presence of cBiTE but not of Mock or ICO15K supernatants.

We then performed further gating analysis only for cocultures containing CAR T-cell preparations based on CAR and CD25 expression. We confirmed that T cells expressing CD25 in the cocultures of L55 cells treated with mock or ICO15K supernatants were only those expressing the CAR (Figure 49B). In contrast, both CAR^+ and CAR^- T cells expressed CD25 in cocultures containing the cBiTE. Importantly, in A431 cocultures both CAR^+ and CAR^- T cells could only be activated when treated with the ICO15K-cBiTE supernatant. These results demonstrate that CAR^+ T cells can be activated by BiTE antibodies in a scenario in which the CAR T-cell-targeted antigen has been lost.

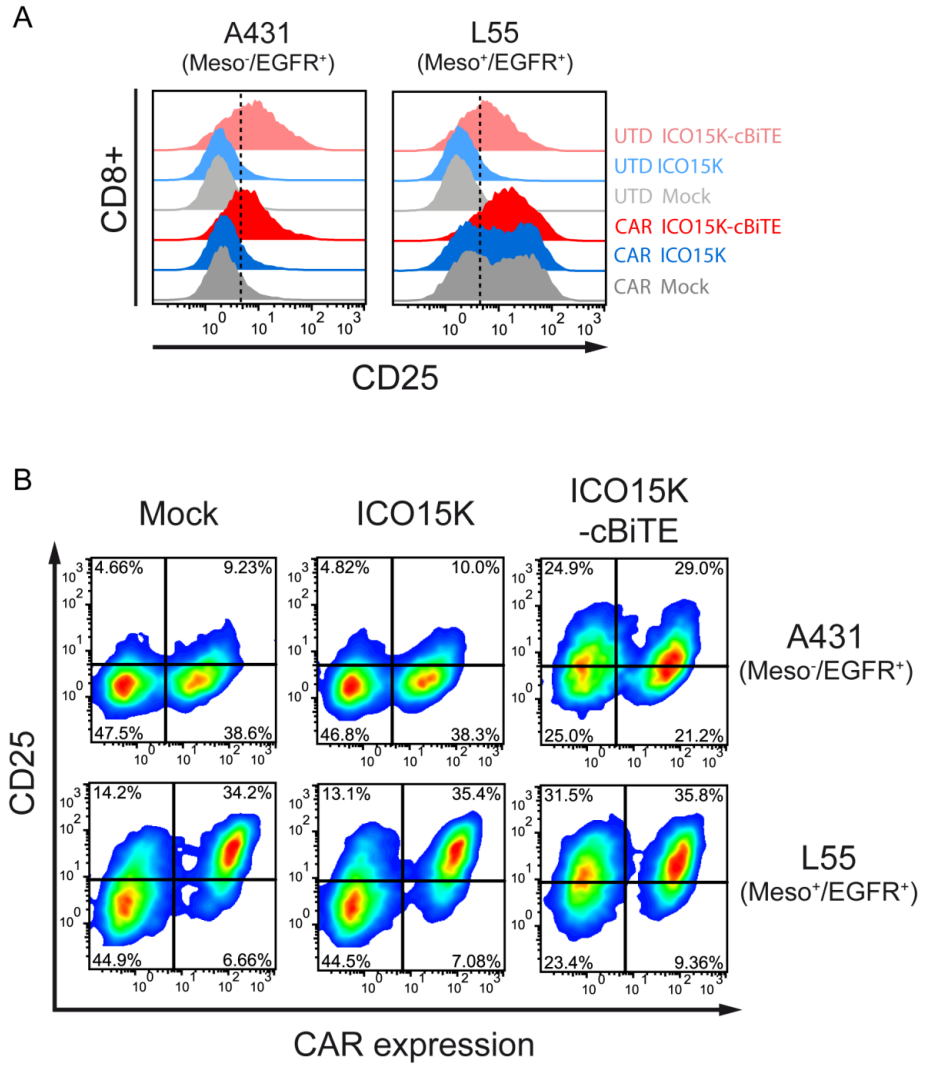

Figure 49. ICO15K-cBiTE supernatants activate CAR T cells in the absence of mesothelin. (A) CAR or untransduced (UTD) T-cell preparations were cocultured with A431 or L55 cells (E:T = 2) in the presence of the indicated supernatants. 24 h after coculture, the expression levels of the CD25 activation marker on $CD8^+$ cells was determined by flow cytometry. **(B)** Cocultures including CAR T-cell preps were evaluated for CD25 and CAR expression on the $CD8^+$ subpopulation. Representative results from one of two healthy donors are shown.

4.2.3 CAR T-cell preparations show increased cytokine productionin combination with ICO15K-cBiTE supernatants

We next tested the cytokine production of CAR T-cell preparation in cocultures treated with the different supernatants for 48 hours. As expected, UTD control T cells secreted high levels of IFN-γ and TNF-α when cocultured with A431 or L55 cells only in the presence of the cBiTE supernatant (Figures 50A and B). Consistent with the results described above for T-cell activation, only cocultures of CAR T cells with A431 cells and cBiTE led to high cytokine production. Importantly, when both mesothelin and EGFR were present (*i.e.* L55 cells), CAR

T-cell preparations treated with ICO15K-cBiTE supernatants secreted significantly higher cytokine levels than the mock-treated cocultures, which are the positive control for the action of CAR$^+$ cells. Interestingly, cocultures of L55 cells and CAR T cells treated with ICO15K supernatants led to a decrease in cytokine production compared to the mock control, which suggests a moderate interference of the virus with CAR-mediated T-cell activation.

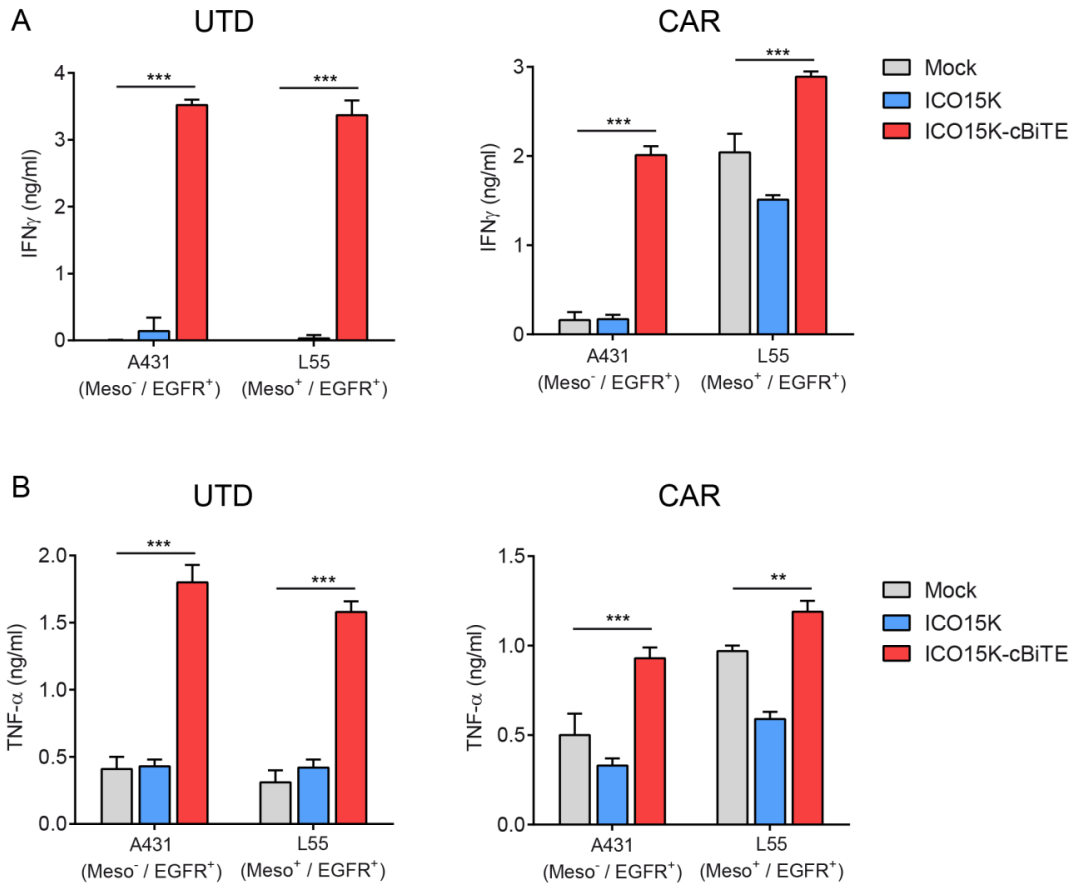

Figure 50. CAR T-cell preparations show increased cytokine production in combination with ICO15K-cBiTE supernatants. CAR or untransduced (UTD) T-cell preparations were cocultured with A431 or L55 cells (E:T = 2) in the presence of the indicated supernatants. 48h later, the coculture supernatants were assessed for IFN-γ **(A)** and TNF-α **(B)** production by ELISA. Representative results from one of two healthy donors are shown. The mean ± SD of triplicates is shown. **, $P < 0.01$; ***, $P < 0.001$ by One-way ANOVA with Tukey post-hoc test.

4.2.4 CAR T-cell preparations show increased proliferation in combination with ICO15K-cBiTE supernatants

Proliferation after antigen recognition is a key feature of CAR T cells. We therefore evaluated whether ICO15K-cBiTE supernatants could enhance the proliferation of CAR T-cell preparations. Cocultures with the same settings described above were incubated for 5 days and the proliferation of total $CD4^+$ and $CD8^+$ T cells was assessed by flow cytometry. In cocultures with A431 cells, T cells from UTD and CAR T-cell preparations proliferated only when treated with the cBiTE supernatants (Figures 51A). As expected, T cells from CAR T-cell preparations proliferated in cocultures with L55 cells in the presence of all three treatments, which indicated the engagement of the CAR towards meosthelin. Notably, ICO15K-cBiTE treatment caused a significant increase in the proliferation of CAR T-cell preparations compared to the mock- or ICO15K-treated ones (Figures 51B).

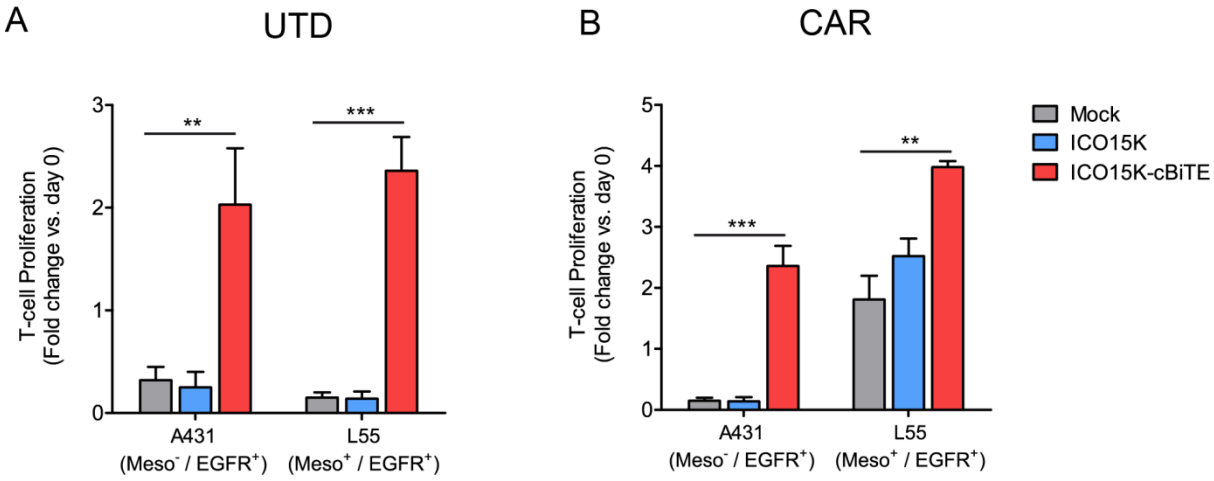

Figure 51. CAR T-cell preparations show increased proliferation in combination with ICO15K-cBiTE supernatants. Untransduced (UTD; **A**) or CAR **(B)** T-cell preparations were cocultured with A431 or L55 cells (E:T = 2) in the presence of the indicated supernatants. 5 days later, the total number of live T cells within the cocultures was determined by flow cytometry using counting beads. Total cell count at the end of the experiment was normalized to the total cell count at day 0. Representative results from one of two healthy donors are shown. The mean ± SD of triplicates is shown. *, $P < 0.05$; **, $P < 0.01$; ***, $P < 0.001$ by One-way ANOVA with Tukey post-hoc test.

4.2.5 ICO15K-cBiTE improves the cytotoxic potential of CAR T-cell preparations *in vitro*

To test whether ICO15K-cBiTE could improve the killing capacity of CAR T cells in an oncolysis setting, cocultures of L55 cells and CAR or UTD T cells were infected with ICO15K or ICO15K-cBiTE and cell death was monitored with the xCELLigence system. UTD T cells alone had no effect on tumor cell growth in contrast to CAR T cells alone which reduced tumor cell growth. Similarly to what we observed in the xCELLigence experiments described above, ICO15K-cBiTE in combination with UTD cells improved the overall killing of L55 cells when compared with the combination of UTD and ICO15K (Figure 52). L55 cells treated with the combination of ICO15K and CAR T cells led to increased cell death compared to the UTD/ICO15K treatment, and it was similar to that of the UTD/ICO15K-cBiTE treatment. Importantly, the combination of ICO15K-cBiTE with CAR T cells reduced the time of killing of L55 cells compared to any of the other treatments. These results demonstrate that ICO15K-cBiTE can improve the overall cytotoxic potential of mixed populations of CAR^+ and CAR^- T cells *in vitro*.

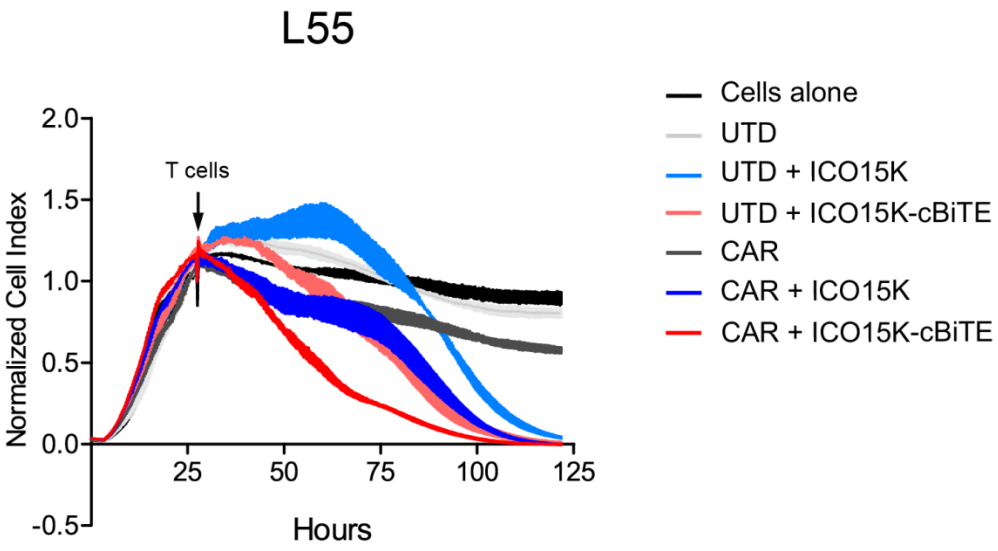

Figure 52. ICO15K-cBiTE-mediated oncolysis improves the cytotoxic potential of CAR T cells. L55 cells were seeded and infected with ICO15K or ICO15K-cBiTE at an MOI of 1 at t_0. CAR or untransduced (UTD) T cells were added 24 hours later at an E:T ratio of 1. Impedance at well bottoms was measured every 20 min for 120h and normalized to baseline impedance values with medium only. The mean ± SD of duplicates is shown. One representative experiment from three independent T-cell preparations from different healthy donors is shown.

Altogether, the results from this chapter demonstrate that ICO15K-cBiTE can engage CAR^+ T cells even in the absence of its primary target, and that simultaneous engagement of UTD and CAR^+ T cells via the cBiTE and CAR, respectively, can improve the overall immune functions of CAR T-cell preparations. The potential of these observations *in vivo* will be evaluated humanized mouse models of cancer by Sonia Guedan at the University of Pennsylvania.

5. DISCUSSION

5.1 BiTE-ARMED ONCOLYTIC ADENOVIRUSES

The immune system represents one of the major hurdles for the success of oncolytic adenoviruses (OAds) in cancer patients. Despite the highly immunosuppressive tumor microenvironment (TME), OAd-infected cancer cells can be efficiently cleared from the organism by infiltrating Ad-specific CTLs without compromising the tumor load [57]. Most of the strategies used to date to improve virotherapy have aimed at arming OAds with molecules which elicit a general but unspecific activation of the immune system [114]. We hypothesized that arming OAds with BiTEs that redirect immune response towards cancer cells would solve key challenges in oncolytic virotherapy.

In this thesis, we have genetically engineered the OAd ICO15K to encode EGFR-targeting BiTEs that are produced by and secreted from infected cells. We chose the EGFR as the tumor-associated antigen (TAA) being targeted by the BiTEs encoded in the viruses for several reasons. This receptor has been widely studied in the context of cancer and it is recognized as one of the best models to describe oncogenes [191]. Furthermore, the EGFR is overexpressed in a wide range of human solid tumors [180, 181], and the role of its intracellular signaling in colorectal cancer has been well characterized [192]. The important role of the EGFR in cancer has led to the development of several targeted therapies, including the monoclonal antibody Cetuximab (Erbitux) [191, 193].

5.1.1 Molecular considerations for the design of BiTE-armed oncolytic adenoviruses

For the construction of a BiTE with potential for translation into patients (cBiTE), we chose the scFVs derived from the monoclonal antibodies Cetuximab and L2K. Cetuximab is routinely used in patients with colorectal cancer and head-and-neck squamous cell cancer [194, 195], and its mode of action has been extensively studied [196, 197]. Most importantly, the functionality of the Cetuximab-derived scFV as a BiTE format has been validated in a preclinical study [176]. The scFV from the L2K antibody was the same that is used in the Blinatumomab BiTE, which is optimized for binding to the CD3 in this format [177], and has been used in BiTEs targeting different TAAs [175, 198, 199] . Given the well-documented preclinical studies with these two scFV, the design of our cBiTE would facilitate the potential translation of ICO15K-cBiTE into patients.

The rationale behind the molecular design of the BiTEs described in this work was based on the literature of antibody engineering studies. For the cBiTE, the anti-EGFR (Cetuximab)

and anti-CD3 (L2K) scFVs were located at the N- and C-terminus, respectively. This format was chosen based on the fact that all BiTEs with clinical development so far have this conformation [161]. Furthermore, it has been reported that placing the OKT3 or L2K anti-CD3 scFVs at the N-terminus negatively affects the binding capabilities of some BiTEs [200, 201]. In contrast to the cBiTE, all BiTEs containing the 145.2C11 scFV (*i.e.* mBiTE and mcBiTE) were designed to place the anti-mCD3 scFV at the N-terminus since its function is improved at this location [173, 179]. One concern for these BiTEs was the potential malfunction of the TAA-targeting scFV placed at the C-terminus in the soluble molecule. In the case of the mcBiTE, this arrangement did not affect the binding capabilities of the Cetuximab scFV, which is in agreement with a previous study in which the same scFV placed at the C-terminus of a fusion protein retained its functionality [202]. In contrast to the mcBiTE, we could not detect functional mBiTEs in the supernatants from ICO15K-mBiTE-infected cells. Since no scFVs versions of the 7A7 have been described in the literature and we only evaluated one arrangement for this BiTE, we cannot discard the possibility that this particular antibody needs a specific arrangement for its optimal folding and activity as a scFV.

The arrangement of the scFV variable domains in BiTEs is also relevant for their optimal functionality. Although most of the BiTEs described so far retain binding capacities in any of the arrangements tested, some specific orientations show superior binding and cytotoxic activities than others [201, 203]. The cBiTE was comprised of the anti-EGFR scFV in the VL-VH orientation linked through a G4S linker to the L2K scFV in the VH-VL orientation, which is the arrangement that more closely resembles Blinatumoamb [204].

cBiTE secretion by infected cells was confirmed by flow cytometry-based binding assays. Whereas binding signal to $EGFR^+$ cells was clear using unconcentrated supernatants, only a minor binding signal was detected for the $CD3^+$ with the same supernatants. This indicates that the binding of the cBiTE to the EGFR was of higher affinity than to the CD3. This is a similar behavior to what has been described for Blinatumomab, for which binding saturation to the TAA (*i.e.* CD19) is achieved at lower concentrations (K_d = 1.49 × 10^{-9} M) than to the CD3 (K_d = 2.6 × 10^{-7} M) [205]. In general, AMGEN's BiTE pipeline is structured in a way that the affinity of the L2K scFV remains constant, while the affinity of the other scFV can be adjusted depending on the nature of the TAA and the desired activity of the BiTE [206]. It is worth mentioning that other BiTEs which do not incorporate the L2K scFV have shown potent activity as well. An example is bscEGFRvIIIxCD3, which is composed of an anti-EGFRvIII scFV fused to a scFV derived from the FDA-approved monoclonal antibody

Muromonab (OKT3). This BiTE has demonstrated potent activity *in vitro* and *in vivo* in glioblastoma models [207].

We decided to control BiTE expression from the MLP by incorporating the Adv IIIa splicing acceptor, a strategy that has been widely used by us and others to restrict transgene expression to virus replication [44, 48, 50]. We demonstrated by flow cytometry the secretion of the cBiTE to the supernatant of cell cultures after 72 h of infection with ICO15K-cBiTE. Although we tried to purify the cBiTE from culture supernatants by affinity chromatography to perform quantification assays, unspecific binding of BSA to the anti-FLAG antibody coupled to the agarose beads prevented the proper isolation of pure cBiTE molecules (data not shown). Even though no quantitative analysis of cBiTE secretion could be performed, a rough estimate of the concentration present in our supernatants can be suggested by taking advantage of the similar binding behavior of the L2K scFV in our BiTE and Blinatumomab. Dreier *et al.* used two concentrations (0.4 and 10 µg/ml) for saturation binding assays of the scFVs from Blinatumomab [205]. In the lower concentration, they observed a modest binding to the CD3 and a clear binding (almost half-way to saturation) to the CD19. This is a similar behavior to what we observed with unconcentrated supernatants of ICO15K-cBiTE, although the binding to the CD3 we observed was lower. Thus, we can roughly speculate that the cBiTE concentration in our supernatants was < 0.2 µg/ml. Although BiTE antibodies have potent activities at low concentrations, these levels of BiTE expression seem low compared to what has been reported for other therapeutic proteins encoded from OAds. Since BiTE action is dose-dependent, it would be worth trying to improve BiTE secretion from infected cells. A strategy to achieve this would be modulating BiTE expression with regulatory elements others than the IIIa splicing acceptor. Examples of such regulatory elements are the HAd-40 long fiber gene splice acceptor (40SA) [208] or linking the BiTE and fiber genes with the IRES from the encephalomyocarditis virus [209, 210]. A side-by-side comparison of OAds armed with an anti-CEA scFV-FC whose expression was controlled by these regulatory elements (*i.e.* IIIa, 40SA and IRES) demonstrated that the IIIa splicing acceptor showed the weakest activity, making protein undetectable by western blot [211]. This is in agreement with our results, as we could not detect the cBiTE by western blot unless it was concentrated (data not shown). That same study highlighted the superior activity of the 40SA over the other elements evaluated, giving protein concentrations up to 10 µg/ml 120 h after infection at low MOI. Ongoing projects in our group are evaluating the potential of controlling BiTE expression from the MLP via the 40SA in order to increase the concentration of the secreted protein.

The size of the engineered ICO15K genomes encoding the BiTEs was approximately 37.7 kb, which represents a 105% of the original Ad5 genome size. This percentage is the packaging limit that has been described for Ads, as inserts giving a genome size above 105% result in unstable viruses with multiple genomic rearrangements after three to four culture passages [55, 56]. All our BiTE-armed OAds had similar cytopathic effect as the parental virus, and rearrangements during amplification in A549 cells (5 passages until purification) were ruled out by restriction analysis, and sequencing of the *E1a*- and *BiTE*-coding regions. Although we were able to amplify ICO15K-cBiTE and ICO15K-mcBiTE to good titers and ratios, their onocolytic properties were reduced compared to ICO15K. In the case of the cBiTE, the loss in cytotoxicity might be a consequence of the reduced virus production we observed in cancer cells. This loss in production and cytotoxicity is likely the result of the competition between the BiTE and viral genes for the transcription and translation machinery of the cell. A recent study has shown that incorporation of a codon-optimized transgene as an L6 unit under the control of the MLP can attenuate adenoviral fitness [212]. This is in agreement with our experience with several OAds carrying MLP-driven transgenes optimized for human codon usage, which consistently show reduced *in vitro* cytotxic potential compared to the parental virus. Despite this, the cBiTE gene gives a remarkable advantage to the virus in the presence of T cells even at low MOI *in vitro*. Importantly, the *in vitro* loss of production and cytotoxicity of the cBiTE-expressing virus did not translate into a loss in antitumor efficacy *in vivo* in the absence of PBMCs compared to ICO15K. This is likely explained by the excess virus that is produced in one round of replication (ICO15K ≈ 9000 TU/cell and ICO15K-cBiTE ≈ 7000 TU/cell). We do not expect that all virus progeny produced from one infected cell will be able to infect the equivalent amount of cells due to the many barriers encountered in the tumor microenvironment. Thus, the amount of virions produced by ICO15K-cBiTE-infected cells is expected to give a similar antitumor advantage as the parental virus in tumor microenvironments in which stromal cells limit virus spread.

5.1.2 The promise and challenges of BiTE-armed oncolytic adenoviruses

The main goal of this project was to generate an OAd encoding a BiTE antibody that could redirect T-cell responses to $EGFR^+$ cancer cells. ICO15K-cBiTE-infected cells successfully secreted BiTEs that retained key features of BiTE antibodies including target cell-dependent T-cell activation and proliferation, and redirected lysis of cancer cells [162, 213]. We further demonstrate that ICO15K-cBiTE promotes T-cell infiltration into $EGFR^+$ tumors and has superior antitumor efficacy compared to the parental virus.

The potential of BiTE-armed OVs has been previously demonstrated using an oncolytic vaccinia virus with an EphA2-targeting BiTE (vv-EphA2) [214]. Whereas vv-EphA2 induced T-cell activation and PBMCs-mediated bystander killing of cancer cells, no T-cell proliferation was observed in the absence of exogenous IL-2 *in vitro* and *in vivo*. In contrast, we observed that ICO15K-cBiTE induced remarkable proliferation of T cells *in vitro,* without the addition of IL-2 to the cocultures. This difference could be related to the BiTE design or the O used. Another noteworthy finding from our *in vivo* experiments was the increased T-cell infiltration and expansion observed in subcutaneous tumors treated with the cBiTE-expressing virus after intravenous T-cell administration. With regard to antitumor efficacy, vv-EphA2 prevented tumor growth of subcutaneous A549 tumors that were coimplanted with PBMCs immediately followed by an intraperitoneal injection of the virus, and delayed growth of 7-day established lung A549 tumors after the coadministration of vv-EphA2 and PBMCS. In our antitumor efficacy experiments we chose to use tumors established for longer periods (three and two weeks for A549 and HCT116, respectively), and efficacy was observed even in this setting. Altogether, our work confirms the potential or arming OVs with BiTEs.

The strategy of arming OAds with BiTE antibodies represents a unique opportunity to exploit the best features of both therapies simultaneously, while overcoming many of the hurdles encountered by both agents as monotherapies. From the point of view of the BiTE, its localized expression from infected cancer cells would reduce the adverse side effects commonly observed in preclinical and clinical studies of BiTEs, some of which can be fatal if not treated appropriately [215]. Additionally, the continuous production of BiTE molecules from infected cancer cells would likely increase its availability at the tumor site. This would be advantageous given the short half-life of BiTEs in the serum, requiring the continuous infusion of the drug to patients for extended periods of time (*i.e.* 4-6 weeks) [216]. Conversely, the mode of action of BiTE antibodies could help to overcome some of the limitations in oncolytic virotherapy. Although OAds have been shown to elicit specific T-cell responses to tumor neo-epitopes *in vivo* [104], the immunodominance of adenoviral epitopes is known to mask immune responses to delivered transgenes or capsid-displayed tumor antigens [155, 156]. We and others have successfully developed different approaches to favor MHC-I-restricted antitumor rather than antiviral immune responses [112, 158, 159]. However, these strategies rely on the expression of MHC-I, which is known to be downregulated on cancer cells as one mechanism to escape from antitumor immune responses [100, 101]. The MCH-I-independent and polyclonal mode of action of BiTEs offers

a unique opportunity to theoretically activate and redirect any tumor infiltrating T cell, including Ad-specific CTLs, to cancer cells. Interestingly, it has been recently reported that BiTE antibodies can engage cytomegalovirus-specific enriched CTLs to kill cancers cells *in vitro* [217]. Since we have demonstrated the cBiTE-mediated polyclonal engagement of unstimulated and preactivated $CD4^+$ and $CD8^+$ T cells towards cancer cells, we speculate that redirecting Ad-specific CTLs is also feasible. In addition to the antiviral immune responses, limited virus spread within the tumor due to stromal barriers is another limitation for OAds [1, 50]. The small size of BiTEs (~55 kDa) is advantageous for efficient penetration and distribution throughout the tumor as demonstrated by imaging preclinical studies [218]. This would allow improving the overall bystander effect of OAds even if their spread is limited. Furthermore, this strategy can be expanded to attack the tumor stroma by using BiTEs targeting, for example, the fibroblast activation protein (FAP) alpha on cancer-associated fibroblasts. Such a BiTE has been validated *in vitro* [219], and its expression from infected cells would focus the bystander effect to stromal cells which are normally resistant to the oncolytic effect of the virus. An OAd encoding a BiTE targeting the FAP is currently under investigation in our group.

In addition to the advantages described above, the nature of the cBiTE could offer a positive impact for colorectal cancer patients. One of the major mechanisms of resistance to standard chemotherapy and targeted therapies in this type of cancer is the mutation of downstream signaling genes such as *BRAF*, *KRAS PIK3CA* and *PTEN* [220, 221]. Furthermore, *KRAS* mutation is a negative predictor of Cetuximab efficacy in colorectal cancer patients [222, 223], and the use of this mAb has been restricted to patients bearing tumors with wild-type *KRAS* status [220]. An important advantage of BiTE antibodies is that their mode of action is independent of such somatic mutations [224]. Specifically relevant for our virus is the study of a Cetuximab-derived BiTE, similar to our cBiTE, which has been shown to overcome resistance by successfully redirecting T cells to kill *BRAF*- and *KRAS*-mutated colorectal cancer cells *in vitro* and *in vivo* [176]. Here we have also demonstrated that ICO15K-cBiTE induces a T-cell mediated killing of *KRAS*-mutated HCT116 cells *in vitro* and *in vivo*. Thus, ICO15K-cBiTE represents a potential alternative for colorectal cancer therapies that are susceptible to tumor resistance due to somatic mutations in intracellular signaling pathways.

The progress in the understanding of tumor immunology, along with the development of novel immunotherapies, has led to the classification of tumor according to their T-cell

infiltration status. T-cell-inflamed tumors (also termed “hot” tumors) are characterized by the presence of numerous $CD8^+$ T cells whose function is impaired by a highly immunosuppressive microenvironment (*e.g.* upregulation of PD-1/PD-L1, T_{reg}-cell recruitment and loss of antigen presentation) [225]. In contrast, non-T-cell-inflamed tumors (also termed “cold” tumors) are those in which no T-cell infiltrate is observed due to a lack of innate immune recognition and impaired recruitment of effector T cells due to the loss of chemokine production. Importantly, clinical trials with anti-PD-1 antibodies have shown that clinical benefit of this therapy is almost exclusive to T-cell-inflamed tumors [226, 227]. These observations have led to the identification of one the current most challenging hurdles in immunotherapy: how to overcome non-T-cell inflamed tumor microenvironments to promote T-cell infiltration. In this regard, OVs have gained interest in the past years as potential immunostimulatory agents that can potentiate T-cell infiltration. Indeed, clinical trials have demonstrated the potential of OVs to induce T-cell infiltration and anti-tumor immune responses even in untreated distal lesions [105, 228-232]. Although an increase in melanoma-specific T cells has been observed in patients treated with T-VEC [229], those studies have not addressed whether virus-specific CTLs are also present in the tumor-infiltrating T-cell population. Antiviral immune responses have been identified in patients treated with OAds [105], and it is most likely that antiviral T cells are also present in tumors of patients treated with any OV. Furthermore, antiviral CTLs seem to be fully functional in the immunosuppressive tumor microenvironment [57, 233]. In this regard, ICO15K-cBiTE might represent an attractive candidate to turn cold tumors into hot ones. We demonstrated that our cBiTE-expressing virus promotes infiltration of adoptively transferred T-cells into tumors. Although these results were obtained in immunodeficient mouse models in which no antiviral immune responses are elicited, they support the notion that local delivery of the cBiTE can recruit polyclonal T cells into tumors. We anticipate that in an immunocompetent setting, antiviral immune responses will provide a continuous source of effector virus-specific T cells migrating to the tumor site, where they can be redirected to cancer cells by the cBiTE. Importantly, the potential of antiviral T cells for cancer therapy has been demonstrated *in vitro* and in clinical trials in which EBV-, varicella zoster virus- or Adv-specific T cells modified to express CARs retained their antiviral properties while gaining antitumor-specific activities [234-237]. Altogether, these studies support our hypothesis that Adv-specific T cells redirected to cancer cells by the cBiTE hold potential to improve anticancer therapies, and that the mode of action of ICO15K-cBiTE can potentially overcome non-T-cell-inflamed tumor microenvironments (Figure 53).

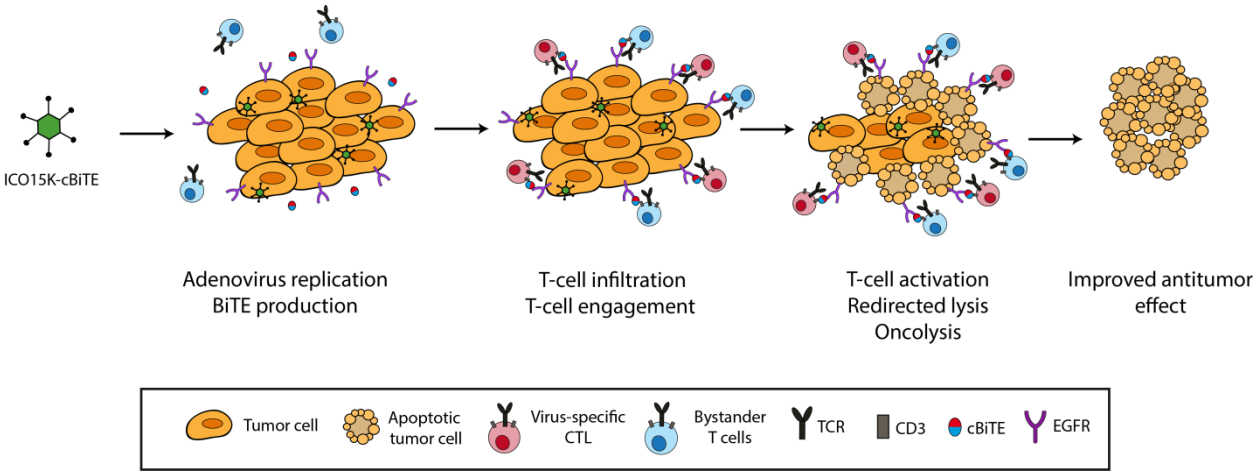

Figure 53. Proposed mode of action of ICO15K-cBiTE. Infection and replication of ICO15K-cBiTE in cancer cells leads to cBiTE secretion to the tumor microenvironment. Virus replication also triggers the infiltration of adenovirus-specific CTLs which target infected cells. However, secreted cBiTEs can redirect these cells and any other $CD3^+$ resident or infiltrating T cells to lyse $EGFR^+$ uninfected cancer cells. The action of virus-mediated oncolysis in combination with BiTE-mediated redirected lysis of cancer cells by T cells results in improved antitumor efficacy.

Despite the advantages of ICO15K-cBiTE as novel candidate for cancer therapy, cBiTEs secreted from infected cells face the same challenges as any other BiTE in the tumor microenvironment. As any other targeted therapy that relies on the expression of surface markers, BiTE action can be evaded by tumors if the targeted antigen is lost. It has been recently reported that four patients with ALL under Blinatumomab treatment developed relapses with $CD19^-$ B-cell phenotype [238]. Deeper analysis of one of these patients revealed that CD19 loss was the results of impaired trafficking of the antigen from the endoplasmic reticulum to the cell surface. We did not determine the expression of EGFR in the tumors from the *in vivo* antitumor efficacy studies. Although it is tempting to assume that EGFR downregulation will occur in cancer cells during BiTE treatment, data from the literature argue against this. One of the mechanisms of action of Cetuximab is the induction of EGFR internalization and degradation which leads to reduced proliferation of cancer cells [197]. However, it has been shown that cancer cells acquire resistance to Cetuximab by impairing this internalization and degradation, which leads to its stabilization in the membrane and cross-talk with other members of the ErbB family [239]. These studies suggest that that loss of EGFR is detrimental for cancer cells due to its central role in carcinogenesis. More importantly, the activation of the *EGFR* pathway plays a central role in the evasion of the antitumor immune response by inducing expression of *PD-L1* [240, 241].

Thus, the combined mechanisms of EGFR-induced carcinogenesis and tumor immune evasion suggests that EGFR is a good target for immunotherapies and that its downregulation, as a result of selective therapeutic pressure, might be detrimental for cancer cells. Despite this, future studies will have to address potential loss of this receptor under ICO15K-cBiTE therapy.

Another challenge for BiTE antibodies that has been recently suggested is the potential induction of T-cell exhaustion during BiTE treatment. Exhausted T cells are characterized by upregulation and co-expression of inhibitory receptors, a particular transcriptional signature, and loss of effector functions (*i.e.* cytokine production, proliferation and cytotoxic potential) as a result of chronic exposure to antigens [183, 184]. Although the precise exhaustion status of T cells after BiTE treatment is still unclear, recent studies demonstrate that BiTE-engagement of T cells leads to phenotypes that share some of the hallmarks of T-cell exhaustion. *In vitro*, T cells that have been cultured in the presence of target cells and BiTEs show reduced cytotoxic potential in second rounds of treatment due to an increase in expression of PD-1 and PD-L1 on T cells and tumor cells, respectively [242]. In line with these observations, cocultures of AML patient T cells and blasts treated with the anti-CD33 BiTE AMG-330 showed increased PD-L1 and PD-1 expression on blasts and T cells, respectively, compared to baseline conditions [243]. It is worth noting, however, that PD-1 is also expressed in recently activated effector T cells and, thus, its expression cannot be designated as a unique feature to define exhausted T cells. In fact, Köhnke and colleagues reported a case study in which T cells from one ALL patient refractory to Blinatumomab treatment showed reduced cytokine production and cytotoxic potential, even though PD-1 expression levels were not different from those on healthy donor T cells [244]. Additionally, a recent study has demonstrated that T cells from ALL patients show increased expression of PD-1, TIM-3 and LAG-3, when compared to T cells from healthy donors after coculture with autologous blasts in the presence of Blinatumomab [245]. Most of the studies described above have demonstrated that PD-1 blockade can restore T cell function *in vitro*, indicating that BiTE-induced dysfunction of T cells can be reverted. Most importantly, Feucht and colleagues have reported that an ALL patient refractory to Blinatumomab therapy showed increased PD-L1 expression on blasts and that combination of the same BiTE with anti-PD-1 blockade can result in clinical responses. Due to all this evidence and because of the importance of checkpoint regulation in immunotherapies, we performed *in vitro* phenotypical characterizations of T cells after ICO15K-cBiTE treatment. ICO15K-cBiTE-mediated oncolysis induced the expression of the inhibitory receptors PD-1, TIM-3, CD200

and LAG-3 on T cells. Although this increased expression suggests an exhausted T-cell phenotype, a deeper phenotypic T-cell characterization is required to determine the potential dysfunctional level after BiTE-mediated T-cell engagement. This characterization is becoming more relevant for the field of oncolytic virotherapy given the increase in the number of studies combining OVs with checkpoint inhibitors [246]. Furthermore, the importance of such analysis for virotherapy applications has been recently highlighted by the study Shim *et al*., in which the antitumor efficacy of a TAA-expressing VSV oncolytic virus was not improved when combined with checkpoint inhibitors, despite the detection of $CD8^+$ effector T cells expressing high levels of PD-1 and TIM-3 after treatment with TAA-VSV as monotherapy [247]. These results suggest that PD-1 and TIM-3 expression on those T cells represented markers of acute T-cell activation rather than exhaustion. Thus, we cannot rule out the possibility that this is also happening in the context of ICO15K-cBiTE-mediated oncolysis. Although a more thorough evaluation of the exhaustion status of T cells after ICO15K-cBiTE treatment is needed, our results encourage the evaluation of BiTE-armed OAds in combination with checkpoint inhibitors as a strategy to improve antitumor efficacy.

5.2 THE CHALLENGE OF ESTABLISHING MURINE MODELS FOR THE *IN VIVO* EVALUATION OF BiTE-ARMED ONCOLYTIC ADENOVIRUSES

5.2.1 Humanized mouse models of cancer

One of the major challenges in this thesis was the *in vivo* evaluation of our BiTE-armed OAds. In the case of ICO15K-cBiTE, the design of the BiTE (both scFV strictly recognize human antigens) restricted its evaluation to “humanized” immunodeficient mouse models bearing human-derived tumor xenografts in which human PBMCs or T cells are transferred to mice. Taking this into account, a series of decisions had to be taken based on the potential therapy setting for ICO15K-cBiTE. First, it was necessary to choose a mouse strain with a high level of immunodeficiency to allow sufficient engraftment of human PBMCs/T cells. Mice strains with the *scid* mutation background, which impairs T- and B-cell maturation and circulation, have been extensively studied in this context [248, 249]. Additionally, SCID, NOD/SCID and SCID/beige mice have been used for the preclinical evaluation of BiTE antibodies [176]. SCID/beige mice combine the *scid* mutation with the *beige* mutation, which reduces NK cell activity, resulting in a more stable background with reduced leakiness of mature T and B cells compared to SCID mice [175, 250]. This strain has been used for Yu *et al.* for the evaluation of the BiTE-expressing vaccinia virus [214]. Furthermore, SCID/beige mice have served as an

important model to elucidate the role of E1a in the hepatotoxicity associated with oncolytic adenoviruses [251]. Due to all the reasons described above, we decided to choose the SCID/beige strain as the model to evaluate ICO15K-cBiTE.

We next needed to decide the route of inoculation for cancer cells and PBMCs/T cells. The most frequently strategy used for the preclinical evaluation of BiTEs is the subcutaneous co-implantation of cancer cells and PBMCs, and the subsequent BiTE treatment (4-5 administrations) in the first twelve days post tumor inoculation. Hence, in this setting, the end objective is the prevention of tumor formation. However, we discarded this strategy for several reasons. The first pilot study we performed using this strategy led to the rejection of the A549 tumors when co-implanted with PBMCs even before treatment, whereas tumors without PBMCs showed normal growth (data not shown). Furthermore, Schlereth and colleagues have shown that NOD/SCID mice co-engrafted with tumor cells and human PBMCs subcutaneously only respond to the therapy if BiTE treatment is started in the first eight days after engraftment [198]. Also, the later the treatment is started after engraftment, the more variability is observed in antitumor efficacy. In our experience, none of the cell lines used in this thesis will form measurable tumors eight days after inoculation. This limits the delivery window of our OAds which should be administered either intratumorally or systemically when tumors have been established. Another strategy that has also been used for the evaluation of anti-cancer therapies, including the vv-EphA2 virus, is the establishment of lung xenografts by intravenous injection of luciferase-expressing cancer cells into the mice [252]. In this setting, virus and PBMCs are co-administered intravenously few days after tumor inoculation (4-7 days) and tumor growth is measured by *in vivo* imaging [214]. This model is ideal, since all its components (cancer, virus and T cells) are injected into the bloodstream, directing them unequivocally to the lung. However, in our experience, luciferase-expressing A549 cells take longer than 4-7 days (approximately 3 weeks) to form fully established tumors that are detectable with the IVIS system. Once at this stage, tumors are too aggressive to be controlled and the therapeutic window for this model is short before euthanasia is required. Based on all the above, we decided to use subcutaneous xenograft tumors of approximately 100 mm^3, which allows to deliver ICO15K-cBiTE intravenously or intratumorally, followed by intravenous adoptive transfer of PBMCs/T cells. Such a model has been successfully tested in a study evaluating the combination of oncolytic adenoviruses with CAR T-cells [152].

The dose and route of administration of human PBMCs or T cells transferred to immunodeficient mice were also important factors to take into account for our *in vivo* model. There are two common routes for adoptive transfer of humans cells into mice: intravenous (tail vein injection) and intraperitoneal. In contrast to intravenous administration in which cells are directly injected into the circulation of the host, the intraperitoneal administrations requires the migration of the T cells from the peritoneal cavity to the circulation which delays their biodistribution in the mice [253]. Since T cells do not persist long in our SCID/beige model (see below), we decided to use intravenous administration to increase the time of the cells in the bloodstream before clearance from the mice. A major concern with this intravenous approach is the potential development of PBMCs-mediated graft versus host disease (GvHD), which is well described in experiments involving adoptive transfer of human PBMCs or T cells to highly immunodeficient mice [248, 254]. It has been described that NOD/SCID mice receiving less than 30 million PBMCs intravenously are unlikely to develop GvHD before 60 days after cell transfer [255]. We therefore decided to administer a total of 20 million PBMCs per mouse in two administrations (10 million/each) at day 4 and 18 after virus administration. With this experimental setting we did not detect any signs of GvHD in our mice at the end of the A549 antitumor efficacy study, which was 45 days after the first PBMCs administration.

The *in vivo* experimental settings used in this thesis allowed us to study the antitumor efficacy of ICO15K-cBiTE and also the distribution behavior of luciferase-expressing T cells in tumors treated with the BiTE-expressing virus. However, one of the major drawbacks from our model was the limited immunological analysis we could perform during the course of the *in vivo* experiments. We could not detect $CD3^+$ infiltrating cells in tumors at the end of the A549 antitumor efficacy experiment (31 days after the last PBMCs administration) neither by flow cytometry or immunohistochemical analysis. This is most likely explained by the short persistence of human T cells in SCID/beige mice. In our *in vivo* imaging studies, whole body T-cell signal in PBS- and ICO15K-treated animals decrease after 3 days and infiltrating T cells persisted up to 9 days only in ICO15K-cBiTE-treated tumors. This is in agreement with BiTE studies in which human unstimulated T cells transferred to SCID mice by tail-vein injection have a half-life in spleens of 11 hours, although some residual circulating cells are still detected 3 days after injection [175]. Thus, this short persistence limited the analysis of immunological responses and phenotyping of those TILs. One potential alternative to solve this limitation is the use of NSG mice, which have arisen in the past years as an important tool for the preclinical evaluation of immunotherapies such as CAR T cells. These mice have

higher levels of engraftment of human PBMCs/T cells than other SCID strains, allowing a more robust analysis of T-cell responses in mice. The potential of this model for the evaluation of immunovirotherapy applications is exemplified by a recent study in which NSG mice engrafted with human PBCMs have been used to evaluate the potential of a vaccinia OV armed with DNA-dependent activator of IFN-regulatory factors (DAI) [256]. It is worth mentioning that by the time we started this project, to our knowledge, all human BiTE studies reported in the literature were evaluated either in SCID, NOD/SCID or SCID/Beige mice. The only exception we have found is a recent study evaluating a BiTE targeting the fetal tight junction molecule claudin 6 (CLDN6) [257]. In that study, NSG mice were engrafted with PBMCs 4 or 11 days prior to BiTE treatment, and this setting allowed a thorough phenotypic analysis of TILs. Given the advantages of NSG, all OAds armed with BiTEs targeting human antigens that are currently under development in our group will be evaluated in this mouse strain. The short persistence of T cells in SCID/Beige also narrowed the therapeutic window for ICO15K-cBiTE. We designed our *in vivo* experiments so that virus administration was performed 4-7 days prior to PBMC- or T-cell administration to maximize virus replication and cBiTE accumulation in tumors prior to T-cell infiltration. In this way we aimed at maximizing the cytotoxic potential of TILs before their clearance from the host.

We evaluated ICO15K-cBiTE systemically, which is the preferred route of administration for OAds in clinical trials to maximize the delivery of the virus to primary and metastatic tumors. Furthermore, we have previously described that replacing the KKTK domain in the shaft of the fiber with an RGD motif enhances the systemic antitumor efficacy of ICO15K by reducing liver targeting and increasing virus bioavailability in the blood [47]. In our study, the systemic administration of ICO15K to SCID/beige mice led to a decrease, although not significant, in HCT116 tumor volume when compared to the PBS group. This modest antitumor efficacy might be explained by the low dose of virus administered to the mice. It has been demonstrated that SCID/beige mice are more sensitive to oncolytic adenovirus infection than BALB/c nude mice due to their increased immunodeficiency [251]. Based on our preliminary studies, we determined that the highest systemic tolerated dose of our viruses in SCID/beige mice was $1x10^{10}$ VP/mouse. This dose is five times lower than the one used for the antitumor efficacy studies of ICO15K in nude mice, in which a clear advantage was observed in several human cancer xenografts. Note, however, that this low dose was enough to observe the advantage of ICO15K-cBiTE in the aggressive and fast-growing HCT116 tumor model.

Since the EGFR is expressed on the cancer cells targeted by the virus, we were concerned about the potential interference of the cBiTE-mediated cell killing with virus replication and persistence *in vivo*. Nevertheless, we were able to detect the Ad E1a protein in all virus-treated tumors at the end of both antitumor efficacy studies. Of note, no differences were observed for E1a staining in A549 tumors, indicating that virus persistence was independent of PBMCs administration. Furthermore, we detected similar levels of hexon mRNA transcripts in ICO15K- and ICO15K-cBiTE-treated tumors after 4 days of T-cell administration. These results show that, at least in our models, cBiTE-mediated cancer cell death does not compromise the short- or long-term persistence of the virus in the tumor. It is worth mentioning again that these results are likely underrepresented due to the transient persistence of human T cells in SCID/beige mice.

5.2.2 Immunocompetent mouse models of cancer

Although the humanized models described above are important for the preclinical evaluation of immunotherapies, the restriction of BiTEs to human antigens hinder the study of their toxicological and pharmacological parameters in immunocompetent models. Furthermore, these models lack fully functional adaptive immunity, which limits the evaluation of our hypothesis regarding the redirection of virus-specific CTLs. To overcome these restrictions, researchers have developed mouse surrogates of the human version of BiTE antibodies by using scFVs recognizing murine TAAs and murine CD3. One example is muS110, a surrogate of the human BiTE MT110 that was generated by fusing scFVs targeting murine EpCam and murine CD3. This BiTE has shown potent antitumor efficacy in syngeneic mouse models of cancer and has provided insightful observation regarding the pharmacokinetics of BiTEs [185, 186, 258]. Furthermore, the pattern of expression of EpCam in human and murine in normal tissue is similar, which has allowed toxicological safety studies regarding potential off-target toxicities of BiTEs. With the design of the mBiTE, we aimed at generating a surrogate of cBiTE by fusing the 7A7 scFV, which targets human and murine EGFR, with the scFv of the anti-mCD3 145.2C11 antibody. We could not detect mBiTE production by infected cells in flow cytometry binding assays in which $EGFR^+$ or $mCD3^+$ cells were used. As discussed above, the lack of functionality of this BiTE is likely a failure in the particular arrangement tested. It is worth mentioning that, despite the advantages of BiTE surrogates, the biological and molecular patterns between mouse and humans are often not overlapping. For example, the administration of mus110 to mice can lead to off-target side effects due to the engagement of BiTEs towards a subpopulation of circulating $EpCam^+$ T and

B cells [186]. Of note, this $EpCam^+$ population is not observed in human PBMCs, highlighting the importance of being prudent when extrapolating results in murine models to humans.

Due to the lack of a functional murine surrogate of the cBiTE, we used another approach by generating a chimeric BiTE (mcBiTE) recognizing the human EGFR and murine CD3. We detected the mcBiTE in supernatants from ICO15K-mcBiTE cells and it retained key features of BiTE antibodies, including target cell-dependent T-cell activation and proliferation, and MHC-I-independent redirected lysis of hEGFR-expressing murine cancer cells *in vitro*. Although mcBiTE induced high expression levels of activation markers on $CD4^+$ and $CD8^+$ T cells, T-cell proliferation was clearly skewed towards $CD8^+$ cells. To our knowledge, there are no reports in the literature describing mouse T-cell proliferation for any of the surrogate BiTE developed to date. Despite this, Amann and colleagues have shown that systemic administration of muS110 results in a faster onset of activation for $CD8^+$ compared to $CD4^+$ cells [186]. Thus, we cannot discard the possibility that faster T-cell activation can lead to earlier proliferation of $CD8^+$ T cells.

The *in vivo* evaluation of ICO15K-mcBiTE required the generation of mouse cancer cell lines expressing the human EGFR. A major limitation for the evaluation of the OAds in immunocompetent mouse models is the reduced permissiveness of murine cancer cell lines to HAd infection. Although there have been reports of productive Ad infection in some murine cancer cell lines, we decided to use B16CAR which have been previously used in our group. Ad infection does not produce progeny in this cell line, but the increased Ad transduction efficiency and the expression of late proteins in these cells suggest that it could be an interesting model to evaluate the mcBiTE-expressing OAd. Furthermore, this cell line has been used in our group to evaluate the immunotherapeutic potential of OAds expressing TAAs to be presented in a TAP-independent manner [159]. We confirmed that B16CAR cells supported the expression of MLP-driven transgenes, as evidenced by the detection of functional mcBiTE in the supernatants from ICO15K-mcBiTE-infected cells. We generated the B16CAR-EGFR cell lines by transfection and demonstrated that Ad transduction efficiency was retained despite a reduction in CAR expression. However, mcBiTE production in this cell lines was clearly reduced compared to the parental cell line. This is likely the result of a competition of CAR and EGFR transcripts with viral-encoded transcripts for the translational machinery of the cells. Despite this, mcBiTE could still be detected in supernatants from B16CAR-EGFR cells, and this expression level would likely have been sufficient *in vivo* given the potent action of BiTEs at low concentrations. However, B16CAR-EGFR cells implanted in

the flanks of C57BL/6 mice failed to generate tumors, restricting the *in vivo* evaluation of ICO15K-mcBiTE. It is uncertain why these cells failed to establish tumors in immunocompetent mice. Several groups have successfully used B16 cells as platforms to establish tumors expressing human antigens such as EpCam, CD20 and CAR [159, 179, 259]. One possibility is that the coexpression of CAR and human EGFR (hEGFR) rendered the cells with higher immunogenicity leading to their immune rejection. Another possibility is that the nature of the wild-type (wt) hEGFR is already immunogenic enough to induce its immune rejection by the mouse. Our results are in disagreement with the study by Yang *et al.*, who successfully established $hEGFR^+$ tumors in C57BL/6J mice in order to study tumor resistance to antibody therapy [260]. Furthermore, that same group has successfully established TUBO-hEGFR and MC38-hEGFR tumors in BALB/c and C57BL/6J mice, respectively [260-262]. The main difference between those studies and ours is the nature of the sequence of the hEGFR. In the study by Yang *et al.*, murine cell lines were transduced with a lentiviral vector encoding the human EGFR bearing the L858R mutation. In contrast, the pcDNA3.EGFR plasmid we used for the generation of B16CAR-EGFR cells contains the WT hEGFR. Unfortunately, we have failed to contact the group describing these cell lines, and we do not know whether this is the critical point for successful engraftment in immunocompetent mice. The L858R mutation substitutes an arginine for a leucine at codon 858 in the tyrosine kinase domain of the EGFR protein, leading to increased kinase activation, tumor selective growth and survival advantage [263]. Furthermore, constitutively activated EGFR due to the L858R mutation has been shown to induce expression of *PD-L1* and other immunosuppressive factors which leads to evasion of the antitumor immune responses in a hEGFR-driven lung cancer mouse model [240]. Given these considerations, we are currently generating WT or L858R-mutated hEGFR-expressing mouse syngeneic cancer cell lines with either BALB/c or C57BL/6 background by lentiviral transduction. We these models we expect to study the ability of virus-delivered BiTEs to activate infiltrating T cells under the highly immunosuppressive environment of the tumor and also to confirm the potential BiTE-mediated redirection of Adv-specific T cells towards cancer cells.

Despite the challenges of murine models for the evaluation of BiTE-armed OAds, the results presented in this thesis highlight the potential of ICO15K-cBiTE as novel anticancer agent and encourage its further evaluation in preclinical and clinical studies.

5.3. COMBINATION OF ICO15K-cBiTE WITH CAR T-CELL THERAPY

CAR T-cell therapy has shown enormous potential for the treatment of hematological cancers, but its success for treatment of solid tumors is still limited. In the second chapter of this thesis, we hypothesized that ICO15K-cBiTE could improve the outcome of CAR T cell therapy by overcoming some of the known limitations encountered by CAR T cells in the tumor microenvironment.

As described above, targeted therapies are susceptible to tumor immune evasion by antigen loss, and CAR T cells are not the exception. Among B-ALL patients responding to anti-CD19 CAR T-cell therapy, 18-36% develop $CD19^-$ relapses [146]. It has been demonstrated that several mechanisms are involved in this tumor immune evasion including mutations in the *CD19* locus, and alternative splicing of *CD19* mRNA species which results in truncated versions of CD19 [151]. Similar observations have been described for a patient suffering from mediastinal large B cell lymphoma, who was refractory to several immunotherapies, including anti-CD19 CAR T cells, due to multiple chromosomal aberrations that resulted in downregulation of the targeted antigens [264]. Furthermore, preclinical mouse studies with mesothelin-targeting CAR T cells have shown that, after a partial response, tumors relapse mainly due to the loss of mesothelin expression within the tumor microenvironment (Sonia Guedan, personal communication and unpublished data). We hypothesized that cBiTE antibodies secreted from Ad-infected cells could address mesothelin loss by re-directing CAR T cells to EGFR-expressing tumor cells. In order to demonstrate this *in vitro*, the A431 ($EGFR^+/Meso^-$) cell line was used as model for antigen loss given its lack of mesothelin expression. We demonstrated that, in the absence of mesothelin (*i.e.* A431 cells), cytokine secretion and proliferation of anti-mesothelin CAR T-cell preparations only occurred in the presence of supernatants from ICO15K-cBiTE-infected cells. Given that CAR T-cell preparations contain mixed populations of CAR^- (UTD) and CAR^+ T cells, we were concerned by the possibility that cytokine secretion and T-cell proliferation was the result of engagement of UTD but not of CAR^+ T cells due to possible interferences of the BiTE with the CAR. However, we demonstrated that CAR^+ T cells expressed the CD25 activation marker when cocultured with A431 cells in the presence of cBiTE-containing supernatants. Thus, the use of ICO15K-cBiTE represents a promising strategy to engage CAR T cells in a scenario in which the targeted antigen has been lost. Although these results have to be confirmed *in vivo*, the simultaneous targeting of different tumor antigens by CAR T cells has already been described as a solution for antigen loss. Ruella and colleagues have used bi-specific CAR T

cells simultaneously expressing anti-CD123 and anti-CD19 CARs to demonstrate that this approach can overcome immune evasion in a mouse model of CD19-negative relapsed B-ALL [265]. Another strategy involves the generation of tandem CAR constructs, in which the scFV is either fused to a second scFV targeting a different antigen or to mutein ligands of tumor-associated receptors. This tandem CARs have demonstrated potent antitumor efficacy with reduced tumor immune escape due to antigen loss in different preclinical models of cancer [266, 267]. Taken together, these studies support the notion that increasing the number antigens being targeted can improve the outcome of cancer therapies.

FDA regulations for the generation of CAR T cells recommend that lentivirus-transduced T cells have ≤ 4 vector copies/cell [147, 268]. These restrictions limit the MOI at which T-cell preparations can be transduced, resulting in preparations with 5%-45% CAR^+ T cells [147]. Taking this into account, we hypothesized that ICO15K-cBiTE could further improve CAR T cell therapy by cBiTE-mediated engagement of the unstransduced (UTD; CAR^-) T-cell population present in CAR T cells preparations. In order to evaluate this, we generated preparations containing 50% CAR^+ and 50% UTD (CAR^-) T cells. These percentages were chosen to simulate the highest lentiviral transduction outcome (*i.e.* 45% CAR^+ cells) reported for clinical trial infusion products [147]. We demonstrated that UTD T cells within CAR T-cell preparations were efficiently activated only when cBiTE supernatants were added to A431 or L55 cocultures. Additionally, cBiTE antibodies induced increased cytokine secretion, T-cell proliferation and tumor cell cytotoxicity in cocultures with L55 cells which expressed both the EGFR and mesothelin. These results likely reflect the combined action of CAR engagement towards mesothelin and $CD3^+$ T-cell engagement towards the EGFR via the cBiTE, leading to improved anti-cancer responses by CAR T-cell preparations *in vitro*. These results might have important implications for improving CAR T cell therapy given the potent cytotoxic potential of these cells. UTD T cells expanded with anti-CD3 and anti-CD28-coated beads show predominantly effector memory (T_{EM}) and central memory (T_{CM}) phenotypes [269, 270]. Importantly, BiTE-mediated redirected lysis of cancer cells is mainly supported by T_{EM} cells [271]. Thus, the strategy of redirecting the UTD fraction of CAR T-cell preparation proposed in this thesis holds promise as an improvement for this kind of immunotherapies.

Several studies have demonstrated the feasibility of generating genetically-modified T cells expressing BiTEs targeting TAAs such as EphA2, CD19 and CD123 [270, 272-274]. These modified T cells induce T-cell infiltration into tumors, promote expansion of bystander T cells and result in potent antitumor efficacy *in vivo*. Given these advantages, it would not be

surprising if this strategy is expanded to CAR T cells. BiTE-secreting CAR T cells would likely promote T-cell infiltration and activation and, if the CAR and BiTE target different antigens, it could also aid in avoiding tumor escape by antigen loss. However, the unselective and continuous production of BiTE by T cells is also likely to induce the severe off-target side effects often observed during BiTE treatment. A possible solution to this limitation is the engineering of BiTE-secreting cells to express the suicide CD20 gene which, in combination with the anti-CD20 antibody Rituximab, leads to the eradication of these cells [274]. This approach, however, only represents a safety measure and does not solve the unselective and continuous expression of BiTEs by these cells. In this regard ICO15K-cBiTE is more attractive than the BiTE-T-cells, since BiTE expression is restricted to virus replication in cancer cells. Thus, localized BiTE expression adds another level of selectivity which is lacking in BiTEs as monotherapies, but also in other combinatorial approaches such as BiTE-expressing T cells. Furthermore, the combined action of virus, BiTE and CAR T cells is likely to induce a more potent antitumor efficacy than BiTE-expressing T cells due to their multimodal killing mechanisms.

As mentioned above, OVs have been gained attention in the past years as potent immunostimulators to generate T-cell inflamed tumor microenvironments. In this context, OAds have been evaluated in combination with CAR T cells. It has been shown that a Δ24-based OAd promotes infiltration of CAR T cells into tumors, and this infiltration and persistence can be further improved if the virus is armed with chemokines (*e.g.* RANTES) and cytokines (*e.g.* IL-15) [152]. Additionally, a recent study demonstrated that a helper-dependent Ad expressing a PD-L1-blocking mini-body composed of the scFV and CH2 and CH3 regions of human IgG (CAd-VEC*PDL1*) in combination with an OAd improves the antitumor of anti-HER2 CAR T cells [275]. Although it is difficult to compare the strategies used by us and others to approach the combination of OAds and CAR T cells, some aspects can be contrasted. Regarding antitumor efficacy, ICO15K-cBiTE could offer an advantage over Ad5Δ24.RANTES.IL15 as the cBiTE can engage any $CD3^+$ T that infiltrates or that is already present in the tumors. In contrast, Ad5Δ24.RANTES.IL15 is likely to promote improved persistence and survival of CAR T cells due to the action of IL-15 compared to ICO15K-cBiTE. In the future, however, it would also be possible to further arm ICO15K-cBiTE with cytokines involved in survival of memory T cells. Although the genome size of ICO15K-cBiTE is at the packaging limit for adenoviruses, further modifications, such as the deletion of the *6.7K/gp19K* genes (965 bp) from the E3 region, would allow the insertion of cytokine genes with small size such as IL-15 (486 bp). This strategy has been widely used to generate

armed OAds with improved immunological properties [139, 276, 277], although it might come at expenses of oncolytic potency and virus persistence in immunocompetent hosts [278, 279]. Future studies will have to address the cost-benefits of these modifications in terms of antitumor efficacy in immuncompetent settings. Regarding CAd-VEC*PDL1*, expressing a PD-L1 blocking antibody from infected cell would allow to evade tumor PD-1/PD-L1-mediated adaptive immune resistance not only by CAR T cells but also by any tumor-specific T cell infiltrating the tumor. However, from a regulatory point of view, the fact that CAd-VEC*PDL1* relies on the combination of two different adenoviral vectors makes it difficult to translate into patients. A potential solution for this limitation would be to incorporate the anti-PD-L1 mini-body into the genome of OAds as it has been described for anti-CTLA-4 or anti-HER2 antibodies [139, 280]. In contrasts to CAd-VEC*PDL1*, ICO15K-cBiTE can engage tumor resident T cells as well as infiltrating CAR^+ and UTD T cells present in clinical preparations. Furthermore and as described above, the continuous infiltration of Ad-specific T cells into tumors represent a potential source of T cells with intact immunological properties to be engaged by the cBiTE. Although CAR and BiTE-mediated engagement can lead to physiological expression of immune checkpoints receptors and their ligand in the tumor microenvironment, the fact that different ckeckpoint inhibitors have been approved by the FDA for different malignancies could facilitate the combination of ICO15K-cBiTE to overcome this limitation. Finally and in contrast to ICO15K-cBiTE, neither Ad5Δ24.RANTES.IL15 nor CAd-VEC*PDL1* address tumor escape by antigen loss, which is on the major challenges for the success of CAR T-cell therapy in solid tumors. Despite these considerations, the results in this thesis and the studies described above support the potential of combining oncolytic virotherapy with CAR T cells

Finally, we propose a model in which ICO15K-cBiTE-mediated oncolysis and cBiTE secretion improves CAR T-cell therapy by: (i) evading tumor immune escape due to simultaneous targeting of two tumor antigens and (ii) engaging CAR^+ and UTD T cells towards the EGFR (Figure 54). Although further *in vivo* validation is needed, the results in this thesis support the combination of BiTE-armed OAds with CAR T cells and encourage its further preclinical and clinical development.

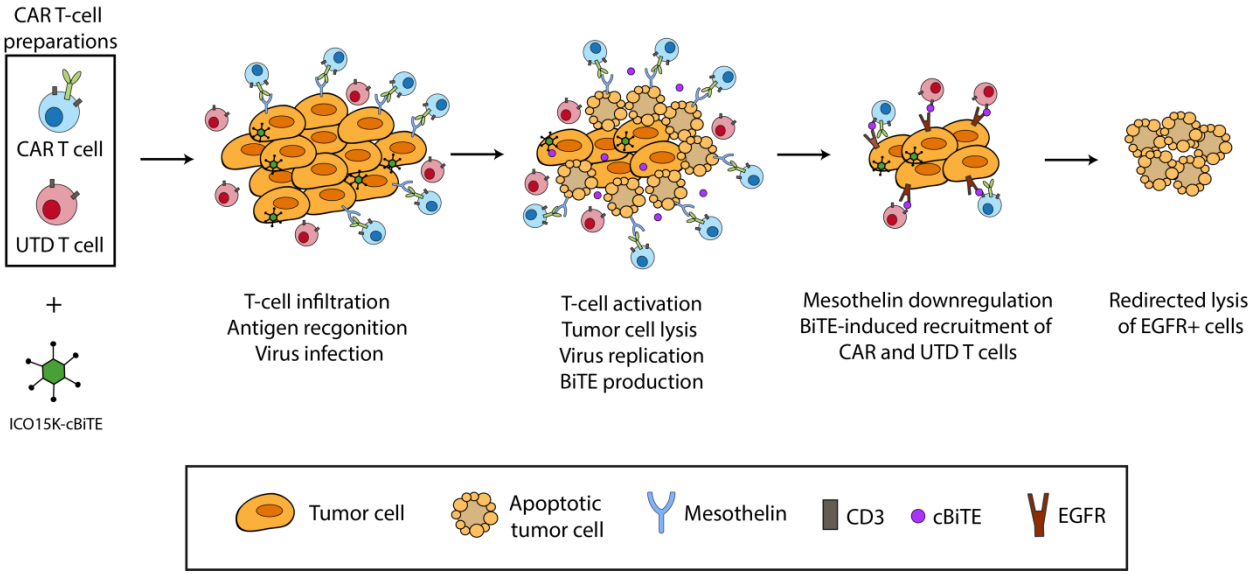

Figure 54. Proposed model of the combined action of ICO15K-cBiTE and CAR T cells. ICO15K-cBiTE infection and replication leads to cBiTE production, while CAR T cells infiltrate the tumor and target mesothelin-positive cancer cells. CAR T therapy induce tumor immune escape by loss of mesothelin expression, but the cBiTE can engage CAR+ and also UTD T cells to the EGFR. The combined action of CARs, BiTEs and adenoviruses leads to improved antitumor efficacy.

5.4 Outlook and future perspectives

Despite the potential of BiTE-armed OAds, key questions are still open and will have to be addressed in the future. Some of these include: What is the safety and pharmacological profile of BiTE-armed OAds? Does localized cBiTE production lead to exhaustion of infiltrating T cells? Can ICO15K-cBiTE be combined with checkpoint inhibitors to improve antitumor efficacy? Can OAds persistence in tumors be improved by redirecting antiviral immune responses to cancer cells in immunocompetent hosts? Is the concentration of BiTE produced by infected cells enough to control tumor growth? Many of the answers to these questions are restricted to the assessment of ICO15K-cBiTE in the context of immunocompetence. This means that such studies can only be achieved either in immunocompetent mouse/hamster models or directly in clinical trials with cancer patients. Thus, we believe that the development of immunocompetent mouse models, such as the one described above for the evaluation of the chimeric mcBiTE, will be of great importance to accelerate the translation of BiTE-armed OAds into the clinic.

The promising results obtained in the past years with novel immunotherapies have brought excitement to the field of cancer therapies. Furthermore, the recently FDA approval

of checkpoint blocking antibodies and Blinatumomab for several cancer malignancies has paved the way for rationale design of combinatorial approaches of immunotherapies with standard cancer treatments [281]. Among the several combination strategies proposed to date, OVs emerge as attractive candidates given their tumor selectivity and favorable immunostimulatory properties. Indeed, the recent marketing approval in the United States of the GM-CSF-armed OV T-VEC for the treatment of advance melanoma has encouraged the development of OV with improved immunotherapeutic potential. The results described in this thesis demonstrate that BiTE-armed OAds hold the unique properties of inducing specific and redirected anti-tumor immune responses. This strategy has the potential to solve key limitations in oncolytic virotherapy, encouarging its further evaluation and development.

6. CONCLUSIONS

1. The oncolytic adenovirus ICO15K-cBiTE, expressing a BiTE targeting the EGFR, was successfully rescued and showed similar oncolytic properties as the parental *in vitro*.
2. cBiTE antibodies expressed and secreted from ICO15K-cBiTE-infected cells bound specifically and simultaneously to the EGFR on target cells and to the CD3 on effector cells, leading to T-cell activation and proliferation, and promoting cytotoxicity and bystander effect of cancer.
3. Intratumoral administration of ICO15K-cBiTE increase the persistence and infiltration of tumor-infiltrating T cells compared to ICO15K, resulting in enhanced antitumor efficacy in humanized mouse models of cancer.
4. The oncolytic adenovirus ICO15K-mBiTE, encoding a murine surrogate of cBiTE targeting murine EGFR and murine CD3, was successfully rescued but it failed to secrete functional mBiTEs from infected cells.
5. The oncolytic adenovirus ICO15K-mcBiTE, expressing a chimeric BiTE targeting human EGFR and murine CD3, was successfully rescued and showed similar oncolytic properties as ICO15K *in vitro*.
6. mcBiTE antibodies expressed and secreted from ICO15K-mcBiTE-infected cells bound specifically to the human EGFR on target cells and to the murine CD3 on effector cells, leading to T-cell activation and proliferation, and promoting cytotoxicity of human EGFR-expressing mouse cancer cells.
7. B16CAR-EGFR cells failed to establish tumors in C57BL/6 mice and were therefore not suitable for the evaluation of ICO15K-mcBiTE in an immunocompetent animal model.
8. Supernatants from ICO15K-cBiTE-infected cells triggered the activation of anti-mesothelin CAR^+ T cells in an *in vitro* setting which mimics the loss of mesothelin-expressing cells from tumors.
9. cBiTEs secreted from infected cancer cells enhanced the activation, proliferation, and cytotoxic potential of anti-mesothelin CAR T-cell preparations when both EGFR and mesothelin were co-expressed on cancer cells.

7. REFERENCES

1. Russell SJ, Peng K-W and Bell JC. **Oncolytic virotherapy**. *Nature Biotechnology.* (2012), 30(7):658-670.

2. Kaufman HL, Kohlhapp FJ and Zloza A. **Oncolytic viruses: a new class of immunotherapy drugs**. *Nature Reviews Drug Discovery.* (2015), 14(9):642-662.

3. Cattaneo R, Miest T, Shashkova EV and Barry MA. **Reprogrammed viruses as cancer therapeutics: targeted, armed and shielded**. *Nat Rev Micro.* (2008), 6(7):529-540.

4. Miest TS and Cattaneo R. **New viruses for cancer therapy: meeting clinical needs**. *Nature Reviews Microbiology.* (2014), 12(1):23-34.

5. Garber K. **China Approves World's First Oncolytic Virus Therapy For Cancer Treatment**. *JNCI: Journal of the National Cancer Institute.* (2006), 98(5):298-300.

6. Coffin R. **Interview with Robert Coffin, inventor of T-VEC: the first oncolytic immunotherapy approved for the treatment of cancer**. *Immunotherapy.* (2016), 8(2):103-106.

7. Howley PM and Livingston DM. **Small DNA tumor viruses: Large contributors to biomedical sciences**. *Virology.* (2009), 384(2):256-259.

8. Berk AJ. **Recent lessons in gene expression, cell cycle control, and cell biology from adenovirus**. *Oncogene.* (2005), 24(52):7673-7685.

9. Vorburger SA and Hunt KK. **Adenoviral Gene Therapy**. *The Oncologist.* (2002), 7(1):46-59.

10. **New Drugs/Drug News**. *Pharmacy and Therapeutics.* (2014), 39(11):733-785.

11. Harrach B. **Adenoviruses: General Features**. In: Encyclopedia of Virology (Third Edition). Edited by Editors-in-Chief: BWJM, Regenmortel MHVv. Oxford: Academic Press; 2008: 1-9.

12. Knipe DM, Howley PM and Griffin DE. **Fields virology**. Philadelphia: Lippincott Williams & Wilkins; 2007.

13. Hall K, Blair Zajdel ME and Blair GE. **Unity and diversity in the human adenoviruses: exploiting alternative entry pathways for gene therapy**. *Biochem J.* (2010), 431(3):321-336.

14. Benkő M. **Adenoviruses: Pathogenesis**. In: Encyclopedia of Virology (Third Edition). Edited by Editors-in-Chief: BWJM, Regenmortel MHVv. Oxford: Academic Press; 2008: 24-29.

15. Evans JD and Hearing P. **Adenovirus replication**. In: Adenoviral vectors for gene therapy. Edited by Curiel D, Douglas JT. Amsterdam; Boston: Academic Press; 2002: 39-64.

16. Russell WC. **Adenoviruses: update on structure and function**. *Journal of General Virology.* (2009), 90(1):1-20.

17. Hong JS and Engler JA. **Domains required for assembly of adenovirus type 2 fiber trimers**. *Journal of Virology.* (1996), 70(10):7071-7078.

18. Acheson NH. **Fundamentals of molecular virology**. Hoboken, NJ: Wiley; 2007.

19. Arnberg N. **Adenovirus receptors: implications for tropism, treatment and targeting**. *Reviews in Medical Virology.* (2009), 19(3):165-178.

20. Wickham TJ, Mathias P, Cheresh DA and Nemerow GR. **Integrins αvβ3 and αvβ5 promote adenovirus internalization but not virus attachment**. *Cell.* (1993), 73(2):309-319.

21. Wiethoff CM, Wodrich H, Gerace L and Nemerow GR. **Adenovirus Protein VI Mediates Membrane Disruption following Capsid Disassembly**. *Journal of Virology.* (2005), 79(4):1992-2000.

22. Henaff D, Salinas S and Kremer EJ. **An adenovirus traffic update: from receptor engagement to the nuclear pore**. *Future Microbiology.* (2011), 6(2):179-192.

23. Moran E. **DNA tumor virus transforming proteins and the cell cycle**. *Curr Opin Genet Dev.* (1993), 3(1):63-70.

24. Bennett EM, Bennink JR, Yewdell JW and Brodsky FM. **Cutting edge: adenovirus E19 has two mechanisms for affecting class I MHC expression**. *J Immunol.* (1999), 162(9):5049-5052.

25. Burgert HG, Maryanski JL and Kvist S. **"E3/19K" protein of adenovirus type 2 inhibits lysis of cytolytic T lymphocytes by blocking cell-surface expression of histocompatibility class I antigens**. *Proc Natl Acad Sci U S A.* (1987), 84(5):1356-1360.

26. Windheim M, Hilgendorf A and Burgert HG. **Immune evasion by adenovirus E3 proteins: exploitation of intracellular trafficking pathways**. *Curr Top Microbiol Immunol.* (2004), 273:29-85.

27. Flint SJ, Racaniello VR, Rall GF, Skalka AM and Enquist LW. **Principles of Virology Volume I: Molecular Biology**: ASM Press; 2015.

28. Tomko RP, Xu R and Philipson L. **HCAR and MCAR: The human and mouse cellular receptors for subgroup C adenoviruses and group B coxsackieviruses**. *Proceedings of the National Academy of Sciences.* (1997), 94(7):3352-3356.

29. Miller CR, Buchsbaum DJ, Reynolds PN, Douglas JT, Gillespie GY, Mayo MS, Raben D and Curiel DT. **Differential Susceptibility of Primary and Established Human Glioma Cells to Adenovirus Infection: Targeting via the Epidermal Growth Factor Receptor Achieves Fiber Receptor-independent Gene Transfer**. *Cancer Research.* (1998), 58(24):5738-5748.

30. Kim M, Zinn KR, Barnett BG, Sumerel LA, Krasnykh V, Curiel DT and Douglas JT. **The therapeutic efficacy of adenoviral vectors for cancer gene therapy is limited by a low level of primary adenovirus receptors on tumour cells**. *European Journal of Cancer.* (2002), 38(14):1917-1926.

31. Glasgow JN, Everts M and Curiel DT. **Transductional targeting of adenovirus vectors for gene therapy**. *Cancer Gene Ther.* (2006), 13(9):830-844.

32. Coughlan L, Alba R, Parker AL, Bradshaw AC, McNeish IA, Nicklin SA and Baker AH. **Tropism-Modification Strategies for Targeted Gene Delivery Using Adenoviral Vectors**. *Viruses.* (2010), 2(10):2290-2355.

33. Kaufmann JK and Nettelbeck DM. **Virus chimeras for gene therapy, vaccination, and oncolysis: adenoviruses and beyond**. *Trends in Molecular Medicine.* (2012), 18(7):365-376.

34. Koivunen E, Wang B and Ruoslahti E. **Phage libraries displaying cyclic peptides with different ring sizes: ligand specificities of the RGD-directed integrins**. *Biotechnology (N Y).* (1995), 13(3):265-270.

35. Gamble LJ, Borovjagin AV and Matthews QL. **Role of RGD-containing ligands in targeting cellular integrins: Applications for ovarian cancer virotherapy (Review)**. *Exp Ther Med.* (2010), 1(2):233-240.

36. Hesse A, Kosmides D, Kontermann RE and Nettelbeck DM. **Tropism Modification of Adenovirus Vectors by Peptide Ligand Insertion into Various Positions of the Adenovirus Serotype 41 Short-Fiber Knob Domain**. *Journal of Virology.* (2007), 81(6):2688-2699.

37. Borovjagin AV, Krendelchtchikov A, Ramesh N, Yu D-C, Douglas JT and Curiel DT. **Complex mosaicism is a novel approach to infectivity enhancement of adenovirus type 5-based vectors**. *Cancer Gene Ther.* (2005), 12(5):475-486.

38. Matsui H, Sakurai F, Katayama K, Kurachi S, Tashiro K, Sugio K, Kawabata K and Mizuguchi H. **Enhanced transduction efficiency of fiber-substituted adenovirus vectors by the incorporation of RGD peptides in two distinct regions of the adenovirus serotype 35 fiber knob**. *Virus Research.* (2011), 155(1):48-54.

39. Bayo-Puxan N, Gimenez-Alejandre M, Lavilla-Alonso S, Gros A, Cascallo M, Hemminki A and Alemany R. **Replacement of adenovirus type 5 fiber shaft heparan sulfate proteoglycan-binding domain with RGD for improved tumor infectivity and targeting**. *Human Gene Therapy.* (2009), 20(10):1214-1221.

40. Russell SJ, Peng K-W and Bell JC. **Oncolytic virotherapy**. *Nat Biotech.* (2012), 30(7):658-670.

41. Nettelbeck DM. **Virotherapeutics: conditionally replicative adenoviruses for viral oncolysis**. *Anticancer Drugs.* (2003), 14(8):577-584.

42. Fueyo J, Gomez-Manzano C, Alemany R, Lee PS, McDonnell TJ, Mitlianga P, Shi YX, Levin VA, Yung WK and Kyritsis AP. **A mutant oncolytic adenovirus targeting the Rb pathway produces anti-glioma effect in vivo**. *Oncogene.* (2000), 19(1):2-12.

43. Rodríguez García A. **Enhancing the antitumor activity of oncolytic adenoviruses by combining tumor targeting with hyaluronidase expression or by increasing the immunogenicity of exogenous epitopes**. *Doctoral thesis.* Universitat de Barcelona, 2015. Retrieved from http://hdl.handle.net/2445/65246

44. Nettelbeck DM. **Cellular genetic tools to control oncolytic adenoviruses for virotherapy of cancer**. *Journal of Molecular Medicine.* (2008), 86(4):363-377.

45. Bofill-De Ros X, Gironella M and Fillat C. **MiR-148a- and miR-216a-regulated Oncolytic Adenoviruses Targeting Pancreatic Tumors Attenuate Tissue Damage Without Perturbation of miRNA Activity**. *Molecular Therapy.* (2014), 22(9):1665-1677.

46. Callegari E, Elamin BK, D'Abundo L, Falzoni S, Donvito G, Moshiri F, Milazzo M, Altavilla G, Giacomelli L, Fornari F *et al*. **Anti-Tumor Activity of a miR-199-dependent Oncolytic Adenovirus**. *PLOS ONE.* (2013), 8(9):e73964.

47. Rojas JJ, Gimenez-Alejandre M, Gil-Hoyos R, Cascallo M and Alemany R. **Improved systemic antitumor therapy with oncolytic adenoviruses by replacing the fiber shaft HSG-binding domain with RGD**. *Gene Therapy* (2012), 19(4):453-457.

48. Rojas JJ, Guedan S, Searle PF, Martinez-Quintanilla J, Gil-Hoyos R, Alcayaga-Miranda F, Cascallo M and Alemany R. **Minimal RB-responsive E1A Promoter Modification to Attain Potency, Selectivity, and Transgene-arming Capacity in Oncolytic Adenoviruses**. *Molecular Therapy* (2010), 18(11):1960-1971.

49. Karlseder J, Rotheneder H and Wintersberger E. **Interaction of Sp1 with the growth- and cell cycle-regulated transcription factor E2F**. *Molecular and Cellular Biology.* (1996), 16(4):1659-1667.

50. Guedan S, Rojas JJ, Gros A, Mercade E, Cascallo M and Alemany R. **Hyaluronidase Expression by an Oncolytic Adenovirus Enhances Its Intratumoral Spread and Suppresses Tumor Growth**. *Molecular Therapy.* (2010), 18(7):1275-1283.

51. Rodríguez-García A, Giménez-Alejandre M, Rojas JJ, Moreno R, Bazan-Peregrino M, Cascalló M and Alemany R. **Safety and Efficacy of VCN-01, an Oncolytic Adenovirus Combining Fiber HSG-Binding Domain Replacement with RGD and Hyaluronidase Expression**. *Clinical Cancer Research.* (2015), 21(6):1406-1418.

52. Duffy MR, Parker AL, Bradshaw AC and Baker AH. **Manipulation of adenovirus interactions with host factors for gene therapy applications**. *Nanomedicine.* (2012), 7(2):271-288.

53. Alemany R. **Molecular Design of Oncolytic Adenoviruses** In: Adenoviral Vectors for Gene Therapy (Second Edition). Edited by Curiel DT. San Diego: Academic Press; 2016: 319-334.

54. Jin F, Kretschmer PJ and Hermiston TW. **Identification of novel insertion sites in the Ad5 genome that utilize the Ad splicing machinery for therapeutic gene expression**. *Mol Ther.* (2005), 12(6):1052-1063. Epub 2005 Sep 1013.

55. Ghosh-Choudhury G, Haj-Ahmad Y and Graham FL. **Protein IX, a minor component of the human adenovirus capsid, is essential for the packaging of full length genomes**. *The EMBO Journal.* (1987), 6(6):1733-1739.

56. Bett AJ, Prevec L and Graham FL. **Packaging capacity and stability of human adenovirus type 5 vectors**. *Journal of Virology.* (1993), 67(10):5911-5921.

57. Smith RR, Huebner RJ, Rowe WP, Schatten WE and Thomas LB. **Studies on the use of viruses in the treatment of carcinoma of the cervix**. *Cancer.* (1956), 9(6):1211-1218.

58. Blackford AN and Grand RJA. **Adenovirus E1B 55-Kilodalton Protein: Multiple Roles in Viral Infection and Cell Transformation**. *Journal of Virology.* (2009), 83(9):4000-4012.

59. Bischoff JR, Kirn DH, Williams A, Heise C, Horn S, Muna M, Ng L, Nye JA, Sampson-Johannes A, Fattaey A *et al*. **An Adenovirus Mutant That Replicates Selectively in p53- Deficient Human Tumor Cells**. *Science.* (1996), 274(5286):373-376.

60. Ganly I, Kirn D, Eckhardt SG, Rodriguez GI, Soutar DS, Otto R, Robertson AG, Park O, Gulley ML, Heise C *et al*. **A Phase I Study of Onyx-015, an E1B Attenuated Adenovirus, Administered Intratumorally to Patients with Recurrent Head and Neck Cancer**. *Clinical Cancer Research.* (2000), 6(3):798-806.

61. Nemunaitis J, Khuri F, Ganly I, Arseneau J, Posner M, Vokes E, Kuhn J, McCarty T, Landers S, Blackburn A *et al*. **Phase II Trial of Intratumoral Administration of ONYX-015, a Replication-Selective Adenovirus, in Patients With Refractory Head and Neck Cancer**. *Journal of Clinical Oncology.* (2001), 19(2):289-298.

62. Kirn DH. **The End of the Beginning: OncolyticVirotherapy Achieves Clinical Proof-of-Concept**. *Molecular Therapy.* (2006), 13(2):237-238.

63. O'Shea CC, Johnson L, Bagus B, Choi S, Nicholas C, Shen A, Boyle L, Pandey K, Soria C, Kunich J *et al*. **Late viral RNA export, rather than p53 inactivation, determines ONYX-015 tumor selectivity**. *Cancer Cell.* (2004), 6(6):611-623.

64. Kimball KJ, Preuss MA, Barnes MN, Wang M, Siegal GP, Wan W, Kuo H, Saddekni S, Stockard CR, Grizzle WE *et al*. **A Phase I Study of a Tropism-Modified Conditionally Replicative Adenovirus for Recurrent Malignant Gynecologic Diseases**. *Clinical Cancer Research.* (2010), 16(21):5277-5287.

65. Xipell E, Rivera-Molina Y, Gomez-Manzano C, Jiang H, Alonso MM, Alemany R and Fueyo J. **Conditionally Replicative Adenoviruses—Clinical Trials**. In: Adenoviral Vectors for Gene Therapy (Second Edition). Edited by Curiel DT. San Diego: Academic Press; 2016: 335-348.

66. Barouch DH, Kik SV, Weverling GJ, Dilan R, King SL, Maxfield LF, Clark S, Ng'ang'a D, Brandariz KL, Abbink P *et al*. **International seroepidemiology of adenovirus serotypes 5, 26, 35, and 48 in pediatric and adult populations**. *Vaccine.* (2011), 29(32):5203-5209.

67. Mast TC, Kierstead L, Gupta SB, Nikas AA, Kallas EG, Novitsky V, Mbewe B, Pitisuttithum P, Schechter M, Vardas E *et al*. **International epidemiology of human pre-existing adenovirus (Ad) type-5, type-6, type-26 and type-36 neutralizing antibodies: Correlates of high Ad5 titers and implications for potential HIV vaccine trials**. *Vaccine.* (2010), 28(4):950-957.

68. Sumida SM, Truitt DM, Lemckert AAC, Vogels R, Custers JHHV, Addo MM, Lockman S, Peter T, Peyerl FW, Kishko MG *et al*. **Neutralizing Antibodies to Adenovirus Serotype 5 Vaccine Vectors Are Directed Primarily against the Adenovirus Hexon Protein**. *The Journal of Immunology.* (2005), 174(11):7179-7185.

69. Bradley RR, Lynch DM, Iampietro MJ, Borducchi EN and Barouch DH. **Adenovirus Serotype 5 Neutralizing Antibodies Target both Hexon and Fiber following Vaccination and Natural Infection**. *Journal of Virology.* (2012), 86(1):625-629.

70. Gahéry-Ségard H, Juillard V, Gaston J, Lengagne R, Pavirani A, Boulanger P and Guillet J-G. **Humoral immune response to the capsid components of recombinant adenoviruses: Routes of immunization modulate virus-induced Ig subclass shifts**. *European Journal of Immunology.* (1997), 27(3):653-659.

71. Lieber A, He CY, Meuse L, Schowalter D, Kirillova I, Winther B and Kay MA. **The role of Kupffer cell activation and viral gene expression in early liver toxicity after infusion of recombinant adenovirus vectors**. *Journal of Virology.* (1997), 71(11):8798-8807.

72. Vrancken Peeters MJ, Perkins AL and Kay MA. **Method for multiple portal vein infusions in mice: quantitation of adenovirus-mediated hepatic gene transfer**. *Biotechniques.* (1996), 20(2):278-285.

73. Parato KA, Senger D, Forsyth PAJ and Bell JC. **Recent progress in the battle between oncolytic viruses and tumours**. *Nature Reviews Cancer.* (2005), 5(12):965-976.

74. Fisher KD, Stallwood Y, Green NK, Ulbrich K, Mautner V and Seymour LW. **Polymer-coated adenovirus permits efficient retargeting and evades neutralising antibodies**. *Gene Therapy.* (2001), 8(5):341-348.

75. Kim J, Kim P-H, Kim SW and Yun C-O. **Enhancing the therapeutic efficacy of adenovirus in combination with biomaterials**. *Biomaterials.* (2012), 33(6):1838-1850.

76. Bradley RR, Maxfield LF, Lynch DM, Iampietro MJ, Borducchi EN and Barouch DH. **Adenovirus Serotype 5-Specific Neutralizing Antibodies Target Multiple Hexon Hypervariable Regions**. *Journal of Virology.* (2012), 86(2):1267-1272.

77. Rojas LA, Condezo GN, Moreno R, Fajardo CA, Arias-Badia M, San Martín C and Alemany R. **Albumin-binding adenoviruses circumvent pre-existing neutralizing antibodies upon systemic delivery**. *Journal of Controlled Release.* (2016), 237:78-88.

78. Bunuales M, Garcia-Aragoncillo E, Casado R, Quetglas JI, Hervas-Stubbs S, Bortolanza S, Benavides-Vallve C, Ortiz-de-Solorzano C, Prieto J and Hernandez-Alcoceba R. **Evaluation of Monocytes as Carriers for Armed Oncolytic Adenoviruses in Murine and Syrian Hamster Models of Cancer**. *Human Gene Therapy.* (2012), 23(12):1258-1268.

79. Nakashima H, Kaur B and Chiocca EA. **Directing systemic oncolytic viral delivery to tumors via carrier cells**. *Cytokine & Growth Factor Reviews.* (2010), 21(2–3):119-126.

80. Garcia-Castro J, Alemany R, Cascallo M, Martinez-Quintanilla J, del Mar Arriero M, Lassaletta A, Madero L and Ramirez M. **Treatment of metastatic neuroblastoma with systemic oncolytic virotherapy delivered by autologous mesenchymal stem cells: an exploratory study**. *Cancer Gene Ther.* (2010), 17(7):476-483.

81. Yao X, Yoshioka Y, Morishige T, Eto Y, Narimatsu S, Kawai Y, Mizuguchi H, Gao J-Q, Mukai Y, Okada N *et al*. **Tumor Vascular Targeted Delivery of Polymer-conjugated Adenovirus Vector for Cancer Gene Therapy**. *Molecular Therapy.* (2011), 19(9):1619-1625.

82. Hynes RO and Naba A. **Overview of the Matrisome—An Inventory of Extracellular Matrix Constituents and Functions**. *Cold Spring Harbor Perspectives in Biology.* (2012), 4(1):a004903.

83. Kalluri R. **The biology and function of fibroblasts in cancer**. *Nature Reviews Cancer.* (2016), 16(9):582-598.

84. Sauthoff H, Hu J, Maca C, Goldman M, Heitner S, Yee H, Pipiya T, Rom WN and Hay JG. **Intratumoral Spread of Wild-Type Adenovirus Is Limited After Local Injection of Human Xenograft Tumors: Virus Persists and Spreads Systemically at Late Time Points**. *Human Gene Therapy.* (2003), 14(5):425-433.

85. Lopez MV, Viale DL, Cafferata EGA, Bravo AI, Carbone C, Gould D, Chernajovsky Y and Podhajcer OL. **Tumor Associated Stromal Cells Play a Critical Role on the Outcome of the Oncolytic Efficacy of Conditionally Replicative Adenoviruses**. *PLOS ONE.* (2009), 4(4):e5119.

86. Netti PA, Berk DA, Swartz MA, Grodzinsky AJ and Jain RK. **Role of Extracellular Matrix Assembly in Interstitial Transport in Solid Tumors**. *Cancer Research.* (2000), 60(9):2497-2503.

87. Smith E, Breznik J and Lichty BD. **Strategies to Enhance Viral Penetration of Solid Tumors**. *Human Gene Therapy.* (2011), 22(9):1053-1060.

88. Eikenes L, Bruland ØS, Brekken C and Davies CdL. **Collagenase Increases the Transcapillary Pressure Gradient and Improves the Uptake and Distribution of Monoclonal Antibodies in Human Osteosarcoma Xenografts**. *Cancer Research.* (2004), 64(14):4768-4773.

89. Tedcastle A, Illingworth S, Brown A, Seymour LW and Fisher KD. **Actin-resistant DNAse I Expression From Oncolytic Adenovirus Enadenotucirev Enhances Its Intratumoral Spread and Reduces Tumor Growth**. *Molecular Therapy.* (2016), 24(4):796-804.

90. Martínez-Vélez N, Xipell E, Vera B, Acanda de la Rocha A, Zalacain M, Marrodán L, Gonzalez-Huarriz M, Toledo G, Cascallo M, Alemany R *et al*. **The Oncolytic Adenovirus VCN-01 as Therapeutic Approach Against Pediatric Osteosarcoma**. *Clinical Cancer Research.* (2016), 22(9):2217-2225.

91. Kim J-H, Lee Y-S, Kim H, Huang J-H, Yoon AR and Yun C-O. **Relaxin Expression From Tumor-Targeting Adenoviruses and Its Intratumoral Spread, Apoptosis Induction, and Efficacy**. *JNCI: Journal of the National Cancer Institute.* (2006), 98(20):1482-1493.

92. Choi IK, Lee YS, Yoo JY, Yoon AR, Kim H, Kim DS, Seidler DG, Kim JH and Yun CO. **Effect of decorin on overcoming the extracellular matrix barrier for oncolytic virotherapy**. *Gene Therapy.* (2009), 17(2):190-201.

93. Lopez MV, Rivera AA, Viale DL, Benedetti L, Cuneo N, Kimball KJ, Wang M, Douglas JT, Zhu ZB, Bravo AI *et al*. **A Tumor-stroma Targeted Oncolytic Adenovirus Replicated in Human Ovary Cancer Samples and Inhibited Growth of Disseminated Solid Tumors in Mice**. *Molecular Therapy.* (2012), 20(12):2222-2233.

94. Puig-Saus C, Gros A, Alemany R and Cascalló M. **Adenovirus i-Leader Truncation Bioselected Against Cancer-associated Fibroblasts to Overcome Tumor Stromal Barriers**. *Molecular Therapy.* (2012), 20(1):54-62.

95. Alemany R and Cascallo M. **Oncolytic viruses from the perspective of the immune system**. *Future Microbiology.* (2009), 4(5):527-536.

96. Prestwich RJ, Errington F, Diaz RM, Pandha HS, Harrington KJ, Melcher AA and Vile RG. **The Case of Oncolytic Viruses Versus the Immune System: Waiting on the Judgment of Solomon**. *Human Gene Therapy.* (2009), 20(10):1119-1132.

97. Vesely MD, Kershaw MH, Schreiber RD and Smyth MJ. **Natural innate and adaptive immunity to cancer**. *Annual Reviews Immunology.* (2011), 29:235-271.

98. Chen DS and Mellman I. **Oncology meets immunology: the cancer-immunity cycle**. *Immunity.* (2013), 39(1):1-10.

99. Villablanca EJ, Raccosta L, Zhou D, Fontana R, Maggioni D, Negro A, Sanvito F, Ponzoni M, Valentinis B, Bregni M *et al*. **Tumor-mediated liver X receptor-α activation inhibits CC chemokine receptor-7 expression on dendritic cells and dampens antitumor responses**. *Nat Med.* (2010), 16(1):98-105.

100. Carretero R, Romero JM, Ruiz-Cabello F, Maleno I, Rodriguez F, Camacho FM, Real LM, Garrido F and Cabrera T. **Analysis of HLA class I expression in progressing and regressing metastatic melanoma lesions after immunotherapy**. *Immunogenetics.* (2008), 60(8):439-447.

101. Drake CG, Jaffee E and Pardoll DM. **Mechanisms of Immune Evasion by Tumors**. In: Advances in Immunology. vol. 90: Academic Press; 2006: 51-81.

102. Galluzzi L, Buque A, Kepp O, Zitvogel L and Kroemer G. **Immunogenic cell death in cancer and infectious disease**. *Nature Reviews Immunology.* (2017), 17(2):97-111.

103. Chabanon RM, Pedrero M, Lefebvre C, Marabelle A, Soria J-C and Postel-Vinay S. **Mutational Landscape and Sensitivity to Immune Checkpoint Blockers**. *Clinical Cancer Research.* (2016), 22(17):4309-4321.

104. Woller N, Gurlevik E, Fleischmann-Mundt B, Schumacher A, Knocke S, Kloos AM, Saborowski M, Geffers R, Manns MP, Wirth TC *et al*. **Viral Infection of Tumors Overcomes Resistance to PD-1-immunotherapy by Broadening Neoantigenome-directed T-cell Responses**. *Molecular Therapy.* (2015), 23(10):1630-1640.

105. Kanerva A, Nokisalmi P, Diaconu I, Koski A, Cerullo V, Liikanen I, Tähtinen S, Oksanen M, Heiskanen R, Pesonen S *et al*. **Antiviral and Antitumor T-cell Immunity in Patients Treated with GM-CSF–Coding Oncolytic Adenovirus**. *Clinical Cancer Research.* (2013), 19(10):2734-2744.

106. Endo Y, Sakai R, Ouchi M, Onimatsu H, Hioki M, Kagawa S, Uno F, Watanabe Y, Urata Y, Tanaka N *et al*. **Virus-mediated oncolysis induces danger signal and stimulates cytotoxic T-**

lymphocyte activity via proteasome activator upregulation. *Oncogene.* (2007), 27(17):2375-2381.

107. Diaconu I, Cerullo V, Hirvinen MLM, Escutenaire S, Ugolini M, Pesonen SK, Bramante S, Parviainen S, Kanerva A, Loskog ASI *et al*. **Immune Response Is an Important Aspect of the Antitumor Effect Produced by a CD40L-Encoding Oncolytic Adenovirus**. *Cancer Research.* (2012), 72(9):2327-2338.

108. Jiang H, White EJ, Ríos-Vicil CI, Xu J, Gomez-Manzano C and Fueyo J. **Human Adenovirus Type 5 Induces Cell Lysis through Autophagy and Autophagy-Triggered Caspase Activity**. *Journal of Virology.* (2011), 85(10):4720-4729.

109. Rodriguez-Rocha H, Gomez-Gutierrez JG, Garcia-Garcia A, Rao X-M, Chen L, McMasters KM and Zhou HS. **Adenoviruses Induce Autophagy to Promote Virus Replication and Oncolysis**. *Virology.* (2011), 416(1-2):9-15.

110. Liikanen I, Ahtiainen L, Hirvinen MLM, Bramante S, Cerullo V, Nokisalmi P, Hemminki O, Diaconu I, Pesonen S, Koski A *et al*. **Oncolytic Adenovirus With Temozolomide Induces Autophagy and Antitumor Immune Responses in Cancer Patients**. *Molecular Therapy.* (2013), 21(6):1212-1223.

111. Schierer S, Hesse A, Knippertz I, Kaempgen E, Baur AS, Schuler G, Steinkasserer A and Nettelbeck DM. **Human dendritic cells efficiently phagocytose adenoviral oncolysate but require additional stimulation to mature**. *International Journal of Cancer.* (2012), 130(7):1682-1694.

112. Woller N, Knocke S, Mundt B, xFc, rlevik E, Str, ver N, Kloos A, Boozari B, Schache P *et al*. **Virus-induced tumor inflammation facilitates effective DC cancer immunotherapy in a Treg-dependent manner in mice**. *The Journal of Clinical Investigation.* (2011), 121(7):2570-2582.

113. Bristol JA, Zhu M, Ji H, Mina M, Xie Y, Clarke L, Forry-Schaudies S and Ennist DL. **In vitro and in vivo activities of an oncolytic adenoviral vector designed to express GM-CSF**. *Molecular Therapy.* (2003), 7(6):755-764.

114. Cerullo V, Koski A, Vähä-Koskela M and Hemminki A. **Chapter Eight - Oncolytic Adenoviruses for Cancer Immunotherapy: Data from Mice, Hamsters, and Humans**. In: Advances in Cancer Research. Edited by David TC, Paul BF, vol. Volume 115: Academic Press; 2012: 265-318.

115. Ranki T, Pesonen S, Hemminki A, Partanen K, Kairemo K, Alanko T, Lundin J, Linder N, Turkki R, Ristimäki A *et al*. **Phase I study with ONCOS-102 for the treatment of solid tumors – an evaluation of clinical response and exploratory analyses of immune markers**. *Journal for Immunotherapy of Cancer.* (2016), 4:17.

116. Ramesh N, Ge Y, Ennist DL, Zhu M, Mina M, Ganesh S, Reddy PS and Yu D-C. **CG0070, a Conditionally Replicating Granulocyte Macrophage Colony-Stimulating Factor–Armed Oncolytic Adenovirus for the Treatment of Bladder Cancer**. *Clinical Cancer Research.* (2006), 12(1):305-313.

117. Del Vecchio M, Bajetta E, Canova S, Lotze MT, Wesa A, Parmiani G and Anichini A. **Interleukin-12: Biological Properties and Clinical Application**. *Clinical Cancer Research.* (2007), 13(16):4677-4685.

118. Oh E, Choi I-K, Hong J and Yun C-O. **Oncolytic adenovirus coexpressing interleukin-12 and decorin overcomes Treg-mediated immunosuppression inducing potent antitumor effects in a weakly immunogenic tumor model**. *Oncotarget.* (2016), 8(3).

119. Freytag SO, Barton KN and Zhang Y. **Efficacy of oncolytic adenovirus expressing suicide genes and interleukin-12 in preclinical model of prostate cancer**. *Gene therapy.* (2013), 20(12):1131-1139.

120. Choi KJ, Zhang SN, Choi IK, Kim JS and Yun CO. **Strengthening of antitumor immune memory and prevention of thymic atrophy mediated by adenovirus expressing IL-12 and GM-CSF**. *Gene Therapy.* (2012), 19(7):711-723.

121. Kim W, Seong J, Oh HJ, Koom WS, Choi KJ and Yun CO. **A novel combination treatment of armed oncolytic adenovirus expressing IL-12 and GM-CSF with radiotherapy in murine hepatocarcinoma**. *Journal of Radiation Research.* (2011), 52(5):646-654.

122. Bortolanza S, Bunuales M, Otano I, Gonzalez-Aseguinolaza G, Ortiz-de-Solorzano C, Perez D, Prieto J and Hernandez-Alcoceba R. **Treatment of Pancreatic Cancer With an Oncolytic Adenovirus Expressing Interleukin-12 in Syrian Hamsters**. *Molecular Therapy: the Journal of the American Society of Gene Therapy.* (2009), 17(4):614-622.

123. Pei D-S and Zheng J-N. **Oncolytic adenoviruses expressing interleukin: a novel antitumour approach**. *Expert Opinion on Biological Therapy.* (2010), 10(6):917-926.

124. Choi I-K, Li Y, Oh E, Kim J and Yun C-O. **Oncolytic Adenovirus Expressing IL-23 and p35 Elicits IFN-γ- and TNF-α-Co-Producing T Cell-Mediated Antitumor Immunity**. *PLOS ONE.* (2013), 8(7):e67512.

125. Armstrong L, Arrington A, Han J, Gavrikova T, Brown E, Yamamoto M, Vickers SM and Davydova J. **Generation of a Novel, Cox2-Targeted, Interferon-Expressing, Conditionally-Replicative Adenovirus for Pancreatic Cancer Therapy**. *American journal of surgery.* (2012), 204(5):741-750.

126. Franciszkiewicz K, Boissonnas A, Boutet M, Combadière C and Mami-Chouaib F. **Role of Chemokines and Chemokine Receptors in Shaping the Effector Phase of the Antitumor Immune Response**. *Cancer Research.* (2012), 72(24):6325-6332.

127. Elgueta R, Benson MJ, de Vries VC, Wasiuk A, Guo Y and Noelle RJ. **Molecular mechanism and function of CD40/CD40L engagement in the immune system**. *Immunological Reviews.* (2009), 229(1):10.1111/j.1600-1065X.2009.00782.x.

128. Pesonen S, Diaconu I, Kangasniemi L, Ranki T, Kanerva A, Pesonen SK, Gerdemann U, Leen AM, Kairemo K, Oksanen M *et al*. **Oncolytic Immunotherapy of Advanced Solid Tumors with a CD40L-Expressing Replicating Adenovirus: Assessment of Safety and Immunologic Responses in Patients**. *Cancer Research.* (2012), 72(7):1621-1631.

129. Chen L and Flies DB. **Molecular mechanisms of T cell co-stimulation and co-inhibition**. *Nat Rev Immunol.* (2013), 13(4):227-242.

130. Choi KJ, Kim JH, Lee YS, Kim J, Suh BS, Kim H, Cho S, Sohn JH, Kim GE and Yun CO. **Concurrent delivery of GM-CSF and B7-1 using an oncolytic adenovirus elicits potent antitumor effect**. *Gene Therapy.* (2006), 13(13):1010-1020.

131. Lee YS, Kim JH, Choi KJ, Choi IK, Kim H, Cho S, Cho BC and Yun CO. **Enhanced Antitumor Effect of Oncolytic Adenovirus Expressing Interleukin-12 and B7-1 in an Immunocompetent Murine Model**. *Clinical Cancer Research.* (2006), 12(19):5859-5868.

132. Sharma P and Allison James P. **Immune Checkpoint Targeting in Cancer Therapy: Toward Combination Strategies with Curative Potential**. *Cell.* (2015), 161(2):205-214.

133. Bardhan K, Anagnostou T and Boussiotis VA. **The PD1:PD-L1/2 Pathway from Discovery to Clinical Implementation**. *Frontiers in Immunology.* (2016), 7:550.

134. Pardoll DM. **The blockade of immune checkpoints in cancer immunotherapy**. *Nature Reviews Cancer.* (2012), 12(4):252-264.

135. Topalian SL, Drake CG and Pardoll DM. **Immune checkpoint blockade: a common denominator approach to cancer therapy**. *Cancer Cell.* (2015), 27(4):450-461.

136. Ito A, Kondo S, Tada K and Kitano S. **Clinical Development of Immune Checkpoint Inhibitors**. *BioMed Research International.* (2015), 2015:605478.

137. Sharon E, Streicher H, Goncalves P and Chen HX. **Immune checkpoint inhibitors in clinical trials**. *Chinese Journal of Cancer.* (2014), 33(9):434-444.

138. Mahoney KM, Rennert PD and Freeman GJ. **Combination cancer immunotherapy and new immunomodulatory targets**. *Nature Reviews Drug Discovery.* (2015), 14(8):561-584.

139. Dias JD, Hemminki O, Diaconu I, Hirvinen M, Bonetti A, Guse K, Escutenaire S, Kanerva A, Pesonen S, Loskog A *et al*. **Targeted cancer immunotherapy with oncolytic adenovirus coding for a fully human monoclonal antibody specific for CTLA-4**. *Gene Therapy.* (2012), 19(10):988-998.

140. Wu R, Forget M-A, Chacon J, Bernatchez C, Haymaker C, Chen JQ, Hwu P and Radvanyi L. **Adoptive T-cell Therapy Using Autologous Tumor-infiltrating Lymphocytes for Metastatic Melanoma: Current Status and Future Outlook**. *Cancer Journal* (2012), 18(2):160-175.

141. Tran E, Turcotte S, Gros A, Robbins PF, Lu Y-C, Dudley ME, Wunderlich JR, Somerville RP, Hogan K, Hinrichs CS *et al*. **Cancer Immunotherapy Based on Mutation-Specific CD4+ T Cells in a Patient with Epithelial Cancer**. *Science.* (2014), 344(6184):641-645.

142. Hinrichs CS and Rosenberg SA. **Exploiting the curative potential of adoptive T-cell therapy for cancer**. *Immunological Reviews.* (2014), 257(1):56-71.

143. Tähtinen S, Grönberg-Vähä-Koskela S, Lumen D, Merisalo-Soikkeli M, Siurala M, Airaksinen AJ, Vähä-Koskela M and Hemminki A. **Adenovirus Improves the Efficacy of Adoptive T-cell**

Therapy by Recruiting Immune Cells to and Promoting Their Activity at the Tumor. *Cancer Immunology Research.* (2015), 3(8):915-925.

144. Siurala M, Vähä-Koskela M, Havunen R, Tähtinen S, Bramante S, Parviainen S, Mathis JM, Kanerva A and Hemminki A. **Syngeneic Syrian hamster tumors feature tumor-infiltrating lymphocytes allowing adoptive cell therapy enhanced by oncolytic adenovirus in a replication permissive setting**. *OncoImmunology.* (2016), 5(5):e1136046.

145. Jackson HJ, Rafiq S and Brentjens RJ. **Driving CAR T-cells forward**. *Nature Reviews Clinical Oncology.* (2016), 13(6):370-383.

146. Fesnak AD, June CH and Levine BL. **Engineered T cells: the promise and challenges of cancer immunotherapy**. *Nat Rev Cancer.* (2016), 16(9):566-581.

147. Maude SL, Frey N, Shaw PA, Aplenc R, Barrett DM, Bunin NJ, Chew A, Gonzalez VE, Zheng Z, Lacey SF *et al*. **Chimeric Antigen Receptor T Cells for Sustained Remissions in Leukemia**. *New England Journal of Medicine.* (2014), 371(16):1507-1517.

148. Maus MV and June CH. **Making Better Chimeric Antigen Receptors for Adoptive T-cell Therapy**. *Clinical Cancer Research.* (2016), 22(8):1875-1884.

149. Newick K, Moon E and Albelda SM. **Chimeric antigen receptor T-cell therapy for solid tumors**. *Molecular Therapy - Oncolytics.* (2016), 3:Article 16006.

150. Moon EK, Wang L-C, Dolfi DV, Wilson CB, Ranganathan R, Sun J, Kapoor V, Scholler J, Puré E, Milone MC *et al*. **Multifactorial T-cell Hypofunction That Is Reversible Can Limit the Efficacy of Chimeric Antigen Receptor–Transduced Human T cells in Solid Tumors**. *Clinical Cancer Research.* (2014), 20(16):4262-4273.

151. Sotillo E, Barrett DM, Black KL, Bagashev A, Oldridge D, Wu G, Sussman R, Lanauze C, Ruella M, Gazzara MR *et al*. **Convergence of Acquired Mutations and Alternative Splicing of *CD19* Enables Resistance to CART-19 Immunotherapy**. *Cancer Discovery.* (2015), 5(12):1282-1295.

152. Nishio N, Diaconu I, Liu H, Cerullo V, Caruana I, Hoyos V, Bouchier-Hayes L, Savoldo B and Dotti G. **Armed Oncolytic Virus Enhances Immune Functions of Chimeric Antigen Receptor–Modified T Cells in Solid Tumors**. *Cancer Research.* (2014), 74(18):5195-5205.

153. Watanabe K, Guedan S, Scholler J, McGettigan S, Luo Y, Tähtinen S, Parviainen S, Havunen R, Siurala M, Hemminki A *et al*. **Oncolytic Adenovirus Expressing Cytokines Enhances Anti-Tumor Efficacy of Mesothelin-Redirected CAR-T Cells**. *Blood.* (2016), 128(22):3360-3360.

154. Restifo NP. **Hierarchy, Tolerance, and Dominance in the Antitumor T-Cell Response**. *Journal of Immunotherapy.* (2001), 24(3):193-194.

155. Schirmbeck R, Reimann J, Kochanek S and Kreppel F. **The Immunogenicity of Adenovirus Vectors Limits the Multispecificity of CD8 T-cell Responses to Vector-encoded Transgenic Antigens**. *Molecular Therapy.* (2008), 16(9):1609-1616.

156. Frahm N, DeCamp AC, Friedrich DP, Carter DK, Defawe OD, Kublin JG, Casimiro DR, Duerr A, Robertson MN, Buchbinder SP *et al*. **Human adenovirus-specific T cells modulate HIV-**

specific T cell responses to an Ad5-vectored HIV-1 vaccine. *The Journal of Clinical Investigation.* (2012), 122(1):359-367.

157. Gibson H, Munns S, Freytag S, Barton K, Veenstra J, Bettahi I, Bissonette J and Wei W-Z. **Immunotherapeutic intervention with oncolytic adenovirus in mouse mammary tumors**. *OncoImmunology.* (2015), 4(1):e984523.

158. Capasso C, Hirvinen M, Garofalo M, Romaniuk D, Kuryk L, Sarvela T, Vitale A, Antopolsky M, Magarkar A, Viitala T *et al*. **Oncolytic adenoviruses coated with MHC-I tumor epitopes increase the antitumor immunity and efficacy against melanoma**. *OncoImmunology.* (2016), 5(4):e1105429.

159. Rodriguez-Garcia A, Svensson E, Gil-Hoyos R, Fajardo CA, Rojas LA, Arias-Badia M, Loskog ASI and Alemany R. **Insertion of exogenous epitopes in the E3-19K of oncolytic adenoviruses to enhance TAP-independent presentation and immunogenicity**. *Gene Therapy.* (2015), 22(7):596-601.

160. Wolf E, Hofmeister R, Kufer P, Schlereth B and Baeuerle PA. **BiTEs: bispecific antibody constructs with unique anti-tumor activity**. *Drug Discovery Today.* (2005), 10(18):1237-1244.

161. Baeuerle PA, Reinhardt C and Kufer P. **BiTE: A new class of antibodies that recruit T-cells**. *Drugs of the future.* (2008), 33(2):137-147.

162. Brischwein K, Parr L, Pflanz S, Volkland J, Lumsden J, Klinger M, Locher M, Hammond SA, Kiener P, Kufer P *et al*. **Strictly Target Cell-dependent Activation of T Cells by Bispecific Single-chain Antibody Constructs of the BiTE Class**. *Journal of Immunotherapy.* (2007), 30(8):798-807.

163. Baeuerle PA, Kufer P and Bargou R. **BiTE: Teaching antibodies to engage T-cells for cancer therapy**. *Current Opinion in Molecular Therapy.* (2009), 11(1):22-30.

164. Goebeler M-E, Knop S, Viardot A, Kufer P, Topp MS, Einsele H, Noppeney R, Hess G, Kallert S, Mackensen A *et al*. **Bispecific T-Cell Engager (BiTE) Antibody Construct Blinatumomab for the Treatment of Patients With Relapsed/Refractory Non-Hodgkin Lymphoma: Final Results From a Phase I Study**. *Journal of Clinical Oncology.* (2016), 34(10):1104-1111.

165. Yuraszeck T, Kasichayanula S and E. Benjamin J. **Translation and Clinical Development of Bispecific T cell Engaging Antibodies for Cancer Treatment**. *Clinical Pharmacology & Therapeutics.* (2017), 101(5):634-645.

166. Ribera J-M, Ferrer A, Ribera J and Genescà E. **Profile of blinatumomab and its potential in the treatment of relapsed/refractory acute lymphoblastic leukemia**. *OncoTargets and therapy.* (2015), 8:1567-1574.

167. Pishvaian M, Morse MA, McDevitt J, Norton JD, Ren S, Robbie GJ, Ryan PC, Soukharev S, Bao H and Denlinger CS. **Phase 1 Dose Escalation Study of MEDI-565, Bispecific T-Cell Engager that Targets Human Carcinoembryonic Antigen, in Patients With Advanced Gastrointestinal Adenocarcinomas**. *Clinical Colorectal Cancer.* (2016), 15(4):345-351.

168. Birnboim HC and Doly J. **A rapid alkaline extraction procedure for screening recombinant plasmid DNA**. *Nucleic Acids Research.* (1979), 7(6):1513-1523.

169. Warming S, Costantino N, Court DL, Jenkins NA and Copeland NG. **Simple and highly efficient BAC recombineering using galK selection**. *Nucleic Acids Research.* (2005), 33(4):e36.

170. Stanton RJ, McSharry BP, Armstrong M, Tomasec P and Wilkinson GW. **Re-engineering adenovirus vector systems to enable high-throughput analyses of gene function**. *Biotechniques.* (2008), 45(6):659-662.

171. Wang S, Zhao Y, Leiby M and Zhu J. **A New positive/negative selection scheme for precise BAC recombineering**. *Molecular biotechnology.* (2009), 42(1):110-116.

172. Stavropoulos TA and Strathdee CA. **Synergy between tetA and rpsL Provides High-Stringency Positive and Negative Selection in Bacterial Artificial Chromosome Vectors**. *Genomics.* (2001), 72(1):99-104.

173. Stone JD, Aggen DH, Schietinger A, Schreiber H and Kranz DM. **A sensitivity scale for targeting T cells with chimeric antigen receptors (CARs) and bispecific T-cell Engagers (BiTEs)**. *OncoImmunology.* (2012), 1(6):863-873.

174. Garrido G, Sanchez B, Rodriguez HM, Lorenzano P, Alonso D and Fernandez LE. **7A7 MAb: A New Tool for the Pre-Clinical Evaluation of EGFR-Based Therapies**. *Hybridoma and Hybridomics.* (2004), 23(3):168-175.

175. Hammond SA, Lutterbuese R, Roff S, Lutterbuese P, Schlereth B, Bruckheimer E, Kinch MS, Coats S, Baeuerle PA, Kufer P *et al*. **Selective Targeting and Potent Control of Tumor Growth Using an EphA2/CD3-Bispecific Single-Chain Antibody Construct**. *Cancer Research.* (2007), 67(8):3927-3935.

176. Lutterbuese R, Raum T, Kischel R, Hoffmann P, Mangold S, Rattel B, Friedrich M, Thomas O, Lorenczewski G, Rau D *et al*. **T cell-engaging BiTE antibodies specific for EGFR potently eliminate KRAS- and BRAF-mutated colorectal cancer cells**. *Proceedings of the National Academy of Sciences.* (2010), 107(28):12605-12610.

177. Brischwein K, Schlereth B, Guller B, Steiger C, Wolf A, Lutterbuese R, Offner S, Locher M, Urbig T, Raum T *et al*. **MT110: A novel bispecific single-chain antibody construct with high efficacy in eradicating established tumors**. *Molecular Immunology.* (2006), 43(8):1129-1143.

178. Lutterbuese R, Raum T, Kischel R, Lutterbuese P, Schlereth B, Schaller E, Mangold S, Rau D, Meier P, Kiener PA *et al*. **Potent control of tumor growth by CEA/CD3-bispecific single-chain antibody constructs that are not competitively inhibited by soluble CEA**. *Journal of Immunotherapy.* (2009), 32(4):341-352. doi: 310.1097/CJI.1090b1013e31819b31817c31870.

179. Schlereth B, Kleindienst P, Fichtner I, Lorenczewski G, Brischwein K, Lippold S, Silva Ad, Locher M, Kischel R, Lutterbüse R *et al*. **Potent inhibition of local and disseminated tumor growth in immunocompetent mouse models by a bispecific antibody construct specific for Murine CD3**. *Cancer Immunology, Immunotherapy.* (2006), 55(7):785-796.

180. Rocha-Lima CM, Soares HP, Raez LE and Singal R. **EGFR targeting of solid tumors**. *Cancer Control.* (2007), 14(3):295-304.

181. Sebastian S, Settleman J, Reshkin SJ, Azzariti A, Bellizzi A and Paradiso A. **The complexity of targeting EGFR signalling in cancer: From expression to turnover**. *Biochimica et Biophysica Acta (BBA) - Reviews on Cancer.* (2006), 1766(1):120-139.

182. Miloud T, Henrich C and Hämmerling GJ. **Quantitative comparison of click beetle and firefly luciferases for in vivo bioluminescence imaging**. *BIOMEDO.* (2007), 12(5):054018.

183. Blackburn SD, Shin H, Haining WN, Zou T, Workman CJ, Polley A, Betts MR, Freeman GJ, Vignali DAA and Wherry EJ. **Coregulation of CD8+ T cell exhaustion by multiple inhibitory receptors during chronic viral infection**. *Nature Immunology.* (2009), 10(1):29-37.

184. Pauken KE and Wherry EJ. **Overcoming T cell exhaustion in infection and cancer**. *Trends in Immunology.* (2015), 36(4):265-276.

185. Amann M, Brischwein K, Lutterbuese P, Parr L, Petersen L, Lorenczewski G, Krinner E, Bruckmeier S, Lippold S, Kischel R *et al*. **Therapeutic Window of MuS110, a Single-Chain Antibody Construct Bispecific for Murine EpCAM and Murine CD3**. *Cancer Research.* (2008), 68(1):143-151.

186. Amann M, Friedrich M, Lutterbuese P, Vieser E, Lorenczewski G, Petersen L, Brischwein K, Kufer P, Kischel R, Baeuerle PA *et al*. **Therapeutic window of an EpCAM/CD3-specific BiTE antibody in mice is determined by a subpopulation of EpCAM-expressing lymphocytes that is absent in humans**. *Cancer Immunology, Immunotherapy.* (2008), 58(1):95.

187. Yamashita M, Ino A, Kawabata K, Sakurai F and Mizuguchi H. **Expression of coxsackie and adenovirus receptor reduces the lung metastatic potential of murine tumor cells**. *International Journal of Cancer.* (2007), 121(8):1690-1696.

188. Halldén G, Hill R, Wang Y, Anand A, Liu T-C, Lemoine NR, Francis J, Hawkins L and Kirn D. **Novel immunocompetent murine tumor models for the assessment of replication-competent oncolytic adenovirus efficacy**. *Molecular Therapy.* (2003), 8(3):412-424.

189. Ho M, Feng M, Fisher RJ, Rader C and Pastan I. **A novel high affinity human monoclonal antibody to mesothelin**. *International journal of cancer Journal international du cancer.* (2011), 128(9):2020-2030.

190. Guedan S, Chen X, Madar A, Carpenito C, McGettigan SE, Frigault MJ, Lee J, Posey AD, Scholler J, Scholler N *et al*. **ICOS-based chimeric antigen receptors program bipolar TH17/Th1 cells**. *Blood.* (2014), 124(7):1070-1080.

191. Wykosky J, Fenton T, Furnari F and Cavenee WK. **Therapeutic targeting of epidermal growth factor receptor in human cancer: successes and limitations**. *Chin J Cancer.* (2011), 30(1):5-12.

192. Arteaga CL. **The epidermal growth factor receptor: from mutant oncogene in nonhuman cancers to therapeutic target in human neoplasia**. *Journal of Clinical Oncology.* (2001), 19(18 Suppl):32S-40S.

193. Vecchione L, Jacobs B, Normanno N, Ciardiello F and Tejpar S. **EGFR-targeted therapy**. *Experimental Cell Research.* (2011), 317(19):2765-2771.

194. Vermorken JB, Trigo J, Hitt R, Koralewski P, Diaz-Rubio E, Rolland F, Knecht R, Amellal N, Schueler A and Baselga J. **Open-Label, Uncontrolled, Multicenter Phase II Study to Evaluate the Efficacy and Toxicity of Cetuximab As a Single Agent in Patients With Recurrent and/or Metastatic Squamous Cell Carcinoma of the Head and Neck Who Failed to Respond to Platinum-Based Therapy**. *Journal of Clinical Oncology.* (2007), 25(16):2171-2177.

195. Jonker DJ, O'Callaghan CJ, Karapetis CS, Zalcberg JR, Tu D, Au H-J, Berry SR, Krahn M, Price T, Simes RJ *et al*. **Cetuximab for the Treatment of Colorectal Cancer**. *New England Journal of Medicine.* (2007), 357(20):2040-2048.

196. Lenz H-J. **Cetuximab in the management of colorectal cancer**. *Biologics : Targets & Therapy.* (2007), 1(2):77-91.

197. Brand TM, Iida M and Wheeler DL. **Molecular mechanisms of resistance to the EGFR monoclonal antibody cetuximab**. *Cancer Biology & Therapy.* (2011), 11(9):777-792.

198. Schlereth B, Fichtner I, Lorenczewski G, Kleindienst P, Brischwein K, da Silva A, Kufer P, Lutterbuese R, Junghahn I, Kasimir-Bauer S *et al*. **Eradication of Tumors from a Human Colon Cancer Cell Line and from Ovarian Cancer Metastases in Immunodeficient Mice by a Single-Chain Ep-CAM-/CD3-Bispecific Antibody Construct**. *Cancer Research.* (2005), 65(7):2882-2889.

199. Aigner M, Feulner J, Schaffer S, Kischel R, Kufer P, Schneider K, Henn A, Rattel B, Friedrich M, Baeuerle PA *et al*. **T lymphocytes can be effectively recruited for ex vivo and in vivo lysis of AML blasts by a novel CD33/CD3-bispecific BiTE antibody construct**. *Leukemia.* (2013), 27(5):1107-1115.

200. Compte M, Álvarez-Cienfuegos A, Nuñez-Prado N, Sainz-Pastor N, Blanco-Toribio A, Pescador N, Sanz L and Álvarez-Vallina L. **Functional comparison of single-chain and two-chain anti-CD3-based bispecific antibodies in gene immunotherapy applications**. *OncoImmunology.* (2014), 3(5):e28810.

201. Kufer P, Lutterbüse R, Kohleisen B, Zeman S and Bäuerle P.**Pharmaceutical compositions comprising bispecific anti-CD3, anti-CD19 antibody constructs for the treatment of B-cell related disorders**. World patent WO/2004/106381. December 9, 2004

202. Fernández-Ulibarri I, Hammer K, Arndt MAE, Kaufmann JK, Dorer D, Engelhardt S, Kontermann RE, Hess J, Allgayer H, Krauss J *et al*. **Genetic delivery of an immunoRNase by an oncolytic adenovirus enhances anticancer activity**. *International Journal of Cancer.* (2015), 136(9):2228-2240.

203. Hofmeister R, Kohleisen B, Lenkkeri-schütz U, Itin C, Bäuerle P, Carr FJ, Hamilton AA and Williams S.**Multispecific Deimmunized CD3-Binders**. World patent WO/2005/040220. May 6, 2005

204. Brinkmann U and Kontermann RE. **The making of bispecific antibodies**. *mAbs.* (2017), 9(2):182-212.

205. Dreier T, Lorenczewski G, Brandl C, Hoffmann P, Syring U, Hanakam F, Kufer P, Riethmuller G, Bargou R and Baeuerle PA. **Extremely potent, rapid and costimulation-independent cytotoxic T-cell response against lymphoma cells catalyzed by a single-chain bispecific antibody**. *International Journal of Cancer.* (2002), 100(6):690-697.

206. Klinger M, Benjamin J, Kischel R, Stienen S and Zugmaier G. **Harnessing T cells to fight cancer with BiTE® antibody constructs – past developments and future directions**. *Immunological Reviews.* (2016), 270(1):193-208.

207. Choi BD, Kuan C-T, Cai M, Archer GE, Mitchell DA, Gedeon PC, Sanchez-Perez L, Pastan I, Bigner DD and Sampson JH. **Systemic administration of a bispecific antibody targeting EGFRvIII successfully treats intracerebral glioma**. *Proceedings of the National Academy of Sciences.* (2013), 110(1):270-275.

208. Carette JE, Graat HCA, Schagen FHE, Abou El Hassan MAI, Gerritsen WR and van Beusechem VW. **Replication-dependent transgene expression from a conditionally replicating adenovirus via alternative splicing to a heterologous splice-acceptor site**. *The Journal of Gene Medicine.* (2005), 7(8):1053-1062.

209. Jang SK, Kräusslich HG, Nicklin MJ, Duke GM, Palmenberg AC and Wimmer E. **A segment of the 5' nontranslated region of encephalomyocarditis virus RNA directs internal entry of ribosomes during in vitro translation**. *Journal of Virology.* (1988), 62(8):2636-2643.

210. Martínez-Salas E. **Internal ribosome entry site biology and its use in expression vectors**. *Current Opinion in Biotechnology.* (1999), 10(5):458-464.

211. Dorer D. **Developing novel strategies for oncolytic adenovirus therapy by host cell gene expression profiling and arming with therapeutic antibodies**. *Doctoral dissertation.* Heidelberg University, 2011.Retrieved from http://www.ub.uni-heidelberg.de/archiv/11844

212. Villanueva E, Martí-Solano M and Fillat C. **Codon optimization of the adenoviral fiber negatively impacts structural protein expression and viral fitness**. *Scientific Reports.* (2016), 6:27546.

213. Mølhøj M, Crommer S, Brischwein K, Rau D, Sriskandarajah M, Hoffmann P, Kufer P, Hofmeister R and Baeuerle PA. **CD19-/CD3-bispecific antibody of the BiTE class is far superior to tandem diabody with respect to redirected tumor cell lysis**. *Molecular Immunology.* (2007), 44(8):1935-1943.

214. Yu F, Wang X, Guo ZS, Bartlett DL, Gottschalk SM and Song X-T. **T-cell Engager-armed Oncolytic Vaccinia Virus Significantly Enhances Antitumor Therapy**. *Molecular Therapy.* (2014), 22(1):102-111.

215. Teachey DT, Rheingold SR, Maude SL, Zugmaier G, Barrett DM, Seif AE, Nichols KE, Suppa EK, Kalos M, Berg RA *et al*. **Cytokine release syndrome after blinatumomab treatment related**

to abnormal macrophage activation and ameliorated with cytokine-directed therapy. *Blood.* (2013), 121(26):5154-5157.

216. Klinger M, Brandl C, Zugmaier G, Hijazi Y, Bargou RC, Topp MS, Gökbuget N, Neumann S, Goebeler M, Viardot A *et al*. **Immunopharmacologic response of patients with B-lineage acute lymphoblastic leukemia to continuous infusion of T cell–engaging CD19/CD3-bispecific BiTE antibody blinatumomab**. *Blood.* (2012), 119(26):6226-6233.

217. Schmittnaegel M, Levitsky V, Hoffmann E, Georges G, Mundigl O, Klein C and Knoetgen H. **Committing Cytomegalovirus-Specific CD8 T Cells to Eliminate Tumor Cells by Bifunctional Major Histocompatibility Class I Antibody Fusion Molecules**. *Cancer Immunology Research.* (2015), 3(7):764-776.

218. Warnders FJ, Waaijer SJH, Pool M, Lub–de Hooge MN, Friedrich M, Terwisscha van Scheltinga AGT, Deegen P, Stienen SK, Pieslor PC, Cheung HK *et al*. **Biodistribution and PET Imaging of Labeled Bispecific T Cell–Engaging Antibody Targeting EpCAM**. *Journal of Nuclear Medicine.* (2016), 57(5):812-817.

219. Wüest T, Moosmayer D and Pfizenmaier K. **Construction of a bispecific single chain antibody for recruitment of cytotoxic T cells to the tumour stroma associated antigen fibroblast activation protein**. *Journal of Biotechnology.* (2001), 92(2):159-168.

220. Bardelli A and Siena S. **Molecular Mechanisms of Resistance to Cetuximab and Panitumumab in Colorectal Cancer**. *Journal of Clinical Oncology.* (2010), 28(7):1254-1261.

221. Souglakos J, Philips J, Wang R, Marwah S, Silver M, Tzardi M, Silver J, Ogino S, Hooshmand S, Kwak E *et al*. **Prognostic and predictive value of common mutations for treatment response and survival in patients with metastatic colorectal cancer**. *British Journal of Cancer.* (2009), 101(3):465-472.

222. Benvenuti S, Sartore-Bianchi A, Di Nicolantonio F, Zanon C, Moroni M, Veronese S, Siena S and Bardelli A. **Oncogenic Activation of the RAS/RAF Signaling Pathway Impairs the Response of Metastatic Colorectal Cancers to Anti–Epidermal Growth Factor Receptor Antibody Therapies**. *Cancer Research.* (2007), 67(6):2643-2648.

223. Lièvre A, Bachet J-B, Le Corre D, Boige V, Landi B, Emile J-F, Côté J-F, Tomasic G, Penna C, Ducreux M *et al*. ***KRAS* Mutation Status Is Predictive of Response to Cetuximab Therapy in Colorectal Cancer**. *Cancer Research.* (2006), 66(8):3992-3995.

224. Oberst MD, Fuhrmann S, Mulgrew K, Amann M, Cheng L, Lutterbuese P, Richman L, Coats S, Baeuerle PA and Hammond SA. **CEA/CD3 bispecific antibody MEDI-565/AMG 211 activation of T cells and subsequent killing of human tumors is independent of mutations commonly found in colorectal adenocarcinomas**. *mAbs.* (2014), 6(6):1571-1584.

225. Spranger S. **Mechanisms of tumor escape in the context of the T-cell-inflamed and the non-T-cell-inflamed tumor microenvironment**. *International Immunology.* (2016), 28(8):383-391.

226. Topalian SL, Hodi FS, Brahmer JR, Gettinger SN, Smith DC, McDermott DF, Powderly JD, Carvajal RD, Sosman JA, Atkins MB *et al*. **Safety, Activity, and Immune Correlates of Anti–PD-1 Antibody in Cancer**. *New England Journal of Medicine.* (2012), 366(26):2443-2454.

227. Tumeh PC, Harview CL, Yearley JH, Shintaku IP, Taylor EJM, Robert L, Chmielowski B, Spasic M, Henry G, Ciobanu V *et al*. **PD-1 blockade induces responses by inhibiting adaptive immune resistance**. *Nature.* (2014), 515(7528):568-571.

228. Hwang T-H, Moon A, Burke J, Ribas A, Stephenson J, Breitbach CJ, Daneshmand M, De Silva N, Parato K, Diallo J-S *et al*. **A Mechanistic Proof-of-concept Clinical Trial With JX-594, a Targeted Multi-mechanistic Oncolytic Poxvirus, in Patients With Metastatic Melanoma**. *Molecular Therapy.* (2011), 19(10):1913-1922.

229. Kaufman HL, Kim DW, DeRaffele G, Mitcham J, Coffin RS and Kim-Schulze S. **Local and Distant Immunity Induced by Intralesional Vaccination with an Oncolytic Herpes Virus Encoding GM-CSF in Patients with Stage IIIc and IV Melanoma**. *Annals of Surgical Oncology.* (2010), 17(3):718-730.

230. Mastrangelo MJ, Maguire HC, Jr., Eisenlohr LC, Laughlin CE, Monken CE, McCue PA, Kovatich AJ and Lattime EC. **Intratumoral recombinant GM-CSF-encoding virus as gene therapy in patients with cutaneous melanoma**. *Cancer Gene Therapy.* (1999), 6(5):409-422.

231. Kaufman HL, Amatruda T, Reid T, Gonzalez R, Glaspy J, Whitman E, Harrington K, Nemunaitis J, Zloza A, Wolf M *et al*. **Systemic versus local responses in melanoma patients treated with talimogene laherparepvec from a multi-institutional phase II study**. *Journal for Immunotherapy of Cancer.* (2016), 4:12.

232. Andtbacka RHI, Ross M, Puzanov I, Milhem M, Collichio F, Delman KA, Amatruda T, Zager JS, Cranmer L, Hsueh E *et al*. **Patterns of Clinical Response with Talimogene Laherparepvec (T-VEC) in Patients with Melanoma Treated in the OPTiM Phase III Clinical Trial**. *Annals of Surgical Oncology.* (2016), 23(13):4169-4177.

233. Gajewski TF. **The Next Hurdle in Cancer Immunotherapy: Overcoming the Non–T-Cell–Inflamed Tumor Microenvironment**. *Seminars in Oncology.* (2015), 42(4):663-671.

234. Rossig C, Bollard CM, Nuchtern JG, Rooney CM and Brenner MK. **Epstein-Barr virus–specific human T lymphocytes expressing antitumor chimeric T-cell receptors: potential for improved immunotherapy**. *Blood.* (2002), 99(6):2009-2016.

235. Landmeier S, Altvater B, Pscherer S, Eing BR, Kuehn J, Rooney CM, Juergens H and Rossig C. **Gene-Engineered Varicella-Zoster Virus–Reactive CD4+ Cytotoxic T Cells Exert Tumor-Specific Effector Function**. *Cancer Research.* (2007), 67(17):8335-8343.

236. Pule MA, Savoldo B, Myers GD, Rossig C, Russell HV, Dotti G, Huls MH, Liu E, Gee AP, Mei Z *et al*. **Virus-specific T cells engineered to coexpress tumor-specific receptors: persistence and antitumor activity in individuals with neuroblastoma**. *Nature Medicine.* (2008), 14(11):1264-1270.

237. Cruz CRY, Micklethwaite KP, Savoldo B, Ramos CA, Lam S, Ku S, Diouf O, Liu E, Barrett AJ, Ito S *et al*. **Infusion of donor-derived CD19-redirected virus-specific T cells for B-cell malignancies relapsed after allogeneic stem cell transplant: a phase 1 study**. *Blood.* (2013), 122(17):2965-2973.

238. Braig F, Brandt A, Goebeler M, Tony H-P, Kurze A-K, Nollau P, Bumm T, Böttcher S, Bargou RC and Binder M. **Resistance to anti-CD19/CD3 BiTE in acute lymphoblastic leukemia may be mediated by disrupted CD19 membrane trafficking**. *Blood.* (2016).

239. Wheeler DL, Huang S, Kruser TJ, Nechrebecki MM, Armstrong EA, Benavente S, Gondi V, Hsu KT and Harari PM. **Mechanisms of acquired resistance to cetuximab: role of HER (ErbB) family members**. *Oncogene.* (2008), 27(28):3944-3956.

240. Akbay EA, Koyama S, Carretero J, Altabef A, Tchaicha JH, Christensen CL, Mikse OR, Cherniack AD, Beauchamp EM, Pugh TJ *et al*. **Activation of the PD-1 Pathway Contributes to Immune Escape in EGFR-Driven Lung Tumors**. *Cancer Discovery.* (2013), 3(12):1355-1363.

241. Concha-Benavente F, Srivastava RM, Trivedi S, Lei Y, Chandran U, Seethala RR, Freeman GJ and Ferris RL. **Identification of the Cell-Intrinsic and -Extrinsic Pathways Downstream of EGFR and IFNγ That Induce PD-L1 Expression in Head and Neck Cancer**. *Cancer Research.* (2016), 76(5):1031-1043.

242. Osada T, Patel SP, Hammond SA, Osada K, Morse MA and Lyerly HK. **CEA/CD3-bispecific T cell-engaging (BiTE) antibody-mediated T lymphocyte cytotoxicity maximized by inhibition of both PD1 and PD-L1**. *Cancer Immunology, Immunotherapy.* (2015), 64(6):677-688.

243. Krupka C, Kufer P, Kischel R, Zugmaier G, Lichtenegger FS, Kohnke T, Vick B, Jeremias I, Metzeler KH, Altmann T *et al*. **Blockade of the PD-1/PD-L1 axis augments lysis of AML cells by the CD33/CD3 BiTE antibody construct AMG 330: reversing a T-cell-induced immune escape mechanism**. *Leukemia.* (2016), 30(2):484-491.

244. Köhnke T, Krupka C, Tischer J, Knösel T and Subklewe M. **Increase of PD-L1 expressing B-precursor ALL cells in a patient resistant to the CD19/CD3-bispecific T cell engager antibody blinatumomab**. *Journal of Hematology & Oncology.* (2015), 8:111.

245. Feucht J, Kayser S, Gorodezki D, Hamieh M, Döring M, Blaeschke F, Schlegel P, Bösmüller H, Quintanilla-Fend L, Ebinger M *et al*. **T-cell responses against CD19 + pediatric acute lymphoblastic leukemia mediated by bispecific T-cell engager (BiTE) are regulated contrarily by PD-L1 and CD80/CD86 on leukemic blasts**. *Oncotarget.* (2016), 7(47).

246. Rajani K and Vile R. **Harnessing the Power of Onco-Immunotherapy with Checkpoint Inhibitors**. *Viruses.* (2015), 7(11):2914.

247. Shim KG, Zaidi S, Thompson J, Kottke T, Evgin L, Rajani KR, Schuelke M, Driscoll CB, Huff A, Pulido JS *et al*. **Inhibitory Receptors Induced by VSV Viroimmunotherapy Are Not Necessarily Targets for Improving Treatment Efficacy**. *Molecular Therapy.* (2017).

248. Bankert RB, Egilmez NK and Hess SD. **Human-SCID mouse chimeric models for the evaluation of anti-cancer therapies**. *Trends in Immunology.* (2001), 22(7):386-393.

249. Shultz LD, Ishikawa F and Greiner DL. **Humanized mice in translational biomedical research**. *Nature Reviews Immunology.* (2007), 7(2):118-130.

250. Mosier DE, Stell KL, Gulizia RJ, Torbett BE and Gilmore GL. **Homozygous scid/scid;beige/beige mice have low levels of spontaneous or neonatal T cell-induced B cell generation**. *The Journal of Experimental Medicine.* (1993), 177(1):191-194.

251. Engler H, Machemer T, Philopena J, Wen S-F, Quijano E, Ramachandra M, Tsai V and Ralston R. **Acute hepatotoxicity of oncolytic adenoviruses in mouse models is associated with expression of wild-type E1a and induction of TNF-α**. *Virology.* (2004), 328(1):52-61.

252. Hoyos V, Del Bufalo F, Yagyu S, Ando M, Dotti G, Suzuki M, Bouchier-Hayes L, Alemany R and Brenner MK. **Mesenchymal Stromal Cells for Linked Delivery of Oncolytic and Apoptotic Adenoviruses to Non-small-cell Lung Cancers**. *Molecular Therapy.* (2015), 23(9):1497-1506.

253. Pearson T, Greiner DL and Shultz LD. **Creation of "Humanized" Mice to Study Human Immunity**. *Current protocols in immunology / edited by John E Coligan [et al].* (2008), CHAPTER:Unit-15.21.

254. Murphy WJ, Bennett M, Anver MR, Baseler M and Longo DL. **Human-mouse lymphoid chimeras: host-vs.-graft and graft-vs.-host reactions**. *European Journal of Immunology.* (1992), 22(6):1421-1427.

255. Gorin N-C, Piantadosi S, Stull M, Bonte H, Wingard JR and Civin C. **Increased Risk of Lethal Graft-Versus-Host Disease-like Syndrome after Transplantation into NOD/SCID Mice of Human Mobilized Peripheral Blood Stem Cells, As Compared to Bone Marrow or Cord Blood**. *Journal of Hematotherapy & Stem Cell Research.* (2002), 11(2):277-292.

256. Hirvinen M, Capasso C, Guse K, Garofalo M, Vitale A, Ahonen M, Kuryk L, Vähä-Koskela M, Hemminki A, Fortino V *et al*. **Expression of DAI by an oncolytic vaccinia virus boosts the immunogenicity of the virus and enhances antitumor immunity**. *Molecular Therapy - Oncolytics.* (2016), 3:Article 16002.

257. Stadler CR, Bähr-Mahmud H, Plum LM, Schmoldt K, Kölsch AC, Türeci Ö and Sahin U. **Characterization of the first-in-class T-cell-engaging bispecific single-chain antibody for targeted immunotherapy of solid tumors expressing the oncofetal protein claudin 6**. *OncoImmunology.* (2016), 5(3):e1091555.

258. Amann M, D'Argouges S, Lorenczewski G, Brischwein K, Kischel R, Lutterbuese R, Mangold S, Rau D, Volkland J, Pflanz S *et al*. **Antitumor activity of an EpCAM/CD3-bispecific BiTE antibody during long-term treatment of mice in the absence of T-cell anergy and sustained cytokine release**. *Journal of Immunotherapy.* (2009), 32(5):452-464. .

259. Engeland CE, Grossardt C, Veinalde R, Bossow S, Lutz D, Kaufmann JK, Shevchenko I, Umansky V, Nettelbeck DM, Weichert W *et al*. **CTLA-4 and PD-L1 Checkpoint Blockade Enhances Oncolytic Measles Virus Therapy**. *Molecular Therapy.* (2014), 22(11):1949-1959.

260. Yang X, Zhang X, Fu May L, Weichselbaum Ralph R, Gajewski Thomas F, Guo Y and Fu Y-X. **Targeting the Tumor Microenvironment with Interferon-β Bridges Innate and Adaptive Immune Responses**. *Cancer Cell.* (2014), 25(1):37-48.

261. Yang X, Zhang X, Mortenson ED, Radkevich-Brown O, Wang Y and Fu Y-X. **Cetuximab-mediated Tumor Regression Depends on Innate and Adaptive Immune Responses**. *Molecular Therapy.* (2013), 21(1):91-100.

262. Tang H, Wang Y, Chlewicki LK, Zhang Y, Guo J, Liang W, Wang J, Wang X and Fu Y-X. **Facilitating T Cell Infiltration in Tumor Microenvironment Overcomes Resistance to PD-L1 Blockade**. *Cancer Cell.* (2016), 29(3):285-296.

263. Gazdar AF. **Activating and resistance mutations of EGFR in non-small-cell lung cancer: role in clinical response to EGFR tyrosine kinase inhibitors**. *Oncogene.* (2009), 28(Suppl 1):S24-S31.

264. Yu H, Sotillo E, Harrington C, Wertheim G, Paessler M, Maude SL, Rheingold SR, Grupp SA, Thomas-Tikhonenko A and Pillai V. **Repeated loss of target surface antigen after immunotherapy in primary mediastinal large B cell lymphoma**. *American Journal of Hematology.* (2017), 92(1):E11-E13.

265. Ruella M, Barrett DM, Kenderian SS, Shestova O, Hofmann TJ, Perazzelli J, Klichinsky M, Aikawa V, Nazimuddin F, Kozlowski M *et al*. **Dual CD19 and CD123 targeting prevents antigen-loss relapses after CD19-directed immunotherapies**. *The Journal of Clinical Investigation.* (2016), 126(10):3814-3826.

266. Hegde M, Mukherjee M, Grada Z, Pignata A, Landi D, Navai SA, Wakefield A, Fousek K, Bielamowicz K, Chow KKH *et al*. **Tandem CAR T cells targeting HER2 and IL13Rα2 mitigate tumor antigen escape**. *The Journal of Clinical Investigation.* (2016), 126(8):3036-3052.

267. Zah E, Lin M-Y, Silva-Benedict A, Jensen MC and Chen YY. **T Cells Expressing CD19/CD20 Bispecific Chimeric Antigen Receptors Prevent Antigen Escape by Malignant B Cells**. *Cancer Immunology Research.* (2016), 4(6):498-508.

268. Hollyman D, Stefanski J, Przybylowski M, Bartido S, Borquez-Ojeda O, Taylor C, Yeh R, Capacio V, Olszewska M, Hosey J *et al*. **Manufacturing validation of biologically functional T cells targeted to CD19 antigen for autologous adoptive cell therapy**. *Journal of immunotherapy (Hagerstown, Md : 1997).* (2009), 32(2):169-180.

269. Li Y and Kurlander RJ. **Comparison of anti-CD3 and anti-CD28-coated beads with soluble anti-CD3 for expanding human T cells: Differing impact on CD8 T cell phenotype and responsiveness to restimulation**. *Journal of Translational Medicine.* (2010), 8:104-104.

270. Liu X, Barrett DM, Jiang S, Fang C, Kalos M, Grupp SA, June CH and Zhao Y. **Improved anti-leukemia activities of adoptively transferred T cells expressing bispecific T-cell engager in mice**. *Blood Cancer Journal.* (2016), 6:e430.

271. Kischel R, Hausmann S, Baeuerle P and Kufer P. **Effector memory T cells make a major contribution to redirected target cell lysis by T cell-engaging BiTE antibody MT110 (Abstract #3252)**. *Cancer Research.* (2009), 69(9 Supplement):3252-3252.

272. Iwahori K, Kakarla S, Velasquez MP, Yu F, Yi Z, Gerken C, Song X-T and Gottschalk S. **Engager T Cells: A New Class of Antigen-specific T Cells That Redirect Bystander T Cells**. *Molecular Therapy.* (2015), 23(1):171-178.

273. Velasquez MP, Torres D, Iwahori K, Kakarla S, Arber C, Rodriguez-Cruz T, Szoor A, Bonifant CL, Gerken C, Cooper LJN *et al*. **T cells expressing CD19-specific Engager Molecules for the Immunotherapy of CD19-positive Malignancies**. *Scientific Reports.* (2016), 6:27130.

274. Bonifant CL, Szoor A, Torres D, Joseph N, Velasquez MP, Iwahori K, Gaikwad A, Nguyen P, Arber C, Song X-T *et al*. **CD123-Engager T Cells as a Novel Immunotherapeutic for Acute Myeloid Leukemia**. *Molecular Therapy.* (2016), 24(9):1615-1626.

275. Tanoue K, Rosewell Shaw A, Watanabe N, Porter CE, Rana B, Gottschalk S, Brenner MK and Suzuki M. **Armed oncolytic adenovirus expressing PD-L1 mini-body enhances anti-tumor effects of chimeric antigen receptor T-cells in solid tumors**. *Cancer Research.* (2017), 77(8):2040-2051.

276. Bauzon M, Castro D, Karr M, Hawkins LK and Hermiston TW. **Multigene expression from a replicating adenovirus using native viral promoters**. *Molecular Therapy.* (2003), 7(4):526-534.

277. Cerullo V, Pesonen S, Diaconu I, Escutenaire S, Arstila PT, Ugolini M, Nokisalmi P, Raki M, Laasonen L, Särkioja M *et al*. **Oncolytic Adenovirus Coding for Granulocyte Macrophage Colony-Stimulating Factor Induces Antitumoral Immunity in Cancer Patients**. *Cancer Research.* (2010), 70(11):4297-4309.

278. Wang Y, Hallden G, Hill R, Anand A, Liu T-C, Francis J, Brooks G, Lemoine N and Kirn D. **E3 gene manipulations affect oncolytic adenovirus activity in immunocompetent tumor models**. *Nat Biotech.* (2003), 21(11):1328-1335.

279. Bortolanza S, Bunuales M, Alzuguren P, Lamas O, Aldabe R, Prieto J and Hernandez-Alcoceba R. **Deletion of the E3-6.7K/gp19K region reduces the persistence of wild-type adenovirus in a permissive tumor model in Syrian hamsters**. *Cancer Gene Ther.* (2009), 16(9):703-712.

280. Liikanen I, Tähtinen S, Guse K, Gutmann T, Savola P, Oksanen M, Kanerva A and Hemminki A. **Oncolytic Adenovirus Expressing Monoclonal Antibody Trastuzumab for Treatment of HER2-Positive Cancer**. *Molecular Cancer Therapeutics.* (2016), 15(9):2259-2269.

281. Apetoh L, Ladoire S, Coukos G and Ghiringhelli F. **Combining immunotherapy and anticancer agents: the right path to achieve cancer cure?** *Annals of Oncology.* (2015), 26(9):1813-1823.

8. ANNEXES

Annex 1. cBiTE construct

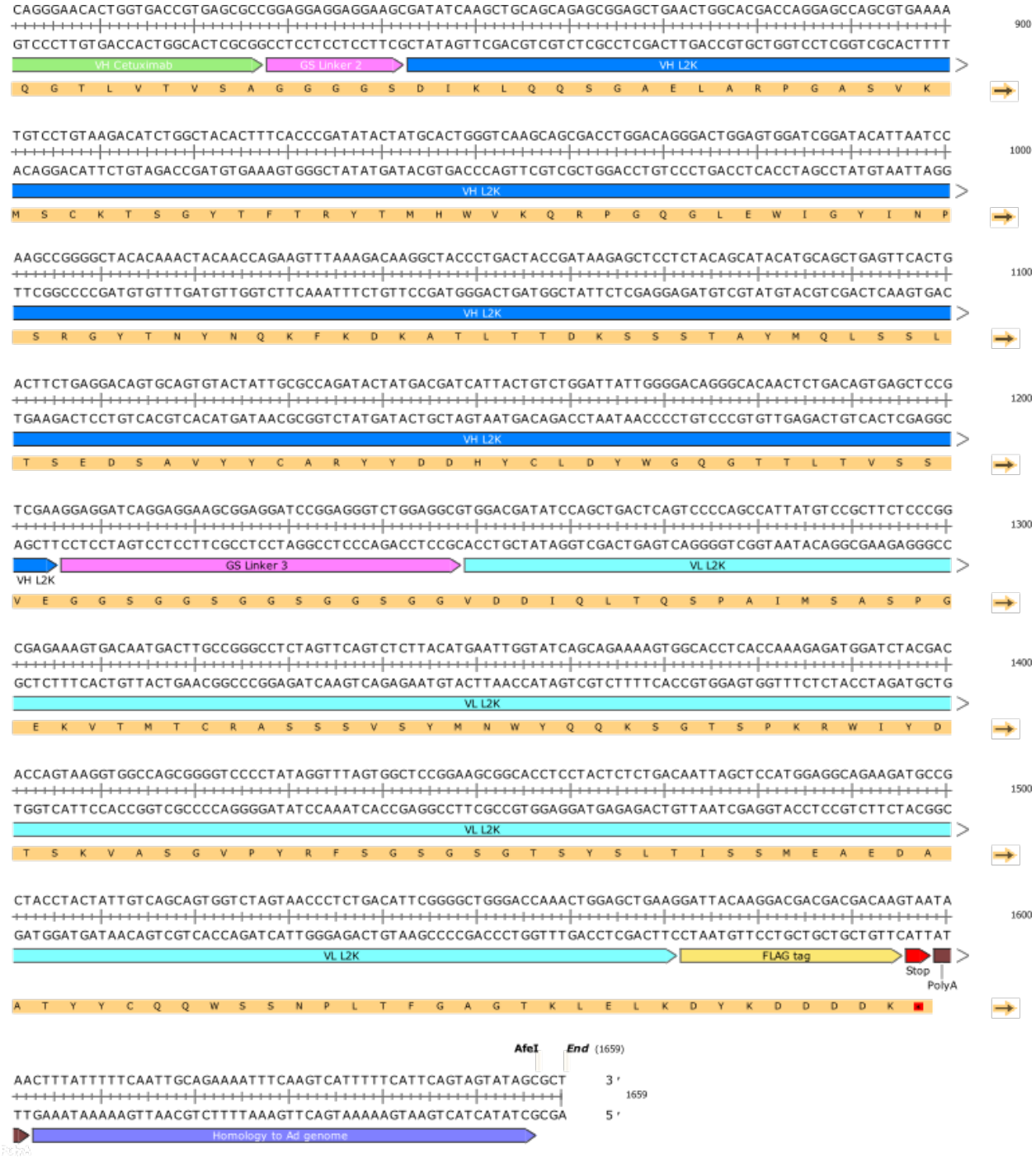
CAGGGAACACTGGTGACCGTGAGCGCCGGAGGAGGAGGAAGCGATATCAAGCTGCAGCAGAGCGGAGCTGAACTGGCACGACCAGGAGCCAGCGTGAAAA
GTCCCTTGTGACCACTGGCACTCGCGGCCTCCTCCTCCTTCGCTATAGTTCGACGTCGTCTCGCCTCGACTTGACCGTGCTGGTCCTCGGTCGCACTTTT
900
VH Cetuximab
GS Linker 2
VH L2K
Q G T L V T V S A G G G G S D I K L Q Q S G A E L A R P G A S V K
TGTCCTGTAAGACATCTGGCTACACTTTCACCCGATATACTATGCACTGGGTCAAGCAGCGACCTGGACAGGGACTGGAGTGGATCGGATACATTAATCC
ACAGGACATTCTGTAGACCGATGTGAAAGTGGGCTATATGATACGTGACCCAGTTCGTCGCTGGACCTGTCCCTGACCTCACCTAGCCTATGTAATTAGG
1000
VH L2K
M S C K T S G Y T F T R Y T M H W V K Q R P G Q G L E W I G Y I N P
AAGCCGGGGCTACACAAACTACAACCAGAAGTTTAAAGACAAGGCTACCCTGACTACCGATAAGAGCTCCTCTACAGCATACATGCAGCTGAGTTCACTG
TTCGGCCCCGATGTGTTTGATGTTGGTCTTCAAATTTCTGTTCCGATGGGACTGATGGCTATTCTCGAGGAGATGTCGTATGTACGTCGACTCAAGTGAC
1100
VH L2K
S R G Y T N Y N Q K F K D K A T L T T D K S S S T A Y M Q L S S L
ACTTCTGAGGACAGTGCAGTGTACTATTGCGCCAGATACTATGACGATCATTACTGTCTGGATTATTGGGGACAGGGCACAACTCTGACAGTGAGCTCCG
TGAAGACTCCTGTCACGTCACATGATAACGCGGTCTATGATACTGCTAGTAATGACAGACCTAATAACCCCTGTCCCGTGTTGAGACTGTCACTCGAGGC
1200
VH L2K
T S E D S A V Y Y C A R Y Y D D H Y C L D Y W G Q G T T L T V S S
TCGAAGGAGGATCAGGAGGAAGCGGAGGATCCGGAGGGTCTGGAGGCGTGGACGATATCCAGCTGACTCAGTCCCCAGCCATTATGTCCGCTTCTCCCGG
AGCTTCCTCCTAGTCCTCCTTCGCCTCCTAGGCCTCCCAGACCTCCGCACCTGCTATAGGTCGACTGAGTCAGGGGTCGGTAATACAGGCGAAGAGGGCC
1300
VH L2K
GS Linker 3
VL L2K
V E G G S G G S G G S G G S G G V D D I Q L T Q S P A I M S A S P G
CGAGAAAGTGACAATGACTTGCCGGGCCTCTAGTTCAGTCTCTTACATGAATTGGTATCAGCAGAAAAGTGGCACCTCACCAAAGAGATGGATCTACGAC
GCTCTTTCACTGTTACTGAACGGCCCGGAGATCAAGTCAGAGAATGTACTTAACCATAGTCGTCTTTTCACCGTGGAGTGGTTTCTCTACCTAGATGCTG
1400
VL L2K
E K V T M T C R A S S S V S Y M N W Y Q Q K S G T S P K R W I Y D
ACCAGTAAGGTGGCCAGCGGGGTCCCCTATAGGTTTAGTGGCTCCGGAAGCGGCACCTCCTACTCTCTGACAATTAGCTCCATGGAGGCAGAAGATGCCG
TGGTCATTCCACCGGTCGCCCCAGGGGATATCCAAATCACCGAGGCCTTCGCCGTGGAGGATGAGAGACTGTTAATCGAGGTACCTCCGTCTTCTACGGC
1500
VL L2K
T S K V A S G V P Y R F S G S G S G T S Y S L T I S S M E A E D A
CTACCTACTATTGTCAGCAGTGGTCTAGTAACCCTCTGACATTCGGGGCTGGGACCAAACTGGAGCTGAAGGATTACAAGGACGACGACGACAAGTAATA
GATGGATGATAACAGTCGTCACCAGATCATTGGGAGACTGTAAGCCCCGACCCTGGTTTGACCTCGACTTCCTAATGTTCCTGCTGCTGCTGTTCATTAT
1600
VL L2K
FLAG tag
Stop
PolyA
A T Y Y C Q Q W S S N P L T F G A G T K L E L K D Y K D D D D K
AfeI
End (1659)
AACTTTATTTTTCAATTGCAGAAAATTTCAAGTCATTTTTCATTCAGTAGTATAGCGCT 3'
1659
TTGAAATAAAAAGTTAACGTCTTTTAAAGTTCAGTAAAAAGTAAGTCATCATATCGCGA 5'
Homology to Ad genome

Annex 2. mBiTE construct

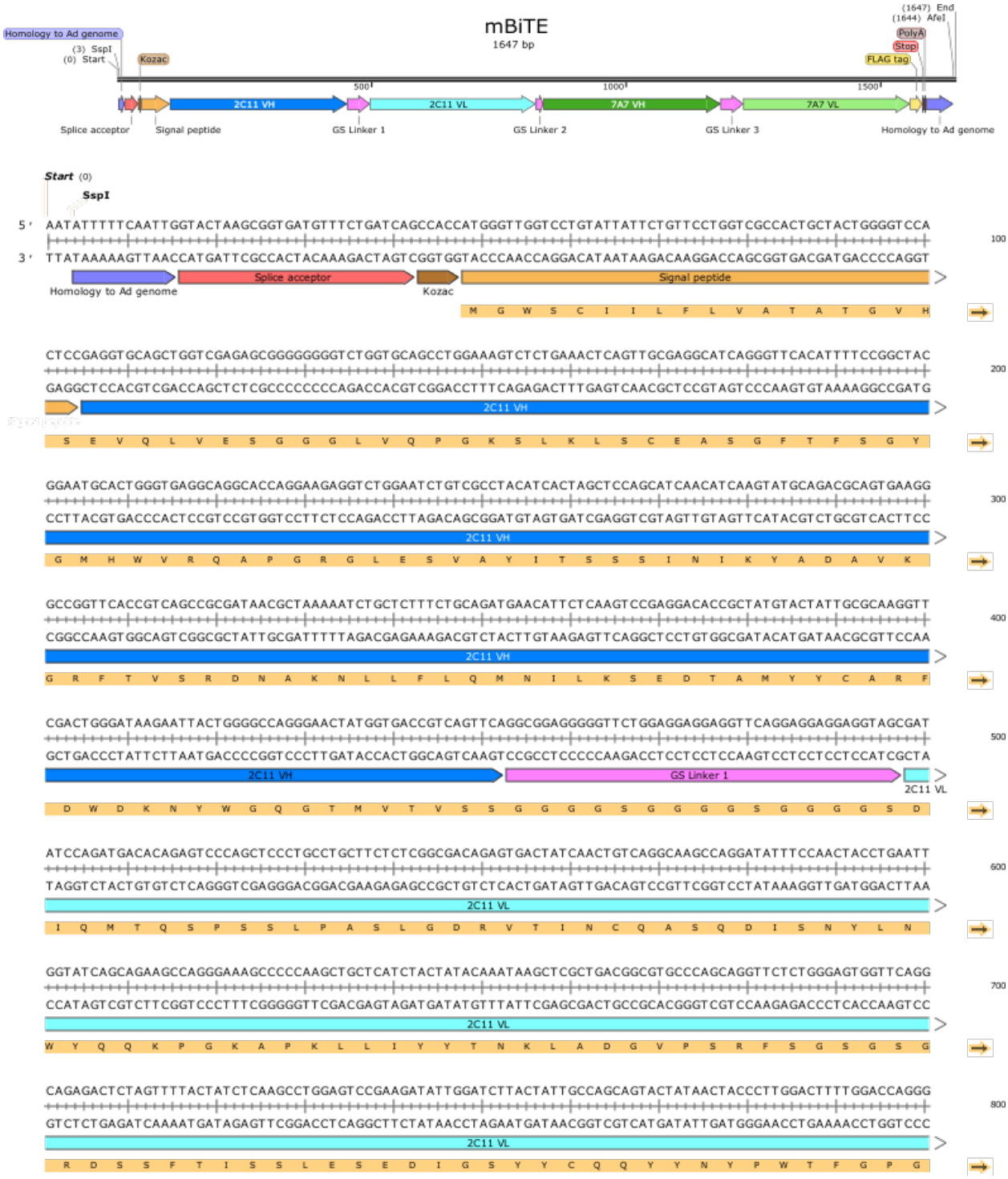

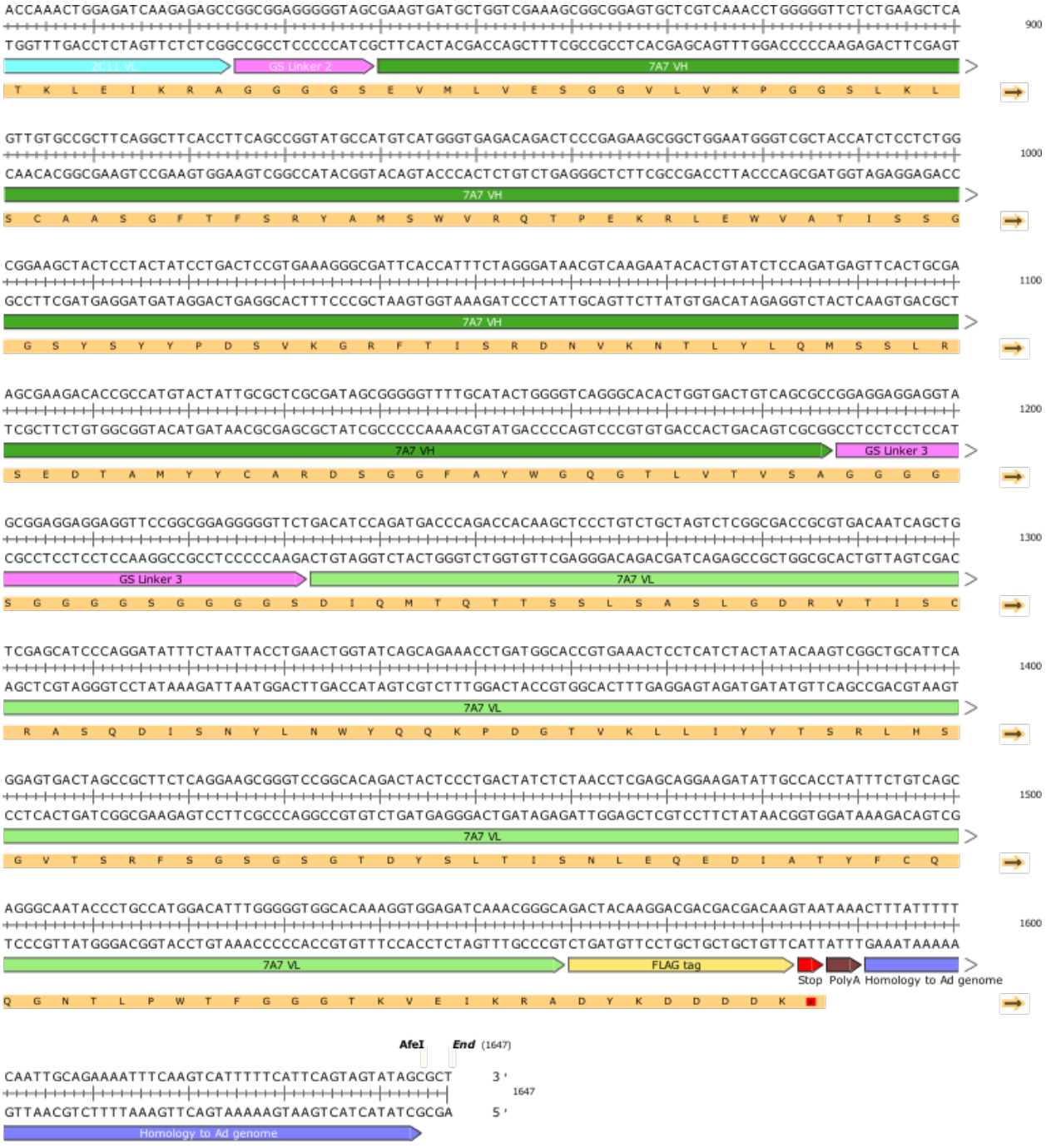
ACCAAACTGGAGATCAAGAGAGCCGGCGGAGGGGGTAGCGAAGTGATGCTGGTCGAAAGCGGCGGAGTGCTCGTCAAACCTGGGGGTTCTCTGAAGCTCA
900
TGGTTTGACCTCTAGTTCTCTCGGCCGCCTCCCCCATCGCTTCACTACGACCAGCTTTCGCCGCCTCACGAGCAGTTTGGACCCCCAAGAGACTTCGAGT
2C11 VL
GS Linker 2
7A7 VH
T K L E I K R A G G G G S E V M L V E S G G V L V K P G G S L K L
GTTGTGCCGCTTCAGGCTTCACCTTCAGCCGGTATGCCATGTCATGGGTGAGACAGACTCCCGAGAAGCGGCTGGAATGGGTCGCTACCATCTCCTCTGG
1000
CAACACGGCGAAGTCCGAAGTGGAAGTCGGCCATACGGTACAGTACCCACTCTGTCTGAGGGCTCTTCGCCGACCTTACCCAGCGATGGTAGAGGAGACC
7A7 VH
S C A A S G F T F S R Y A M S W V R Q T P E K R L E W V A T I S S G
CGGAAGCTACTCCTACTATCCTGACTCCGTGAAAGGGCGATTCACCATTTCTAGGGATAACGTCAAGAATACACTGTATCTCCAGATGAGTTCACTGCGA
1100
GCCTTCGATGAGGATGATAGGACTGAGGCACTTTCCCGCTAAGTGGTAAAGATCCCTATTGCAGTTCTTATGTGACATAGAGGTCTACTCAAGTGACGCT
7A7 VH
G S Y S Y Y P D S V K G R F T I S R D N V K N T L Y L Q M S S L R
AGCGAAGACACCGCCATGTACTATTGCGCTCGCGATAGCGGGGGTTTTGCATACTGGGGTCAGGGCACACTGGTGACTGTCAGCGCCGGAGGAGGAGGTA
1200
TCGCTTCTGTGGCGGTACATGATAACGCGAGCGCTATCGCCCCCAAAACGTATGACCCCAGTCCCGTGTGACCACTGACAGTCGCGGCCTCCTCCTCCAT
7A7 VH
GS Linker 3
S E D T A M Y Y C A R D S G G F A Y W G Q G T L V T V S A G G G G
GCGGAGGAGGAGGTTCCGGCGGAGGGGGTTCTGACATCCAGATGACCCAGACCACAAGCTCCCTGTCTGCTAGTCTCGGCGACCGCGTGACAATCAGCTG
1300
CGCCTCCTCCTCCAAGGCCGCCTCCCCCAAGACTGTAGGTCTACTGGGTCTGGTGTTCGAGGGACAGACGATCAGAGCCGCTGGCGCACTGTTAGTCGAC
GS Linker 3
7A7 VL
S G G G G S G G G G S D I Q M T Q T T S S L S A S L G D R V T I S C
TCGAGCATCCCAGGATATTTCTAATTACCTGAACTGGTATCAGCAGAAACCTGATGGCACCGTGAAACTCCTCATCTACTATACAAGTCGGCTGCATTCA
1400
AGCTCGTAGGGTCCTATAAAGATTAATGGACTTGACCATAGTCGTCTTTGGACTACCGTGGCACTTTGAGGAGTAGATGATATGTTCAGCCGACGTAAGT
7A7 VL
R A S Q D I S N Y L N W Y Q Q K P D G T V K L L I Y Y T S R L H S
GGAGTGACTAGCCGCTTCTCAGGAAGCGGGTCCGGCACAGACTACTCCCTGACTATCTCTAACCTCGAGCAGGAAGATATTGCCACCTATTTCTGTCAGC
1500
CCTCACTGATCGGCGAAGAGTCCTTCGCCCAGGCCGTGTCTGATGAGGGACTGATAGAGATTGGAGCTCGTCCTTCTATAACGGTGGATAAAGACAGTCG
7A7 VL
G V T S R F S G S G S G T D Y S L T I S N L E Q E D I A T Y F C Q
AGGGCAATACCCTGCCATGGACATTTGGGGGTGGCACAAAGGTGGAGATCAAACGGGCAGACTACAAGGACGACGACGACAAGTAATAAACTTTATTTTT
1600
TCCCGTTATGGGACGGTACCTGTAAACCCCCACCGTGTTTCCACCTCTAGTTTGCCCGTCTGATGTTCCTGCTGCTGCTGTTCATTATTTGAAATAAAAA
7A7 VL
FLAG tag
Stop
PolyA
Homology to Ad genome
Q G N T L P W T F G G G T K V E I K R A D Y K D D D D K
AfeI
End (1647)
CAATTGCAGAAAATTTCAAGTCATTTTTCATTCAGTAGTATAGCGCT 3'
1647
GTTAACGTCTTTTAAAGTTCAGTAAAAAGTAAGTCATCATATCGCGA 5'
Homology to Ad genome

Annex 3. mcBiTE construct

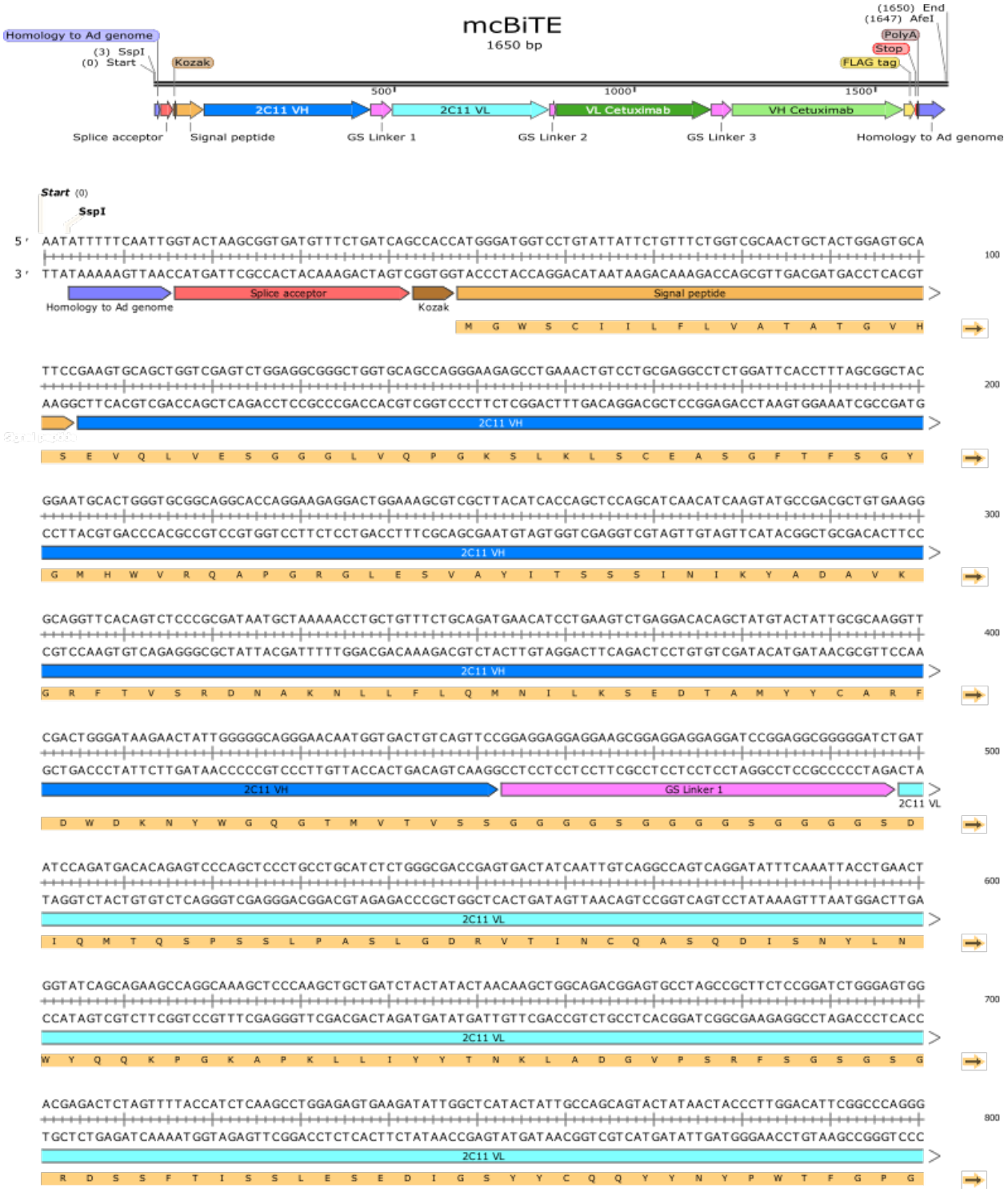

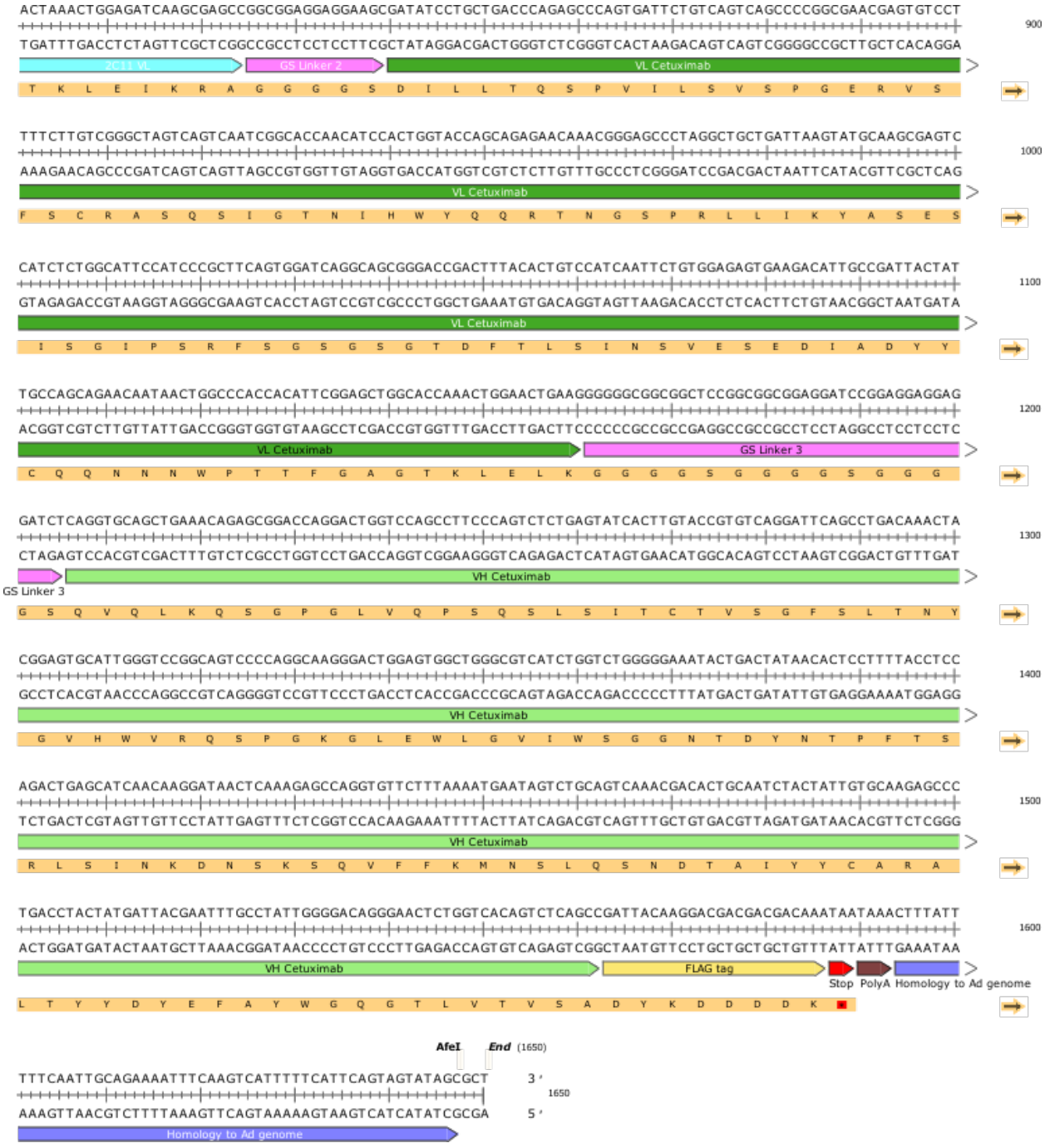
ACTAAACTGGAGATCAAGCGAGCCGGCGGAGGAGGAAGCGATATCCTGCTGACCCAGAGCCCAGTGATTCTGTCAGTCAGCCCCGGCGAACGAGTGTCCT
900
TGATTTGACCTCTAGTTCGCTCGGCCGCCTCCTCCTTCGCTATAGGACGACTGGGTCTCGGGTCACTAAGACAGTCAGTCGGGGCCGCTTGCTCACAGGA
2C11 VL
GS Linker 2
VL Cetuximab
T K L E I K R A G G G G S D I L L T Q S P V I L S V S P G E R V S
TTTCTTGTCGGGCTAGTCAGTCAATCGGCACCAACATCCACTGGTACCAGCAGAGAACAAACGGGAGCCCTAGGCTGCTGATTAAGTATGCAAGCGAGTC
1000
AAAGAACAGCCCGATCAGTCAGTTAGCCGTGGTTGTAGGTGACCATGGTCGTCTCTTGTTTGCCCTCGGGATCCGACGACTAATTCATACGTTCGCTCAG
VL Cetuximab
F S C R A S Q S I G T N I H W Y Q Q R T N G S P R L L I K Y A S E S
CATCTCTGGCATTCCATCCCGCTTCAGTGGATCAGGCAGCGGGACCGACTTTACACTGTCCATCAATTCTGTGGAGAGTGAAGACATTGCCGATTACTAT
1100
GTAGAGACCGTAAGGTAGGGCGAAGTCACCTAGTCCGTCGCCCTGGCTGAAATGTGACAGGTAGTTAAGACACCTCTCACTTCTGTAACGGCTAATGATA
VL Cetuximab
I S G I P S R F S G S G S G T D F T L S I N S V E S E D I A D Y Y
TGCCAGCAGAACAATAACTGGCCCACCACATTCGGAGCTGGCACCAAACTGGAACTGAAGGGGGGCGGCGGCTCCGGCGGCGGAGGATCCGGAGGAGGAG
1200
ACGGTCGTCTTGTTATTGACCGGGTGGTGTAAGCCTCGACCGTGGTTTGACCTTGACTTCCCCCCGCCGCCGAGGCCGCCGCCTCCTAGGCCTCCTCCTC
VL Cetuximab
GS Linker 3
C Q Q N N N W P T T F G A G T K L E L K G G G G S G G G G S G G G
GATCTCAGGTGCAGCTGAAACAGAGCGGACCAGGACTGGTCCAGCCTTCCCAGTCTCTGAGTATCACTTGTACCGTGTCAGGATTCAGCCTGACAAACTA
1300
CTAGAGTCCACGTCGACTTTGTCTCGCCTGGTCCTGACCAGGTCGGAAGGGTCAGAGACTCATAGTGAACATGGCACAGTCCTAAGTCGGACTGTTTGAT
VH Cetuximab
GS Linker 3
G S Q V Q L K Q S G P G L V Q P S Q S L S I T C T V S G F S L T N Y
CGGAGTGCATTGGGTCCGGCAGTCCCCAGGCAAGGGACTGGAGTGGCTGGGCGTCATCTGGTCTGGGGGAAATACTGACTATAACACTCCTTTTACCTCC
1400
GCCTCACGTAACCCAGGCCGTCAGGGGTCCGTTCCCTGACCTCACCGACCCGCAGTAGACCAGACCCCCTTTATGACTGATATTGTGAGGAAAATGGAGG
VH Cetuximab
G V H W V R Q S P G K G L E W L G V I W S G G N T D Y N T P F T S
AGACTGAGCATCAACAAGGATAACTCAAAGAGCCAGGTGTTCTTTAAAATGAATAGTCTGCAGTCAAACGACACTGCAATCTACTATTGTGCAAGAGCCC
1500
TCTGACTCGTAGTTGTTCCTATTGAGTTTCTCGGTCCACAAGAAATTTTACTTATCAGACGTCAGTTTGCTGTGACGTTAGATGATAACACGTTCTCGGG
VH Cetuximab
R L S I N K D N S K S Q V F F K M N S L Q S N D T A I Y Y C A R A
TGACCTACTATGATTACGAATTTGCCTATTGGGGACAGGGAACTCTGGTCACAGTCTCAGCCGATTACAAGGACGACGACGACAAATAATAAACTTTATT
1600
ACTGGATGATACTAATGCTTAAACGGATAACCCCTGTCCCTTGAGACCAGTGTCAGAGTCGGCTAATGTTCCTGCTGCTGCTGTTTATTATTTGAAATAA
VH Cetuximab
FLAG tag
Stop
PolyA
Homology to Ad genome
L T Y Y D Y E F A Y W G Q G T L V T V S A D Y K D D D D K ■
AfeI
End (1650)
TTTCAATTGCAGAAAATTTCAAGTCATTTTTCATTCAGTAGTATAGCGCT 3'
1650
AAAGTTAACGTCTTTTAAAGTTCAGTAAAAAGTAAGTCATCATATCGCGA 5'
Homology to Ad genome